UNIVERSITE DE LIMOGES

ECOLE DOCTORALE Sciences et Ingénierie pour l'Information

FACULTE DES SCIENCES ET TECHNIQUES
XLIM OSA

Année : 2012 **Thèse N°56-2012**

THESE

pour obtenir le grade de

DOCTEUR DE L'UNIVERSITE DE LIMOGES

Discipline : "Electronique des Hautes Fréquences, Photonique et Systèmes"

Spécialité : "Télécommunications"

présentée et soutenue par

ABDALLAH Yasser

le 13 décembre 2012

«Effects of the mutual couplings on the EM properties of reflectarrays. Definition of a strategy of design»

« Influence des couplages sur les propriétés des antennes à réseau réflecteur. Définition d'une méthodologie de conception »

Thèse dirigée par Monsieur Thierry Monediere

Encadrée par Monsieur Marc Thevenot et Monsieur Cyrille Menudier

JURY :

Monsieur B. Jarry	Président	*Professeur, Université de Limoges*
Monsieur H. Aubert	Rapporteur	*Professeur, Université de Toulouse*
Monsieur R. Gillard	Rapporteur	*Professeur, Université de Rennes*
Monsieur H. Legay	Examinateur	*Ingénieur Antennes, Thales Alenia Space, Toulouse*
Monsieur B. Palacin	Examinateur	*Ingénieur Antennes, Cnes, Toulouse*
Monsieur T. Monediere	Examinateur	*Professeur, Université de Limoges*
Monsieur M. Thevenot	Examinateur	*Chargé de Recherche CNRS, Xlim, Limoges*
Monsieur C. Menudier	Examinateur	*Maître de conférences, Université de Limoges*

To my familly and beloved ones

INFLUENCE DES COUPLAGES SUR LES PROPRIETES DES ANTENNES A RESEAU REFLECTEUR. DEFINITION D'UNE METHODOLOGIE DE CONCEPTION

L'objectif de la thèse est d'étudier de façon précise et rigoureuse les propriétés électromagnétiques des antennes reflectarray (RA). Pour atteindre cet objectif, ce travail de thèse propose une architecture de reflectarray spécifique associée à une méthodologie de synthèse. Après avoir présenté un état de l'art sur les reflectarray et leurs applications, une méthodologie complète de conception sera détaillée. Celle-ci sera ensuite mise en oeuvre, notamment pour montrer l'impact des couplages et la nécessité de les considérer dans la conception d'un Reflectarray. L'intérêt de ce travail consiste aussi à améliorer la compréhension des propriétés électromagnétique du RA afin d'optimiser leurs performances. La démarche adoptée permet également d'analyser des contraintes particulières comme celles liées à la technologie des cellules utilisées dans un RA agile (effet de la quantification, par exemple). Cette facette de la thèse, qui peut servir de support à l'ingénierie du système, complète le point de vue donné sur les phénomènes physiques intervenant dans les reflectarrays.

I. CONTEXTE ET ENJEUX DE L'ETUDE

Les antennes à réseau réflecteur, ou reflectarray (RA), en technologie imprimées ont été l'objet de beaucoup d'attention ces dernières années. Une large gamme d'applications avec des conceptions passives ou reconfigurables ont été présentées. Ces antennes combinent la simplicité et la performance élevée des antennes à réflecteur avec les capacités des réseaux d'antennes pour contrôler la forme et/ou l'angle de pointage des diagrammes de rayonnement. L'alimentation par distribution spatiale de l'énergie réduit les pertes et la complexité du circuit de distribution par rapport aux réseaux d'antennes planaires, minimisant ainsi les pertes d'insertion et autorisant des gains réalisés élevés.

Cependant, le principal défi à relever lors de la conception de ces antennes est de réaliser une modélisation efficace, de façon à obtenir des résultats numériques suffisamment fiables avant de passer au processus de fabrication. En se basant uniquement sur les théories de l'optique géométrique (GO) ou physique (PO), une conception imprécise est fortement probable, car ces théories ne permettent pas de prendre en compte les interactions locales entre le champ électromagnétique incident provenant de la source primaire et les cellules du reflectarray. Dans la pratique, une erreur importante sur les déphasages appliqués à chaque élément peut se produire et le champ diffracté résultant est altéré, conduisant à une réduction des performances par rapport à l'objectif défini pour le rayonnement.

Des avancées significatives ont néanmoins été faites sur la modélisation électromagnétique (EM) des reflectarrays, et illustrées à travers diverses applications. Cependant, certains comportements EM intéressants ne sont pas encore bien détaillés dans la littérature scientifique, ce qui ne permet d'éliminer toutes les zones d'ombres dans la conception de ces antennes, freinant leur développement à grande échelle. Il est bien connu par la communauté que les performances des antennes réseaux sont affectées par le couplage mutuel entre les éléments. En se basant sur les formulations bien établies sur les réseaux d'antennes et en tirant parti de l'analogie possible avec les reflectarray, il est possible d'établir une formulation rigoureuse pour concevoir et étudier ces antennes fonctionnant en réflexion. **Notre principal objectif dans cette thèse sera notamment d'étudier les effets du couplage et leurs conséquences dans les reflectarray, de façon à comprendre en détails quels peuvent être les mécanismes pouvant être utilisés pour optimiser leurs performances**. Pour cela, nous proposons une architecture spécifique et un formalisme associé pour la conception des RA. Cette approche va permettre l'analyse fine de leurs performances, ainsi

qu'une conception couplée à une méthodologie de synthèse. Dans ce cadre, le travail sera focalisé sur une modélisation précise des effets du couplage plutôt que sur la recherche de performances en termes de temps de calcul ou sur une conception de cellules spécifique.

En utilisant un procédé de synthèse spécifique, nous allons démontrer que le couplage mutuel influence à la fois les phases et les amplitudes des excitations des cellules du RA, tandis que l'hypothèse classique suppose que leurs amplitudes sont uniquement proportionnelles à l'éclairement de la source primaire. Afin de démontrer ces effets, l'étude est basée sur un panneau réflecteur composé de cellules identiques connectées à des charges réactives. Ces charges sont situées à l'arrière du panneau afin de minimiser les interactions entre rayonnement et circuit déphaseur. En outre, un avantage déterminant de cette architecture est de **séparer l'étude du problème électromagnétique** (coté des éléments rayonnants) **et le circuit actif** (coté des charges réactives). **Les deux domaines sont reliés par des ports électromagnétiques qui vont nous permettre de résoudre le problème avec une grande précision**, notamment en termes de bilan énergétique. Du point de vue d'un concepteur, une telle architecture est intéressante, car les charges peuvent être directement soudées au dos du substrat d'accueil, qui contiendra également le routage pour piloter et distribuer des tensions continues aux circuits dans le cas d'un reflectarray agile.

Une autre motivation importante de cette thèse concerne le domaine des applications du reflectarray. En fait, les RA sont souvent limités à des applications à coût élevé, dans des secteurs spécifiques, où ils sont destinés à remplacer les réflecteurs ou réseaux de grandes dimensions. Dans ces cas, le RA contient plusieurs milliers de cellules. Dans un scénario reconfigurable, cette antenne nécessite alors un grand nombre de contrôles augmentant considérablement le coût final. Du point de vue de la modélisation, les formalismes faisant recours à une périodicité infinie (modes de Floquets) sont souvent utilisés. Même si ceux-ci impliquent des approximations (cellules et couplages identiques) les performances obtenues peuvent être suffisantes pour certaines applications.

Cependant, si quelqu'un veut concevoir un RA ayant une taille moyenne, par exemple pour des applications terrestres, il va souffrir d'une dégradation des performances si des formalismes à périodicité infinie sont utilisés. **Dans notre cas, nous voulons démontrer qu'une conception efficace est possible si un formalisme approprié est utilisé, quelle que soit la taille du problème électromagnétique.**

Le manuscrit est divisé en quatre chapitres:

Dans le premier chapitre, un état de l'art des antennes RA est présenté. Il contient l'historique des développements sur cette catégorie d'antenne ainsi que son positionnement vis-à-vis des antennes à réflecteurs et des réseaux. Un résumé des principales techniques d'analyse est aussi donné.

Dans le deuxième chapitre, le formalisme théorique ainsi que l'architecture d'antenne étudiée est présentée. Ce formalisme, reposant sur l'utilisation de ports électromagnétiques, est ensuite implanté dans un solveur analytique permettant d'effectuer la synthèse des charges réactives associées au RA. Celui-ci s'appuie sur une 'carte d'identité' des grandeurs caractéristiques du RA, obtenues par une simulation rigoureuse ou par la mesure. Ces grandeurs sont stockées dans une base de données.

Dans le troisième chapitre, la validation numérique du formalisme établi est effectuée. Elle repose sur un RA de dimensions moyennes. Le panneau réflecteur est composé de centaines de cellules patch micro-ruban. Les résultats présentés démontrent la précision de l'architecture proposée et du solveur analytique qui synthétise la distribution des déphasages.

Dans le quatrième chapitre, une étude détaillée des caractéristiques EM de l'antenne est menée, en caractérisant précisément les couplages mutuels entre les cellules. Ces phénomènes seront détaillés ainsi que d'autres aspects liés aux contraintes technologiques, telles que les effets de la quantification.

II. PRINCIPAUX RESULTATS

I.1 - **Définition du formalisme**

Le deuxième chapitre de la thèse a permis de définir un schéma équivalent des cellules d'un reflectarray et de leurs interactions, comme le montre la Figure 1.

Ce formalisme a permis d'écrire la relation Eq.1. (voir développement complet dans le chapitre 2). Celle-ci montre la dépendance des poids d'excitation de chaque cellule par rapport à :

- b_0 : ondes incidentes couplées en provenance de la source primaire,
- [S] : matrice de couplage entre les différentes cellules,
- p+C : phase définie par rapport à l'objectif de rayonnement, défini à une constante près (C).

(Eq.1) $$\|\vec{a}\| = \left\| \overrightarrow{b_0} + [S].diag\left(e^{+j(p+C)}\right).\|\vec{a}\| \right\|$$

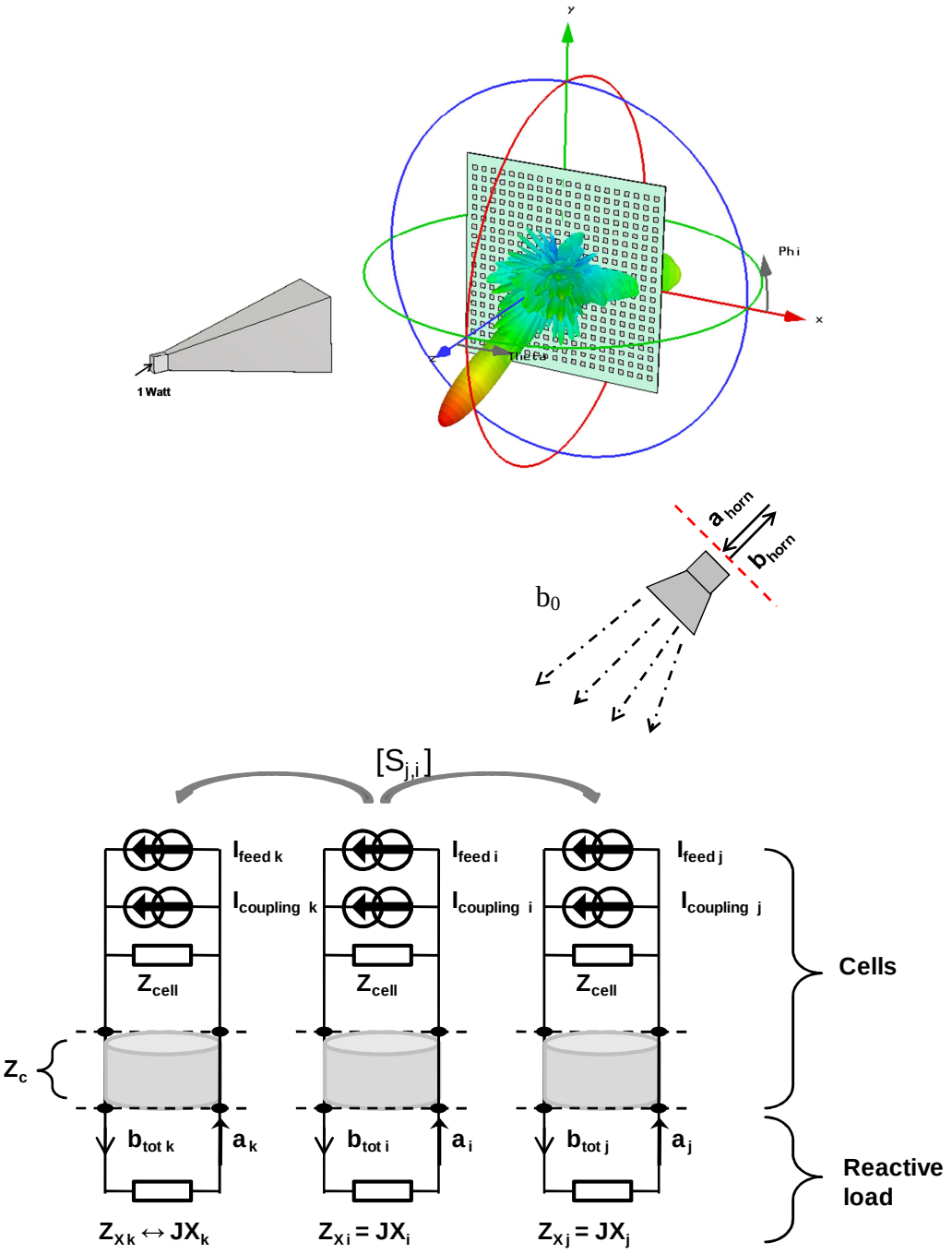

Figure 1. *Schéma équivalent des cellules pour traiter le re-rayonnement en prenant en compte les couplages. Le schéma du reflectarray utilisé est présenté en haut (380 cellules, panneau de 10λx10λ, illumination par un cornet pyramidal en offset)*

I.2 - **Développement du solveur analytique**

Une fois le formalisme établi, celui-ci a été implanté dans un solveur analytique à architecture modulaire, tel que représenté par le synoptique de la Figure 2. Celui-ci a été développé entièrement sous Matlab et permet d'effectuer en quelques secondes ou minutes les différentes tâches de la conception du reflectarray :

- Synthèse des charges réactives à implanter pour réaliser un objectif de rayonnement,
- Détermination des performances électromagnétiques : diagrammes de rayonnement complets, contributions des cellules en courants et tensions, bilan de puissance,
- Etudes de contraintes particulières : effets d'un offset de la phase de référence, impact de la quantification.

Pour fonctionner, ce solveur utilise une base de données qui contient une carte d'identité de la configuration du reflectarray :

- Matrice [S] réduite du panneau,
- Diagramme de rayonnement d'une cellule environnée,
- Diagramme de rayonnement et position de la source primaire,
- Coefficients de couplage entre l'onde incidente de la source primaire et les cellules,
- Diagramme diffracté par le panneau réflecteur (SER).

Les éléments constitutifs de cette base de données sont obtenus essentiellement par un simulateur électromagnétique « full-wave » ou par des mesures. C'est cette phase de construction de la carte d'identité qui est la plus consommatrice en temps de calcul. Néanmoins, dans un contexte où nous cherchons à concevoir des reflectarrays qui contiennent « seulement » quelques centaines d'éléments et compte tenu de la puissance de calcul de la moindre station de travail aujourd'hui, cette phase de calcul reste tout à fait raisonnable (inférieure à 10 heures). De plus, une fois cette carte d'identité établie, il n'est plus nécessaire d'avoir recours à un calcul full-wave, l'intégralité de la synthèse, des études paramétriques et la détermination des performances finales se font avec le solveur analytique.

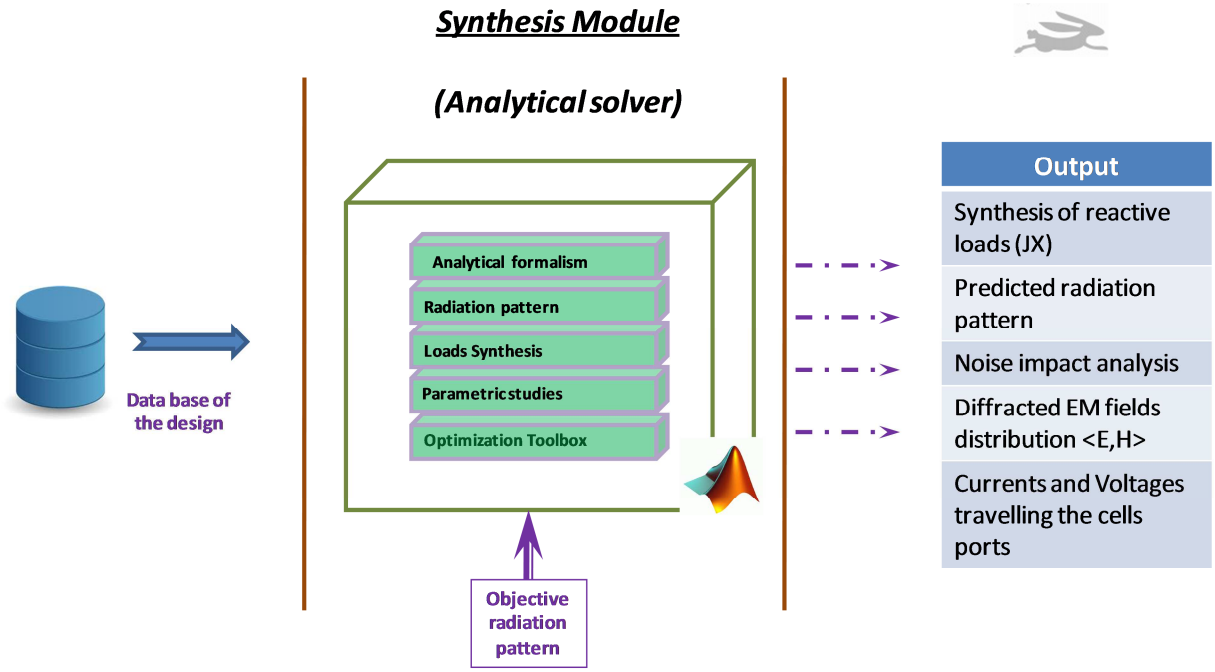

Figure 2. *Schéma descriptif du solveur analytique.*

Une fois le solveur analytique validé par confrontation à une simulation complète du reflectarray par une méthode full-wave (Finite Integration Technique) dans CST Microwave Studio, celui-ci a été utilisé pour étudier en détail certaines propriétés des reflectarrays.

I.3 - **Mise en évidence de l'impact des couplages**

De façon à montrer l'impact des couplages qui apparaît dans l'équation Eq. 1, une étude a été faite de façon à montrer l'impact sur les performances entre un reflectarray modélisé avec la dépendance vis-à-vis des couplages et un autre où ces derniers ont été négligés. L'exemple d'un dépointage dans la direction $\{\theta_0 = 15°; \varphi_0 = 90°\}$ est illustré sur les Figure 4 et 5 représentant respectivement les diagrammes de rayonnement et les phases des coefficients a_{mxn} pour un reflectarray contenant 380 cellules.

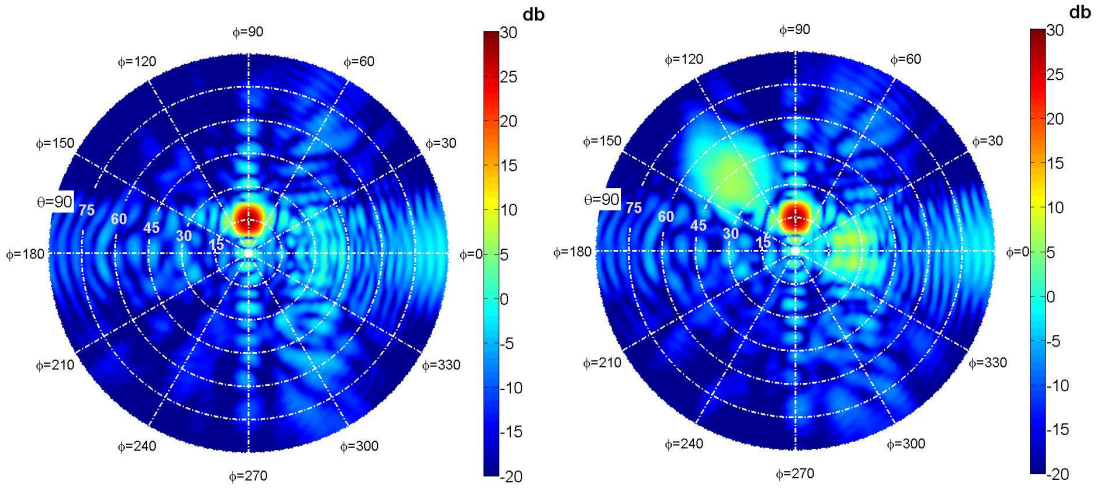

Figure 3. *Diagrammes de rayonnement obtenu pour un pointage dans la direction {θ_0 =15°; φ_0 =90°}, en négligeant les couplages (à droite) et en les intégrant dans le processus de synthèse (à gauche).*

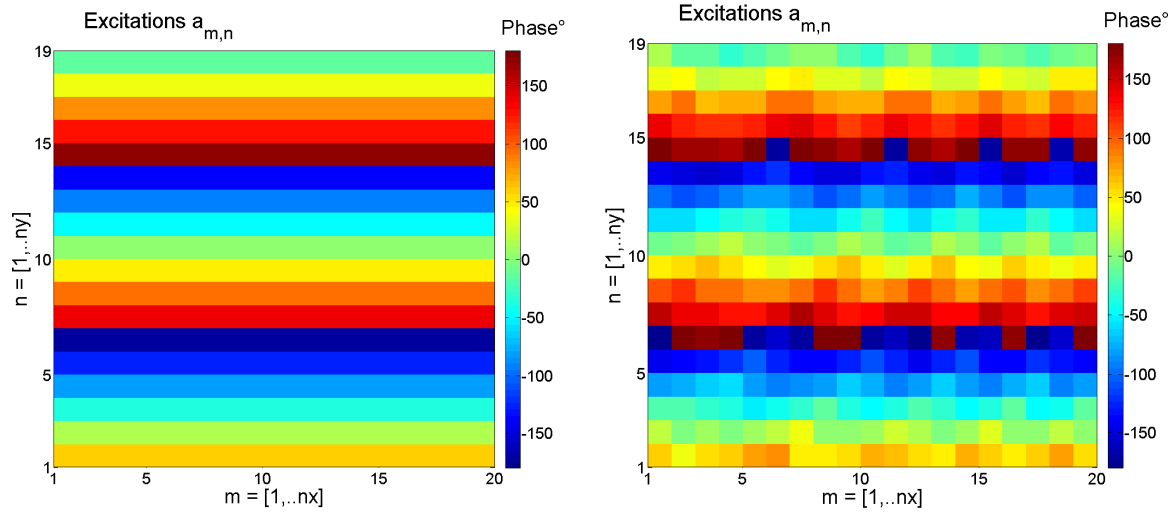

Figure 4. *Cartographies de phases des coefficients a_{mxn} pour un pointage dans la direction {θ_0 =15°; φ_0 =90°}, en négligeant les couplages (à droite) et en les intégrant dans le processus de synthèse (à gauche)*

Les résultats montrent une dégradation de la directivité d'environ 0.4 dB pour cette direction de pointage lorsque les couplages sont négligés. Bien que modéré, cette dégradation est clairement visible sur les remontées de lobes secondaires de la Figure 3 et sur le bruit introduit sur les phases des coefficients a_{mxn} de la Figure 4. Dans un contexte d'application de télécommunications, ces remontées de lobes secondaires peuvent être préjudiciables. Il faut également noter que l'impact des couplages est aussi lié à la nature des cellules et à l'objectif de rayonnement, ce qui veut dire que la dégradation de 0.4 dB observée ici peut être plus importante dans certains cas.

Au-delà de cet impact, la thèse a permis de mettre en avant l'influence du couplage, à la fois sur le module et la phase des coefficients d'excitations a_{mxn}, alors que l'approximation usuelle est de considérer que seules les phases sont affectées, les modules étant directement proportionnels à l'illumination de la source primaire. Pour illustrer cet impact dans ce résumé, un exemple est montré sur la Figure 5.

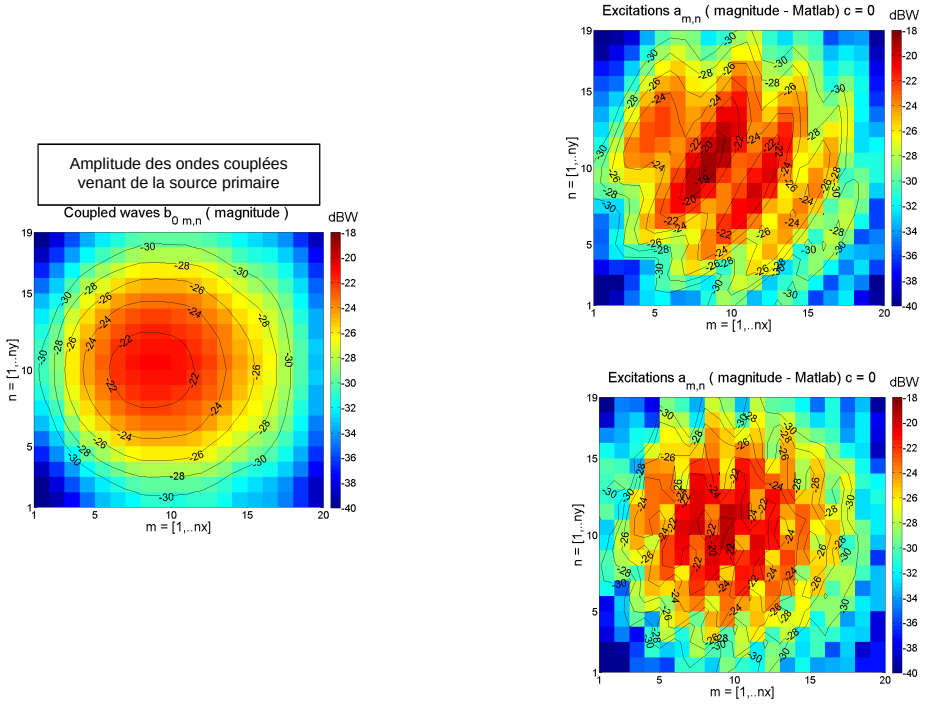

Figure 5. *Cartographies des ondes couplées par les cellules en fonction des directions de pointage à satisfaire {θ_0 =15°; φ_0 =90°} en haut à droite, et {θ_0 =25°; φ_0 =135°} en bas à droite. On notera la différence notable avec les ondes couplées directement en provenance de la source primaire (à gauche)*

Outre ces observations, le solveur analytique permet également d'étudier finement de nombreuses caractéristiques électromagnétiques du reflectarray, comme l'impact d'un offset de phase ainsi que le bilan de puissance à travers la décomposition des différentes contributions du rayonnement (puissance interceptée, SER, re-rayonnement des cellules chargées). Ces aspects sont abordés dans les chapitres 3 et 4.

I.4 - **Prise en compte de contraintes technologiques**

De façon à pouvoir prendre en compte des critères réalistes lorsqu'une conception de reflectarray reconfigurable est envisagée, le solveur analytique permet d'intégrer des

contraintes de quantifications et d'étudier leur impact sur les performances finales. Il est notamment utile de connaître la dégradation inhérente à une réduction des états de quantifications, de façon à trouver le meilleur compromis performances/complexité du déphaseur. Cette possibilité d'étude avec le solveur représente une autre facette, cette fois-ci plus orientée du côté ingénierie.

Parmi les études effectuées, une comparaison des dégradations de performances en fonction des états de quantification a été faite pour différentes direction de pointage. Un graphique résumant les résultats est présenté sur la Figure 6.

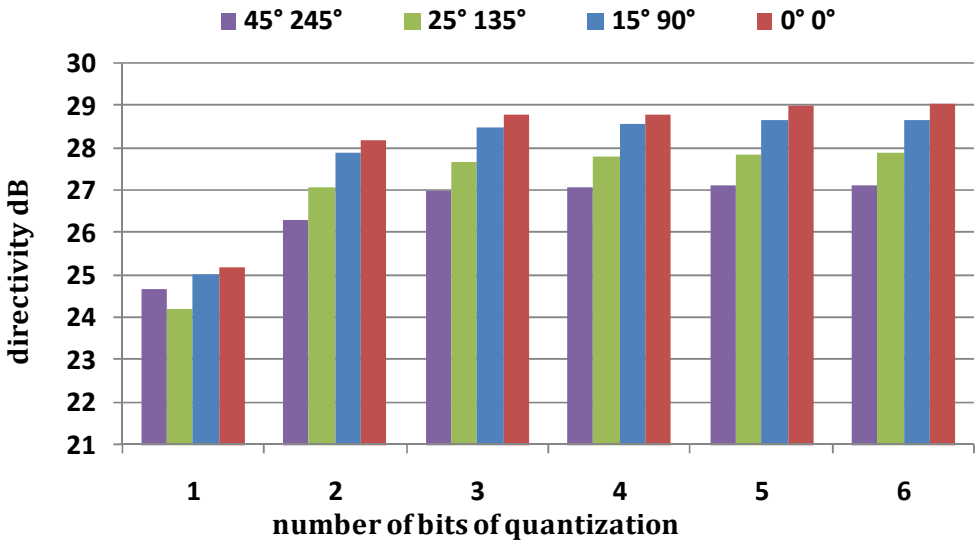

Figure 6. *Evolution de la directivité en fonction du nombre de bits de quantification et pour différents objectifs de pointage.*

Les résultats montrent notamment que pour le reflectarray étudié, la dégradation observée à partir de 3 bits de quantification, soit 8 états de phases possibles, est négligeable. Pour une quantification sur 2 bits, la dégradation est de l'ordre de 0.4 à 0.8 dB et si seulement deux états de phases sont possibles, une baisse de l'ordre de 1.5 à 3 dB est observable. Il faut noter qu'ici, seules les pertes liées à la quantification sont prises en compte, les pertes intrinsèques des déphaseurs sont négligées alors qu'elles peuvent être importantes en fonction de la technologie utilisée. Cette prise en compte est possible dans le solveur, mais ici, l'objectif était seulement d'étudier les dégradations liées à la quantification de la phase. On peut aussi remarquer qu'une quantification sur 2 états, même si elle entraîne des pertes importantes, peut être une perte acceptable en fonction des applications. En effet, en maîtrisant la conception de reflectarrays de petites dimensions et en employant des

technologies de déphaseurs simples et bas coût, il serait possible de développer le marché des reflectarrays dans des applications de masse contrairement à ce qui est fait aujourd'hui.

III. CONCLUSIONS ET PERSPECTIVES

Le sujet de cette thèse porte sur une conception précise d'antennes à panneau réflecteur (Reflectarray) en portant une attention particulière aux éléments qui pourraient affecter leurs performances. Afin de caractériser les RA, un formalisme théorique analytique détaillé a été défini dans le chapitre 2. Ce formalisme est associé à une architecture particulière de panneau réflecteur (cellules chargés par un élément réactif à l'arrière du panneau). Grâce à ce formalisme, nous avons démontré théoriquement que les excitations des cellules dépendent des ondes incidentes couplées b_0, de la matrice de couplage [S], de la loi de phase à réaliser et d'une constante de phase 'C'. Même si ce résultat est relativement évident d'un point de vue physique, il faut noter que les couplages affectent les amplitudes et les phases des excitations des cellules et non uniquement leurs phases, contrairement à l'approximation rencontrée usuellement dans la littérature.

Le solveur analytique développé est divisé en deux modules séparés. Le premier permet l'analyse et la caractérisation du panneau du RA. L'objectif est de construire une base de données utilisée par le deuxième module pour synthétiser d'une façon rapide un objectif de rayonnement. À la fin de cette phase d'analyse, quatre paramètres sont calculés:

- la matrice de couplage [S],
- le diagramme actif $F(\theta,\phi)$,
- les ondes incidents couplées $b_{0,}$
- le champ diffracté (spéculaire).

Le deuxième module porte sur la synthèse des charges réactives qui assure la bonne distribution de déphasage (loi de phase) nécessaire à la formation du diagramme de rayonnement. Nous utilisons la base de données comme entrée et nous définissons différentes directions de pointage comme objectifs de rayonnement. Ce solveur analytique nous permet d'effectuer les tâches suivantes :

- Synthétiser une distribution des déphasages,
- Calculer le diagramme de rayonnement de l'antenne,
- Effectuer une étude paramétrique afin d'optimiser les résultats (comme la constante de phase),

- étudier l'effet de la quantification.

Ce solveur analytique est capable d'interagir avec les modules d'optimisation de Matlab afin d'utiliser différents moteurs de synthèse (MinMax, Algorithme Génétique, Moindres Carrés …).

Après validation du solveur, les études menées nous ont montré que les cellules du RA sont soumises à l'influence des couplages mutuels comme les réseaux classiques. Par contre, contrairement au réseau classique, les cellules ne souffrent pas du problème du 'TOS actif'. Il apparaît donc que le RA peut être une solution plus favorable que les réseaux, surtout si un objectif d'agilité est recherché.

Cette thèse a montré que les contributions énergétiques des cellules sont liées aux paramètres suivants :

1. les ondes incidentes couplées,
2. la matrice de couplage [S],
3. la loi de phase (distribution des déphasages) liée à l'objectif de rayonnement,
4. la constante de phase 'C'.

L'importance d'un offset de phase 'C' appliqué aux phases des excitations $a_{m,n}$ des cellules a aussi été détaillée. Celui-ci affecte la directivité en modifiant la sommation du champ re-rayonné par le réseau avec le champ diffracté. Il s'agit donc d'un degré de liberté non négligeable.

Dans la dernière partie de la thèse, une étude sur les effets de la quantification a été faite de façon à évaluer le compromis entre complexité des déphaseurs et la dégradation due à à la discrétisation des phases. Les pertes sont estimés à 3-4 dB quand le niveau de la quantification est égal à 1 (1 bit /2 états de phases), et sont estimés à 0.7 dB quand le niveau de la quantification est égal à 2. Les pertes de quantification sont négligeables avec un niveau supérieur.

Toutes ces conclusions et ces études doivent se rapporter à l'exactitude et la validité de du solveur analytique. En effet, celui-ci donne des résultats précis si on lui fournit des données en entrée exactes. Il interagit avec une base de données, dont les caractéristiques sont alors primordiales pour obtenir un résultat fiable. Ceci implique un travail sur cette base de données pour obtenir un compromis fiable entre temps de calcul et précision. Aujourd'hui, nous avons opté pour la rigueur au détriment du temps de calcul, bien que ce dernier reste raisonnable. Ce point particulier sera abordé dans les perspectives. Celles-ci sont orientées

vers un **support de recherche expérimentale**. Le laboratoire XLIM-OSA souhaite développer et réaliser un prototype de reflectarray agile. Pour mettre au point ce prototype, le laboratoire met en place un banc de caractérisation et de conception permettant :

1. L'obtention des caractéristiques EM des cellules du panneau le plus fidèlement possible,
2. Le pilotage des ports des cellules conformément au calcul issu de la synthèse,
3. La mesure des performances EM (rayonnement) correspondant aux états pilotés.

Ces différentes étapes seront accomplies grâce à un banc de pilotage dédié aux antennes à multiéléments rayonnants. Il est composé de plusieurs équipements capables de fournir les caractéristiques citées précédemment. Ce banc est relié au solveur analytique et utilise une base compacte. Cette procédure est automatisée pour accélérer l'analyse et la synthèse du reflectarray. Un synoptique est donné sur la Figure 7.

Ces différents éléments et fonctionnalités sont chainés suivant le schéma ci-dessous. L'un des objectifs est de disposer de la **configuration la plus polyvalente possible** pour s'adapter aux différents besoins et technologies :

- La matrice S est mesurée par un arrangement particulier de multiplexeurs RF. Leur nombre est extensible pour s'adapter aux nombres des cellules du panneau.
- Les alimentations DC couvrent l'intervalle -/+ 60V. Celles-ci permettent de piloter des architectures différentes de cellules agiles (à base de MEMS, diodes PIN, varactors,…).
- Un processus de diagnostic sera possible grâce au couplage entre le système d'acquisition et le solveur analytique. Un asservissement des états de phase par rapport aux consignes sera donc accessible.

Cette chaîne permettra de capitaliser le travail accompli au cours de cette thèse, afin de concevoir avec plus de précision des reflectarrays agiles, de détailler leurs propriétés physiques et d'inclure des contraintes technologiques (modèles de déphasage issues des mesures, états quantifiés, ...).

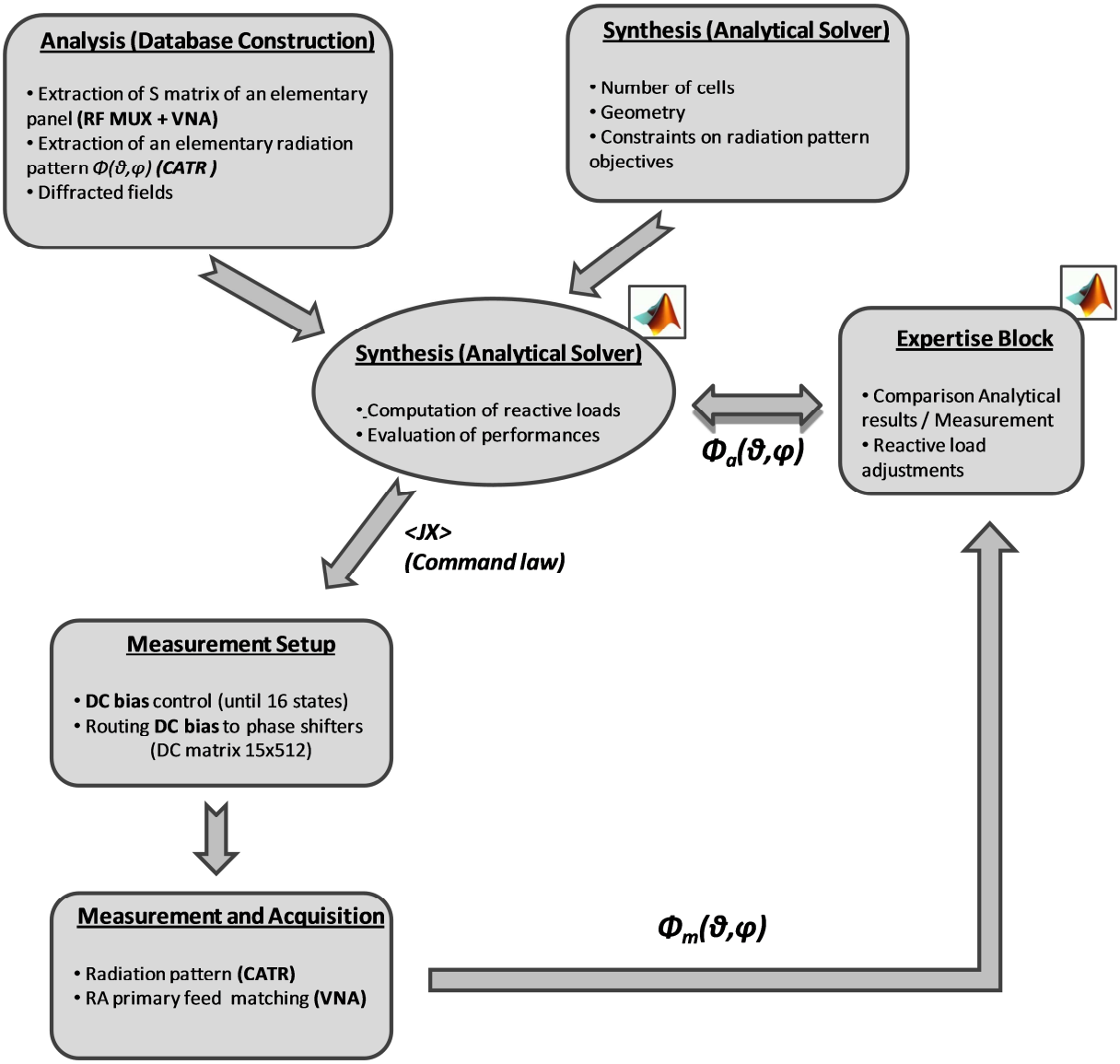

Figure 7. *Synoptique du banc de mesure et de son interfaçage avec le solveur analytique*

Acknowledgements

This thesis was carried out in the XLIM laboratory of Limoges, OSA department (Waves and Associated Systems).

I would like to thank Mr. Thierry Monediere, Professor at the University of Limoges and the head of department of OSA, for welcoming me in his team and providing the framework of my work. Many Thanks and Appreciations.

My sincere thanks to Mr. Marc Thevenot, CNRS researcher, for supervising this thesis. His enthusiasm and support have contributed greatly in my research. I am pleased to have the opportunity to work with him in the last three years, his knowledge and advices were invaluable to the completion of this work. At the same time I also appreciate the confidence and the autonomy that he granted me, much appreciated.

I express my deep gratitude to Mr. Cyrille Menudier, Associate Professor, for supervising this thesis and for participating to this Jury. His advices contributed greatly in the advance of my thesis.

I would like also to thank the former head of department of the OSA Pr. Bernard Jecko.

I express my gratitude to Mr. Bernard Jarry, Professor at the University of Limoges, who has accepted to be the president of this Jury.

I sincerely thank Mr. Raphael Gillard, Professor at the University of Rennes, and Hervé Aubert, Professor at the INP-ENSEEIHT Engineering School of Toulouse, for accepting to be part of the Jury and to perform the reporters task.

I would like also to thank Mr. Hervé Legay, Antenna Engineer at the Thales Alenia Space in Toulouse, and Mr. Palacin Baptiste, Antenna Engineer at the French space Agency (CNES) antenna service, for doing me the honor in being part of this Jury.

A big thanks to M. Patricia Leroy, Secretary of the OSA department for her hard work and availability.

Finally I would like to thank my fellow OSA colleagues. They are too numerous to count. However I can mention M. S. Toubet and J. Chabane for sharing the office with me and the former members A. S. Ahmed and M. Koubeissi for their precious advices. I wish good luck for the new comer Hussein Abou TAAM.

TABLE OF CONTENT

CHAPTER II

CHAPTER III

CHAPTER IV

Microstrip reflectarray antennas have raised significant interest in the last years because a wide range of applications with passive and active design has been demonstrated. These antennas combine the simplicity and high performances of the reflector antennas with the capability of array antennas in controlling the shape and/or scan angle of the radiation patterns. The spatial feeding reduces the losses and eliminates the complexity of the feeding network used in planar array antennas, thus minimizing insertion losses and providing higher gains. However, the main challenge faced by engineers in designing these antennas is to provide an efficient modeling, where accurate simulation results should be considered before proceeding to the manufacturing process. Relying only on the geometrical optic theory (GO) might lead to inaccurate conclusions since it does not take into account the local interactions between the incident electromagnetic field coming from the feed antenna and the reflectarray cells. In fact, a significant error on the phase shifts applied to each element might occur and the resulting scattered field is altered, leading to a lack of performances compared to the objective radiation patterns.

Some significant advances are made on reflectarray modeling to analyze their final electromagnetic performances; however some interesting behaviors are not well detailed. It is well known by the community that the performances of phased arrays are affected by the mutual coupling in many aspects. The resemblance between the array antenna and the reflectarray is evident. It is our goal to show this connection by studying the effects of the mutual couplings on the EM behavior of the panel. Therefore, we will propose a specific architecture to design the reflectarray antenna and the corresponding analysis and synthesis technique. Our focus is on an accurate coupling modeling impact rather than computation time or specific reflectarray cell's design.

By using a specific synthesis procedure, we will demonstrate that the couplings impact both the phases and the amplitude of the excitation weightings of the reflectarray cells, whereas the classical assumption is to consider that their amplitudes are only proportional to the primary feed illumination. In order to demonstrate these effects, the study is based on a reflectarray panel of identical cells connected to the reactive loads, acting as phase shifting elements. These loads are located at the rear of the panel, in order to minimize the interactions between the radiating elements and the loads. Moreover, a significant advantage of this architecture is to separate the study in an electromagnetic problem (for the radiating elements) and a circuit formalism (for the loads). Both domains are linked through electromagnetic ports interfaces, used to solve the problem with a great accuracy, especially in terms of energy

balance. From a designer's point of view, such an architecture is interesting because the loads can be directly soldered on a printed circuit board (PCB), linked to the radiating elements with via holes. The PCB can also be used to add drivers, distribute DC bias and circuits in the case of a reconfigurable reflectarray. As this architecture is suitable to demonstrate the couplings effects and to realize a prototype in a future issue, we have focused our studies on a layout with identical periodic cells.

Another important motivation for this thesis concerns the field of applications of tunable reflectarrays. In fact, RAs are most often restricted to high cost applications, where they are dedicated to replace large arrays or reflectors. In such cases, reflectarrays contain several thousands of cells and, in reconfigurable scenarios; it requires a high number of controls, drastically increasing the final cost. On the particular point of modeling, local periodicity approach is often used and, even if it implies approximations (identical cells and coupling states) the performances achieved can be sufficient.

However, if someone wants to design a reflectarray with a moderate size, e.g. for terrestrial applications, it will suffer from a degradation of performances if couplings are considered identical. In our case, we want to demonstrate that efficient designs can be made if suitable formalism is used, whatever the electromagnetic size of the problem.

This manuscript is divided into four chapters:

In Chapter one, I present a detailed literature review of reflectarray antennas. It contains the developments history of this antenna since the day of its invention. And by doing that we shall recognize the major researchers and laboratories and the wide application domain of the reflectarray. Of course, due to the many features that reflectarrays share with phased arrays and reflectors, a comparison was being presented along the different application domains, in term of performances, feasibility and cost. Finally I present the state of art of the analysis techniques which will help me define the objective of this thesis.

In chapter Two, I will present the analysis and synthesis tool to analyze and synthesis a reflectarray antenna. This tool which was developed during the thesis is based on the approach of adding EM ports at the cells in order to traduce their EM behaviors. It also combines several separated modules to study in details all the EM properties of the RA.

In Chapter Three, I present a small-sized reflectarray test case designed and simulated inside CST MWS. The reflectarray panel to be studied is made from a couple of hundred of square microstrip patches. Thanks to full-wave simulations, the antenna will be studied and synthesized inside the analytical formalism. The presented results will provide a good idea on

the accuracy of the proposed architecture as well the analytical solver that synthesizes the required phase shift distribution.

In Chapter Four, I focus on a particular behavior of the reflectarray panel which is the mutual couplings between the reflectarray cells. Held responsible of some lack of performances, the interactions between the radiating elements affects the energetic contribution of the cells which is considered equal to the illumination law in magnitude. This phenomenon will be detailed as well as some technological constraints like the quantization effects.

Chapter 1

LITERATURE REVIEW

I - Introduction

Most of RF, microwave applications and long distance space communications require high gain antennas that can compensate the attenuation losses due to the propagation of the electromagnetic waves in space. For some other applications, such as radar communications for civil or military purposes, a highly directive scan beam to certain angle is required. To achieve this high directivity, a progressive phase shift on the aperture is required. Traditionally, high-gain applications have relied upon parabolic reflectors and array antennas [1].

However, the fixed parabolic reflector in many cases, due to its specifically curved surface, is difficult to manufacture, in particularly at higher microwave frequencies. It also lacks the ability to achieve wide angle electronic beam scanning. On the other hand, the high gain array antenna, when equipped with controllable phase shifters, can achieve wide angle beam scanning electronically, but generally becomes very expensive due to its complicated beamformer and many high cost amplifier modules. The amplifier modules must be used to alleviate the problem associated with the power inefficiency that occurs in the high loss distribution circuits. As a result, a new type of antenna emerged to combine the best features of reflector antennas and phased array antennas and to overcome their disadvantages. This antenna is named the “reflectarray”.

This chapter presents an overview on the past state and current state of reflectarrays and their applications. First, it provides the reader with the necessary background on reflector antennas and array antennas. The purpose is not to deviate from the objective of the thesis, but to explain in few pages the features that reflectors and arrays share with reflectarrays. The chapter then gives a detailed script on the history of reflectarray antennas, the major actors working on this type of antennas and the international organizations that are funding their researches such as the European Space agency (ESA). Those topics are followed by the recent developments on the reflectarray, and I mention their applications. The last part of the chapter presents a brief overview of analysis and synthesis methods for reflectarrays.

II - Reflector antennas

Reflector antennas have been in use since the discovery of electromagnetic waves propagation in 1888 by Hertz who designed and built the first parabolic cylinder reflector [2]. However, the fine art of analyzing and designing reflectors of many various geometrical shapes did not forge ahead until the days of World War II, when numerous radar applications evolved such as radio-astronomy, space tracking and communications. Although reflector antennas can take various geometrical configurations (corner, cylindrical, paraboloidal...), as seen in Fig .I.1. The most popular shape is the paraboloid because of its excellent ability to produce a high gain with low side lobes and good cross-polarization characteristics in the radiation pattern [3]. This antenna benefits from its curved-parabolic geometry to create a uniform phase and uniform amplitude radiating aperture. It allows focusing the beam when the reflector is illuminated by a feed antenna.

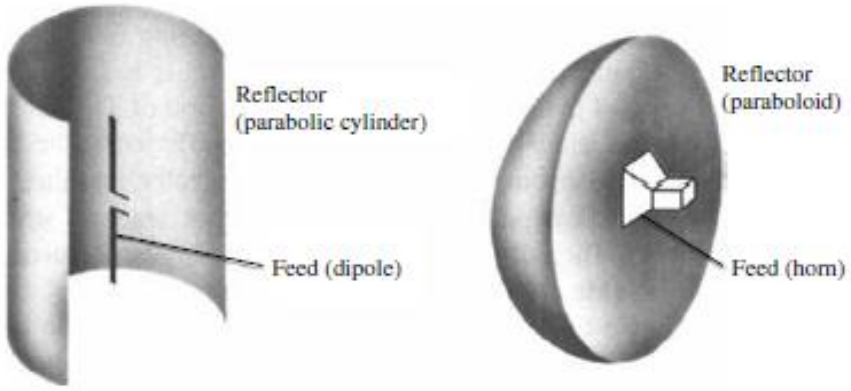

Figure. I.1. *(left) Hertz's cylindrical reflector, (right) paraboloidal reflector*

II.1 - Parabolic reflector antennas

The paraboloid reflector principle is simple. It has been shown by geometrical optics (GO) that if a beam of parallel rays is incident upon a reflector whose geometrical shape is a parabola, the radiation will converge at a spot which is known as the *focal point* F_0. In the same manner, if a point source is placed at the *focal point*, the rays reflected by a parabolic reflector will emerge as a parallel beam [4]. Therefore by matching the *phase center* of the feed antenna with the *focal point* F_0 of the parabolic reflector, the rays radiated by the reflector antenna will emerge as a plane wave belonging to the same plane called the *aperture plane* as illustrated in Fig .I.2.

The *phase center* of the feed antenna is the point from which the electromagnetic radiation spreads spherically outward, with the phase of the signal being equal at any point on the sphere [5,6]. The distribution of the electromagnetic fields in the aperture plane shows a circular spot with equiphase and non-equiamplitude fields.

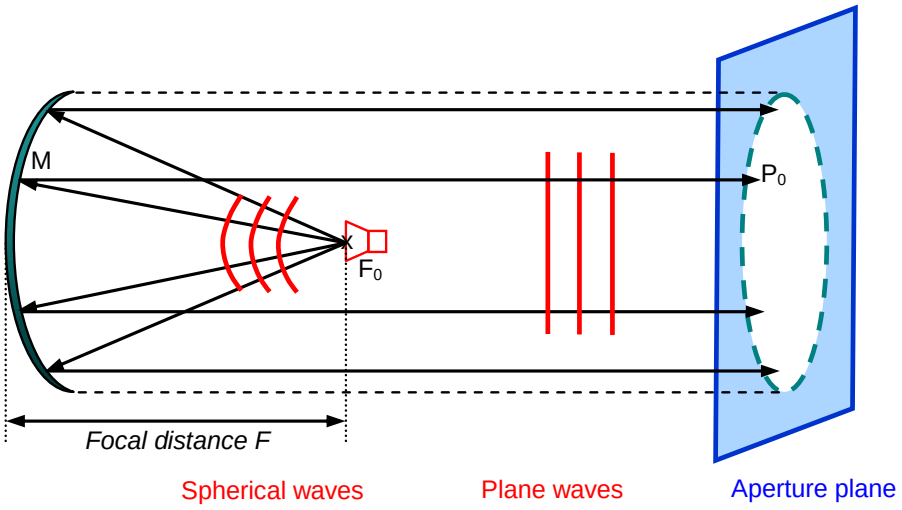

Figure. I.2. *Principle of a parabolic reflector*

Among the different possible configurations for a parabolic antenna [7] we can note the following main categories. For a single reflector design, designated **prime focus**, two geometric configurations are possible. The first one is when the feed antenna illuminates the reflector's center and in this case the reflector is **axial** or **front fed**. The second one is when the feed illuminates an asymmetrical segment of the reflector, and in this case, the reflector is **offset-fed** [8]. The second type is mostly used because the feed and its support do not block a portion of the beam.

Space communication applications often require a high focal length to diameter ratio, i.e. F/D (>1.5) to minimize the phase aberrations that can damage the performances of a mutli-spot antenna [9]. D**ual-reflector** systems satisfy this requirement while keeping the antenna compact and small to be deployed on a satellite. In dual-reflector systems a secondary sub-reflector is placed in front of the main parabolic reflector [10]. Its focal collocates with the focal of the main reflector. In conventional architectures the configuration is called **cassegrain** when the sub-reflector is hyperbolic (convex) and placed behind the focal of the main reflector. The configuration is called **Gregorian** when the sub-reflector is an ellipsoid (concave) placed after the focus of the main reflector. Another substantial advantage of dual-reflector configurations is the possibility to optimize the directivity and the cross-polarization [11].

For some other applications such space telecommunications, shaping the reflector antenna can provide higher performance in terms of total efficiency by lowering the cross-polar radiation [12], or to achieve a specific contour beam coverage for the radiated pattern [13,14] .

II.2 - Performances of a parabolic reflector antenna

Let us consider in this section a prime focus parabolic reflector. A directive feed antenna is placed at the focal point F_0 of a parabolic reflector. The feed antenna emits spherical rays that will be diffracted by the metallic conductive materiel of the reflector (point M_i) to plane waves radiating towards the aperture plane. The travelled path P_i corresponding to a diffracted ray R_i is constant according to Eq.I.1. The ray phases are given in Eq.I.2.

(I.1). $$\overrightarrow{P_i} = \overrightarrow{F_0M_i} + \overrightarrow{M_iP_0} = 2F + M_iP_0 = cst$$

(I.2). $$\angle R_i = -\vec{k}.\overrightarrow{P_i} = -\beta \times P_i = -\frac{2\pi f}{c} \times (2F + F_0P_0)$$

Theoretically, we conclude from (1) and (2) that the bandwidth of a parabolic reflector is infinite, since the path vectors $\overrightarrow{P_i}$ for the different rays are constant and independent from the frequency. The phases of the electromagnetic waves are equal in the aperture plane at any given frequency. Practically, this is not true since, feed antennas, such as standard gain horns, have their own resonance frequency and an unstable phase center over a large bandwidth [15]. In other terms, if the feed antenna is broadband and its phase center is stable versus the frequency, the diffracted rays will always be equiphase in the aperture plane forming a directive beam. The phase errors caused by the misplacement of the feed phase center are called *phase aberrations*. The performances of the parabolic antenna depend also from other numerous parameters. We can mention the feed's *radiation efficiency* which is around 80% for a standard gain horn [16], the *illumination efficiency* and *spillover efficiency* on the aperture, *polarization efficiency* and the *F/D ratio*.

Nowadays, paraboloidal (parabolic) reflector antennas remain the most widely used large aperture ground-based antennas. At the time of its construction in the 70's, the world's largest fully steerable reflector was the 100-m diameter radio telescope of the Max Planck Institute for Radioastronomy at Effelsberg [17], while the largest in the United States was the 64-m diameter reflector at Goldstone, California built primarily for deep-space applications [18] as seen in Fig .I.3.

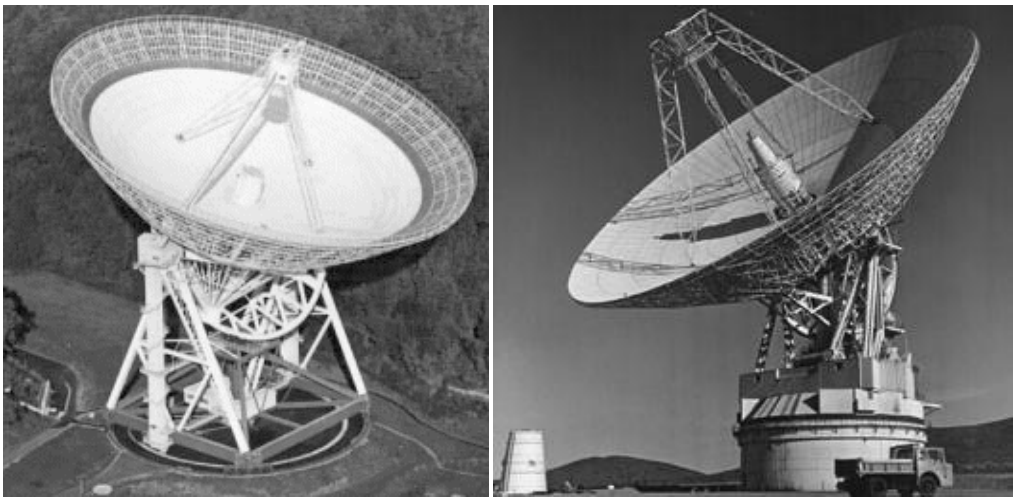

Figure. I.3. *(left) Max Planck Institute radio telescope, (right) 64-m diameter Goldstone reflector for deep space applications*

For 29 years the Effelsberg Radio Telescope remained the largest fully steerable radio telescope on Earth. In 2000, it was surpassed by the Robert C. Byrd Green Bank Telescope *(GBT)* in Green Bank, West Virginia with an elliptical 100 by 110-metre aperture [19]. The GBT is the world's largest fully steerable radio telescope nowadays with a gain of 80 dB at 10 GHz. The telescope operates at prime focus in the 290-1200 MHz frequency range and at Gregorian focus in the 1.15 GHz to 100 GHz range. The ***beam steering*** is done mechanically thanks to eight 40 hp motors. The azimuth tracking has a range of 270° and has a maximum rate of 40° per minute. The elevation tracking is between 5° and 95° with a maximum speed of 20° per minute. The telescope was available on August 25 2000, after nearly 10 years of construction as seen in Fig .I.4.

Figure. I.4. *Green Bank Telescope (GBT)*

III - Antenna Arrays

Although there are several families of antenna arrays, **phased array** is the one concerned when arrays are compared to reflectarrays. The reason is that reflectarrays use phase shifters behind the elements to shape a highly directive beam similarly to phased arrays. Basically, the phased array antenna is composed of groups of radiating elements which are distributed and oriented in a linear or two-dimensional spatial configuration. The phase excitations of each element can be individually controlled to form a radiated beam of any desired shape in space [4,20,21]. The radiated beam is determined by the vectoral addition of the electromagnetic fields radiated by the individual elements. It can vary from a directive pencil beam to a fan (shaped) beam depending on the application. The position of the beam in space is controlled electronically by adjusting the phase of the excitation signals at the individual elements. Hence, beam scanning is accomplished while the antenna aperture remains fixed in space without the involvement of mechanical motion in the scanning process. In other words, this is scanning without inertia. In most cases, the elements of an array are identical. But this is not necessary, elements can vary in form and shape but it will make the analysis and synthesis process more complicated.

III.1 - Basic concept of phased arrays

Phased arrays are composed from radiating elements, phase shifters and attenuators. The easiest way to begin with is a linear array made from N elements equally spaced along a line. To simplify even more the study we consider that the elementary radiation pattern is isotropic and the elements are excited with the same amplitude but with a progressive controllable phase shift $\Delta_{\emptyset}$ as illustrated in Fig .I.5. In order to focus the beam in a direction θ_0, the different radiated patterns must have the same phase so they add in a constructive manner. Since the isotropic element means that its radiation is the same in every direction, we know that the far-field radiation from such an isotropic element can be expressed as $\mathrm{E}_0(\theta, \varphi) = \frac{e^{-jkr}}{4\pi r}$.

For a given point in the space M, the total far-field radiation is given in Eq.I.3.

(I.3). $$E_{tot}(\theta, \varphi) = \sum_{i=1}^{N} E_i(\theta, \varphi) \times J_i = \frac{e^{-jkr}}{4\pi r} \sum_{i=1}^{N} A_i e^{j\, i * \Delta_{\phi}} = E_0(\theta, \varphi) \times AF$$

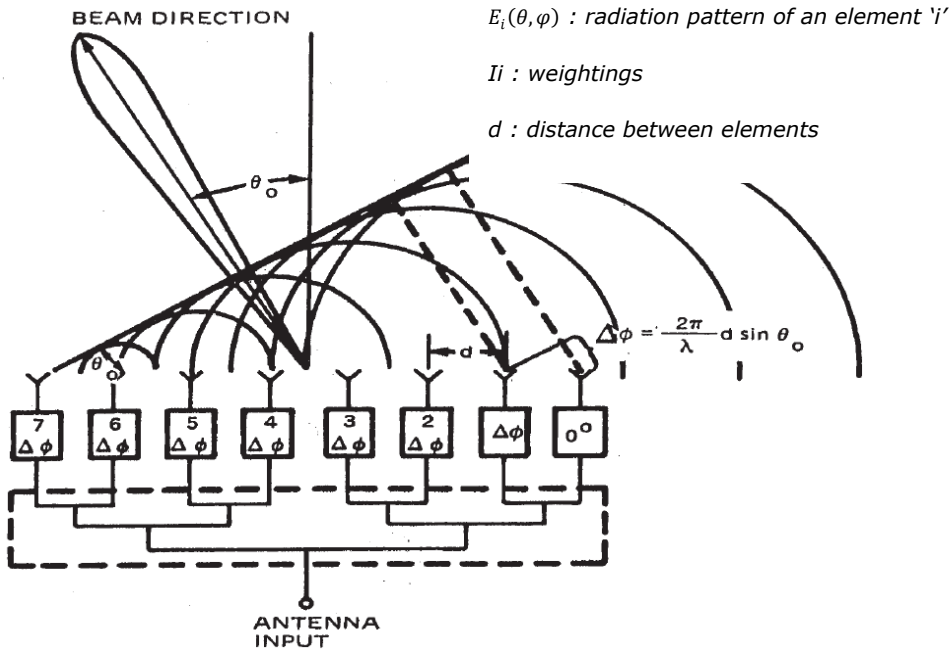

Figure. I.5. *Beam steering principle using phase shifters at each radiating element*

The second factor in Eq.I.3 is called the isotropic array factor. It contains the amplitude A_i and the relative phasing Δ_ϕ of an element 'i'. In our case we have chosen to apply the same amplitude on the elements. This array is referred to *uniform array*. The normalized array factor can be written in Eq.I.4.

$$AF = \frac{1}{N}\frac{\sin\left(N\Psi/2\right)}{\sin\left(\Psi/2\right)} \qquad (I.4).$$

Where $\Psi = \left(\beta d \sin\theta + \Delta_\phi\right)$, is the radiated fields phase difference between two adjacent elements and the first element is chosen as the reference antenna. The radiation pattern is maximum in the direction θ when $\Psi = 0$ as seen in Eq.I.5:

$$\begin{cases} \Delta_\phi = -\beta d \sin(\theta) \\ or \\ \theta = -\sin^{-1}\left(\frac{\lambda\Delta_\phi}{2\pi d}\right) \end{cases} \qquad (I.5).$$

We can scan the beam by changing the phase Δ_ϕ or the wavelength. This is the principle of a phase/frequency scanned array. The phase change is accomplished electronically by the use of ferrite (sensitive to magnetic field) or diode (sensitive to bias voltage) phase shifters. Switched transmission lines are also commonly used. Controlling the beam is one of the most appealing features of arrays. This approach permits beams to be moved from point to point in space in just microseconds, whereas mechanical scanning of a large antenna could take several seconds or longer. Phased antenna arrays (1D and 2D) are widely used, especially for military applications.

III.2 - Multi-beam arrays

Multiple simultaneous beams exist when an array of N elements is connected to a beamformer with M beam ports, where N and M may be different. The amplitude and phase excitation of each element for a defined beam direction are generated at the output of the beam former. Multiple beamformers are either networks (Butler Matrix [22], Blass Matrix [23]) or quasi-optical lenses (Rotman lenses [24]). It is usual to call either type a **beamforming network** (BFN). In general, with a BFN, beam crossover levels are independent of frequency, while beamwidths and beam angles change with frequency. With a lens BFN, beam angles are fixed, while beamwidths, hence crossover levels, change with frequency [25]. For higher frequency band solutions based on waveguide technology were introduced [26] as illustrated in Fig .I.6. Beamforming networks are dominated by their complexity when the array is bigger or the number of beams is higher, and by the loss power introduced in the beam forming network [27,28].

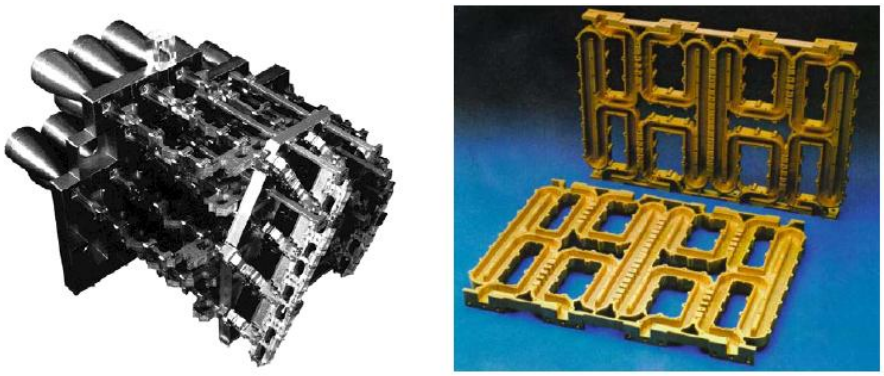

Figure. I.6. *BFN examples, wave guide technology and butler matrix*

During his thesis at XLIM OSA, A.S. Ahmed showed that the gain loss tends to grow exponentially with the number of couplers added to the design and that it is very difficult to surpass a gain of 27dB when the array is fed with a BFN [28].

III.3 - Electronically scanned array

We can find two types of electrically scanned arrays: passive and active. **Passive Electronically Scanned Array** (PESA) have a central transmitter and receiver, with phase shifters located at each radiating element or subarray [29]. The central source is a high-power

RF generator that includes traveling wave tube (TWT), magnetrons, or solid state transmitter (SST) components. **Active Electronically Scanned Array** (AESA) [30] use Transmit/Receive (T/R) modules to provide the last stage of amplification for transmitted signals, the first stage of amplification for receive signals, and provide both amplitude and phase control at each radiating element . The use of T/R modules in active arrays provides the advantages of amplitude control, low loss, and graceful degradation over passive arrays.

In an AESA configuration, T/R components are usually located in hermetically sealed T/R modules, as seen in Fig .I.7. RF losses in AESA configurations are smaller than PESA configurations due to the close proximity of the T/R modules to the radiators. However, the requirement of having a discrete T/R module at each radiator site is **costly**. In a PESA configuration, the T/R components may be lumped together for more cost-efficient packaging because they are remote to the radiators. However, because these devices are remote from the radiators, increased RF losses tend to lower the overall system performance.

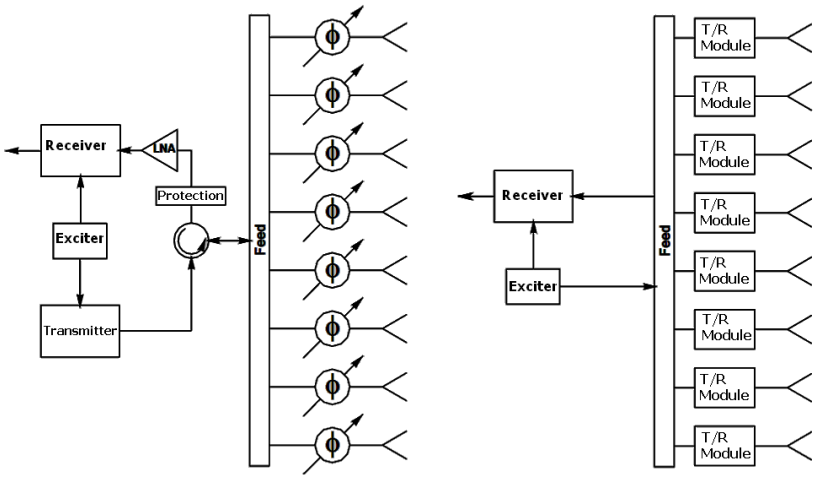

Figure. I.7. *Block diagrams of passive and active phased arrays*

To summarize, AESA provides higher performances but at higher cost. The passive array is the least expensive phased array because of its lower number and cost of components [29]. However passive array technology must be accomplished at high power to position the transmit beam. For example, the magnetron used in the **AN/SPN-43** radar [31] (Pulsed air surveillance radar installed in warships) produces 850 KW peak. High-power phase control technology is dominated by power loss concerns. Typical total losses in early systems resulted in a factor of 10 reduction in radiated power.

Most of the ground missile guided radars, such as the **AN/MPQ-53** radar installed in the **MIM-104 Patriot** designated by the **Raytheon** company [32] (Fig .I.8), or the airborne

radar systems, such as the **AN/APG-77** radar installed in the F22 raptor fighter aircraft, use Electronically Scanned Array radars. It is unlikely that any new fighter radar will be produced in the future without AESA technology.

Figure. I.8. *A closer look to the AN/MPQ-53* ***PESA*** *radar installed in the patriot systems*

In July 2004 a 90 million Euros-worth contract was signed for the development and integration of an AESA in the RBE2 of the Rafale French combat aircraft which uses PESA. It was reported that Thales will start delivering the new radar in August 2010 for use on the fourth tranche of Rafale aircraft with the first AESA-equipped squadron to become operational in 2012 [33]. The Rafale will then become the first European combat aircraft to benefit from the operational advantages of AESA radar technology as seen in Fig .I.9.

Figure. I.9. ***RBE2*** *radar installed inside the RAFALE combat aircraft*

IV - Reflectarray antennas – Early innovations and developments

To summarize the previous section, reflectors and arrays are specialized to perform in a domain but they suffer from certain disadvantages. If we are looking for a passive highly directive beam for satellite communications and large bandwidth, reflector antennas are the best in this domain. Although they are efficient radiators, due to their curved reflecting surface, they are generally bulky in size and can be difficult to deploy for space applications. In addition, the main beam of a parabolic reflector can be designed scan only a few beamwidths away from its broadside direction, unless heavy mechanical rotations and alignments devices are used to tilt in the azimuth or elevation planes. If we are looking to steer the beam and scan a volume in a matter of microseconds phased arrays come handy but at a high cost, since we either need to inject high power to encounter the high losses, or else pay for the expensive T/R amplifier modules. In the case of contoured coverage applications, shaped parabolic reflectors suffer from the manufacturing complexity and arrays suffer from the BFN complexity and losses.

In any case, it would be interesting to combine some of the attractive features of reflectors and arrays in a compact and flat low cost antenna [34]. From here came the need of **reflectarray antennas**.

A reflectarray is a class of antennas that utilizes arrays of elementary antennas as reflecting surface [35]. It has been found that a reflectarray combines the simplicity of reflector antennas with the performance and versatility of array antennas. A reflectarray is an antenna consisting of a flat or slightly curved reflecting surface containing hundreds of thousands of radiating elements. Likewise a reflector antenna, a feed antenna illuminates the reflecting surface instead of the high loss conventional beam-formers network. The elements are designed and optimized to reradiate the incident fields with proper phase shifts to form the desired pattern. Phase shifts are opted to compensate the different phases associated with the different path lengths for the incident fields.

IV.1 - Waveguide reflectarray in the 1960s

The first reflectarray was introduced by Berry, Malech and Kenedy in 1963 [35]. It was made from a primary feed antenna and an array of short-ended waveguides. The incident

coupled waves from the feed travelled long the tubes to shorted ends. The shorted ends reflected the electromagnetic waves and reradiated from the open ends.

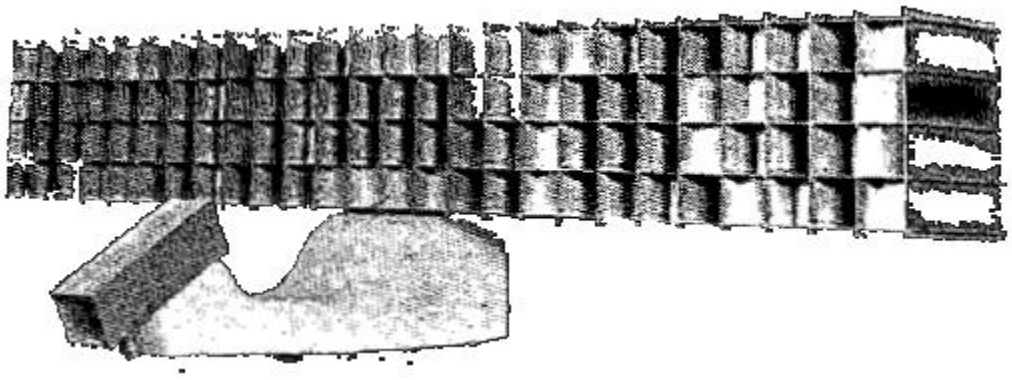

Figure. I.10. *reflectarray with open-ended waveguide array*

Berry used geometrical optics (GO) to estimate the phase of the incident fields at each open end waveguide and adjusted the length of each waveguide so the reradiated waves would form a directive beam. The use of low microwave frequencies resulted in very bulky and heavy structures as illustrated in Fig .I.10. The resulting radiation patterns were indicated on what a reflectarray would achieve, however the efficiencies were not studied or optimized.

IV.2 - Spiral reflectarray in 1977

In 1977, a very clever concept of "spiralphase" reflectarray was developed by Phelan where switching diodes, as illustrated in Fig .I.11, were used in a four-arm spiral or dipole element of a circularly polarized reflectarray to electronically scan its main beam to large angles from the broadside direction [36].

It is known that, if a circularly polarized antenna element is rotated from its original position by φ degrees, the phase of the element will be either advanced or delayed by the same φ degrees, hence, the technique of rotating circularly polarized elements to achieve the required phases for a conventional array to scan its beam has been previously demonstrated [37]. Due to the thick spiral cavity (quarter-wavelength depth) and large electronic components, the spiralphase reflectarray was still relatively bulky and heavy. Its aperture efficiency was still relatively poor. Thus, no continued development effort was followed until recently.

Figure. I.11. *4-arm spiralphase circularly polarized reflectarray with switching diodes in the center*

IV.2.1 – Recent researches on spiralphase reflectarray

In 2004, a new reflectarray antenna design based on spiralphase type elements was presented in [38]. This work was followed by a reconfigurable spiralphase type reflectarray based on ring slot resonators with switchable radial stubs [39], as seen in Fig .I.12. The antenna radiates circularly polarized focused beams in the millimeter-wave frequencies (36.5GHz). The antenna has 277elements optimized to achieve beam scanning in the elevation plane between 0° and 50°. Switching pin diodes are added behind each element to control the beam.

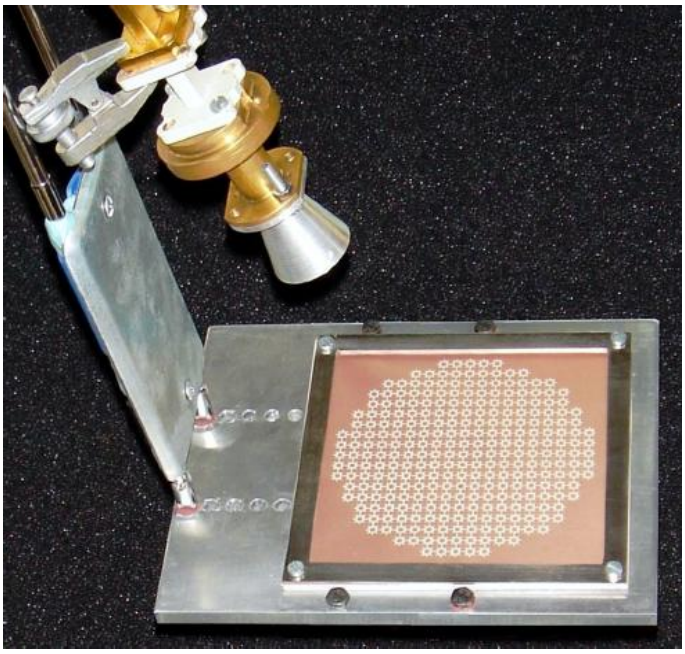

Figure. I.12. *Fabricated spiralphase-type reflectarray antenna*

Even though beam scanning capabilities were obtained, the measured aperture efficiency of the reconfigurable reflectarray is quite poor at the different scan angles (between 40% and 12% for beam angles between 0° and 50°).

IV.3 - Printed Reflectarray in the 1980-90s

Due to the invention of the low-profile microstrip antenna, various printed microstrip reflectarrays were developed in the late 80's and early 90's. The printed reflectarray antenna consists of a very thin and flat (can be slightly curved) reflecting surface and an illuminating feed, as shown in Fig .I.13. On the reflecting surface, there are many isolated elements (e.g. patches, dipoles or rings). The feed antenna illuminates these microstrip elements which are designed to scatter the incident field with phases that are required to form a planar phase front. This operation is similar in concept to the use of a parabolic reflector that naturally scatters a planar phase front when a feed is placed at its focus. For large deployable apertures, the antenna's reflecting surface, being flat, can be more easily and reliably deployed than the curved parabolic reflector. Thus the term *"flat reflector"* is sometimes used to describe the printed reflectarray [40].

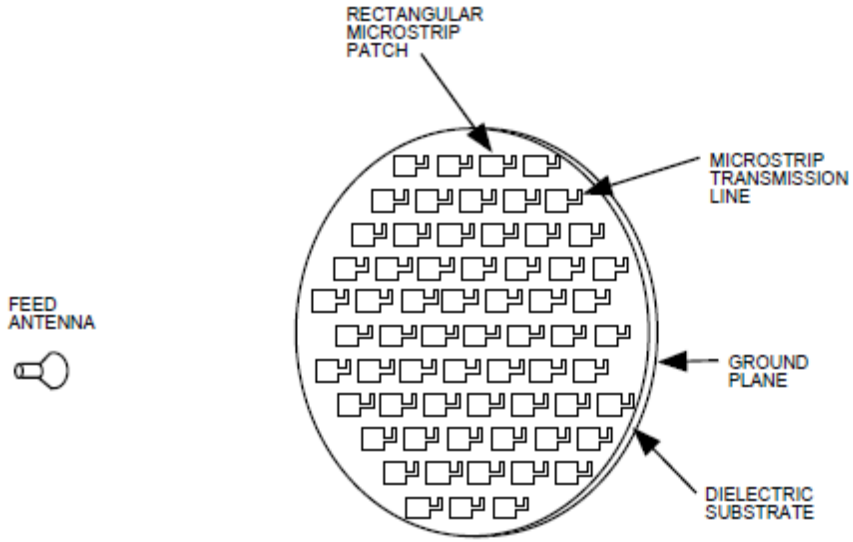

Figure. I.13. *Flat printed microstrip reflectarray*

They came in various forms, but all with flat low-profile and low-mass reflecting surfaces. Some of them used identical patch elements with different-length phase delay lines [41,42,43,44], as depicted in Fig .I.14.a. The phase delay lines, having half-wavelength long or shorter, are used to compensate the different path lengths from the illuminating feed. This

can also be accomplished by using elements made of printed dipoles with variable dipole sizes, as depicted in Fig .I.14.b. Different dipole sizes will yield different scattering impedances which then provide the different phases to compensate for the different path-length delays [45].

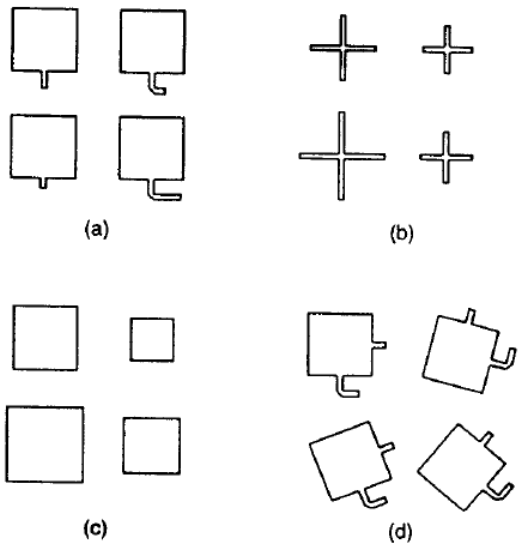

Figure. I.14. *Printed reflectarray with various elements technology. (a) Identical elements with variable length phase delay lines. (b) Variable size dipoles. (c) Variable size patch. (d) variable rotation angles*

Similarly, microstrip patches with variable patch sizes [46] were developed, as depicted in Fig .I.14.c. Printed dipole elements were also used to form a frequency scanned grating-reflector antenna [47]. Printed annular rings of variable sizes arranged in Fresnel Zone configuration were used to focus the beam [48]. Circularly polarized microstrip patches with identical size but variable angular rotations were designed to form a highly-efficient high performance reflectarray [49], as depicted in Fig .I.14.d.

V - Microstrip patch Reflectarrays

V.1 - Introduction and Developments History

The microstrip patch antenna was first introduced by Munson in a symposium paper in 1972 [50], which was followed by a journal paper in 1974 [51]. These papers discussed both the wraparound microstrip antenna and the rectangular patch. Shortly after Munson's symposium paper, Howell also discussed rectangular patch antennas in another symposium paper followed by a journal paper [52].

Microstrip patch reflectarrays belong to the family of printed microstrip reflectarrays. So, there is nothing much to add on the basic concept of the antenna. However, we can supplement that the reflecting surface consists of array microstrip patches printed on a thin-grounded dielectric substrate, as depicted in Fig .I.15.

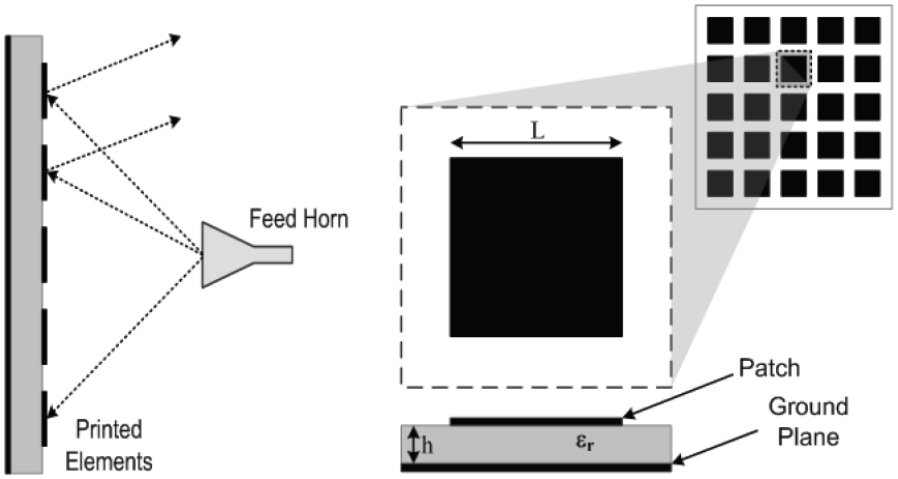

Figure. I.15. *Microstrip patch reflectarray antenna*

It is easy to track the chronology of the microstrip reflectarray antenna developments between the years **1978** and **2000**. The first mention of using microstrip elements for reflectarray was by Malagisi in **1978** [53]. During the same year, the first attempt to analyze the microstrip reflectarray element was carried out by Montgomery [54]. Montgomery's approach was based on the analysis of the scattering by an infinite periodic array of microstrip disks using a Galerkin solution of a vector integral equation [55]. In **1987**, Munson and Haddad proposed identical microstrip patches with *different microstrip transmission delay lines* to form the microstrip reflectarray antenna [41].

Their work was followed in the years **1991** and **1992**, by J. Huang, D.C. Chang and M.C Huang [56,57]. J. Huang calculated the reradiated fields from a finite array of microstrip patches connected to microstrip transmission delay lines and illuminated by a feed antenna. It included the fields pattern from the microstrip array that radiate in the desired beam direction and two specular patterns which do no radiate in the beam's direction. One is the specular reflected field from the flat ground plane and the other is the diffracted field from the edge of the ground plane. The specular fields were calculated using the Uniform Geometrical theory of Diffraction UTD [58]. Huang estimated the worst case of the specular patterns. He later admitted that further work need to be done to accurately predict the backscattered fields from thousand of non-uniformly illuminated microstrip patches with un-equal lengths of microstrip lines.

Fig .I.16 (left) shows the radiation pattern for a reflectarray having a diameter of 144 wavelengths. The main scan beam is fixed to 36° and the sidelobes were below -60dB. For the same antenna, when Huang included the backscattered the sidelobes were near -40dB which is still considered very low for many applications. Fig .I.17 shows the radiation patterns for a smaller reflectarray (diameter is 10 wavelengths). For the same given beam direction 36°, the peak sidelobe is near -30dB when the backscattered fields are not included, however the sidelobes level is near -15dB when the two specular field components are added. Huang concluded that the diffracted patterns are more than significant when a smaller reflectarray is used, and the microstrip reflectarray is more efficient when its aperture is electrically larger.

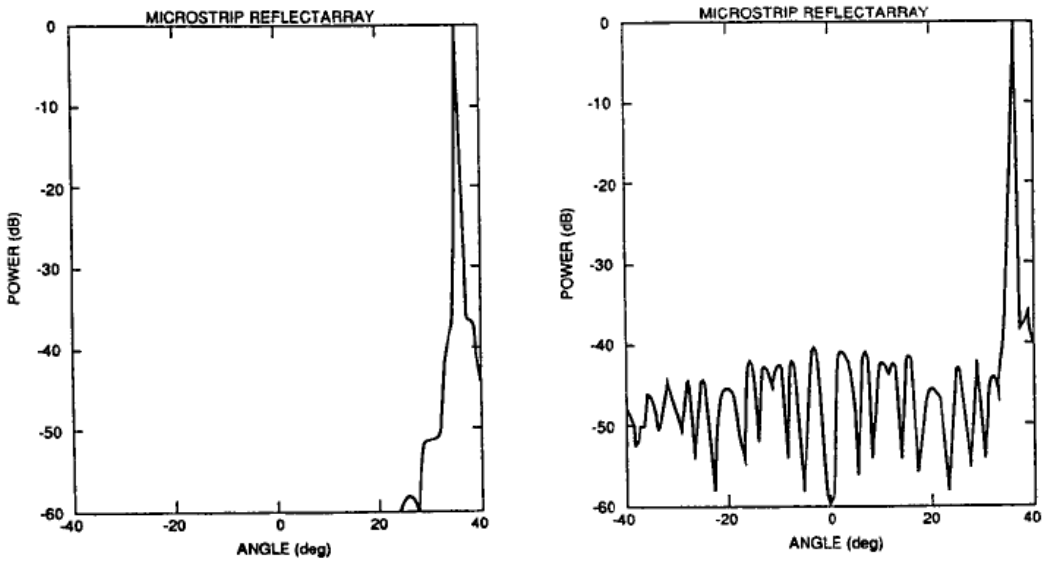

Figure. I.16. *(Left) pattern without including backscattered fields components. (right) pattern with backscattered fields included, aperture diameter =144 wavelengths [56]*

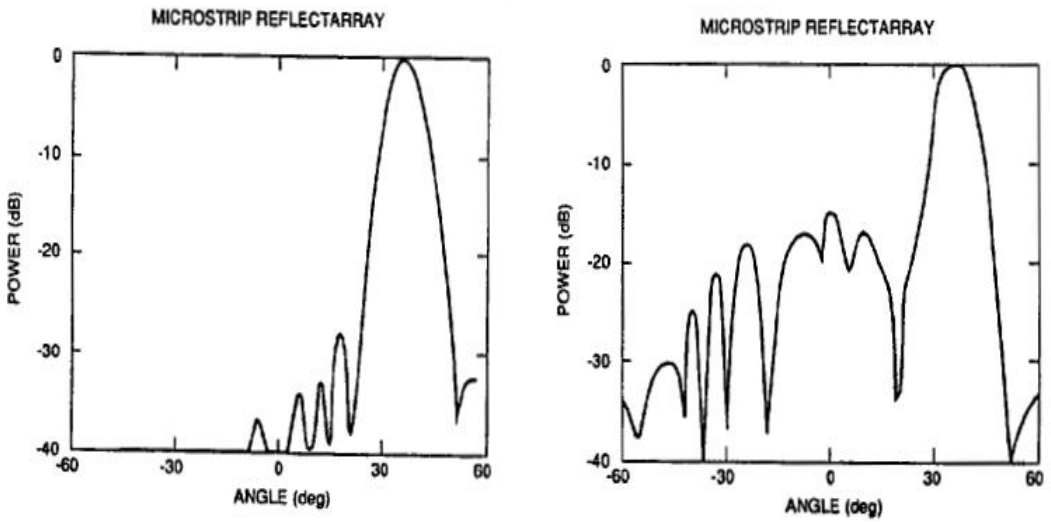

Figure. I.17. *Left) pattern without including backscattered fields components. (right) pattern with backscattered fields included, aperture diameter =10 wavelengths [56]*

In **1993-1994**, Pozar introduced the *variable-size microstrip patches* reflectarray [59,46]. Pozar changed the size of the microstrip square patches to generate the required phase shifts needed to focus the beam. In his analysis technique, Pozar calculated the phase of the reflected field from an infinite array of microstrip patches illuminated by a plane wave. He then assumed that each element in the reflectarray scatters with the same phase as the same infinite array is then invoked. The angle of the incidence wave at the cell was included as seen in Fig .I.18. Pozar gave no details of the manufactured prototype, what we knew is that the peak gain was around 27 dB and the gain bandwidth was 4.6%.

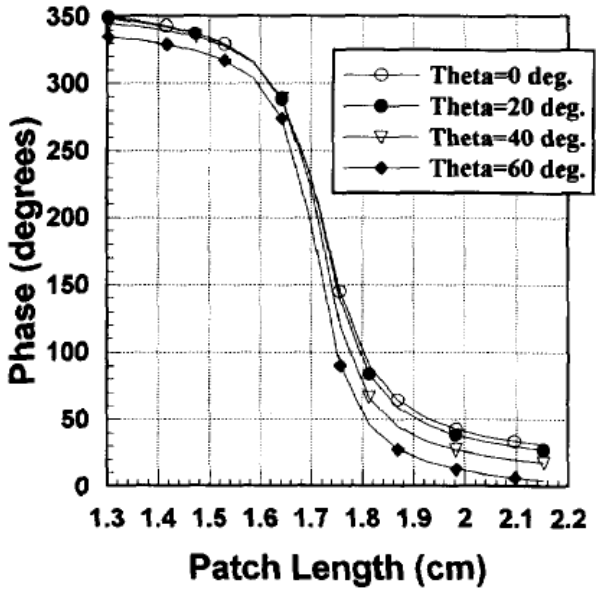

Figure. I.18. *Reflected field phase versus patch length for an infinite array of microstrip patches with plane wave incidence at various angles (taken from Pozar's paper)*

In **1994**, R.D. Javor, X.D Wu and K. Chang presented three separated papers on the same 12 elements square patch microstrip reflectarray antenna which operates at 10 GHz. The first paper demonstrated the offset feed microstrip reflectarray [60], the second demonstrated a dual-polarization microstrip reflectarray antenna [61] and the last paper was on the beam steering capabilities using a 1-bit digital phase shifter.

In **1995**, J. Huang studied the bandwidth performance of reflectarrays that use identical patches with different-length transmission delay [62] and in a second paper he presented a dual-band microstrip reflectarray for mobile communications by using two stacked arrays of stub loaded patches [63]. In his second paper, mutual couplings between the stacked patches were not included.

In **1996**, J. Encinar improved the accuracy of this work by adding the scattering matrix in the calculus of the required phase shifts of the cells. The multi-layer periodic array was analyzed in a full-wave method and the reflection phases were calculated for two different frequencies using a Generalized Scattering Matrix (GSM) computation method [64]. A 16x16 elements reflectarray was designed to radiate two focused beams using this method at the frequencies 6.5 GHz and 10.6 GHz [65].

Few years later (**2001** and **2003**), J. Encinar used the multi-layer concept to improve the bandwidth of the antenna by 10% as depicted in Fig .I.18. The bandwidth of reflectarrays can be improved if the phase's responses of the radiating cells occupy more than 360° range to counter the differential phase spatial phase delay. A two layer stacked patch structure can yield a smooth phase versus size characteristic, and more importantly, can yield phase ranges far in excess of 360° [66]. By varying the dimensions of three stacked patches, over 600° of phase range was demonstrated [67].

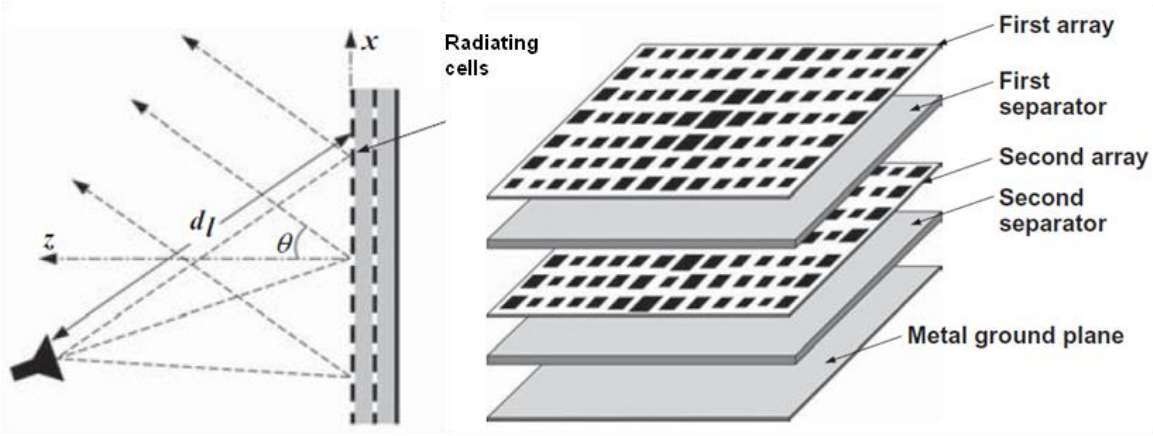

Figure. I.19. *Dual-layer stacked patches reflectarray to achieve wider bandwidth*

In **1997-1998**, J. Huang and R.J. Pogorzelski designed two circularly polarized reflectarrays in the Ka-Band [49]. One has identical square patches with variable-length phase delay lines. The other uses identical square patches and delay lines with variable element rotation angles. Although both antennas demonstrated excellent efficiencies, adequate bandwidths, and low average sidelobe and cross-polarization levels, the one with variable rotation angles achieved superior overall performance. At that time these antennas were electrically the largest microstrip reflectarrays (6924 elements with 42 dB gain) as seen in Fig .I.20.

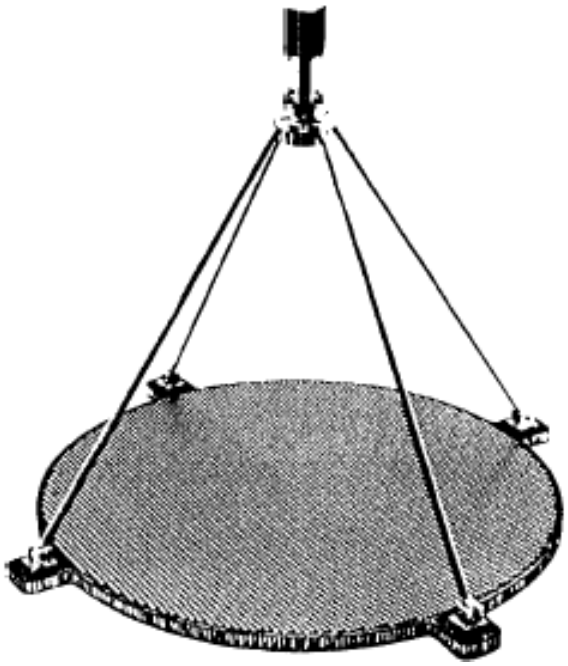

Figure. I.20. *Half meter flat microstrip reflectarray with 6924 rotating patches*

In **1999**, a worth mentioning paper presented by Pozar is a reflectarray designed to produce a shaped-beam pattern using a phase-only synthesis, as depicted in Fig .I.21. The concept was originally developed in 1994, however its publication was postponed "to protect the proprietary nature of this work" according to Pozar.

The linearly polarized reflectarray functioned at the Ku-band and provided coverage of the European continent [68]. Results validated the shaped-beam reflectarray concept, although he noticed some disadvantages to the reflectarray such as narrow bandwidth and reduced aperture efficiency that may offset the mechanical and cost advantages of the flat surface of the reflectarray.

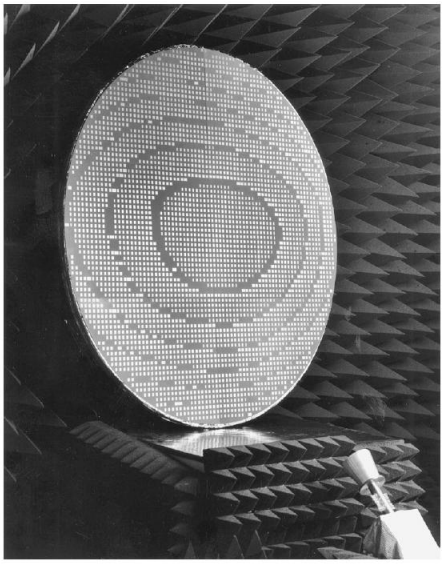

Figure. I.21. *Shaped beam reflectarray for the European coverage*

In the early 2000's, the development of the reflectarray has mushroomed and several performance improvement techniques are worth mentioning here. *Encinar* was focusing on improving the bandwidth of the reflectarray antenna by using stacked patches array. An amplifying reflectarray was developed by *Bialkowski*. The element performance was optimized by using the Genetic algorithm by *Zich*. The reflectarray using a sub-reflector and array feed configuration was also studied by *Rahmat-Samii*. The dual-band reflectarray was being studied by *Chang, Zawadzki* and *Huang*.

A good summary of recent developments can be found in [69,70].

V.2 - Advantages of microstrip reflectarrays

Good efficiency

The low-profile printed microstrip reflectarray can achieve very good efficiency (> 50%) for very large aperture. According to *Huang*, it can reach more than 66% [71]. This is because no high-loss beamforming network is needed thus very little insertion loss is encountered.

Wide-angle beam and beam scan abilities

On the other hand, very similar to an array antenna, the reflectarray can have its main beam designed to tilt at a large angle (> 50 deg) from its broadside direction, while the parabolic antenna can tilt the beam only several beamwidths without mechanical steering.

Scanning the beam is also possible thanks to controllable Pin diodes or Varactor diodes installed behind the radiating elements.

Low manufacturing cost

The reflectarray being in the form of a printed microstrip antenna can be fabricated with a simple and low-cost etching process, especially when it is produced in large quantities. The antenna also can be cost effective just because of its flat structure. For example, the special molding process that is generally required for fabricating a curved paraboloid is not needed for a flat structure. The low-profile compact form of a microstrip makes the microstrip patch reflectarray suitable for satellite communications due to its compactness, simple packaging requirements, conformal abilities, and low manufacturing cost.

Easier deployment in Satellites

Another significant advantage is that a very large aperture reflectarray could exhibits simpler and cheaper deployment in space-crafts than the reflector antennas since the flat reflectarray doesn't occupy much space and it can folded and unfolded by simple mechanism. To save even more volume in the spacecraft two configurations for the reflectarray can be opted; inflatable and folded reflectarray antennas.

Other features

Many other possible features of microstrip reflectarray antennas such synthesizing accurate contoured beams for continent communication coverage, multibeam capabilities, amplifying reflectarrays, reflectarray in cassegrain offset configurations etc … all those features are the subject of a detailed discussion in the section 6 of this chapter.

V.3 - Disadvantages of microstrip reflectarrays

Printed Microstrip reflectarray antennas are governed by their narrow bandwidth behavior. This is its inherent narrow bandwidth which generally cannot exceed 10%. This narrow band behavior is no match to that of a parabolic reflector where theoretically infinite bandwidth exists. For a microstrip patch reflectarray antenna, its bandwidth is caused by two factors [62] . One is the narrow bandwidth behavior of the radiating patches and the other is the differential spatial phase delay.

V.3.1 - Limited Bandwidth by element

The bandwidth of microstrip elements depends on the bandwidth of the radiating elements and from the phase response. For the radiating element, a microstrip patch element on a thin dielectric substrate generally has a bandwidth of about 3 to 5 percent. It can be improved if we use a thicker substrate. A second result for the narrow band of the patch is the nonlinearity of the phase response versus the frequency. Ideally a broadband element should provide smooth phase curves at different frequencies parallel to each other, independently from the incident angle. In this case, the phase distribution of the elements will vary by a constant when the frequency changes. In reality we should expect S-shaped phase curves with nonlinear behavior versus the frequency as seen in Fig .I.22.

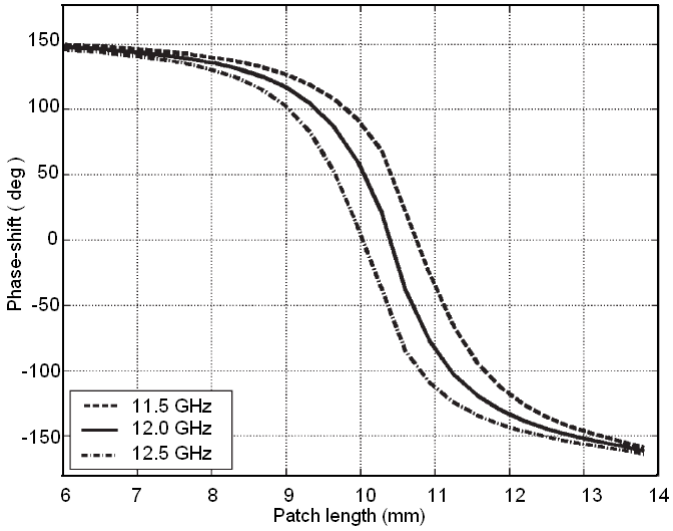

Figure. I.22. *Typical S curve phase shift of an infinite periodic array of variable size square patches for three given frequencies at normal incidence. [59]*

Broadband techniques

To achieve wider bandwidth, techniques such as stacking multiple patches [66,67], using aperture coupled patches [72] or adding slots to the patches [73] have been employed. Bandwidths of more than 15 percent have been reported by Encinar.

V.3.2 - Limited Bandwidth by differential spatial phase delay

The bandwidth limitation due to the differential spatial phase delay is easier to understand if we look at the Fig .I.23. The incident electromagnetic waves from the feed travels different paths d_i. The difference between the paths is Δ_d and it can be many multiples of the wavelengths $\Delta_d = (N + d)\lambda_0$, where N is an integer number and d $\in$ [0 1] . Solving

the phase delay caused by *d* is easy by adding phase shifters at the elements, however N is the problem since we need phase shifters that can cover phase ranges exceeding 360° by multiples times. The second issue is that the phase shifts at the elements are calculated at the center frequency f_0, as the frequency varies, the factor $(N+d)\lambda_0$ becomes$(N+d)(\lambda+\Delta_\lambda)$. Since the compensating phases are calculated at the center frequency, a frequency excursion error will occur in the reradiated phase front. The amount of phase change in each path is related to $(N+d)\Delta_\lambda$ and it can be a significant portion of a wavelength.

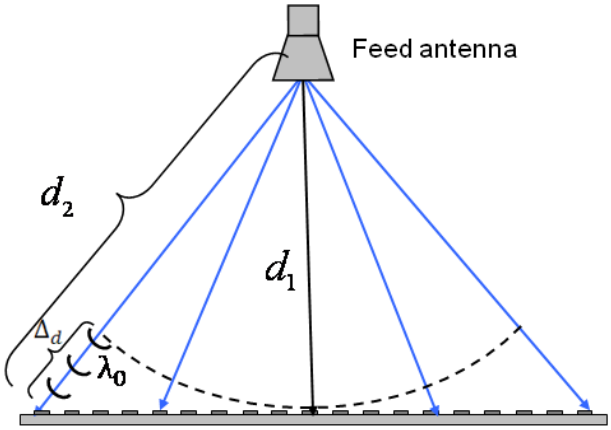

Figure. I.23. *Differential spatial phase delay of microstrip flat reflectarray*

To reduce the amount of frequency excursion error, N must be reduced. Many solutions are offered. One is to design the reflectarray with a larger focal/diameter ratio (F/D). Another solution to minimize the frequency excursion error and avoid phase shifts of multiple wave lengths is to use curved reflectarray antenna by dividing its surface into several panels and align them on a parabolic curve [74], as depicted in Fig .I.24. Another solution is to use time delay phase shifter lines [75].

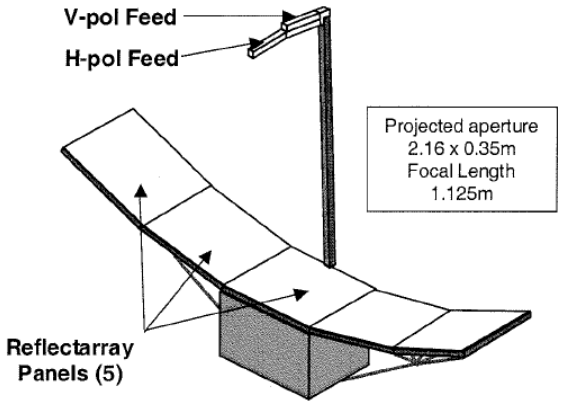

Figure. I.24. *Curved reflectarray design by [76] for space borne radar altimeter*

VI - Microstrip Reflectarray Application domains

VI.1 - Electronically Tunable Microstrip Reflectarrays

Planar reflectarrays are a very attractive solution for implementing reconfigurable, steerable or switchable-beam antennas for ground communications, space applications like Synthetic Aperture Radar [76] or space telemetry [77], and for airborne communication and Internet via satellite applications [78]. The use of tunable materials such as Pin diodes, Varactor diodes, MEMS devices or liquid crystals allows the control of the reflected field on the reflectarray surface. By introducing a phase-shift of the impinging wave at each element of the antenna, a pencil or a shaped-beam can be generated. The beam can be switched or reconfigured if this phase-shift is changed by the introduction of controllable phase-shifters.

VI.1.1 - Beam switching/Steering using Pin diodes and varactors diodes

Diodes are widely used in tunable reflectarrays due to their reliability, easy implantation, moderate congestion and fast commutation time (0.1-0.01 µs). Pin diodes offer the simplest solution to switch the beam, however it is important to optimize their implantation and minimize their consumption otherwise the efficiency of the reflectarray will be impacted.

CNES and *Thales Airborne System*s (TAS) have been working together for years on developing antennas with electronic beam scanning using **PIN diode**s for space applications such as X-band Synthetic Aperture radars on low earth orbit microsatellite [79]. For this purpose, a reflectarray was designed to function in the frequency range 8.025 and 8.4 GHz [76]. The gain of the linearly polarized antenna should be greater than 17.5dB and it should achieve a beam scan till +-63°. To satisfy these objectives, the reflectarray panel is made from 288 cells and its dimensions are 300x300x15 mm. The primary source is a pyramidal horn in an offset position. The elementary cell is based on a waveguide structure associated to a motherboard distributing DC bias and command signals to the phase shifters. The phase control is provided by 4 PIN diodes located on the printed circuit of each cell, as depicted in Fig .I.25. Therefore, the phase shifter is driven by a 2-bits command. The measured results were satisfying and further works were initiated to develop the flight model of the antenna [77].

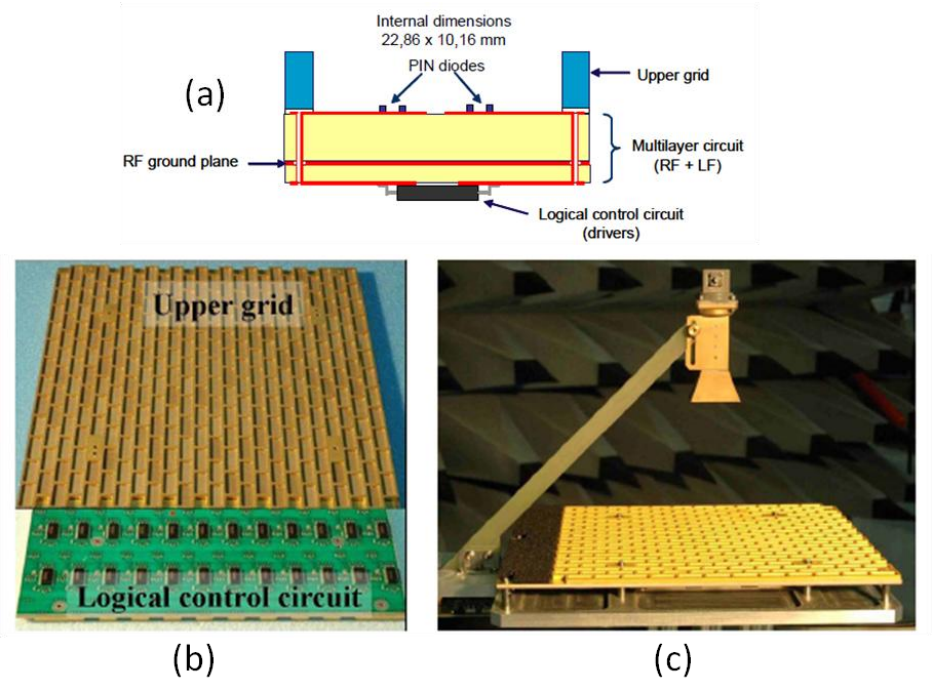

Figure. I.25. *(a) elementary cell model. (b) X-band panel. (c) Engineering model*

Another tunable reflectarray developed by the university of Mexico [80], was to use 3bit spatial phase shifters to steer the beam and radiate a circularly polarized pattern in a frequency band between 18.3 and 20.5 GHz. The idea was to connect 8 PIN diodes to each radiating ring slot resonator and use them to switch between different stubs located at different rotation angles, as seen in Fig .I.26. Only one diode is ON at a time and the other diodes are OFF. This configuration allowed switching the beam between -38° and 38° in the elevation plane while maintaining an overall good efficiency for the reflectarray antenna.

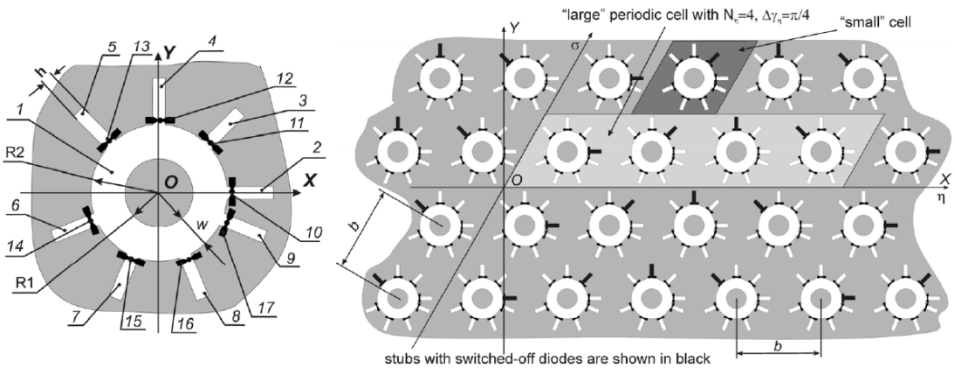

Figure. I.26. *(left) Three-bit spatial phase shifter. (right) Geometry of the reflectarray*

Another solution is to use **varactors diodes** to control the reflected phase of the radiating elements [81]. It consists of a microstrip patch antenna printed on a dielectric substrate over a ground plane and loaded by a varactor diode on one radiating edge. The

voltage controlled tuning varactor introduces at the open end of the antenna a variable capacitive reactance which modifies the resonant frequency of the antenna within a specified range [82], as demonstrated in Fig .I.27 (left). This capability is beneficial for reflectarray antennas because the small shift in the resonant frequency introduced by the tuning diodes changes the reflection phase of the single element, so allowing a dynamic phase control, as demonstrated in Fig .I.27 (right).

A recent realization by *S.V HUM* [83], has shown the possibility of using this technology to electronically tune the reflectarray. The antenna operating at the frequency 5.8 GHz is made from 70 phase shifting cells based on varactor diodes, as depicted in Fig .I.28 (left). The varactors diodes were controlled with a bias DC volt (0 to 25 V) to scan the beam between -/+50° in a 5° steps. The cross polarized pattern were 25-30 dB down the main beam. Despite these performances, 4.4 dB of power loss were consumed by the varactor diodes damaging therefore the efficiency of the reflectarray design.

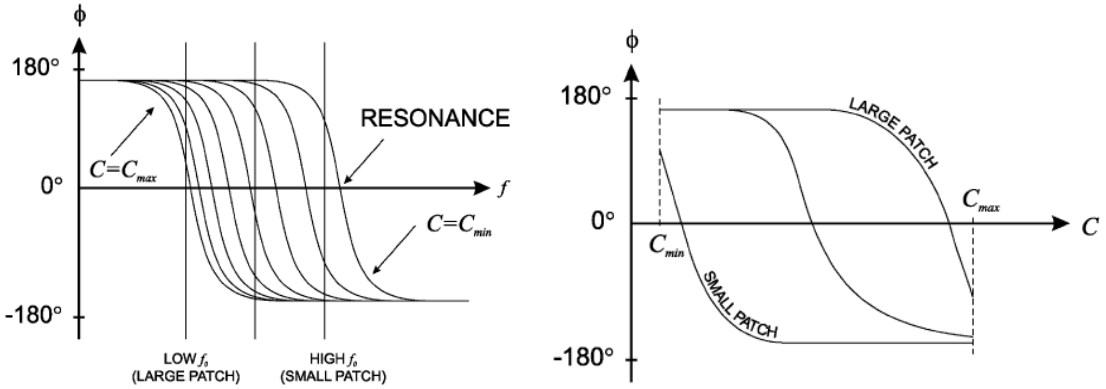

Figure. I.27. *Frequency agile antenna tuning characteristics. (left) Scattered field phase versus frequency. (right) Scattered field phase versus capacitance*

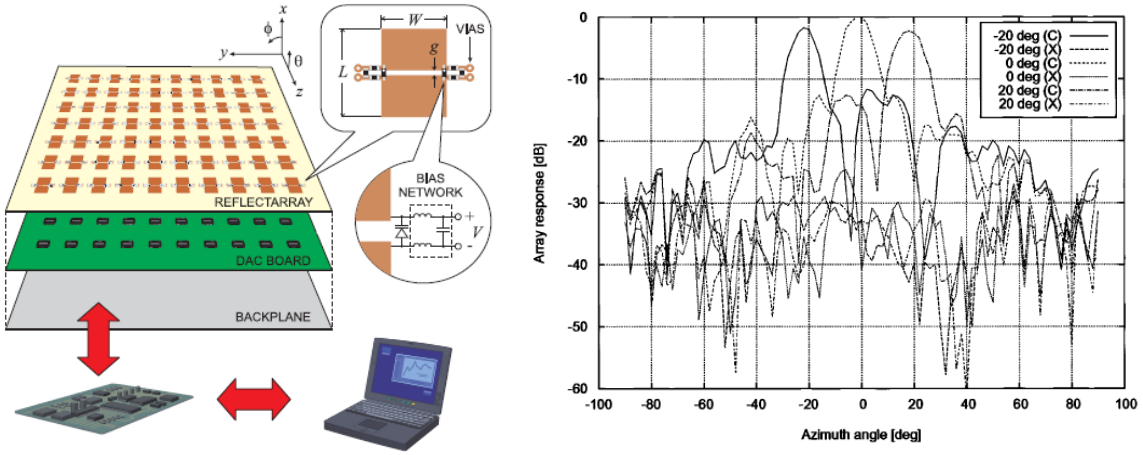

Figure. I.28. *(left) Electronically tunable reflectarray. (right) Measured co-polarized and cross-polarized radiation patterns for 3 reflectarray configurations*

VI.1.2 – RF MEMS Switches and Capacitors technology

MEMS (Micro-electro-mechanical Systems) technology plays a key role in the ongoing miniaturization of electronic modules and systems in future telecommunications, observation and space exploration satellites and probes. While MEMS operating in the low frequency region are currently being employed in commercial products e. g. as acceleration sensors in automotive applications, the field of RF (radio frequency) MEMS is still in a state of research and early development. Microelectromechanical system circuits have the potential to be inexpensive, low loss, and high quality phase-shifting capability [84]. They can also be integrated circuit (IC) compatible, and are thus harmonized with the quest of achieving integrated and ever smaller radio frequency (RF) front ends. These properties made the RF MEMS a research subject for reflectarray antennas. Two strategies are offered by the MEMS technology to control the phase shifts of the reflectarray cells.

The first strategy is to use **MEMS switches** that will vary the length of transmission lines or modify the dimensions of the radiating elements (patch with coupled slot) in order to change the phase shift of the element. RF MEMS switches exhibit excellent RF properties such as low insertion loss, high linearity, low power consumption and high isolation [85]. These components offer the capability to control the phase shifts or the beam digitally via Microcontrollers. The other is to use **MEMS capacitors (**also called **MEMS varactors)** [86]**.**

MEMS switches

In 2003, Under the French research project **ARRESAT**, a tunable reflectarray in the Ka-band was being developed by two French research centers, *IETR* (*Institut d'électronique et de télécommunication de Rennes*) led by *E. Girard* and *R. Gillard* and *TAS (Thales Alenia Space)* led by *H. Legay*. The aim of the project was to design a circularly polarized reconfigurable reflectarray with phase shifting elements based on MEMS switches [87]. The phase shifting cell is shown in Fig .I.29. The Upper etching is composed of 12 dipole elements set out concentrically around a central node. This etching is located a quarter wavelength from a ground plane. Two opposed dipole elements are then connected using low-loss MEMS switches to the centre node to create 6 resonating dipoles with different rotating angles. The idea was to pick a switch to change the phase of the reflected phase, so 6 states per cell were available. This phase shifting cell principle was published in a US patent in 2005 [88].

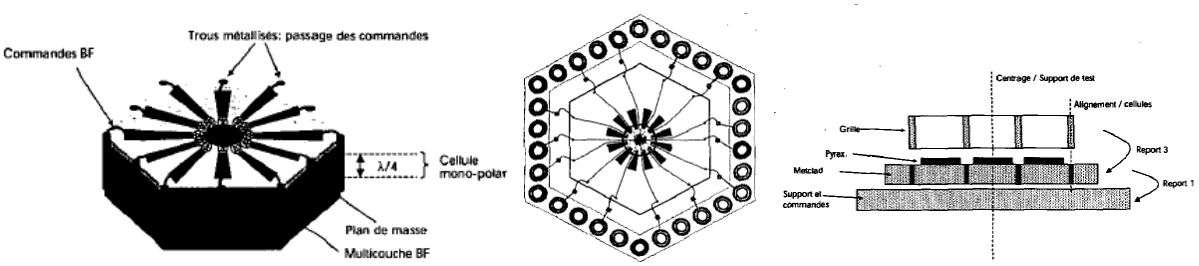

Figure. I.29. *Phase shifting elements for a circularly polarized reflectarray antenna*

In 2005, another study on RF MEMS switches for microstrip reflectarrays was carried out by *TAS* and *IETR*. The phase shifting cell was an extension of the slot-loaded patch concept [73]. MEMS switches were used to control both the size of the patch and of the loading slots as seen in Fig .I.30. Although the phase range complied with the 360° requirement, the frequency dispersion was quite high as both resonators (patch and slot) were used close to their resonances. In addition, the cell size was quite large (>0.6 lambda). To minimize the number of MEMS controls while taking advantage of the capability of the updated structure to provide the same phase with different MEMS configurations, specific optimization tools were developed in [89]. Further researches led to an optimized 8-MEMS cell configuration that overcomes the nonlinearity of the phase shift versus the frequency at any given MEMS configuration [90]. The updated version was obtained by using several concentric metallic rings and by loading the slots in between MEMS switches as seen in Fig.I.31. Another improved cell was presented in [91]. It should be noticed that most of these developments were supported and funded by the European Space Agency (*ESA*) within the **MERCURY** project.

Let's not forget the following interesting papers that dealt with tunable reflectarray cells based on RF MEMS switches, especially the work of *Rahmat-Samii* [92,93,94,95].

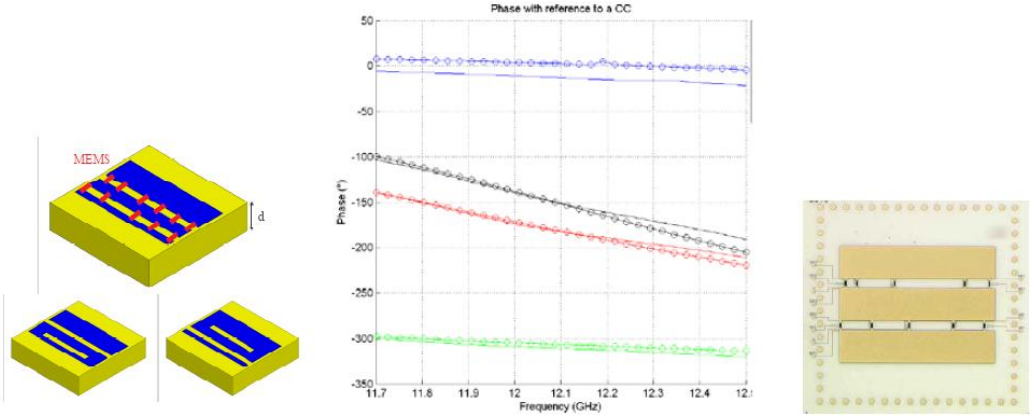

Figure. I.30. *MEMS controlled cell developed by TAS and IETR [96], and the phase response for 4 different MEMS states*

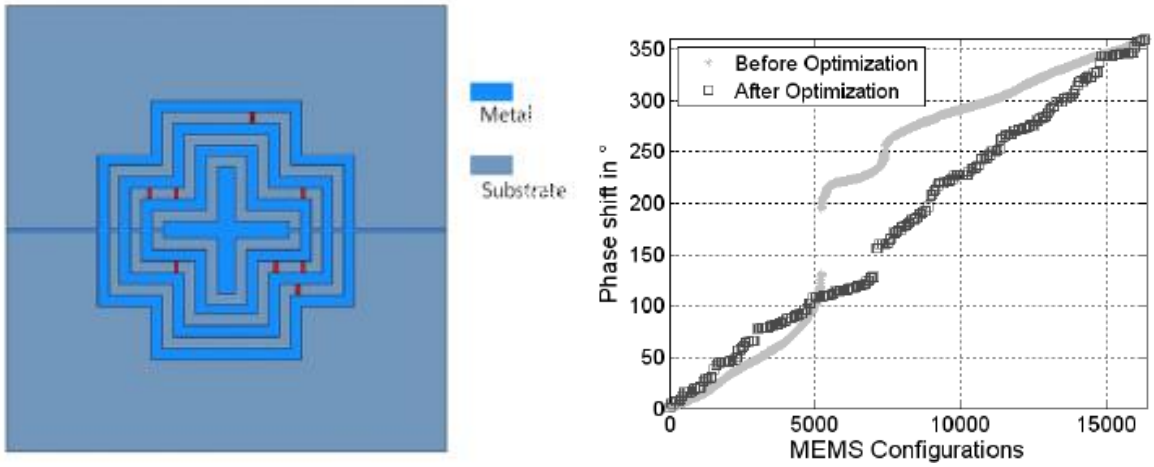

Figure. I.31. *Optimized" pharmacist cross" cell and cell's characteristic table [90]*

MEMS Capacitors

MEMS capacitors have been recently studied as phase shifters for reflectarray antennas by the *University of Toronto* (led by *S.V. Hum* and *M. Okoniewski)* and *TAS*. According to *Hum*, MEMS capacitors are potential candidates to replace Varactor diodes [97], due to lower losses which reach 3.5dB [98]. In the design of MEMS capacitors, electrostatic actuation of MEMS beams is easily achievable with tunable parallel plate capacitor design as seen in Fig .I.32. The capacitance of the MEMS is controlled with bias voltage. The first prototype was a Ku band reflectarray fabricated by *TAS* [99]. The antenna, which was supported and funded by *CNES* and *ESA,* is shown in Fig .I.33.

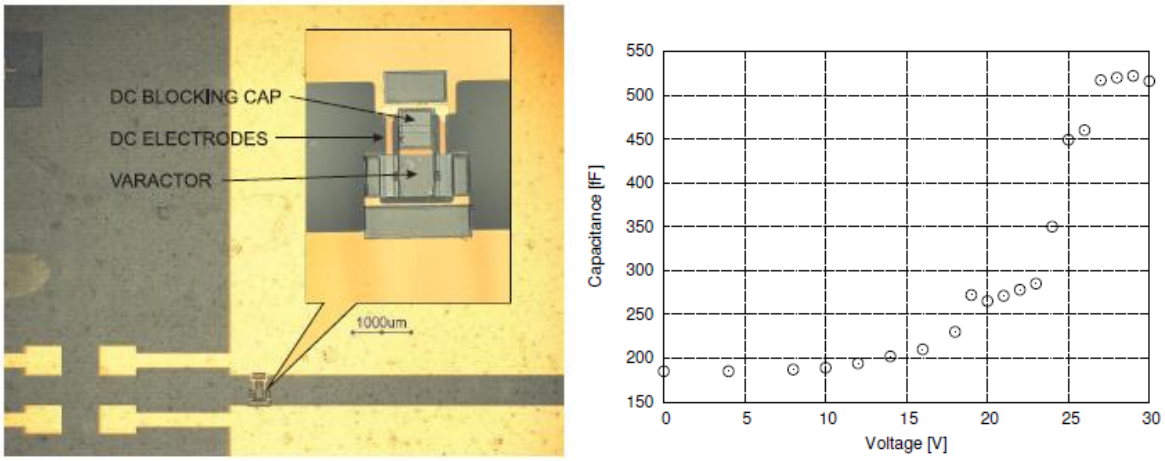

Figure. I.32. *(lef) MEMS varactor*. (right) Capacitance versus voltage at 5 GHz.

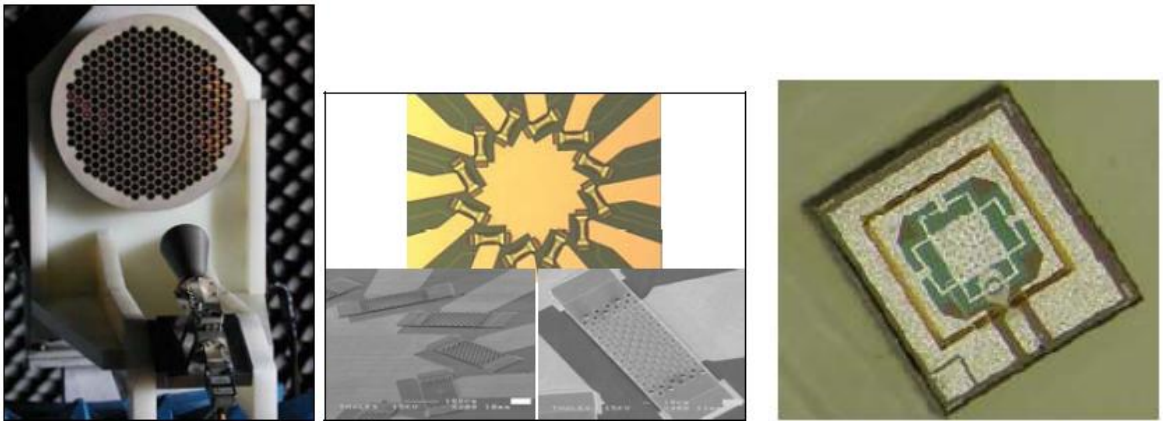

Figure. I.33. *Reflectarray prototype (left). A close up look to the phase shifting elements (middle). MEMS Capacitors(right)*

ESA (European Space agency) have funded some studies on reflectarray antennas with RF MEMS switches/capacitors under the **MERCURY** project [91] [100]. *The European community* has also funded studies on tunable reflectarrays that use RF MEMS switches/capacitors or ferroelectric thin phase sifters, under the RETINA project [78].

VI.1.3 - RRA based on Liquid crystal cells for millimeter/sub-millimeter wave range applications

The anisotropy properties of liquid crystals and the manufacturing technology are well known from the Liquid Crystal Displays (LCD), but only recently, some works have reported the direct use of microwave anisotropy for phase control in reflectarray antennas [101,102,103]. If a LC substrate is used in the reflectarray cell, when a bias voltage is applied, the molecules are reoriented in the direction of the electric field, producing an increase of the dielectric constant at macroscopic level, see Fig .I.34 (c). Several works have reported experimental results for reconfigurable reflectarray cells and antenna demonstrators [101,102,103] using LC mixtures as substrate.

An X-band proof of concept for a reconfigurable monopulse reflectarray antenna with a liquid crystal substrate was developed by QUB (*Queens University Belfast)*, *UPM (Universidad Politécnica de Madridad)* and *EADS Astrium* [104]. In this pilot study, numerical and experimental techniques were employed to demonstrate that the dielectric anisotropy property of liquid crystals can be used to create a reconfigurable reflectarray antenna which generates a beam that can be electronically switched from a sum to a difference radiation pattern. The demonstrator is shown in Fig .I.34 (b).

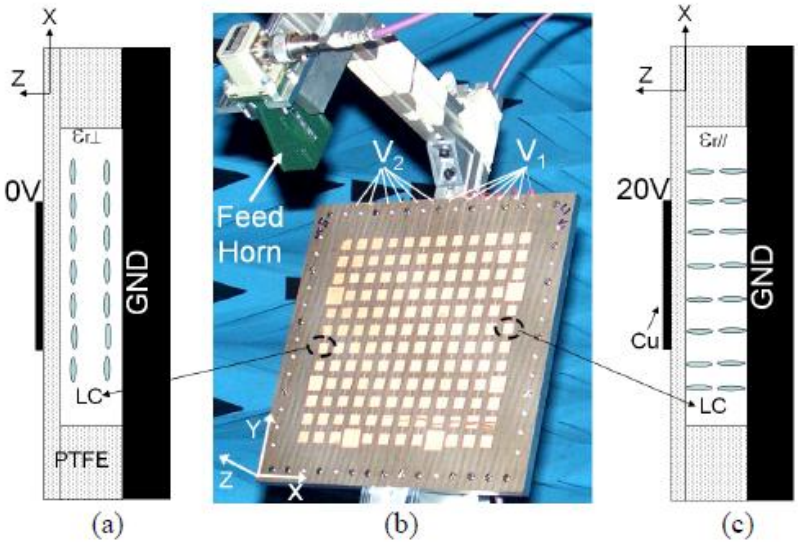

Figure. I.34. *Lateral view of the reflectarray cells in the two bias states (a) and (c), and photo of the demonstrator for switchable sum and difference pattern (b).*

For applications in the millimeter and sub-millimeter wave range, electronic beam scanning has been proposed and demonstrated by using reflectarrays based on Liquid Crystals (LC) [101], [104]. This technology is very appropriate for sub-millimeter and THz range, where other technologies for beam reconfiguration cannot be used.

VI.1.4 - Other Techniques

NASA Space agency is funding studies on low loss phase shifters for space communications. Phase shifters based thin ferrites films, GaAs MMIC or MEMS designs were presented [105] [106], as depicted in Fig .I.35. Ferrite phase shifters demonstrated low phase error, fast transient response and acceptable insertion loss (<3dB).

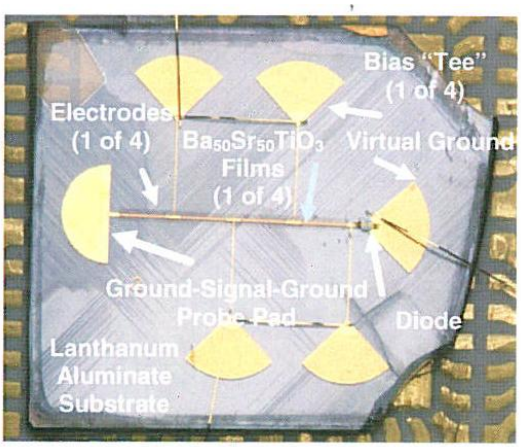

Figure. I.35. *Hybrid X-band ferroelectric/semiconductor phase shifter on 0.5mm lanthanum aluminate*

VI.1.5 – ARASCOM Project: Agile Reflectarray Antennas for Security and COMmunication

ARASCOM is a STREP (Specific Targeted Research Project) supported by the *European Commission*, in the frame of the *7th Framework Research Program "FP7"* [107]. It has begun on May 15th, 2008, and was planned for 3 years. In April 2011, The EC extended the project's duration by 9 moths till Feb.2012. Nine partners are involved (*TAS*, *SELEX*, *MOYANO*, *CEA*, *FBK*, *UNIPG*, *UPM*, *TUD* and *EADS*).

We will just summarize the objectives of this project because it aims at comparing the different up-to-date technologies to make agile beam with the most recent capabilities. This project is a good benchmark to illustrate the potentialities of tunable RA.

ARASCOM aims to proof that agile reflectarrays with **integrating micro & nano technologies** (MEMS switches & nematic Liquid Crystals) can provide the following:

(1) Key equipment for more performing systems in a large set of applications: security imaging; vehicles safety: against collisions for securing landing of airplanes or helicopters; communications via terrestrial networks and satellite; all requiring to scan and/or re-shape the antenna beam.

(2) Much cheaper, compact and less power-consuming than "fully active antennas" composed of hundreds of complex T/R Modules.

More precisely:

(1) Design large MEMS-based reflectarrays with 1D (base-stations) / 2D (satellites) beam scanning and re-shaping fitted to actual mission requirements

(2) Design New Liquid-Crystal Reflectarray designs that can reduce the RF-Loss at 77GHz

(3) Combine MEMS and LC technologies -> full 360° phase-range with moderate loss + reduced number of biasing lines.

	Passive array	**Active antennas with T / R modules**	**Reflectarray antennas**
Agile beam (scan, reshape)	NO	Yes	Yes
Mass & volume	Low	Very High	Low
DC-Consumption	Null	High	Negligible
Cost	Low	Very High	Moderate

Table.I: Comparison between different antennas

RF-MEMS and Liquid Crystal presented decisive complementary advantages for phase-control in reflectarrays, when compared with other candidates, as seen in Table.II.

	PIN/varactor Diodes	**RF-MEMS**	**Ferro-electric film**	**Liquid Crystal layer**
Phase-control method	PIN: discrete-bits switching Varactor:continuous voltage	Discrete-bits switching	Continuous voltage	Continuous voltage
Mass & volume	Medium (substrate area)	Very Low	Low	Low
DC-Consumption	Medium	Null	Negligible	Negligible
RF-loss	Moderate	Low	High	Decreasing with frequency
Linearity	Bad	Very good	Good only for thin-film (but very high voltage)	Very good
Cost	Low if automatic bonding & wiring	Low at large wafers scale	Low if integrated in CMOS	Low (LCD process)

Table.II : Comparison between different phase shifting cell technologies for reflectarrays

At the end of the project three prototypes, should have been built, tested and measured:

(1) An advanced LMDS base-station reconfigurable antenna in X-band with variable beamwidth and switchable beams in the azimuth plane [108], as depicted in Fig .I.36.

(2) In Ku band, a fully reconfigurable sub-reflectarray associated with a reflector for on-ground coverage from satellite [109], the “pharmacist cross” design, as seen in Fig.I.31, is used as unit cell.

(3) A W-band radar antenna, combining RF-MEMS & voltage controlled LC, for security imaging and helicopter landing as shown in Fig .I.37. The bandwidth of the antenna is 1GHZ at 75GHz [110], and the tuning speed is 0.2ms/pixel. The beam is scanned using 1-bit MEMS, yet losing only 3 dB from an ideal antenna, as depicted in Fig .I.38.

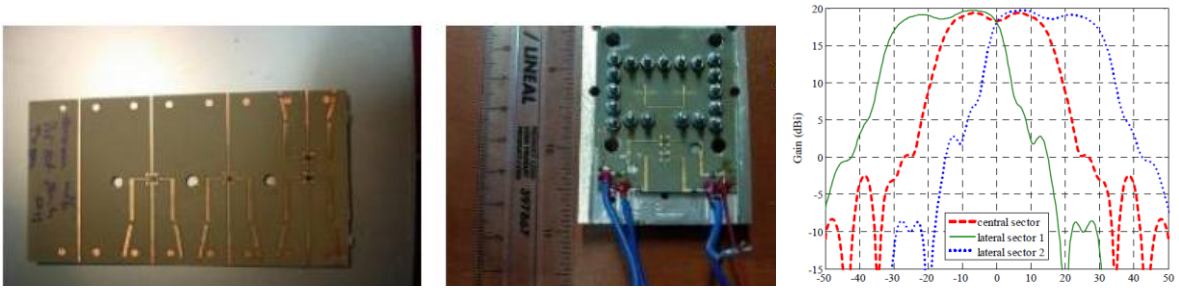

Figure. I.36. *Gathered reflectarray elements with (left) PIN diodes or (center) MEMS devices. (right) Antenna gain for 3 switched beams using 2bit MEMS in the azimuth plane.*

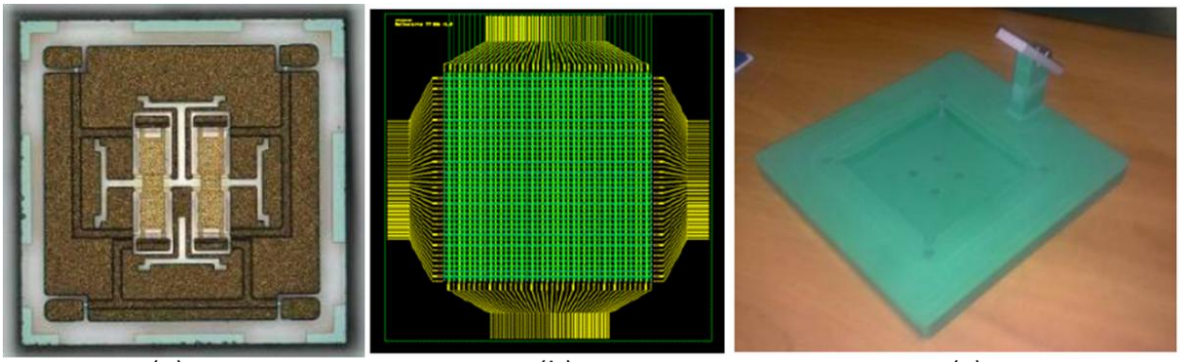

Figure. I.37. *(a)Elementary MEMS cell, (b) packaging board, (c) reflectarray structure*

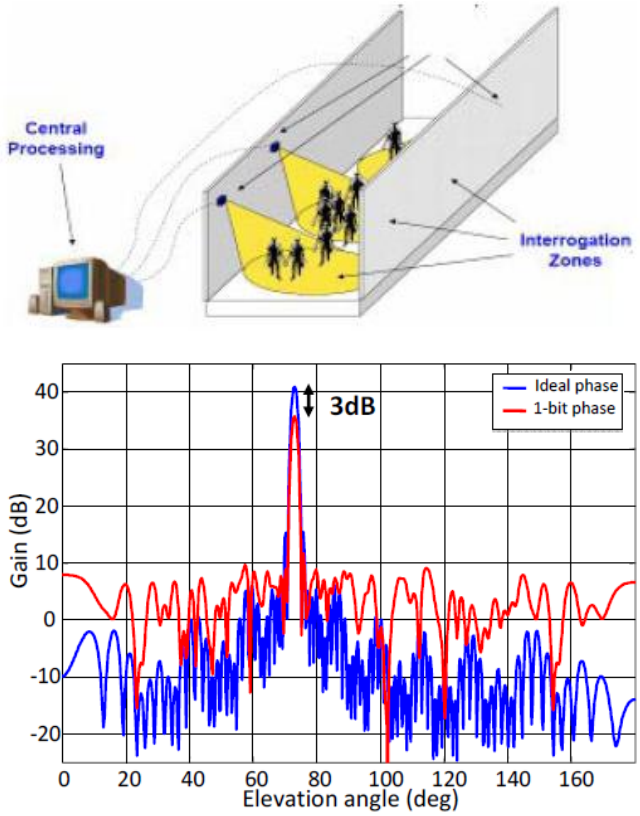

Figure. I.38. *(left) Security application. (right) 1-bit beam scanning of the W-band antenna*

VI.2 - Multi-Beam Reflectarrays

Multi-beam antennas have numerous applications, such as electronic countermeasures, satellite communications, and multiple-target radar systems [25]. Reflectarrays can be designed to generate multiple beams, either with a single feed, or with multiple feeds.

For a single feed antenna, generating simultaneous beams is possible thanks to a specific phase shifts distribution at the radiating cells. Two direct design methods are available. The basic idea behind the first approach, geometrical method, is simply to divide the reflectarray surface into N sub-arrays where each sub-array can then radiate a beam in the required direction [111]. Another approach for multi-beam reflectarray designs is by using the superposition of the aperture fields associated with each beam on the reflectarray aperture [34]. A two-beam single fed prototype was demonstrated by Encinar in [112], as depicted in Fig .I.39.

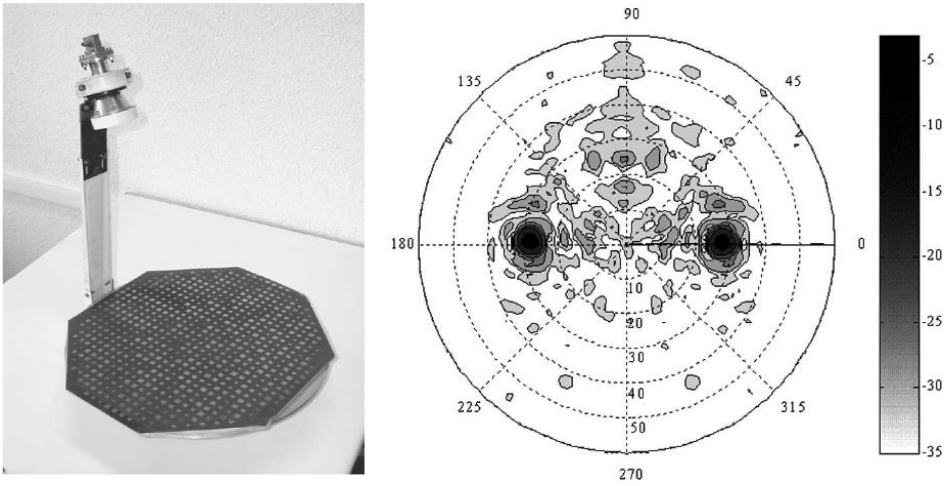

Figure. I.39. *(left) dual-beam single-feed reflectarray. (right) Measured radiation pattern at 11.95 GHZ*

In [113] a very interesting paper on a single-feed quad-beam reflectarray that uses efficient optimization algorithms, such as the Alternative Projection Method (APM), to synthesize multi-beam patterns was presented. The reflectarray design functions at 32 GHz and is shown in Fig .I.40. APM is basically an iterative process that searches for the intersection between two sets, i.e. the set of possible radiation patterns that can be obtained with the reflectarray antenna and the set of radiation patterns that satisfy the mask requirements, as seen in Fig .I.41. When compared to other phase synthesis methods, the authors encountered a significant reduced computational time for convergence of the solution which is suitable for large reflectarray antennas.

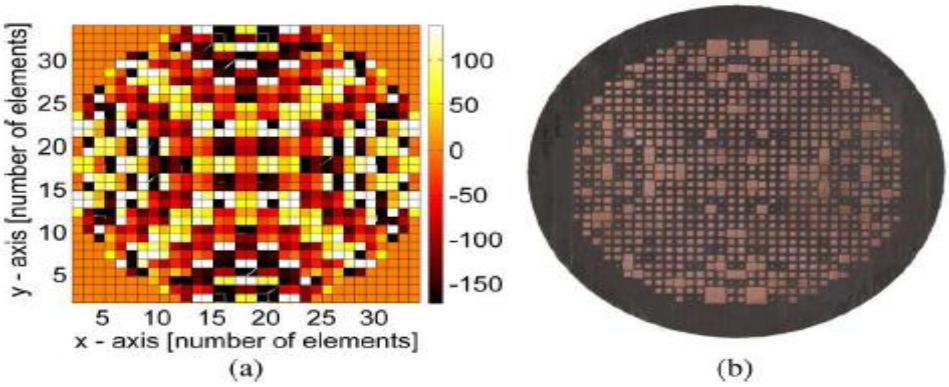

Figure. I.40. *(a) Optimized phase distribution. (b) Reflectarray panel.*

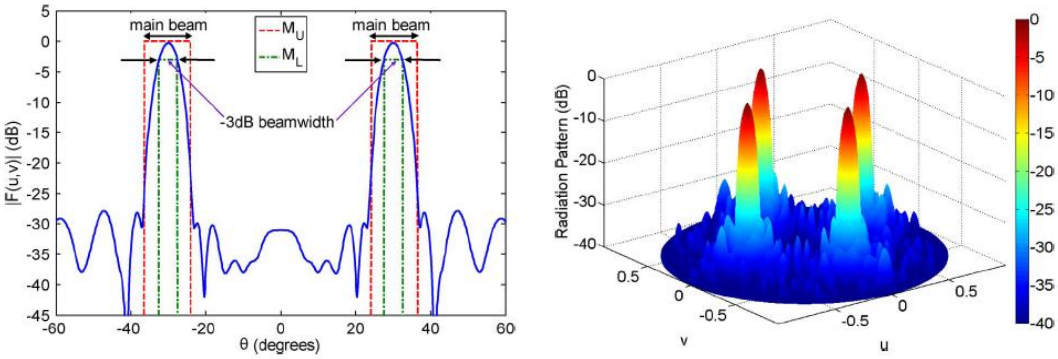

Figure. I.41. *(left) 2D view of the mask model for the quad-beam reflectarray. (right)Radiation pattern of the optimized design at 32 GHz*

For a multi fed reflectarray, the simultaneous beams are generated independently, such as those used in communications with frequency reuse. A reflectarray can be designed to generate a beam in a given direction for each feed, in a similar way as in multi-feed reflectors [34], as shown in Fig .I.42. A multi-feed and multi-beam reflectarray has been designed for a LMDS central station antenna in the 24.5-26.5 GHz band [114].

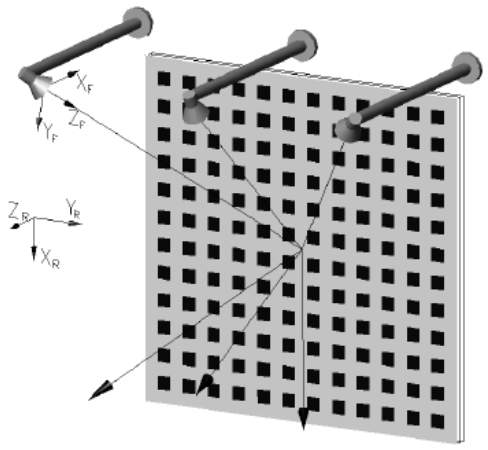

Figure. I.42. *Multi-feed Multi-beam reflectarray configuration*

VI.3 - Contoured Beam Reflectarray for Space Communications

Contoured beams can be easily achieved using reflectarrays by implementing appropriate phase shifts in the reflectarray elements. In reflectarrays, the amplitude at the elements is determined by the feed antenna, while the phase at each element can be adjusted. Thus, a *phase-only* technique is applied to calculate the appropriate phase distribution for the pattern synthesis. Contoured beam reflectarray have been demonstrated for a cosecant squared pattern using a 3600 element reflectarray by *Huang* in [115], and for Direct Broadcast Satellites (DBS) applications such as the reflectarray designed to cover the European continent by *Pozar* in [68].

In the ARTES 5.1 program, *TAS*, *IETR* and *ESA* have developed various advanced concepts and technologies suitable for a Ku band contoured beam reflectarray antenna. A 1.3 m offset reflectarray demonstrator has been developed in [116], as depicted in Fig .I.43. The antenna purpose is to cover Canada, US, Puerto Rico and Hawaii in the KU-Band. So an offset faceted reflectarray with five panels was proposed to increase the bandwidth of the reflectarray. The phoenix cell which was developed by *IETR* is used as phase shifting element [117], and an advanced phase-only synthesis (POS) tool is used to calculate the proper state of each cell. The antenna will be benchmarked with the earth Deck Gregorian configuration antenna which was manufactured for the Galaxy17 satellite.

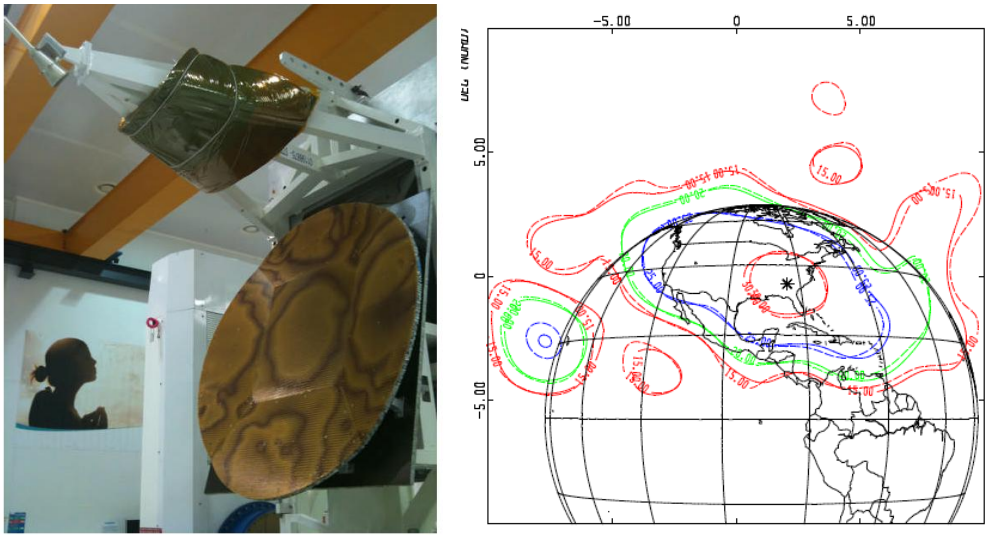

Figure. I.43. *(left) Reflectarray prototype. (right) Simulated galaxy 17 coverage of North America*

VI.4 - Reflectarrays in dual reflector Configuration For satellite applications

The frequency range occupied by the satellites communications are dominated by the attenuation loss due to the propagation through the atmosphere which is around 200dB. The weight of the satellite is a major cost factor, launching 1Kg in a low orbit costs from 10K to 20K$/Kg. Usually satellites are associated to commercial missions with an orbit life between 15 and 18 years, so it is very critical to lower the cost of the satellite and maximize its performances in order to sell the product. In case of a typical mission with 46 RF power amplifiers of 105W, a 1 dB increase in the antenna gain reduces the power consumption of 1,8Kw and lowers the mass of the satellite by 120 Kg. The final cost of the satellite is reduced by 8 Million Euros (8 to 10%) [118]. Traditionally, the shaped dual "parabolic" reflector in offset configuration was considered to yield the best radiation pattern to meet with the above requirements. They can achieve a very high efficiency 85-95%, low cross polarization and a very high gain for focused/shaped beam coverage [119]. Similarly to reflector antennas, microstrip reflectarrays can be designed with a dual reflector configuration using cassegrain or gregorian approach. One advantage as already mentioned in section 5, is the possibility to fill the same mission with less volume, lower mass, cheaper antenna but at the expenses of a smaller bandwidth (at the moment). We should note that during this long time the demand in data traffic and its mission is a subject to change, so the idea of being able to change the mission and the coverage of the satellite is very attractive to operators. Reconfigurable Reflectarrays in dual reflector configuration can satisfy this mission replacing the high mass, high volume expensive phased arrays.

Many dual configurations are possible. One is to use a Cassegrain dual configuration, where the reflectarray is the main reflector and the sub-reflector is a hyperboloid, as depicted in Fig .I.44. The first Cassegrain reflectarray using microstrip patches was developed with a center-fed geometry at 77 GHz by Pozar [120]. The reflectarray has a diameter of 15.5 cm with 5770 linearly polarized rectangular patches using variable-size design. Another Cassegrain reflectarray with an offset configuration was developed for an X/Ka dual-band performance [121]. The antenna has a main reflectarray aperture diameter of 75 cm and uses annular ring elements with each element having two capacitive gaps for circular polarization. The sub-reflector is a convex hyperboloid and has a projected elliptical aperture with major

axis dimension of 150 mm and minor axis of 84 mm. The side-lobe and cross-polar levels were below -25dB, and the efficiency of the antenna was close to 50%.

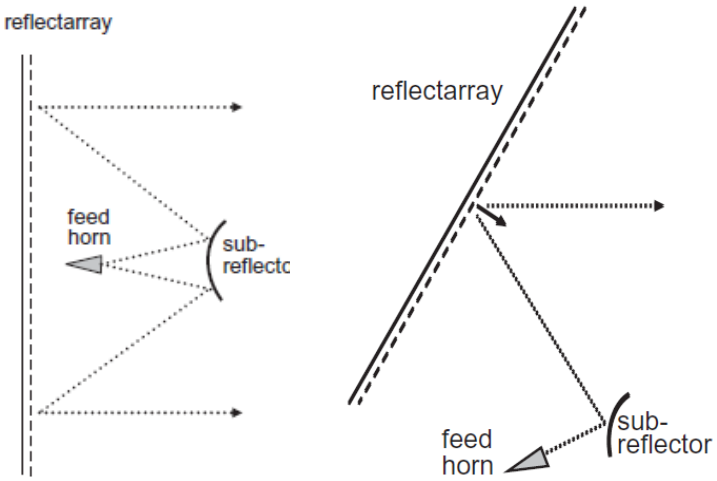

Figure. I.44. *Cassegrain configuration in center-fed and offset-fed positions*

Another is to use a flat reflectarray as sub-reflector and a parabolic main reflector [122] in gregorian configuration. Such configurations are very interesting because it allows to use a reduced-size RA. It has the advantage of improving the radiation bandwidth (reduced spatial phase delay) and reducing the number of control (i.e. complexity and cost). The antenna, shown in Fig .I.45, was designed to produce a focused or contoured beam for DBS applications. In a classical dual-reflector configuration (without RA), contoured beam could be achieved by shaping the sub-reflector, the main parabolic reflector or both.

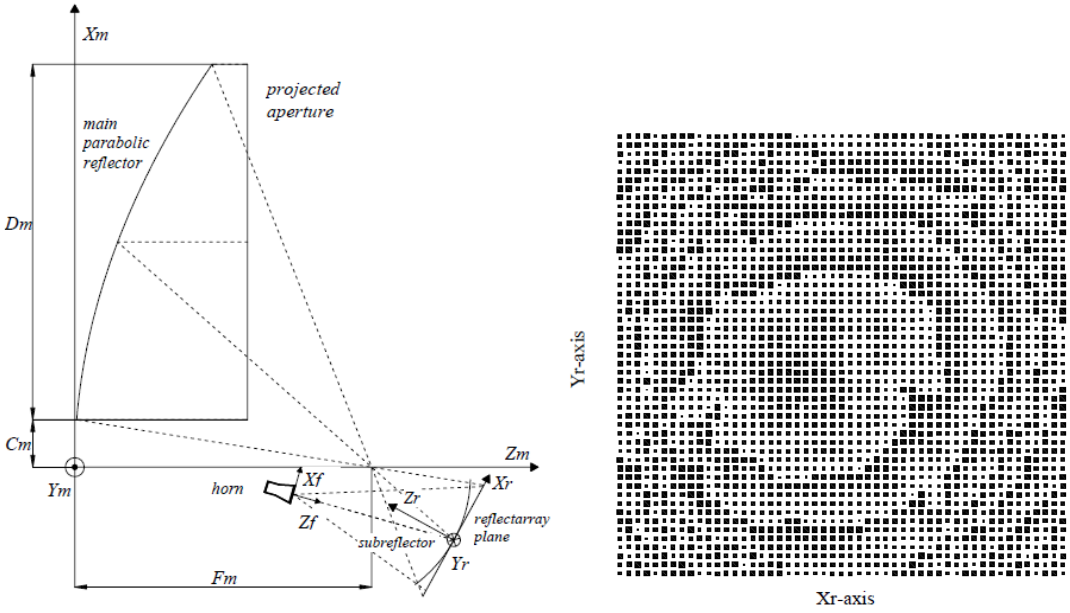

Figure. I.45. *(left) Dual reflector gregorian configuration (right) reflectarray panel*

In the mentioned paper, the authors had chosen to use a sub-reflectarray to realize the progressive phase shift involving the contoured beam, as seen in Fig.I.45 (right). In order to evaluate the beam-shaping performances that can be achieved with a sub-reflectarray and a main parabolic reflector, requirements from a real DBS mission have been selected. The South America coverage of the Amazonas satellite has been chosen, see Fig .I.46. In both cases, the sub-reflectarray panel is made of variable-size patches whose the dimensions are optimized to meet with the objective radiation pattern. This work was supported by the *Spanish Ministry of Science* and *ESA*.

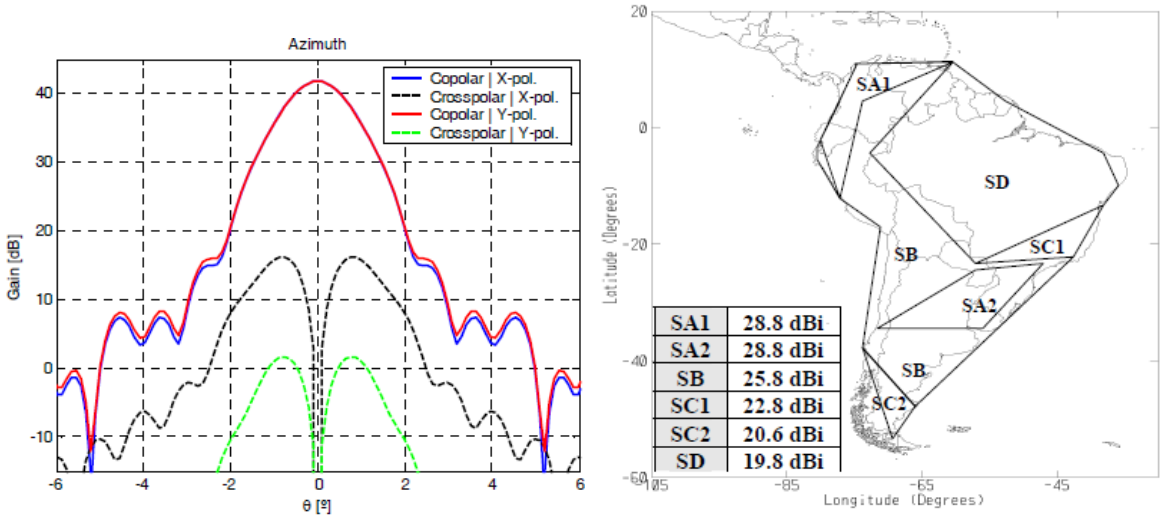

Figure. I.46. *(left) Focused beam case, co-polar and cross-polar radiation pattern. (right) Contoured beam coverage of the south America*

Another possible configuration is the use of a passive reflectarray as a sub reflector associated with a main tunable reflectarray as depicted in Fig .I.47. In [123], preliminary results of a dual-reflectarray antenna made of a passive sub-reflectarray and a main reflectarray with 1-bit electronic control were presented. The antenna was designed to provide a directive beam in receive (10.70-12.75 GHz) and transmit (14.0-14.5GHz) frequency bands with electronic scanning capabilities within a limited angular range. The passive sub-reflectarray is made of two layers of varying-sized patches. In a first step, optimization techniques, already demonstrated for Tx/Rx antennas in Ku-band [124], are used to adjust the patch dimensions to fulfill the required phase distribution at 11.725GHz. From these initial dimensions optimization routines are able to match the required phase-shift distribution at central and extreme frequencies in each of the Tx and Rx bands (10.7-12.75, 14.0-14.5 GHz). In a second step, the appropriate states of all the 1-bit reconfigurable elements are determined

to provide a focused beam in a given scan direction This work was supported by the *Spanish ministry of Science* and *ESA* under the **RESKUE** Project.

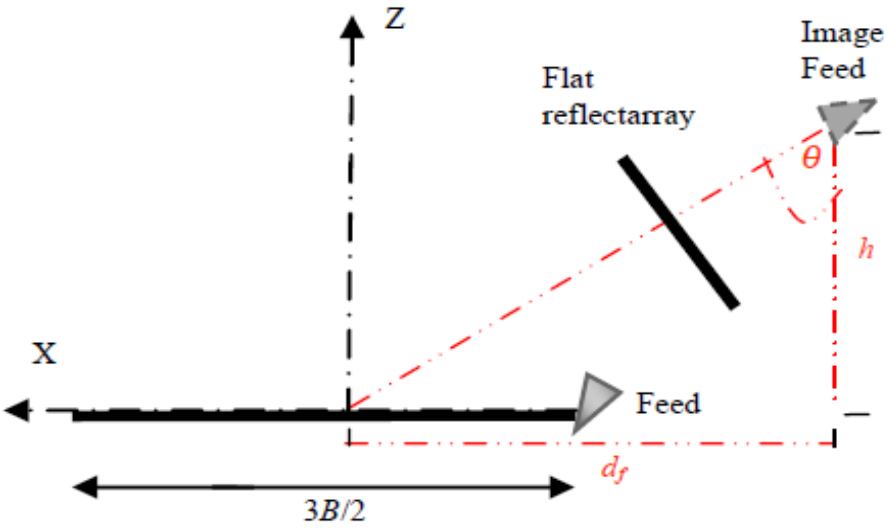

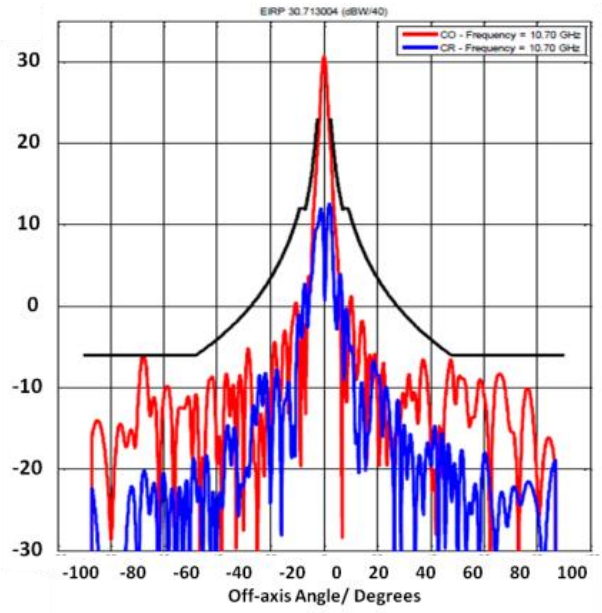

Figure. I.47. *Passive sub-reflectarray in front of a tunable reflectarray as main reflector. (right)co-polar and cross-polar radiated beam at ±5° at 10.7 GHz*

VII - Methods for the analysis and synthesis of the reflectarray antennas

VII.1 - Phase shift distribution according to geometrical optics

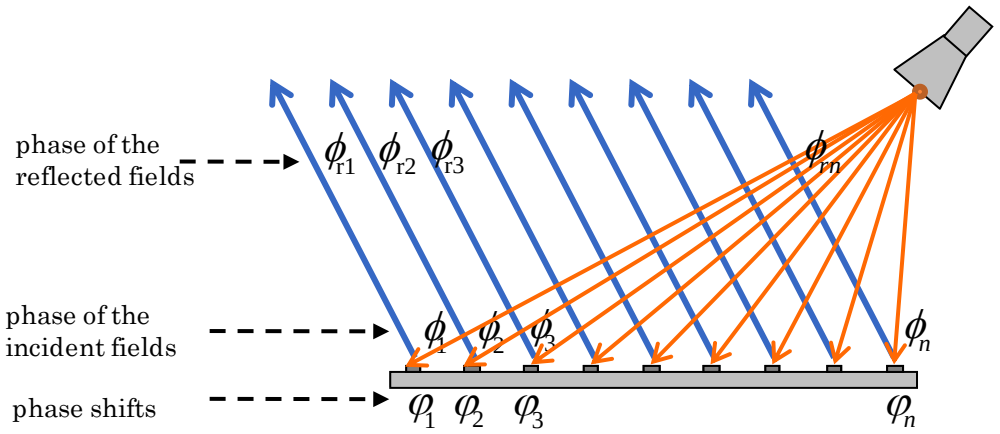

Figure. I.48. *Incident (orange) and reflected (blue) EM fields on the panel.*

According to the classical assumption that employs the geometrical optics [34], the phase shift that must be introduced at each element to produce a collimated beam in a given direction is determined in this section. The progressive phase distribution $\emptyset_r(x_i, y_i)$ on the reflectarray surface that produces a beam in the direction (ϑ_0, φ_0), as known from array theory, is expressed in Eq.I.6:

$$\emptyset_r(x_i, y_i) = -k_0 \sin\vartheta_0 \cos\varphi_0 \, x_i - k_0 \sin\vartheta_0 \sin\varphi_0 \, y_i \tag{I.6}$$

Where: k_0 is the propagation constant in vacuum and (x_i, y_i) are the coordinates of a cell 'i'.

On the other hand, the phase of the reflected field φ_i at each reflectarray element is equal to the phase of the incident field $\emptyset_i(x_i, y_i)$, as a result of propagation from the feed, plus the phase shift introduced by each cell, as shown in Eq.I.7:

$$\emptyset_r(x_i, y_i) = -\emptyset_i(x_i, y_i), +\varphi(x_i, y_i) = -k_0 d + \varphi(x_i, y_i) = -\frac{2\pi f\left(\sqrt{\left((P_x - x_i)^2 + (P_y - y_i)^2 + (P_z - z_i)^2\right)}\right)}{c} + \varphi(x_i, y_i) \tag{I.7}$$

Where $\varphi(x_i, y_i)$ is the phase of the reflection coefficient, or phase shift for the element 'i'. From the equations Eq.I.3 and Eq.I.4, the phase shift required at each element is obtained:

$$(I.8). \qquad \varphi(x_i, y_i) = -k_0 \sin\vartheta_0 \cos\varphi_0 \, x_i - k_0 \sin\vartheta_0 \sin\varphi_0 \, y_i + \frac{2\pi f\left(\sqrt{\left((P_x - x_i)^2 + (P_y - y_i)^2 + (P_z - z_i)^2\right)}\right)}{c}$$

Fig .I.49 shows the required phase shifts on a square reflectarray of 20×19 elements that produces a pencil beam in the direction ($\vartheta_0 = 30°, \varphi_0 = 0°$). For the reflectarray design, the phase of the reflection coefficient must be adjusted in each element to match theses phases. The possibility of an independent phase adjustment for each reflectarray printed element can be used to shape the beam.

Notice that the above definitions are just given to explain the principle of phase shifts. The effects of couplings and of the phase reference of the cells are not taken into account whereas they can drastically affect the performances. We will briefly present the analysis and synthesis techniques for RA in the next part.

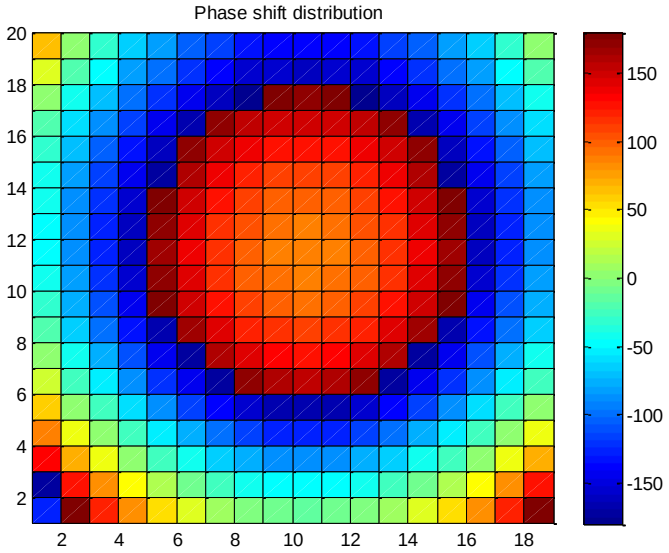

Figure. I.49. *An example of a Phase shift distribution for a square reflectarray panel*

VII.2 - Summary of the analysis techniques

The community analyzes the reflectarray as a reflecting surface, quite similarly to reflector antennas, where different phase shifting elements are lying. The feed antenna is often modeled as a $\cos^q(\theta)$ function and the elements are mostly considered sitting in the far-field region of the feed antenna (Note that the cosines function of the feed antenna can be replaced with more accurate computed or measured radiation patterns). More precisely, the spherical waves of the feed antenna are assumed locally at the cells to be plane waves with variant incidence angles. Based on that assumption, the required phase shift is calculated with different numerical methods to reflect the incident fields with the proper phase in order to focus/shape the beam.

One analysis technique assumes that the cells on the panels are isolated. The mutual coupling between the reflectarray cells is neglected, when the distance between the edges on the radiating patches is larger than 0.25 wavelengths. To meet this criterion, the radiating elements are arranged in a periodic square lattice whose sides are around 0.6-0.7 wavelengths. This approach was used for a reflectarray with attached stubs [125], and for a reflectarray with variable size patches [46]. One disadvantage of such arrangement is the appearance of grating lobes.

Another analysis technique for the reflectarray antenna is to treat the reflectarray panel as a periodic structure. A reflected phase by a cell which belong to an array of infinite elements is calculated versus a given cell parameter such as the size of the patch, or the length of the stub. In a preliminary study, one can consider only the normal incidence for the plane wave, and change the cell's parameter till 360° phase change is obtained. This approach assumes that the phase response is independent versus the angle of the incident field. It might sound adequate for some; however the cells are positioned at different angles from the feed antenna. This assumption can be only true for the cells located at the center of the panel in a center-fed configuration or for high F/D ratio.

It was reported by [46] that if we change the incident angle of the plane on rectangular patches of 40°, the reflected phase can vary around 25°. When the incident angle is 60°, the phase of the reflected phase goes to 50°. The natural consequence was to consider plane waves with different incidence angles [34]. This approach to analyze the reflectarray cells in an infinite array environment and account many incidence angles for the plane waves is well known as the 'local periodicity approach'.

The study is carried out element-by-element, each reflectarray cell that has a given size or stub length is being considered in a periodic environment. The reflected field is then calculated from an infinite array of same size /shape radiating elements illuminated by a plane wave for different incident angles. It is assumed that each element in the reflectarray scatters with the same phase as the same infinite array [126]. Local periodicity has been used since the first realization by Pozar, but with different numerical methods.

One implementation of the method of moments (MoM) in spectral domain for multilayer periodic structures [127] was used for the analysis and design of reflectarrays based on two layers of varying-sized patches, as described in [66]. This technique was used in the manufacture and test of several reflectarrays [128] [129].

The very popular and easy approach to generate periodic conditions around the cell is to use the H-wall waveguide simulator, also called parallel-plate waveguide simulator, where the top and bottom surfaces of the waveguide are electric conductive walls, while the right and left walls are magnetic fields walls [130], as depicted in Fig .I.50. Then the cell is excited by a single plane wave. The reflected phase is then calculated versus a given incidence angle at given frequency. The waveguide simulator which simulates the infinite array can be adapted using the commercial software HFSS [131] (a finite element technique tool).

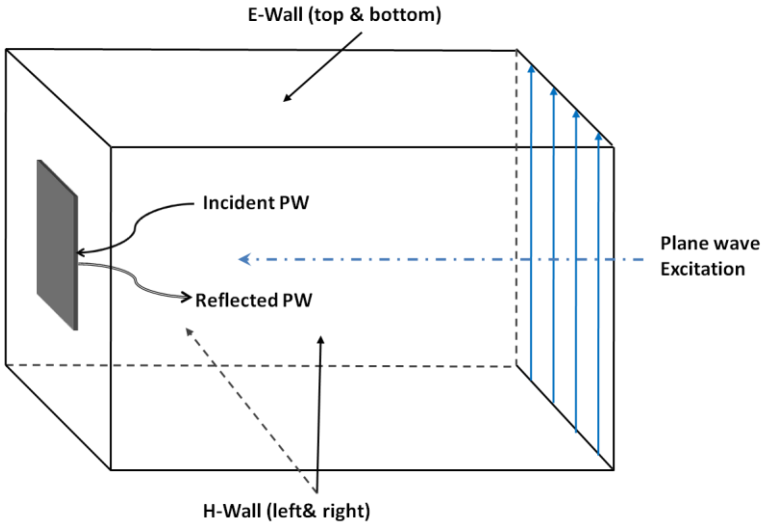

Figure. I.50. *H-Wall waveguide Simulator to calculate the phase response of the cell*

When analyzing arrays with a large number of elements, the element-by-element mutual coupling analysis becomes expensive, the infinite array model is closer to the reality. The study can be done with Floquet theorem [132] [133]. This theorem takes into account the mutual coupling between periodic identical cells and gives good prediction of the element in

the array environment. Floquet theorem can be used to study the cell's phase response or to calculate the mutual impedance/scattering matrix between identical elements belonging to an infinite array. One paper that describes a reflectarray that radiate a circular polarization consisting of an aperture coupled patch with slot and line of variable length, was treated with Floquet modal analysis [134]. The method used here is based on the finite element method (FEM) that uses the Floquet modal expansion theorem to approximate the infinite array model.

Others use the finite-Difference Time-Domain (FDTD) modeling technique to analyze a unit cell of a matrix of elements [135] [136] [137]. In [136], the approach consists in illuminating a single cell of the array and calculating the reflected wave in the presence of the nearest neighbor cells (identical or not), as depicted in Fig .I.51. It permits to obtain the radiation of a surrounded cell in all directions and for any incidence of the incoming wave. This analysis technique which derives from 'local periodicity approach' was called 'surrounded cell approach' [138]. The obtained results proved to be more accurate compared to Floquet analysis.

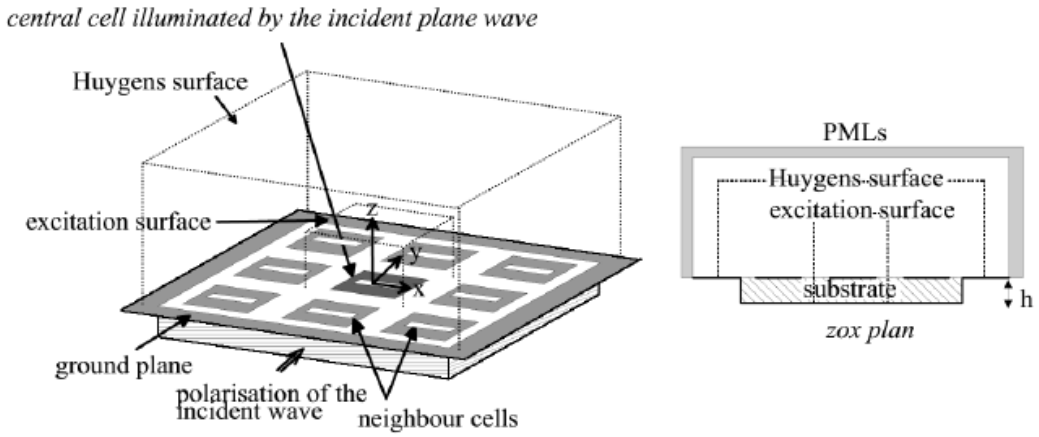

Figure. I.51. *'Surrounded cell approach' simulated in a FDTD numerical model.*

Several full-wave techniques, based on the Method of Moments (MoM) have been recently developed and applied to the analysis of reflectarrays [139,140]. In these techniques, the complete reflectarray is electromagnetically modeled with the real dimensions of all the elements. However, they were developed to analyze only the final performance of the reflectarray after computing the required parameters with a 'Local periodicity' analytical approach. It was reported that these techniques can provide more accurate results, since the mutual coupling is computed with no approximation, but they are much more time-consuming

than those based on local periodicity. So, they cannot be implemented in optimization loops for the reflectarray design. However, they can be used for a more accurate analysis after the design has been completed, in order to find out whether a refinement of the design is required, as 'virtual prototyping'.

Even if the literature contains a lot of references about the reflectarray modeling, it can be noticed that it is difficult to conclude on the best method to design such antennas. Moreover, as the applications and the architecture of the reflectarray often change, it is difficult to state on the accuracy and versatility of these formalisms. Therefore, even if the local periodicity is often mentioned, recent literature presents a keen interest to develop some alternate approaches to design reflectarray. These studies are mainly motivated by the need to overcome some limitations, especially the ones encountered with local periodicity that are leading to a lack of performances in some cases. Among these alternate approaches, we can notice the concept of Extended Local Periodicity (ELP) [141]. It consists in the modeling of a repeated scheme with an extended unit cell with its nearest neighbors, suitable to be included in the Ticra's softwares. The objective of this study is to provide a commercial tool dedicated in part to reflectarray design. In fact, with actual commercial EM software, the only way proposed to analyze reflectarray's performances in a single modeling is to make a Full-wave simulation, involving important computing resources, preventing all synthesis or parametric study. Another promising method, initially developed for arrays, has been derived for reflectarrays, it is the Scale Changing Technique (SCT) [142]. It consists of a sub-domain decomposition with Scale Changing Networks allowing to represent fine details and couplings. Combined with a synthesis algorithm, this method can be a good and efficient way to design a reflectarray. In fact, the electromagnetic characteristics of the elementary cells can be accurately defined in a reduced computation time and coupled to a synthesis process while couplings are accounted. The authors have already applied this technique for passive reflectarray design and comparisons with the EM software HFSS have been made [143].

Few notes can be given about the local periodicity approach. It allows integrating the mutual coupling between cells that belong to a periodic identical infinite array. The local periodicity approach provides accurate results when the variation of the patch dimensions in the reflectarray is smooth, because all the mutual couplings are taken into account under the assumption that all the neighboring elements are identical. In a practical case, this assumption is not 100% correct. By looking at one realized prototype [122] shown in Fig .I.52, we can

clearly notice that the variation between the dimensions of the cells on the panel is not very smooth.

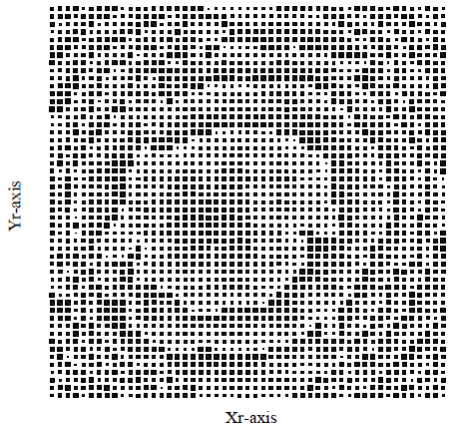

Figure. I.52. *Reflectarray panel designed to radiate a Contoured beam for DBS satellite communication*

Another issue about 'local periodicity' approach is that the reflectarray must be large enough so that the infinite array solution is valid, and the F/D ratio must be large enough so that the incident field at a given cell is locally a plane wave. The smaller the reflectarray is, the less the infinite array model is relevant, and the less the cells are positioned in the farfield region of the feed antenna. It is known that in the far-field zone, the spherical waves radiated by any antenna travel as plane waves [144]. Moreover, the radiation pattern of the reflectarray is computed by integrating the field on the reflectarray, assuming that the field (amplitude and phase) is uniform on each reflectarray cell [34], whose size is normally between 0.5 and 0.8 wavelengths. This is a customary simplification, but it can produce errors in the evaluation of the radiation patterns, which are more significant in the case of contoured beams, as demonstrated by Arrebola [145].

When the reflectarray has a diameter around ten wavelengths and it is placed at a close distance from the feed antenna, using the far-field of the feed antenna to deduce the incident EM fields on the panel becomes less accurate. In [146], the Near-Field radiated by the feed horn is calculated on each reflectarray element and it is taken into account as incident field in the analysis of the reflectarray. The NF of the feed is computed from the measured radiation patterns of the horn by using a FF to NF (FF– NF) transformation technique. The analysis of the reflectarray is carried out as in a 'local periodicity' technique described in [66]. It was reported that the accuracy is significantly improved in the case of reflectarrays illuminated in the Fresnel zone of the feed.

VIII - Objective of the thesis: Small size active reflectarray antennas

In this chapter, I presented a literature review on reflectarrays antennas, the developments history since the day of its invention, its many applications such as DBS satellites communications, space telemetry, image security, agile RA for radars, etc … not to forget the major researchers/laboratories/agencies who are spending their time or money to bring the reflectarray finally to the sells department. Of course due to the many features that reflectarrays share with phased arrays and reflectors, a comparison was being presented along the different application domains, in term of performances, feasibility and cost. We have seen that reflectarrays can fulfill most of the missions occupied by the other antennas at a lower cost, smaller volume/mass but at the expenses of some performances which are today the subject of many researches led by many research centers.

Even if significant advances are made on reflectarray modeling to analyze their final electromagnetic performances, some interesting behaviors are not well detailed. This thesis focus is on an accurate analysis and synthesis method of a small sized tunable reflectarray antenna including the mutual coupling. Therefore, we want to insist on the accurate coupling modeling impact rather than computation time. By using a specific synthesis procedure on a reflectarray with reactive loads, we will demonstrate that the couplings impact both amplitudes and phases of the excitation weightings, whereas the classical assumption is to consider that their amplitudes are only proportional to the primary feed illumination. These observations are the subject of a detailed discussion in the chapter 3 and 4 of this memory.

The analysis tool, which will be presented later, is considered accurate and efficient because it is based on full-wave simulations of the main antenna elements via CST MWS (Microwave Studio). Then, these elements will be used as an input database to synthesize a radiation objective. The reflectarray panel is made of identical periodic microstrip patches antennas. The phase shifting elements are reactive loads connected to the radiating patches. Reactive loads can be varactor diodes or MEMS capacitors or any other technique that allows a phase control.

Our final objective is to provide an accurate formalism that can be used either to study in details the RA EM behavior or to evaluate the impact of some technological constraints, like the quantization of phase shifts.

It should be noted that the frame of the thesis doesn't include any study on the tunable elements. The focus is rather on an accurate study of the required phase shifts distribution including the mutual coupling between the cells, and an accurate calculus of the radiation pattern, especially by describing the energy balance distribution.

IX - References

[1] H. Jasik, "Antenna Engineering Handbook," *MaGraw-Hill*, 1961.

[2] A. W. Love, "Reflector Antennas," *Edition John Wiley and Sons*, 1978.

[3] Yi Huang and Kevin Boyle, "Antennas from theory to practice," *A John Wiley and Sons,* 2008.

[4] C. A. Balanis, "Antenna Theory Analysis and Design," *A JOHN WILEY & SONS*, 2005.

[5] J. D. Dyson, "Determination of the Phase Center and Phase Patterns of Antennas in Radio Antennas for Aircraft and Aerospace Vehicles," *AGARD Conference Proceedings*, no. 15, 1967.

[6] Y.Y. Hu, "A Method of Determining Phase Centers and Its Applications to Electromagnetic Horns," *Journal of the Franklin Institute*, pp. 31-39, January 1961.

[7] W. Rusch and N. A. Adatia, "The current state of the reflector antenna art," *IEEE Trans on antennas and propagation*, vol. 32, pp. 313-329, April 1984.

[8] A. W. Rudge and N.A. Adatia, "Offset parabolic reflector antennas: A review," *In proceedings of IEEE*, vol. 66, pp. 1592-1618, 1978.

[9] C. Menudier, "Caractérisation des performanes d'antennes à reflecteurs paraboliques illuminés par une source focale BIE Application à l'optimization d'une couverture multimédia multi-faisceaux," *These Université de Limoges*, October 2007.

[10] C. Grane, "Designing Axially Symmetric Cassegrain or Gregorian DualReflector Antennas from Combinations of Prescribed Geometric Parameters," *IEEE Antennas and Propagation Magazine*, pp. 76-82, April 1998.

[11] Y. Rahmat-Samii, "Subreflector extension for improved efficiencies in Cassegrain antennas, GTD/PO analysis," *IEEE transactions on antennas and propagations*, vol. AP-34, no. 10, october 1986.

[12] J. J. Lee, Leonard I. Parad, and R. S. CHU, "A Shaped Offset-Fed Dual-ReflectorA ntenna," *IEEE TRANS on antennas and propagation*, 1979.

[13] A. R. Cherrette, L. Shung-Wu, and R. J. Acosta, "A method for producing a shaped contour radiation pattern using a single shaped reflector and a single feed," *IEEE trans on antennas and propagation*, vol. AP-37, pp. 698-706, 1989.

[14] O. Kilic and A.I. Zaghloul, "A method for shaped reflector antenna design," *IEEE trans*, 1998.

[15] W. M. Truman and C. A. Balanis, "Optimum Design of Horn Feeds for Reflector Antennas," *IEEE trans Antennas prop*, pp. 585-586, 1974.

[16] A. W. Love (ed.), "Electromagnetic Horn Antennas," *IEEE Press*, 1976.

[17] O. Hachenberg, B. H. Grahl, and R. Wielebinski, "The 100-Meter Radio Telescope at Effelsberg," *Proc. IEEE*, vol. Vol. 69, no. No. 9, pp. pp. 1288–1295, 1973.

[18] P. D. Potter, W. D. Merrick, and A. C. Ludwig, "Big Antenna Systems for Deep-SpaceCommunications," *Astronaut. Aeronaut*, pp. pp. 84–95, October 1966.

[19] S. Srikanth, R. Norrod, L. King, and D. Parker, "An Overview of the Green Bank Telescope," *IEEE*, 1999.

[20] R.E. Collin, "Antennas and Radiowave Propagation," *McGraw-Hill*, 1985.

[21] Robert J. Mailloux, "Phased Array Antenna Handbook, Second Edition," *Artech house*, 2005.

[22] J. Butler and R. Lowe, "Beam-Forming Matrix Simplifies Design of Electrically Scanned Antennas," *Electronic Design*, April 1961.

[23] J. Blass, "Multi-directional antenna – new approach top stacked beams," *IRE International Convention record*, pp. 48-50, 1960.

[24] W. Rotman and R. F. Turner, "Wide-Angle Microwave Lens for Line Source Applications," *IEEE Transactions on antennas and propagation*, vol. 11, pp. 623-632, 1963.

[25] R.C. Hansen, "Phased array antennas," *John Wiley & Sons*, 1998.

[26] P. Angeletti and M. Lisi, "Twenty-Five Years of Beam Forming Network Developments in Europe," *Proceedings of the 29th ESA Antenna Workshop on multiple beams and reconfigurable antennas*, avril 2007.

[27] M. Koubeissi, "Etude d'antennes multifaisceaux à base d'une nouvelle topologie de matrice de Butler," *Thèse Université de Limoges*, Octover 2007.

[28] A.S. Ahmed, "Conception d'antennes réseaux aux performances optimisées par la prise en compte des couplages inter-éléments.Application à la formation de faisceau et à la polarisation circulaire," *Thèse Université de Limoges*, pp. 126-127, dec 2010.

[29] D. C. Zimmermann and D. Parker, "Phased Arrays - Part I: Theory and Architectures," *IEEE Trans. Microwave Theory and Tech*, vol. 50, pp. 678-687, 2002.

[30] E.D. Cohen, "Trends in the Development of MMICs and Packages for Active Electronically Scanned Arrays (AESAs)," *Proceedings IEEE Symposium on Phased Array Systems and Technology*, October 1996.

[31] D.G. Bodnar and J.D. Adams, "Switchable-PolarizationStudy on AN/SPN-43A Antenna," *Naval Electronics Systems Test AND Evaluation Detachment*, October 1975.

[32] Raytheon Company, *http://www.raytheon.com/*.

[33] P. Tran, "Thales To Deliver AESA Radars Soon," *Defense News*, July 2010.

[34] J. Huang and J. Encinar, "Reflectarray antennas," *Hoboken, NJ: Wiley*, 2005.

[35] D.G. Malech, R.G Berry, and W.A Kennedy, "the reflectarray antenna," *IEEE TRANS on antennas and propation*, pp. 645-651, May 1969.

[36] H.R. Phelan, "spiralphase reflectarray for multi target radar," *Microwave Journal*, vol. 20, pp. 67-73, July 1977.

[37] M.L. Lo. and Y.T Oberhart, "Simple method of experimentally investigating scanning microstrip antenna arrays without phase-shifting devices," *Electronics Letters*, pp. 1042-1043, Aug 1989.

[38] A. E. Martynyuk, J. I. Martinez-Lopez, and N. A. Martynyuk, "Spiraphase-type reflectarrays based on loaded ring slot resonators," *IEEE Trans. Antennas Propag.,* vol. 52, pp. 142-153, June 2004.

[39] J. Rodriguez-Zamudio, J. I. Martinez-Lopez, J. Rodriguez-Cuevas, and A. E. Martynyuk, "Reconfigurable Reflectarrays Based on Optimized Spiraphase-Type Elements," *IEEE transactions on Antennas and Propagation*, 2011.

[40] J. Huang, "review on design of printed reflectarray antennas," *Proc JINA*, pp. 483-490, 1998.

[41] R.E. Muson and H. Haddad, "Microstrip reflectarray for satellite communication and RCS enhancement and reduction," *U.S patent*, August 1987.

[42] J. Huang, "Microstrip reflectarray antenna for the SCANSCAT radar application," *Jet Propulsion laboratory report*, no. 90, Nov 1990.

[43] D.C. Chang and M.C. Huang, "Multiple polarization microstrip reflectarray antenna with high efficiency and low cross-polarization," *IEEE trans. Antennas Propagation*, vol. 43, pp. 829-834, Aug 1995.

[44] Y. Zhang, K.L Wu, C. Wu, and J. Litva, "Microstrip reflectarray: full-wave analysis and design scheme," *IEEE AP-S/URSI Symposium*, pp. 1386-1389, June 1993.

[45] A. Kelkar, "FLAPS : Conformal phased reflecting surfaces," *Proc. IEEE National radar Cnof*, pp. 58-62, March 1991.

[46] S.D. Targonski and D.M. Pozar, "Analysis and Design of a microstrip reflectarray using patches of variable size," *IEEE AP-S/URSI Sumposium*, pp. 1820-1823, June 1994.

[47] F.S. Johansson, "A new planar grating-reflector antenna," *IEEE Trans. Antennas Propagat*, vol. 38, pp. 1491-1495, Sep 1990.

[48] Y.T. Guo and S.K. Barton, "Phase correcting zonal reflector incorporating rings," *IEEE Trans. Antennas Propagation*, vol. 43, pp. 350-355, April 1995.

[49] J. Huang and R.J. Pogorzelski, "A Ka-band microstrip reflectarray with elements having variable rotation angles," *IEEE Trans. Antennas and Propagation*, vol. 46, pp. 650-656, May 1998.

[50] R. E. Munson, "Microstrip Phased Array Antennas," *Proc. of Twenty-Second Symp. on USAF Antenna Research and Development Program*, October 1972.

[51] R. E. Munson, "Conformal Microstrip Antennas and Microstrip Phased Arrays," *IEEE Trans. Antennas Propagat.*, vol. 22, no. 1, pp. 74–78, Jan 1974.

[52] J.Q. Howell, "Microstrip Antennas," *IEEE Trans. Antennas Propagat.*, vol. 22, pp. 90-93, Jan 1974.

[53] C.S. Malagisi, "Microstrip disc element reflect array," *Electronics and Aeorospace Systems Convention*, Sept 1978.

[54] J.P. Montgomery, "A microstrip reflectarray antenna element," *Antenna Applications Symposium*, Sept 1978.

[55] J. Montgomery, "Scattering by an infinite periodic array of microstrip elements," *IEEE Transactions on Antennas and Propagation*, vol. 26, pp. 850 - 854 , Nov 1978.

[56] J. Huang, "Microstrip reflectarray ," *Antennas and Propagation Society International Symposium*, vol. 2, pp. 612-615, june 1991.

[57] D.C. Chang and M.C Huang, "Microstrip reflectarray antenna with offset feed," *Electronics Letters*, pp. 1489 - 1491, 1992.

[58] J. Huang, "The Finite Ground Plane Effect on the Microstrip Antenna Radiation Patterns," *IEEE trans on antennas and Propag.*, July 1983.

[59] D.M Pozar and T.A Metzler, "Analysis of a reflectarray antenna using microstrip patches of variable size," *Electronics Letters*, pp. 657-658, April 1993.

[60] R.D. Javor, X.D. Wu, and K. Chang, "Offset-fed microstrip reflectarray antenna," *Electronics Letters*, pp. 1363-1365, Aug 1994.

[61] R.D. Javor, X.D. Wu, and K. Chang, "Dual polarisation of microstrip reflectarray antenna," *Electronics Letters*, pp. 1018-1019, June 1994.

[62] J. Huang, "Bandwidth study of microstrip reflectarray and a novel phased reflectarray concept," *IEEE APS symp*, pp. 582-585, June 1995.

[63] D.I Wu, R.C Hall, and J. Huang, "Dual-frequency microstrip reflectarray," *Antennas and Propagation Society International Symposium*, pp. 2128 - 2131, 1995.

[64] C. WAN and J. Encinar, "Efficient computation of generalized scattering matrix for analyzing multilayered periodic structures," *IEEE trans. Antennas and Propagat.*, vol. 43, pp. 1233-1242, 1995.

[65] J. Encinar, "Design of a dual frequency reflectarray using microstrip stacked patches of variable size," *Electronics Letters*, vol. 32, pp. 1049-1050 , June 1996.

[66] J. Encinar, "Design of two-layer printed reflectarray using patches of variables size," *IEEE Trans. Antennas Propagation*, vol. 49, pp. 1403-1410, October 2001.

[67] J. A. Zornova and J. A. Encinar, "Broadband design of three-layer printed reflectarrays," *IEEE Trans. Antennas Propagat.*, vol. 51, pp. 1662-1664, July 2003.

[68] D. M. Pozar, S. D. Targonski, and R. Pokuls, "A Shaped-Beam Microstrip Patch Reflectarray," *IEEE Trans On Antennas And Propagation*, vol. 47, no. 7, July 1999.

[69] A. Georgiadis, A. Collado, and J. Perruisseau-Carrier, "Patents on Reconfigurable Reflectarray antennas," *Recent Patents on Electrical Engineering*, pp. 19-26, 2009.

[70] A.G. Roederer, "Reflectarray Antennas," *Proceedings of EUCAP*, 2009.

[71] J. Huang, "Analysis of a Microstrip Reflectarray Antenna for Microspacecraft Applications," *TDA Progress report*, no. 42-120, Feb 1995.

[72] E. Carrasco, M. Barba, and J. Encinar, "Reflectarray element based on aperture-coupled patches with slots and lines of variable lengths," *IEEE Trans. Antennas Propagat.*, vol.

55, no. 3, pp. 820-825, March 2007.

[73] D. Cadoret, A. Laisne, R. Gillard, L. Le Coq, and H. Legay, "Design and measurement of a new reflectarray antenna using microstrip patches loaded with slot," *Electronics Letters*, vol. 41, no. 11, pp. 623-624, May 2005.

[74] R. Hodges and M. Zawadzki, "Design of a large dual polarized Ku-band reflectarray for spaceborne radar altimeter," *IEEE APS symposium*, pp. 4356-4359, June 2005.

[75] E. Carrasco, J. A. Encinar, and M. Barba, "“Bandwidth Improvement in Large Reflectarrays by Using True-Time Delay," *IEEE Trans. on Antennas and Propagat*, vol. 56, pp. 2496 – 2503, Aug 2008.

[76] C. Apert, T. Koleck, P. Dumon, T. Dousset, and C. Renard, "ERASP a new ReflectArray Antenna for Space Application," *Proceedings of EUCAP*, 2006.

[77] C. Cheymol, T. Dousset, P. Dumon, M. Labeyrie, and C. Renard, "A X-band Electronically Scanned ReflectArray Antenna for Space Telemetry," *Proceed. of EUCAP*, 2009.

[78] V. Ziegler and P. Nicole, "RETINA: Reliable, tunable and inexpensive antennas by collective fabrication processes," *Proceedings of the 5th Communities Aeronautics Days, Austria*, June 2006.

[79] C. Chekroun, T. Dousset, C. Renard, M. Déjus, and J-M. Lopez, "ERASP : A Light Weight, Low Power Consumption Phased Array Antenna Concept for a X Band Spaceborne SAR System," *Internationnal Conference on radar systems*, 2004.

[80] J. R. Zamudio and N.A. Martynyuk, "Reflectarray based on three-bit spatial phase shifters: Mathematical model and technology of fabrication," *Proceedings of EUCAP*, 2009.

[81] L. Boccia, F. Venneri, G. Amendola, and G.Di Massa, "Application of Varactor Diodes For Reflectarray Phase Control," *IEEE Symps*, 2002.

[82] P. Barthia and J. Bahl, "Frequency agile microstrip antennas," *Microwave Journal*, 1982.

[83] S. V. Hum, M. Okoniewski, and R. J. Davies, "Modeling and design of electronically tunable reflectarrays," *IEEE Transactions on Antennas and Propagation*, vol. 55, no. 8, pp. 2200-2210, 2007.

[84] Gabrial M. Rebeiz, "RF MEMS Theory, Design and Technology," *John Wiley and sons*, 2003.

[85] G.M. Rebeiz and J.B. Muldavin, "RF MEMS switches and switch circuits," *IEEE Microwave Magazine*, pp. 59-71, Dec 2001.

[86] G. McFeetors and M. Okoniewski, "Distributed MEMS Analog Phase Shifter With Enhanced Tuning," *IEEE Micr. AND Wireless Compenents Letters*, vol. 16, Jan 2006.

[87] H. Legay, B. Pinte, M. Charrier, Afshin ZIAIE, E. Girrard, and R. Gillard, "A steerable reflectarray Antenna with MEMS Controls," *IEEE Int. Proc Symp. on Phased Array Syst. and Tech*, pp. 494-499, Oct 2003.

[88] M. Charrier, T. Dean, A. Ziaei, H. Legay, B. Pinte, R. Gillard, E. Girard, and R. Moulinet, "Phase shifting cell for an antenna reflector," *US patent 2005/0219125*, 2005.

[89] H. Salti, E. Fourn, R. Gillard, and H. Legay, "Robustness Optimization of MEMS-Based Reflectarray Phase-Shiting cells," *Proceeding of EUCAP*, pp. 3742 – 3728, March 2009.

[90] H. Salti, E. Fourn, R. Gillard, E. Girard, and H. Legay, "Pharmacist Cross" phase-shifting cell loaded with MEMS switches for reconfigurable reflectarrays," *Proceedings of EUCAP*, April 2010.

[91] T. Makdissy, R. Gillard, E. Fourn, E. Girard, and H. Legay, "Dual-Annular Slot Phase-Shifting Cell Loaded With MEMS Switches For Reconfigurable Reflectarrays," *Workshop ESA*, 2011.

[92] H. Rajagopalan, Y. Rahmat-Samii, and W. A. Imbriale, "Reconfigurable patch-slot reflectarray elements using RF MEMS switches : a subreflector wavefront controller," *IEEE APS International Conference*, June 2007.

[93] F.A. Tahir, H.Haubert, and E. Girard, "Optimization of MEMS-Controlled Reflectarray Phase Shifter Cell," *IET Microwaves Antennas. Propagat.*, pp. 271-276, Feb 2011.

[94] H. Salti, E. Fourn, R. Gillard, H. Legay, and H. Aubert, "MEMS Breakdown effects on the radiation of a mems based reconfigurable reflectarray," *Proceedings of Eucap*, 2009.

[95] J. P. Gianvittorio and Y. Rahmat-Samii, "Reconfigurable patch antennas for steerable reflectarray applications," *IEEE Trans. Antennas and Prop.*, vol. 54, pp. 1388-1392, May 2006.

[96] H. Legay, G. Caille, E. Girard, P. Pons, P. Calmon, E. Perret, H. Aubert, J. P.Polizzi, A. Laisné, R. Gillard et al., "MEMS controlled phase-shift elements for a linear polarised reflectarray," *28th ESA Antenna Workshop*, pp. 434-439, May 2005.

[97] S. V. Hum, G. McFeetors, and M. Okoniewski, "Integrated MEMS Reflectarray elements," *Proc. EuCAP*, 2006.

[98] S. V. Hum, M. Okoniewski, and R. J. Davies, "Modeling and Design of Electronically Tunable Reflectarray," *IEEE Trans Ant and Prop*, vol. 55, 2007.

[99] O. Vendier, M. Paillard, H. Legay, C. Schaffauser, S. Forrestier, G. Caille, C. Drevon, and J.L. Cazaux, "Main achievements to date toward the use of RF MEMS into space satellite payloads," *IEEE Symp*, 2005.

[100] J. Perruisseau-Carrier, E. Girard, and H. Legay, "Analysis of a Reconfigurable Reflectarray Cell Comprising a Multitude of MEMS Control Elements," *Proceedings of EUCAP*, 2010.

[101] A. Moesinger, R. Marin, S. Mueller, J. Freese, and R. Jakoby, "Electronically reconfigurable reflectarrays with nematic liquid crystals," *Electronic Letters*, vol. 42, pp. 899-900, Aug 2006.

[102] W. Hu, M.Y. Ismail, R. Cahill, H.S. Gamble, R. Dickie, V.F. Fusco, D.Linton, S.P. Rea, and N. Grant, "Tunable liquid crystal reflectarray," *IEE Electronics Letters*, vol.

42, 2006.

[103] W. Hu, M.Y. Ismail, R. Cahill, J.A. Encinar, V.F. Fusco, H.S. Gamble, D. Linton, R. Dickie, N. Grant, and S.P. Rea, "Liquid crystal based reflectarray antenna with electronically switchable monopulse patterns," *IET Electron. Lett.*, pp. 744 -745, 2007.

[104] W. Hu, R. Cahill, J.A. Encinar, R. Dickie, H.S. Gamble, V.F. Fusco, and N. Grant, "Design and Measurement of Reconfigurable mm Wave Reflectarray Cells with nematic Liquid Crystal," *Proc IEEE Antennas and Propagation*, vol. 56, pp. 3112-3117, 2008.

[105] R. Romanofsky, "Special issues and Features of a Scanning Reflectarray Antenna Based on Ferroelectric Thin Film Phase Shifters," *Proceedings of EUCAP*, 2006.

[106] W.J. Taft, A. Katz, G.A. Silverman, W.J. Soohoo, A. Jacomb Hood, and G.J. Matyas, "MEMS Reflectarray Antenna for Satellite Applications," *US Patent n°7030824*, Avril 2006.

[107] "Agile Reflectarray Antennas for Security and Communications," *http://www.arascom.eu/*.

[108] E. Carrasco, M. Arrebola, M. Barba, and J. A. Encinar, "Shaped-Beam Reconfigurable Reflectarray with Gathered Elements in an Irregular Lattice for LMDS Base Station," *Proceedings of EUCAP*, 2011.

[109] H. Legay, D. Bresciani, E. Girard, R. Chiniard, E. Labiole, O. Vendier, and G. Caille, "Recent Developments on Reflectarray antennas at Thales Alenia Space," *Proceedings of EUCAP*, 2009.

[110] S. Montori, L. Marcaccioli, R.V. Gatti, and R. Sorrentino, "1-bit RF-MEMS-Reconfigurable Elementary Cell for Very Large," *GSMM, Incheon, Korea*, 2010.

[111] J. Lanteri, C. Migliaccio, J. Ala-Laurinaho, M. Vaaja, J. Mallat, and A.V. Raisanen, "Four-beam reflectarray antenna for Mm-waves: Design and tests in far-field and near-field ranges," *Proceedings of EUCAP*, 2009.

[112] J. A. Zornoza and J. A. Encinar, "Three-layer printed reflectarrays for contoured beam space applications," *IEEE Trans. Antennas Propag*, vol. 52, pp. 1138–1148, 2004.

[113] P. Nayeri, F. Yang, and A. Z. Elsherbeni, "Design and Experiment of a Single-Feed Quad-Beam," *IEEE Trans. On Ant. Pro.*, vol. 60, 2012.

[114] M. Arrebola, J. A. Encinar, and M. Barba, ", “Multifed Printed Reflectarray With Three Simultaneous Shaped Beams for LMDS Central Station Antenna," *IEEE Trans. Antennas Propag*, vol. 56, no. 6, pp. 1518-1527, June 2008.

[115] D.C. Chang and M.C. Huang, "Feasibility study of ercting cosecant pattern by palanr microstrip reflectarray antenna," *AMPC 93*, vol. 2, pp. 19-24, 1993.

[116] H. Legay, D. Bresciani, E. Labiole, R. Chiniard, E. Girard, G. Caille, D. Calas, R. Gillard, and G. Toso, "A 1.3 M earth Deck Reflectarray For a KU Band Contoured Beam Antenna," *Workshop ESA*, Oct 2011.

[117] L. Moustafa, R. Gillard, F. Peris, R. Loison, H.Legay, and E. Girard, "The Phoenix Cell: A New Reflectarray Cell With Large Bandwidth and Rebirth Capabilities," *IEEE*

Antennas and wireless Prop. LETTERS, vol. 10, pp. 71-74, 2011.

[118] J. Maurel, P. Lepeltier, P. Pelenc, and B. Trancart, "Conception des antennes spatiales pour les charges utiles complexes de télécommunication," *Revue des télécommunications d'Alcatel*, vol. 4, pp. 1-8, 2001.

[119] K. Aok, i S. Makino, T. Katagi, and K. Kagoshima, "Design method for an offset dual-shaped reflector antenna with high efficiency and an elliptical beam," *IEEE APS*, 1993.

[120] D.M. Pozar, S.D. Targonski, and H.D. Surigos, "Design of millimeter-wave microstrip reflectarrays," *IEEE Trans. Antennas. Propagation*, vol. 45, pp. 287-296, Feb 1997.

[121] J. Huang, C.Han, and K.chang, "A cassegrain offset-fed dual band reflectarray," *IEEE APS Symposium*, pp. 2439-2442, July 2006.

[122] M. Arrebola, L. De Haro, J. A. Encinar, and L. F. de la Fuente, "Contoured beam gregorian antenna with a reflectarray as sub-reflector," *Proccedings of Eucap*, 2007.

[123] C. Tienda, J. A. Encinar, S. Montor, R. Vincenti Gatti, M. Arrebola, and R. Sorrentino, "Dual-Reflectarray Antenna for Bidirectional Satellite Links in Ku-band," *Proceedings of EUCAP*, 2011.

[124] J. Encinar, M. Arrebola, L. F. Fuente, and G. Toso, "A Transmit-Receive Reflectarray Antenna for Direct Broadcast Satellite Applications," *IEEE Transactions on Antennas and Propagation*, pp. 3255 -3264, 2011.

[125] D. Shaubert and T. Metzler, "Scattering from a stub loaded microstrip antenna," *Antennas and Propagation Society Internationnal Symposium*, pp. 446-449, 1989.

[126] T.A. Metzler and D.M. Pozar, ""Analysis of a Reflectarray Antenna Using Microstrip Patches of Variable Size," *Electronics Letters*, vol. 29, pp. 657-658, 1993.

[127] J. Encinar and C. WAN, "Efficient computation of generalized scattering matrix for analysing multilayered periodic structures," *IEEE Trans. Antennas Propag.*, vol. 43, pp. 1233–1242, 1995.

[128] J. Encinar, L.Sh. Datashvili, J.A. Zornoza, M. Arrebola, M. Sierra-Castaner, J.L. Besada-Sanmartin, H. Baier, and H. Legay, "Dual polarisation dual-coverage reflectarray for space applications," *IEEE Trans. Antennas Propag.*, vol. 54, pp. 2827–2837, 2006.

[129] J. A. Zornoza, R. Leberer, J. A. Encinar, and W. Menzel, "Folded multi-layer microstrip reflectarray with shaped pattern," *IEEE Trans. Antennas Propag.*, vol. 54, pp. 510-518, 2006.

[130] T. Bialkowski, Feng-Chi E., and Marek E., "An equivalent waveguide approach to designing ofreflect arrays with the use of variable-size microstrip patches," *Microwave and Optical Technology Letters*, vol. 34, pp. 172-175, 2002.

[131] www.ansoft.com,.

[132] K. Bhattacharyya, "Phased Array Antennas, Floquet Analysis and Synthesis," *A John Wiley and sons*, 2006.

[133] D. H. Schaubert and D. M. Pozar, "Analysis of an Infinite Array of Rectangular Microstrip Patches with Idealized Probe Feeds," *IEEE Trans. on Antennas Propagat.*,

vol. 32, pp. 1101-1107, 1989.

[134] M. Albooyeh, N. Komjani, and M.S. Mahani, "A Circularly Polarized Element for Reflectarray Antennas," *IEEE Antennas and Propagation Letters*, 2009.

[135] E. Girard, R. Moulinet, R. Gillard, and H. legay, "An FDTD optimization of a circularly polarized reflectarray unit cell," *IEEE AP-S/URSI symposium*, pp. III-136-139, 2002.

[136] D. Cadore, A. Laisné, M. Milon, R. Gillard, and H. Legay, "FDTD analysis of reflectarray radiating cells," *IEEE ACES*, 2005.

[137] H. Oraizi and K. Keyghobad, "Phase Response of Microstrip Reflectarray Elements by FDTD analysis," *Workshop on Computational Electromagnetics in Time-Domain*, 2007.

[138] M.-A. Milon, D. Cadoret, R. Gillard, and H. Legay, "Surrounded-element approach for the simulation of reflectarray radiating cells," *IET Microwaves Antennas and Propagation*, pp. 289-293, 2007.

[139] P. De Via, A. Freni, F. Vipiana, P. Pirinoli, and G. Vecchi, "Fast analysis of large finite arrays with a combined multiresolution – SM/AIM approach," *IEEE Trans. Antennas Propag.*, vol. 54, pp. 3827–3832, 2006.

[140] I. Gonzalze, E. Garcia, F. Saez De ADana, and F. CAtedra, "Computer tool for the analysis and design of periodic structures taken into account their real size and shape," *Proc. 29th ESA Antenna Workshop on Multiple Beams and Reconfigurable Antennas*, 2007.

[141] M. Zhou, S. B. Sørensen, O. S. Kim, S. Pivnenko, and G. Toso, "Investigations On Accurate Analysis Of Microstrip Reflectarrays," *Proceedings of the 33rd ESA antenna workshop on Challenges for Space Antenna Systems, Estec, Netherland*, October 2011.

[142] H. Aubert, "The Concept of Scale-changing Network in Global Electromagnetic Simulation of Complex Structures," *Progress In Electromagnetics Research B*, vol. 16, pp. 127-154, 2009.

[143] F. A. Tahir and H. Aubert, "Electromagnetic modeling of microstrip reflectarrays using scale changing technique," *International Journal of Numerical Modelling: Electronic Networks, Devices and Fields*, 2012.

[144] Y. Rahmat-Samii, L. I. Williams, and R. G. Yoccarino, "The UCLA bi-polar planar-near-field antenna measurement and diagnostics range," *IEEE Antennas Propag. Mag*, vol. 37, Dec 1995.

[145] M. Arrebola, J.A Encinar, and M. Barba, "Evaluation of a two layer printed reflectarray in K-band with three shaped beams," *Proc. 29th ESA Antenna Workshop on Multiple Beams and Reconfigurable Antennas*, 2007.

[146] M. Arrebola, Y. A. lvarez, J. Encinar, and F. Las-Heras, "Accurate analysis of printed reflectarrays considering the near field of the primary feed," *IET Microw. Antennas Propag*, vol. 3, pp. 187–194, 2009.

Chapter II

MODELING METHODS DEVELOPED DURING THE THESIS

I - Introduction

We have seen in chapter one that a reflectarray is a hybrid antenna that emerged from phased arrays and parabolic reflectors. Indeed, the radiating aperture is composed of hundreds or thousands of elementary units, where each unit will diffract the incident electromagnetic field coming from a feed antenna with the appropriate phase shift in order to focus or shape the beam. Because of that, the reflectarray requires a special attention to accurately calculate the required phase shifts and to predict its radiation pattern. Several analysis and synthesis techniques were developed by the community of reflectarray antennas. Significant advances have been made on reflectarray modeling to analyze their final electromagnetic performances; nevertheless some interesting behaviors are not well detailed.

It is well known by the community that the performances of phased arrays are affected by the mutual coupling in many aspects. At first the input impedances of the cells are subject to a change versus a given beam's direction. This problem is related to the SWR (Standing-wave Ratio) of the active antenna. Secondly, some cells cannot accept and radiate the energy; these cells are called blind cells.

The similarity between the array antenna and the reflectarray is obvious. However, the analysis and synthesis methods which are presented in the literature are unable to find this connection between the reflectarray and the phased array antenna besides than the standard use of the scattering parameters in the calculus of the reflected phase of the cell.

During this thesis, we shall focus on the effects of the mutual couplings that occur between the cells on the behavior of the antenna. Indeed, we will take advantage of the array's heritage during the last 30 years and integrate this accumulated knowledge to design the reflectarray panel.

To achieve this goal, we propose an architecture and analytical formalism to treat the electromagnetic (EM) problems of the reflectarray. This architecture requires adding EM ports at the reflectarray cells. The EM ports are there for a good reason and the potential benefits of using them in a reflectarray analysis will be discussed. Our analysis and synthesis procedure should deliver improved performances to the reflectarray. Therefore, we want to insist on the accurate coupling modeling impact rather than computation time. The analysis and synthesis technique which is presented in this chapter is the substance of my thesis.

II - Architecture of the reflectarray selected for our development

II.1 - Reflectarray cells placed in the near-field of the feed antenna and connected to EM ports

To elevate some of the problematic/approximations listed in the state of art of the analysis techniques, we propose a full-wave approach to analyze the reflectarray antenna. In our approach we design the entire reflectarray antenna including the real dimensions of the finite panel and the exact position of the feed antenna using a 3D EM simulator.

In this approach, we have limited the study to reflectarrays satisfying the conditions depicted in Fig. II.1:

1. The panel is designed with identical periodic radiating elements such as microstrip patches
2. Each cell is connected to a single-mode EM port.

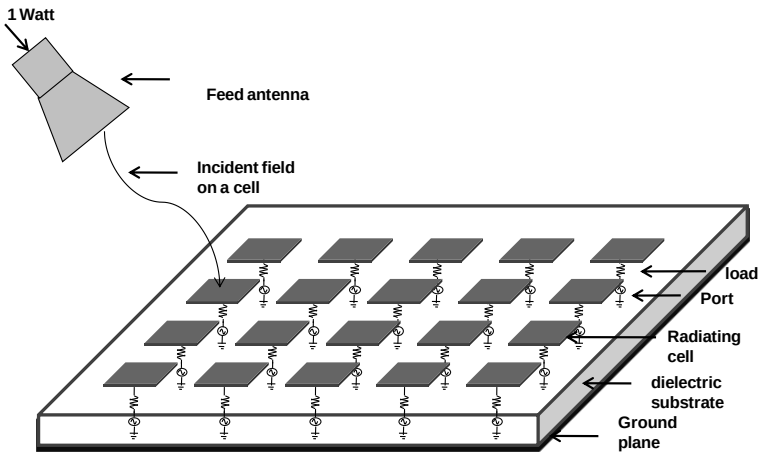

Figure. II.1. *Full-wave simulation principle of the reflectarray antenna. Each cell is connected to EM access to retrieve the S-parameters*

Under these conditions, the reflectarray cells are no longer phase shifting elements and radiating elements at the same time. Instead, we shall uncouple the radiating elements from the phase compensation elements. The panel is responsible only of the electromagnetic radiation through the cells. The phase compensation elements are located under the ground plane and they are controlled by digital or DC bias voltage to generate the required phase

shifts. The phase shifting elements are reactive loads connected behind the cells through vias drilled through the dielectric substrate, as seen in Figure.II.1.

For passive structures that employ reflectarray cells connected to stubs with variable lengths the proposed architecture can be used to compute the required phase shift response. This is possible by connecting below the panel reactive loads to the stubs that will replace the variable-length stubs. The phase shift control will be placed under the panel.

This configuration has many advantages. A major one is to allow an easier analysis of the radiating panel; it will be treated as a usual finite periodic array composed of hundred of elements excited with specifical excitations weightings. Then, we shall study the mutual couplings that occur between the cells in order to evaluate their effects on the behavior of the panel. Secondly, the electric circuits combining the reactive loads and the DC/AC voltage control are totally invisible to the feed antenna thus they will not disturb or be disturbed by the incident/reflected electromagnetic fields components.

For the analysis purpose the cells are connected to single-mode EM access or ports to retrieve some parameters such as the electric voltages and currents, the S-parameters, the illumination intensity … The ports will also allow us to have a complete knowledge about the controlled fields radiated by the cells from the static parasitic diffracted fields by the ground plane and dielectric substrate. Indeed, we will demonstrate that the EM ports allow us to treat the reflectarray problem in the same manner as "*classic phased array antennas*".

The entire reflectarray will be then studied and analyzed under these settings. It might look expensive in term of time and memory consumption; however we want to insist on the accurate analysis and pattern synthesis to design and explain reflectarrays properties, rather than reducing the computation cost with approximations (e.g. infinite periodic models).

II.2 - **Reasons for such an architecture of reflectarray**

The study is based on a reflectarray panel of identical cells connected to the reactive loads, acting as phase shifting elements. These loads are located at the rear of the panel, in order to minimize the interactions between the radiating elements and the loads. Moreover, a significant advantage of this architecture is to separate the study in an electromagnetic problem (for the radiating elements) and a circuit formalism (for the loads). Both domains are linked through electromagnetic ports interfaces, used to solve the problem with a great accuracy, especially in terms of energy budget. From a designer's point of view, such an

architecture is interesting because the loads can be directly soldered on a printed circuit board (PCB), linked to the radiating elements with via holes. The PCB can also be used to add drivers, distribute DC bias and circuits in the case of a reconfigurable reflectarray.

II.3 - **Features offered by the proposed analysis technique**

The features offered by this approach are summarized as follows:

a. The cells are positioned in the near-field region of the feed antenna. The illumination on the cells is no longer approximated from an infinite array excited with plane waves or Floquet modes with different incidences angles.

b. A Full-Wave simulation gives more accurate results when compared to 'Local periodicity' but at the expenses of a higher computation time.

c. The cells are no longer treated as reflecting elements whose the famous S-curve phase response versus the frequency is calculated. It is a novel approach where we treat the panel as an array of elements separated from the phase compensating elements.

d. The full-wave simulation grants an accurate and direct access to the incident EM fields on the panel as well to the reflected and reradiated fields. A main advantage of this technique is to discriminate the contribution of the RCS (Radar Cross Section) and the reradiated field. As a consequence, it should allow an accurate synthesis of the final radiation pattern, leading to higher performances.

e. The approach is flexible, allowing an easy integration of the scattering matrix [S] in the calculus of the phase shifts at the cells and in the final radiation pattern.

f. The discrete ports should give access to the electrical currents and voltages at each cell, as well as the S-parameters. We will make use of those in two separate phases. In the first phase, to calculate the required phase shifts. In the second phase to estimate the energetic contribution of each cell. Contrary to the classic assumption, the energy radiated by the cells is not related only to the illumination law; it is given by the illumination law, the scattering matrix and the objective radiation pattern.

g. Two simulations are required to determine the inputs parameters for the analytical formalism. The final simulation validates the computed reactive loads. Once the

analytical formalism is validated for the pattern synthesis, the parametric studies for the reflectarray synthesis can be done analytically very quickly.

h. The full-wave simulation can be used as a virtual reflectarray prototype to validate the outcome of a 'local periodicity approach' reflectarray synthesis.

The limitations of this approach are:

a. Since the entire reflectarray is designed and simulated the computation domain is big. A powerful machine with an important size of memory is required for a full-simulation.

b. All the reflectarray cells must be connected to discrete ports in order to compute the required input parameters in a full-wave simulation. It is manageable when the panel contains hundreds of elements but it will increase the complexity for more elements.

III - Setting up the equations of the problem

The proposed analysis and synthesis technique of the reflectarray antenna is decomposed in three separated phases, as illustrated in Fig .II.2. In this section, I will describe each phase apart in details. For this purpose I will define the terms of incident power waves b_i and reflected power waves a_i in different electric scheme models. Then, I will present in one equation the connection between these different parameters. Note that I will write the different equations in a generalized form including the impedances of the cells and the discrete ports, even if I have performed the reactive loads synthesis versus 50Ω normalized impedances. I mentioned this to keep in mind that our analysis and synthesis method can be applied to different values of ports impedances. The mutual couplings between the cells, held responsible for the degradation of many antenna performances, are included in this synthesis thanks to a scattering matrix [S].

To sum up, we analyze the reflectarray as depicted in Fig .II.2; we connect discrete ports to the reflectarray cells and we retrieve the amount of power coupled at each cell, designated as 'incident coupled power waves $b_{0\,i}$. Then we define an objective radiation pattern and for this matter we synthesize the reactive loads which will take in consideration the different EM behaviors of the reflectarray antenna.

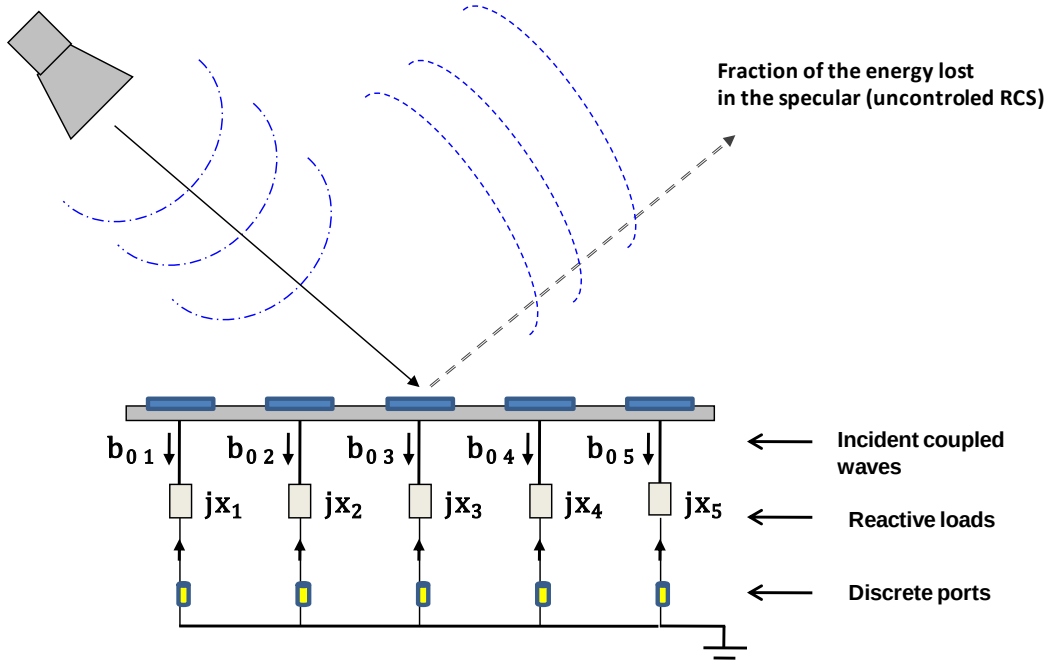

Figure. II.2. *General analysis technique of the reflectarray*

The incident coupled waves $b_{0\,i}$. are a different representation of the incident electromagnetic fields on the cells and are accessible thanks to the ports added to the full-wave simulation. Of course, not the entire energy radiated by the feed antenna is coupled inside the ports. The remaining energy is contained in the uncontrollable diffracted field pattern $E_{diffracted}(\theta,\Phi)$ (RCS). The diffracted field pattern is a mixture of parasitic fields that must be minimized. One portion is contained in the spillover pattern. Another portion is diffracted on the edges of the panel, or simply not accepted inside the ports.

Our reflectarray analysis depends mainly on $b_{0\,i}$. We shall synthesis the EM response and behavior of a panel which is excited by the incident coupled waves $b_{0\,i}$. To satisfy this objective the reactive loads are added behind the cells.

In a more detailed form, let us look at Fig .II.3 to understand how we treat the reflectarray antenna. We decompose the problems of the reflectarray in three separated phases. We treat each phase apart and we compute several EM parameters which are essential to the reactive load synthesis. The connection between these parameters shall be explained inside the analytical formalism.

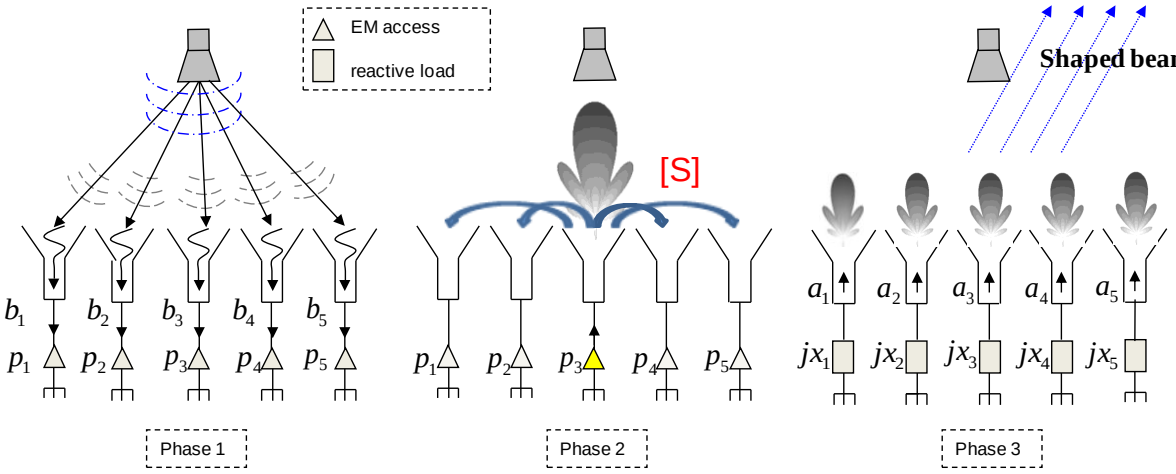

Figure. II.3. *Decomposition of the reflectarray analysis in three phases*

In phase one, the reflectarray cells operate in reception mode, capturing the incident field from the feed, and coupling it into power waves $\{b_{0i}\}$. This is possible thanks to a full-wave simulation where we add ports to the cells and match them with the cells characteristic impedances. A port absorbs the incident power arriving at a cell and enables the calculation of the T transmission parameter from the feed. Since the injected power at the feed is 1Watt by default, the T-parameters lead directly to the coupled waves $\{b_{0i}\}$ in the cells. Therefore these parameters represent directly the amplitude weighting and the phase of the incident wave at

each cell. The remaining energy is lost in the diffracted fields pattern or in the panel's materials.

In phase two, we characterize the scattering parameters of the panel. The reflectarray panel is treated as a classic array. In a full-wave environment we excite the cell near to the center of the panel and compute the scattering parameters [S] and the active radiation pattern $\overrightarrow{F(\theta,\varphi)}$. It should be noted that due to the periodic assembling of the identical cells, these parameters are assumed to be the same for the other cells.

In phase three, the cells operate in radiating mode and are connected to reactive loads through the ground plane. Each cell is excited with a complex excitation weighting called $\{a_i\}$. Thanks to a specific distribution for $\{a_i\}$ on the panel, the reflectarray steers the beam in any desired direction as we are about to see in the following module.

III.1 - **Electrical Circuit model of the reflectarray antenna**

The global electrical model of the reflectarray design is presented in Fig .II.4. The origin of this electrical scheme was developed in [1] for array antennas. The scheme was developed to match to a reflectarray antenna. The only difference from a classical array cell and a reflectarray cell is that in the reflectarray case, the cells are no longer excited directly from a distribution circuit. The cells are excited by the incident coupled waves.

The phase shift that must be introduced at each cell to produce a focused beam or shaped beam can be generated in a first approximation by a reactive load which can be capacitive or inductive. The complex impedance of the reactive load includes a real resistance R_{load} and a purely imaginary 'JX_{load}', where 'X' is the reactance of the load.

In Fig. II.4 we can notice at each antenna 'i' an incident power wave $b_{tot\ i}$ and a reflected power wave a_i, a reflection coefficient Γ_i resulting from an ideal reactive load $Z_{Xi} = JX_i$. Globally we can notice incident waves b_{0i} and a scattering matrix [S]. At each cell, two sources of currents can be defined even if they are not shown in the figure. The first source is the current I_{feed} induced by the electromagnetic fields coming from the feed antenna. The second source is the current $I_{coupling}$ induced by the radiation of the surrounding cells on the panel.

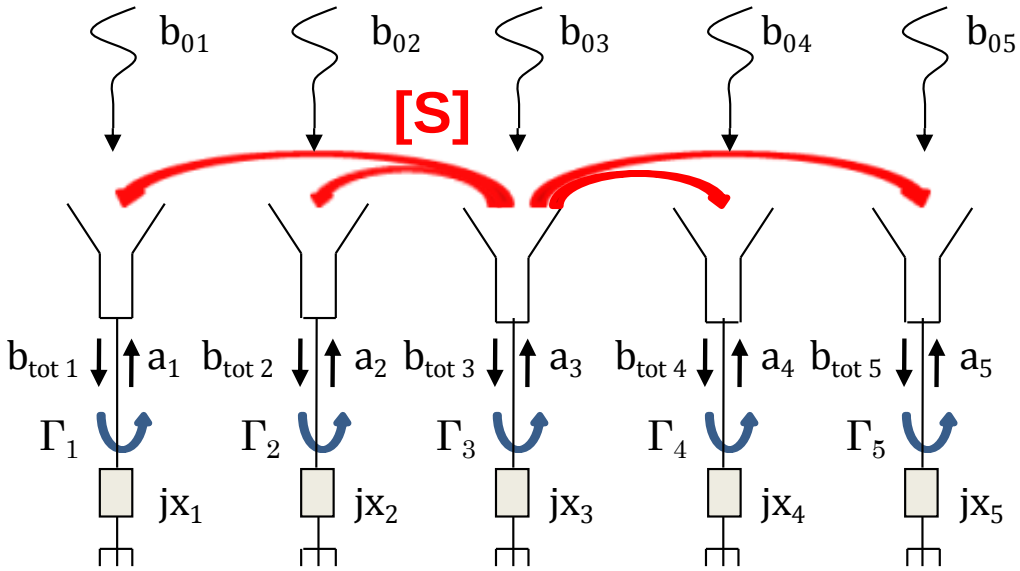

Figure. II.4. *Electrical Circuit Model of a reflectarray*

The two sources are added - using the superposition theorem – leading to the total electric current I_i which circulate between the cell and the ground plane. To help understanding this model lets us divide it into several schemes and analyze them each apart. These various schemes are suitable to all the cells of the panel.

III.1.1 - Detailed description of the proposed electrical circuit model

In the first scheme shown in Fig .II.5, the reflectarray is configured in reception mode (**phase one** Fig. II.3). The feed antenna is excited and each cell is connected to normalized matched impedances. Each incident field induces an electrical current I_{feed} at a given cell. Let us define $b_{0\,i}$ as the coupled incident power wave from the feed to a cell and $a_{0\,i}$ the reflected wave from the port. The objective is to compute the amount of power that a cell is absorbing from the feed. As a natural consequence, we can estimate easily the diffracted parasitic pattern on the panel $\vec{E}_{\text{diffracted}}\ (\theta, \varphi)$.

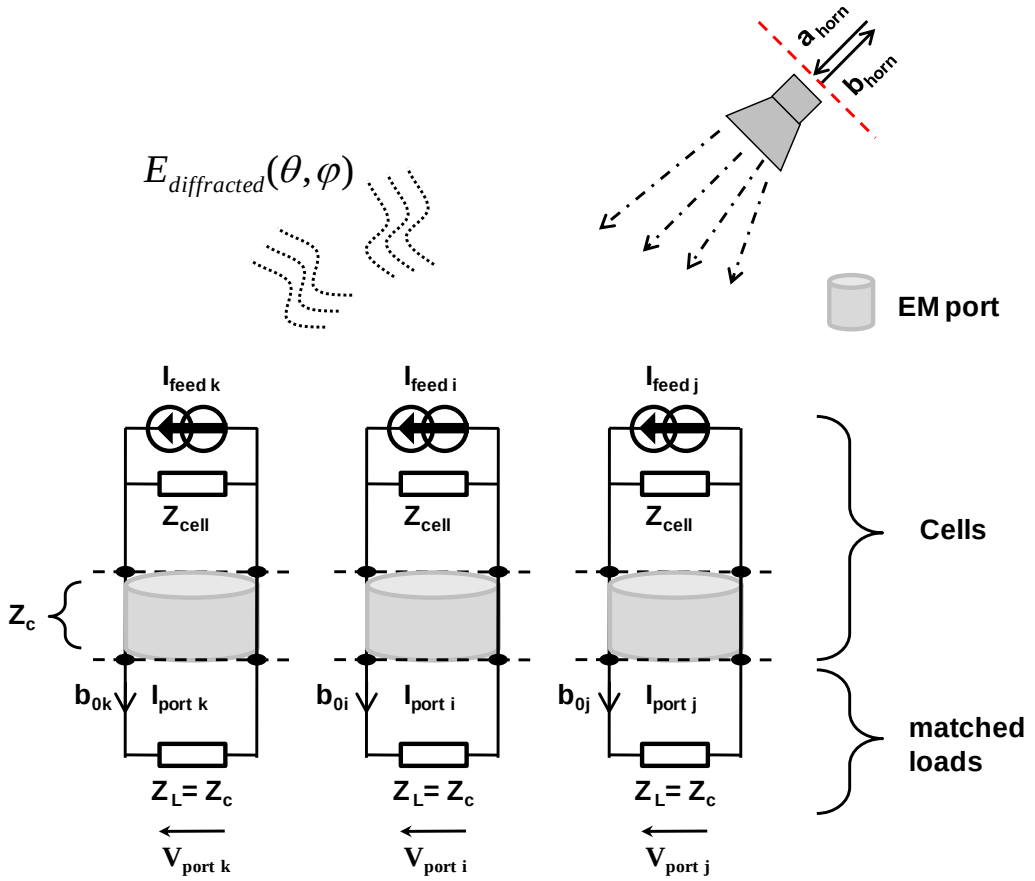

Figure. II.5. *Scheme nb '1' of the electrical circuit model dedicated for the phase one*

The power $b_{0\,i}$ received by a cell from the feed antenna is shown in Eq. II.1. Since the cells are matched and not excited, this power is related directly to the coupling coefficient $S_{i,horn}$ from the feed horn to the cell.

$$(II.1) \qquad S_{i,horn} = \frac{b_{0\,i}}{a_{horn}}$$

The current I_{feed} and voltage V_{feed} computed at the cell's port are defined versus the incident power waves, as in Eq.II.2. The return loss at the feed horn antenna is given in Eq.II.3.

$$(II.2) \qquad \begin{cases} I_{port\ i} = \frac{b_{0i}}{\sqrt{Z_c}} \\ V_{port\ i} = Z_c * I_{port\ i} = \sqrt{Z_c} * (b_{0\,i}) \end{cases}$$

$$(II.3) \qquad \Gamma_{horn} = \frac{b_{horn}}{a_{horn}} \qquad RL = 20 \times log_{10}(\Gamma_{horn})$$

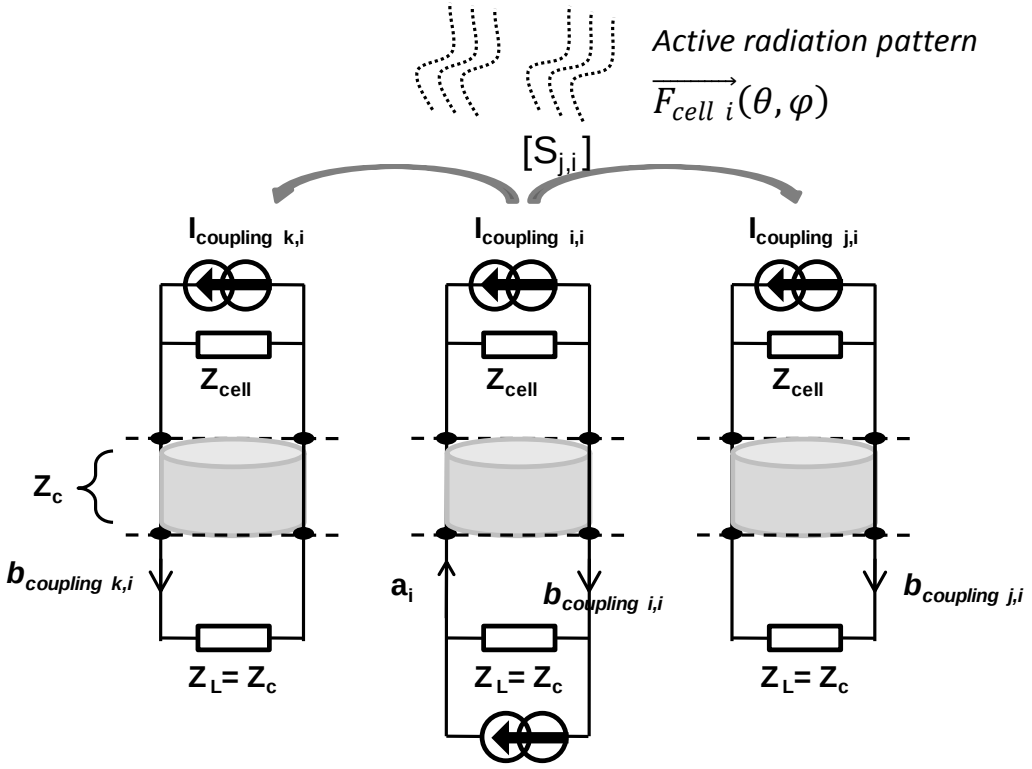

Figure. II.6. *Scheme no '2' of the electrical circuit model dedicated for the mutual couplings*

In the **second scheme** shown in Fig .II.6, one cell is excited and the surroundings cells are not excited and connected to normalized impedances. The reflectarray is configured in **phase 2** (Fig .II.3). We characterize the scattering matrix [S] and the active element pattern $\overrightarrow{F_{cell}}$. The computed S-parameters are illustrated in Eq.II.4. The relation between the excitation of one cell 'i' and the coupling wave 'j' is defined by the scattering vector S_{ji} as given by Eq.II.4.

$$(II.4) \qquad s_{j,i} = \frac{b_{coupling\ \ j,i}}{a_i} \; ; \quad where \begin{Bmatrix} a_{j\neq i} = 0 \\ j \in [1: n_b] \end{Bmatrix}$$

Where: - nb is the total number of cells on the panels.

-'i' and 'j' are the index of the cells on the panel where $i, j \in [1: n_b]$

If the excited cell is taken in the middle of the panel we can construct [S] by extrapolating the single scattering vector $S_{j,i}$. This approximation is valid since the cells on the panel are identical and arranged in a periodic lattice. The scattering matrix [S] is a nb × nb matrix. It allows evaluating the coupling waves $b_{coupling}$ resulting from any simultaneous excitation, as illustrated in Eq.II.5.

$$(II.5)\quad \begin{cases} \begin{bmatrix} b_{coupling\ 1} \\ \vdots \\ b_{coupling\ i} \\ \vdots \\ b_{coupling\ nb} \end{bmatrix} = [S] \begin{bmatrix} a_1 \\ \vdots \\ a_i \\ \vdots \\ a_{nb} \end{bmatrix} \\ [S] = \begin{bmatrix} s_{1,1} & s_{1,2} & \cdots & s_{1,nb} \\ s_{2,1} & s_{2,2} & & \\ \vdots & & \ddots & \vdots \\ \vdots & & & \\ s_{nb,1} & & & s_{nb,nb} \end{bmatrix} \end{cases}$$

The **third scheme** is shown in Fig .II.7. The cells are connected to reactive. For a cell indexed 'i', the total incident coupled power wave and the complex excitation weighting are $b_{tot\ i}$ and a_i respectively. $b_{tot\ i}$ is the result of the sum of the coupled wave from the feed $b_{0\ i}$ using Eq.II.1 and the mutual couplings from the surrounding cells using Eq.II.4 as illustrated in Eq.II.6.

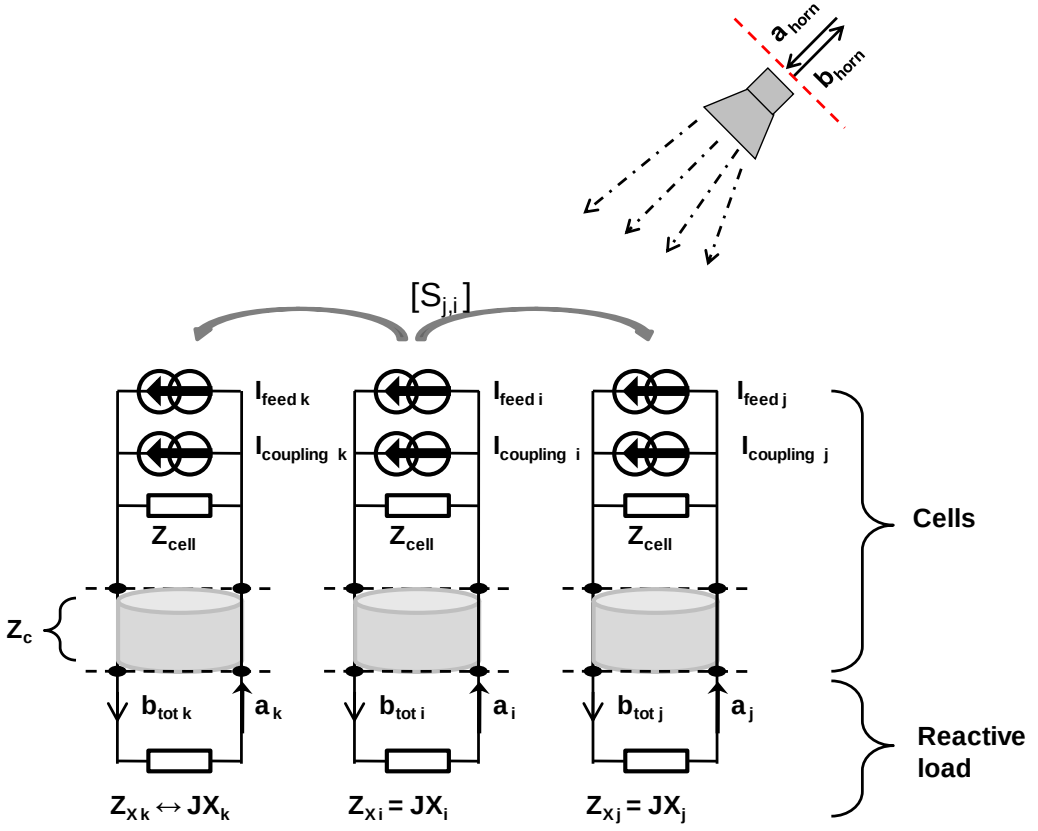

Figure. II.7. *Scheme no'3' of the electric circuit model dedicated for the radiation phase*

$$(II.6)\quad b_{tot\ i} = \left(S_{i,horn} \times a_{horn}\right) + \sum_{k=1}^{nb} s_{i,k} \times a_k$$

The total incident power waves $b_{tot\ i}$ can be related to the weightings a_i via the reflection coefficients Γ_i, as follows:

(II.7) $$a_i = \Gamma_i \times b_{tot\ i}$$

The reflection coefficient between the cell and the equivalent impedance Γ_i is given in Eq.II.8:

(II.8) $$\Gamma_i = \frac{Z_{X\ i} - Z_c}{Z_{X\ i} + Z_c} \approx \frac{JX_i - Z_c}{JX_i + Z_c}$$

I add a note on the electric currents circulating into the cells ports. These currents travel through the reactive loads. They result from the currents induced by the feed horn and the currents induced by the mutual couplings. We can relate them to the total incident coupled waves and the reflected excitation weightings of the cells, as follows (Eq.II.9):

(II.9) $$I_{port\ i} = \frac{b_{tot\ i} - a_i}{\sqrt{Z_c}}$$

III.1.2 - Impedance matching and Power balance Computation for the various schemes

It is crucial to have good awareness of the energy balance of the system. It makes part of the analysis and optimization phase that precedes the design and synthesis process. The proposed electric models allow achieving this objective with a great accuracy and versatility since the incident and reflected waves are expressed in Watt. No wonder why we are able to calculate easily the energy balance of the reflectarray in the various electrical schemes. Usually we focus on the following quantities, which appear in our opinion significant: the power absorbed by the cells from the feed, the power of the diffracted fields pattern and the energetic contribution of the cells (while adding the reactive loads).

We begin with the **first scheme**; the cells are in reception mode. The objective is to maximize the amount of power that the cells could absorb from the feed antenna. As mentioned previously, the controllable reradiated fields (by the cells) boost the efficiency of the antenna, this is achievable if the maximum of energy is transmitted from the feed to the cells and then to the phase shifting circuit. At this stage (phase one Fig.II.3) the cells act like sponges absorbing most of the incident fields without leaking anything back.

In order to maximize the efficiency of the panel we can work with a Floquet model of the cells, illuminated by the dominant mode coming from the feed horn. Variations of certain parameters such as the geometry of the cell allow enhancing the coupling efficiency from the feed to the periodic cells.

With such a particular condition, the cells ports will absorb an important portion of the incident EM fields. In Eq.II.10 we relate the power absorbed by the cells from the feed horn the cells. The remaining power which was not captured by the cells is diffracted into the parasitic RCS of the antenna, designated $\overrightarrow{E_{diffracted}}(\theta,\varphi)$.

$$Power_{absorbed} = \sum_{i=1}^{n}|b_{0\,i}|^2 = \sum_{i=1}^{n}\left|S_{i,horn} \times a_{horn}\right|^2 \quad \textit{(II.10)}$$

As a result of the phase one, the computed radiation pattern is the parasitic pattern RCS which is uncontrollable. The power balance of the first scheme is given as follows (Eq.II.11). Losses can be due to to the dielectric losses $\langle \text{loss}_\varepsilon \rangle$ and conductive losses $\langle \text{loss}_\sigma \rangle$.

$$Power_{total}^{scheme\ 1} = \left\{ \sum_{k=1}^{nb}|b_{0\,k}|^2 + \iint_{\Omega}\left(\left|\overrightarrow{E_{diffracted}}(\theta,\varphi)\right|^2 d\Omega\right) + |b_{horn}|^2 + \langle loss_\varepsilon \rangle + \langle loss_\sigma \rangle \right\} = 1W \quad \textit{(II.11)}$$

We move on to the **second scheme** where we characterize the scattering parameters and the active element pattern. Similarly to the first scheme, all the ports are loaded with matched impedances (ports impedances).

Each cell radiates a portion of its energy or couples the remaining portion to the surrounding cells. The power radiated by a cell is equal to the integral of its active radiation pattern $\vec{F}(\theta,\varphi)$. The remaining power is transmitted to its neighbors by mutual couplings via the scattering coefficient $s_{j,i}$ as given in Eq.II.4. The coupled power from a cell 'j' to the whole cells of the panel is designated $\text{Power}_{\text{coupled j}}$, is given in Eq.II.12.

$$Power_{coupled\ j} = \sum_{k=1}^{nb}\left|b_{coupling\ k,j}\right|^2 = \left(\sum_{k=1}^{nb}\left|s_{k,j}\right|^2\right) \quad \textit{(II.12)}$$

A cell's power is either radiated or transmitted to its surroundings. The power balance of the second scheme is the following (Eq.II.13):

$$Power_{total}^{scheme\ 2} = \left\{ \iint_{\Omega}\left(\left|\vec{F}(\theta,\varphi)\right|^2 d\Omega\right) + \left(\sum_{k=1}^{nb}\left|s_{k,j}\right|^2\right) + \langle loss_\varepsilon \rangle + \langle loss_\sigma \rangle \right\} = 1W \quad \textit{(II.13)}$$

I move now to the **third scheme.** The reflection coefficients at the cells are given in Eq.II.8. One does not need to explain why Γ_i have to be equal to one in magnitude $\{|\Gamma_i| = 1\}$. Let us suppose that the reactive loads are ideal and lossless ($Z_X \approx JX$). The reactive loads are shifting the phase of the incident power waves. The magnitudes of the reflection coefficients defined in Eq.II.14 are equal to one and their arguments contain the phase shift required for the beam synthesis.

(II.14) $$\Gamma_i \approx \frac{JX_i - Z_c}{JX_i + Z_c} \approx e^{j\gamma i} \;\; ; \;\; if \; |\Gamma_i| = 1$$

The power balance of the third scheme is given in Eq.II.15. This equation takes into account the illumination from the feed on the panel, the power radiated by the cells, the mutual coupling between the cells, the diffracted fields pattern, the matching at the feed antenna and the losses.

(II.15) $$Power_{total}^{scheme\ 3} = \left|a_{horn}\right|^2 - \left|b_{horn}\right|^2$$

$$= \left\{ \iint_{\Omega} \left| \left(\sum_{i=1}^{nb} \overrightarrow{F_{cell\ i}}(\theta,\varphi) \times a_i + \overrightarrow{E_{diffracted}}(\theta,\varphi) \right) \right|^2 d\Omega + \langle loss_{\varepsilon} \rangle + \langle loss_{\sigma} \rangle \right\}$$

III.2 - **Analytical formalism for the pattern synthesis**

III.2.1 - Radiation pattern of the reflectarray antenna including the diffracted fields components

One important consequence of using flat reflectarray to shift the incident electromagnetic fields is the appearance of parasitic fields in the specular direction which are added to the useful radiation pattern, as illustrated if Fig .II.7.

When the feed antenna is in offset configuration with respect to the phase shifting panel, the incident waves reach the pixels with different incidence angles θ_p. If we consider that the phase shifting cells are in perfect condition, the reflected electromagnetic fields are divided into two components - in accordance with the laws of optics:

1) The useful EM components designated $\vec{E}_{reradiated}(\theta,\varphi)$, radiating in the desired direction (θ_0,φ_0). This beam is obtained with the proper phase shift distribution on the reflecting elements, as seen in the previous section.
2) The unwanted parasitic EM components $\vec{E}_{diffracted}(\theta,\varphi)$. They are mostly contained in the opposite angular direction of the incident fields. These fields do can interact with ones resulting from the phase shift distribution, which may harm the final performance of the reflectarray antenna. These parasitic fields include the diffracted fields on the ground plane and the metallic surface of the cells, the edges diffracted fields and the spillover patterns.

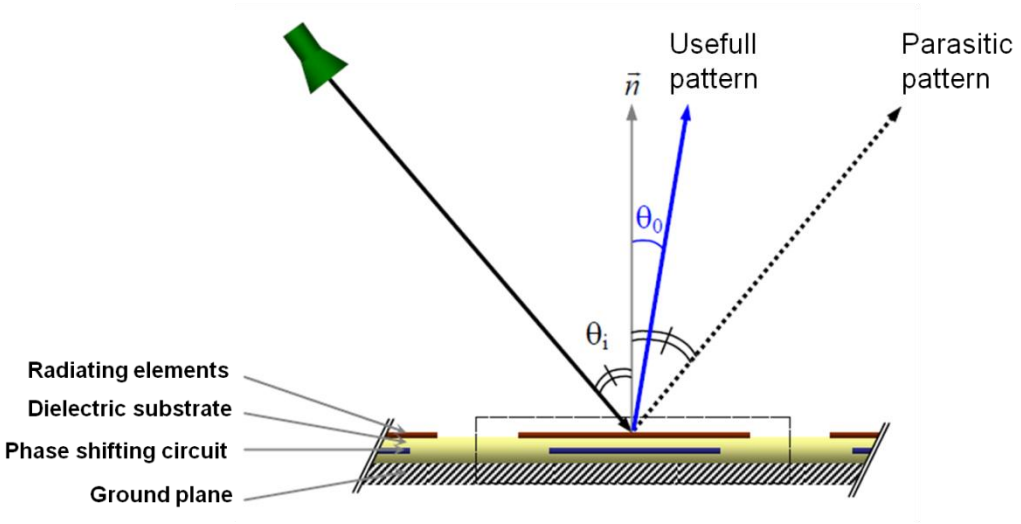

Figure. II.8. *Reflected electromagnetic fields composed from two electromagnetic fields components*

The total radiation pattern of the reflectarray antenna $\overrightarrow{E_{radiated}}(\theta,\varphi)$ is the sum of two major components, the diffracted fields patterns $\overrightarrow{E_{diffracted}}(\theta,\varphi)$and the reradiated fields by the array $\overrightarrow{E_{reradiated}}(\theta,\varphi)$, as depicted in Fig .II.9. The last mentioned contribution is given in Eq.II.16 and Eq.II.17:

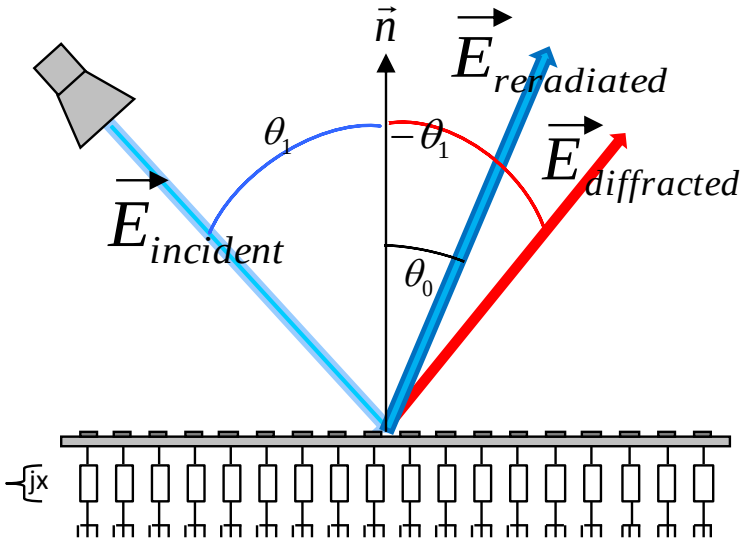

Figure. II.9. *Radiation pattern of reflectarray antennas that employ reactive loads as phase shifting elements*

(II.16) $$\vec{E}_{radiated}(\theta,\varphi) = \vec{E}_{reradiated}(\theta,\varphi) + \vec{E}_{diffracted}(\theta,\varphi)$$

(II.17) $$\overrightarrow{E_{reradiated}}(\theta,\varphi) = \vec{F}(\theta,\varphi) \times \left\{\sum_{i=1}^{nb} a_i([S],\langle b_{0\,i}\rangle,\langle X_i\rangle).e^{-j.\overrightarrow{k_0}.\overrightarrow{V_i}}\right\}$$

Where:

k_0 is the propagation constant in vacuum,

$\vec{F}(\theta,\varphi)$ is the active element pattern referring to the cell in the middle of the panel,

$\langle b_{0\,i}\rangle$ are the incident coupled power waves (scheme n$_o$1 on Fig.II.5),

a_i are the excitation weightings of the cells referring to the reflected power waves (scheme n$_0$ 3 on Fig .II.7),

$\langle X_i\rangle$ are the reactive loads,

$\overrightarrow{V_i} = x_i\vec{x} + y_i\vec{y}$. ($\overrightarrow{V_i}$ refers to the position vector of the different cells),

$\overrightarrow{k_0}(\theta,\varphi) = \overrightarrow{k_x}.\vec{x} + \overrightarrow{k_y}.\vec{y} + \overrightarrow{k_z}.\vec{z} = \frac{2\pi f}{c} \times [\sin(\theta)\cos(\varphi)\,\overrightarrow{x_i} + \sin(\theta)\sin(\varphi)\,\overrightarrow{y_i} + \cos(\theta)\,\vec{z}]$.

$\overrightarrow{k_0}.\overrightarrow{V_I}$ is the spatial delay of the patterns radiated by the different cells on the panel. The excitation weightings of the cells are expressed in terms of $\langle b_{0\,i}\rangle$, $\langle X_i\rangle$ and [S], as we are about to explain in the next section.

III.2.2 - Beam synthesis – criteria for the excitations weightings of the array on the panel

This section consists in the optimization of the excitation weightings a_i versus an objective radiation pattern. The studied case is a focused beam in a single direction (θ_0, φ_0). To satisfy this objective, the phase of the excitation waves a_i must satisfy (Eq.II.18), where p represents the phases weighting distribution to ensure the objective radiation pattern coherence, provided an arbitrary phase constant 'C'. The latter can be used to allow a degree of freedom while choosing realistic reactive elements and/or it can be used to optimize the radiation pattern as it will be discussed in the last part. If we suppose that the classical array phase distribution of the excitation weightings is a sufficient condition to focus the beam [2] (Eq.II.19), this distribution is known provided the arbitrary constant 'C'.

(II.18) $$\angle(a_i) = p_i(\theta_0, \varphi_0) + C$$

(II.19) $$p_i(\theta_0, \varphi_0) = k_0(sin\theta_0 cos\,\varphi_0 . x_i + sin\,\theta_0\, sin\,\varphi_0 . y_i)$$

Where:

C is an arbitrary phase constant,

(θ_0, φ_0) is the direction of the beam,

By using (Eq.II.14) which defined the reflection coefficient Γ_i between a cell and a reactive load, the phase shifts γ can be determined to satisfy the radiation pattern synthesis. In this synthesis, we consider that the reactive loads are lossless and the cells ports are set to the standard 50Ω impedance, as we can notice in the following equation:

(II.20) $$\Gamma_i = \frac{j.X_i - 50}{j.X_i + 50} = e^{j\gamma_i} \; with \quad \|\Gamma_i\| = 1$$

The incident coupled power waves are defined by a column vector $\overrightarrow{b_0}$ and the excitations weightings by a column vector $\overrightarrow{a}$. The length of these two vectors is (nb). These definitions comply with the previous notations, $b_{0\,i}$ and a_i respectively.

$[b_0] = [b_{0\,1}\;\; b_{0\,2} \ldots b_{0\,i} \ldots b_{0\,k} \ldots b_{0\,nb}]'$.

$[a] = [a_1\ a_2\ \dots a_i \dots a_k \dots a_{nb}]'$.

The scattering matrix [S] is a (nb, nb) square matrix. The reflection coefficients Γ_i are defined in the diagonal square matrix [Γ] of (Eq.II.21). Its dimensions are also(nb, nb). Let us remind that nb is the number of the cells on the panel.

$$[\Gamma] = \begin{bmatrix} e^{j\gamma_1} & 0 & 0 & \cdots & \cdots & 0 \\ 0 & e^{j\gamma_2} & \cdots & & & \\ \vdots & \vdots & \ddots & \vdots & & \vdots \\ & \vdots & & e^{j\gamma_i} & & \\ \vdots & \vdots & & & \ddots & \\ 0 & 0 & \cdots & 0 & \cdots & e^{j\gamma_{nb}} \end{bmatrix} \tag{II.21}$$

The total coupled wave $b_{tot\ i}$ in a cell port is defined by the sum of the coupled incident wave $\overrightarrow{b_0}$ and the corresponding mutual coupling from the surrounding cells, as seen in Eq.II.6. Defining $\overrightarrow{b_{tot}}$ as a column vector with a (nb) length, the aforementioned definition leads to (Eq.II.22):

$$\begin{bmatrix} b_{tot\ 1} \\ b_{tot\ 2} \\ \vdots \\ b_{tot\ i} \\ \vdots \\ b_{tot\ nb} \end{bmatrix} = \begin{bmatrix} b_{0\ 1} \\ b_{0\ 2} \\ \vdots \\ b_{0\ i} \\ \vdots \\ b_{0\ nb} \end{bmatrix} + \begin{bmatrix} s_{1,1} & s_{1,2} & \cdots & \cdots & s_{1,nb} \\ s_{2,1} & s_{2,2} & & & \\ \vdots & & \ddots & & \vdots \\ \vdots & & & & \vdots \\ \vdots & & \vdots & \ddots & \\ s_{nb,1} & & \cdots & & s_{nb,nb} \end{bmatrix} \begin{bmatrix} a_1 \\ a_2 \\ \vdots \\ a_i \\ \vdots \\ a_{nb} \end{bmatrix} \tag{II.22}$$

It should be noticed that the excitation weightings $\overrightarrow{a_i}$ are reflected from the total coupled waves $\overrightarrow{b_{tot\ i}}$ (as seen in Eq.II.9). The full matrix form is given in Eq.II.23.

$$\begin{bmatrix} a_1 \\ a_2 \\ \vdots \\ a_i \\ \vdots \\ a_{nb} \end{bmatrix} = \begin{bmatrix} e^{j\gamma_1} & 0 & 0 & \cdots & \cdots & 0 \\ 0 & e^{j\gamma_2} & \cdots & & 0 & \\ \vdots & \vdots & \ddots & \vdots & \vdots & \vdots \\ 0 & \vdots & & e^{j\gamma_i} & & 0 \\ \vdots & \cdots & 0 & \cdots & \ddots & \vdots \\ 0 & 0 & \cdots & 0 & \cdots & e^{j\gamma_{nb}} \end{bmatrix} \begin{bmatrix} b_{tot\ 1} \\ b_{tot\ 2} \\ \vdots \\ b_{tot\ i} \\ \vdots \\ b_{tot\ nb} \end{bmatrix} \tag{II.23}$$

Combining (Eq.II.22) and (Eq.II.23) leads to the final equation (Eq.II.24):

$$(II.24)\qquad \begin{bmatrix} a_1 \\ a_2 \\ \vdots \\ a_i \\ \\ \vdots \\ a_{nb} \end{bmatrix} = \left[\begin{bmatrix} e^{j\gamma_1} & 0 & \cdots & 0 \\ \vdots & \ddots & & \vdots \\ \vdots & & \ddots & \\ 0 & \cdots & \cdots & e^{j\gamma_{nb}} \end{bmatrix}^{-1} - \begin{bmatrix} s_{1,1} & \cdots & s_{1,nb} \\ \vdots & \ddots & \\ s_{nb,1} & & s_{nb,nb} \end{bmatrix}\right]^{-1} \begin{bmatrix} b_{0\,1} \\ b_{0\,2} \\ \vdots \\ b_{0\,i} \\ \vdots \\ \\ b_{0\,nb} \end{bmatrix}$$

$$\leftrightarrows \vec{a} = \left[[\Gamma]^{-1} - [S]\right]^{-1}\overrightarrow{b_0}$$

III.2.3 - Optimization/Convergence Routine of the excitation weightings

In (Eq.II.24) we see the contribution of the reflection matrix [Γ], the scattering matrix [S], and the coupled incident waves $\overrightarrow{b_0}$ in the determination of the excitation weightings a_i which are the unknowns of our synthesis problem. The known parameters in (Eq.II.24) are the arguments of a_i as seen in Eq.II.15, [S] and $b_{0\,i}$. The unknown parameters are the modulus of a_i and Γ_i. These two parameters are correlated; therefore (Eq.II.24) cannot be solved unless one of the unknown parameters is eliminated from the system. However $\|\Gamma_{mxn}\| = 1$, as seen in (Eq.II.20), therefore (Eq.II.24) can be simplified to a much easier system. Replacing $\overrightarrow{b_{tot}}$ in (Eq.II.23) leads to:

$$[\Gamma]^{-1}\vec{a} = \overrightarrow{b_0} + [S].\vec{a}$$

Then the absolute value implies (Eq.II.25):

$$(II.25)\qquad \|\vec{a}\| = \left\|\overrightarrow{b_0} + [S].\vec{a}\right\|$$

By introducing $\overrightarrow{a} = \mathrm{diag}\left(e^{+j(p+C)}\right).\|\vec{a}\|$, we obtain (Eq.II.26):

$$(II.26)\qquad \|\vec{a}\| = \left\|\overrightarrow{b_0} + [S].diag\left(e^{+j(p+C)}\right).\|\vec{a}\|\right\|$$

(Eq.II.26) has only one unknown variable, which is the modulus of the excitations weightings $\|\vec{a}\|$. (Eq.II.26) can be solved using convergence routines like the ***fixed-point method*** used in this approach. A very important result to notice is that the modulus of the weightings is linked to:

1. The scattering matrix [S],
2. The incident coupled waves $b_{0\,i}$,

3. The phase distribution $\angle(a_i)$ referring to the beam direction,
4. The arbitrary phase constant C.

III.2.4 - Calculus of the required phase shifts/ reactive loads for the desired beam direction

Once the excitations weightings a_i are computed versus the objective radiation pattern, the total incident coupled waves $b_{tot\ i}$ are deduced from Eq.II.22. The reflection coefficients Γ_i are then deduced from (Eq.II.7), as follows:

$$\Gamma_i = \frac{a_i}{b_{tot\ i}}$$

The required phase shifts and the reactance of the reactive loads are given by Eq.II.27:

$$\begin{cases} \gamma = argument(\Gamma) \\ X_i = img\left(\frac{50+\Gamma_i}{50-\Gamma_i}\right) \end{cases} \quad (II.27)$$

The real values of the reactive loads to be integrated behind the radiating elements are deduced from Eq.II.28. If the reactive load is negative then we will connect a capacitive load behind the cell. If the reactive load is positive then we will connect an inductive load (Eq.II.28):

$$\begin{cases} C_i = -\frac{1}{X_i \times \omega} \quad (F) & If\ X_i < 0 \\ L_i = +\frac{X_i}{\omega} \quad (H) & If\ X_i > 0 \end{cases} \quad (II.28)$$

IV - Implementation of the theoretical formalism

As all the theoretical elements required for the synthesis and design of the reflectarray have been defined, we will now present the analysis and synthesis tool that integrate this formalism.

IV.1 - Presentation of the design modules

The implementation of the analytical formalism is naturally split into two modules; an analysis module and a synthesis module.

These modules are presented in this section. The first module is illustrated in Fig .II.10. In the first module we analyze the reflectarray. Given the feed's radiation pattern and the geometry of the panel, the first step is to illuminate the reflectarray panel and optimize the aperture efficiency in order to maximize the performances of the antenna. It is possible by simply optimizing the position of the feed and its orientation angles.

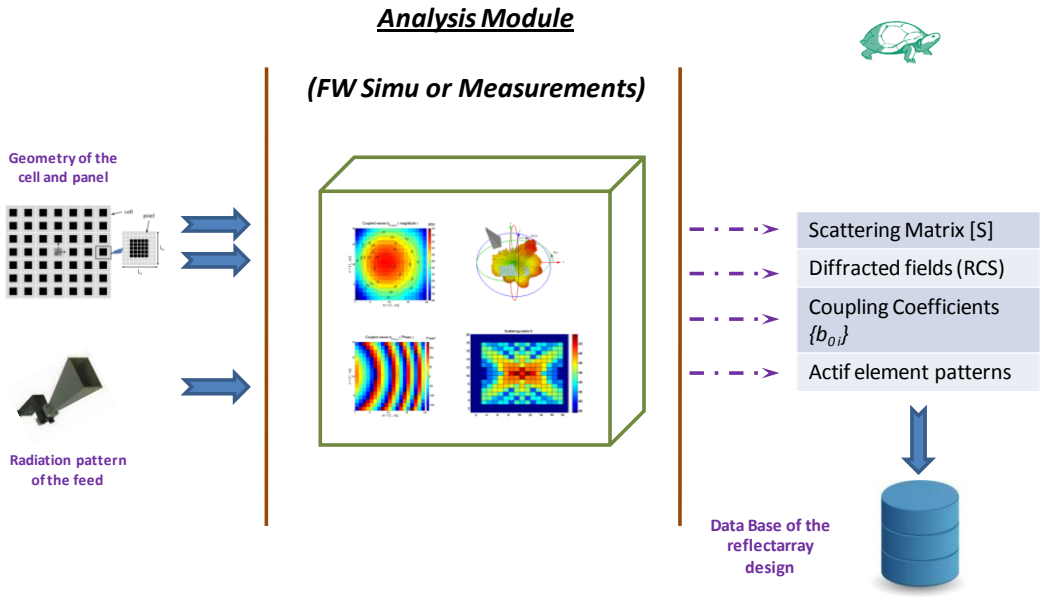

Figure. II.10. *Analysis module of the reflectarray antenna by using full-wave simulations or the measurements*

Once the geometry and the physical configuration of our design are ready we now compute the EM quantities required for the second module, either by full-wave simulations or

by the measurements. These EM quantities construct the identity database of the reflectarray design. This identity database contains the four following parameters:

(1) The incident coupled waves $\{b_{0\,i}\}$,

(2) The diffracted electromagnetic fields pattern on the panel $E_{diffracted}(\theta,\Phi)$ *i.e. (RCS),*

(3) Radiation pattern of the center cell $F(\theta,\Phi)$,

(4) The scattering matrix [S].

Notice that we consider identical radiation pattern for all cells that is why only the radiation pattern of the center cell is evaluated.

The second module is illustrated in Fig .II.11. It operates as follows; the database of the reflectarray design serves as a fixed input and we define an objective radiation pattern, such as a focused beam radiating at a desired direction.

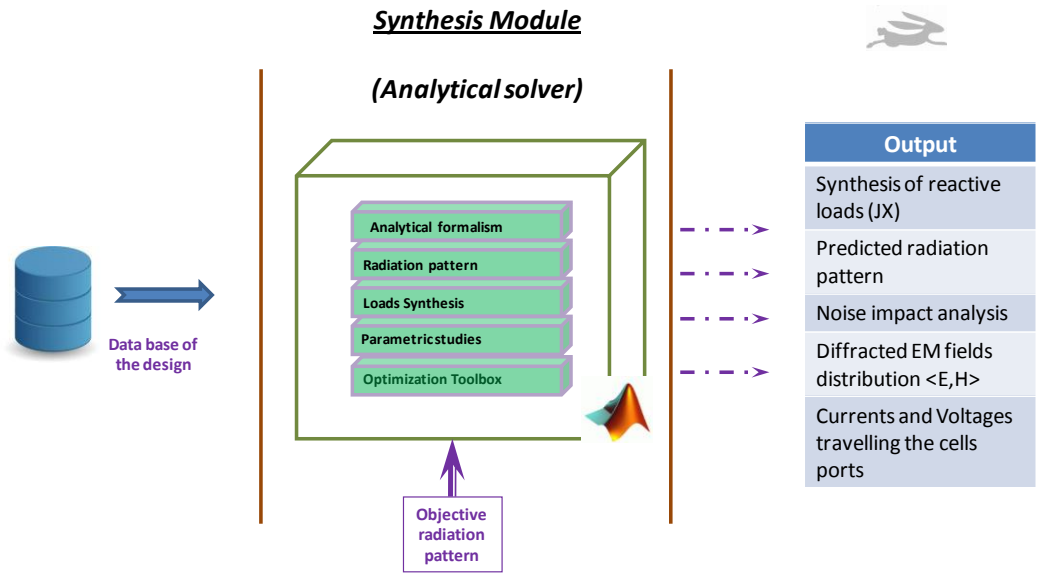

Figure. II.11. *Synthesis module of the reflectarray using an analytical formalism (Matlab)*

The outputs of the analytical solver are the following:

1. A set of synthesized relative loads (JX) / phase shift distribution,
2. An accurate prediction of the radiation pattern including the diffracted fields pattern (RCS),
3. The current and voltages distribution travelling the cells ports including the cells energetic contribution,
4. The diffracted EM fields distribution <E,H>.

On a second note, we can perform the following tasks inside the analytical formalism:

1. Perform a study on a quantized phase shifts/ reactive loads distribution taking into account the effects of the phase constant 'C',
2. Perform a noise impact analysis (Breakdown cells impact),
3. Perform a study on the effects of the mutual couplings between the cells on the radiation pattern as well the energetic contribution of the cells,
4. Couple the analytical formalism to the Optimization toolbox of Matlab where we could optimize the phase distribution or synthesize shaped beam patterns,
5. Perform a study on the energy balance of the reflectarray to check the accuracy of the results.

IV.2 - General notes on the full-wave simulations and the analytical solver

The full-wave simulations are available thanks to the commercial software CST Microwave Studio [3]. CST MICROWAVE STUDIO® is a general-purpose electromagnetic simulator based on the Finite Integration Technique (FIT), first proposed by Weiland in 1976/1977 [4]. The most notable feature given by CST MWS is the meshing strategy thanks to the Perfect Boundary Approximation (PBA) technique [5]. This numerical method provides a universal spatial discretization scheme, applicable to various electromagnetic problems, ranging from static field calculations to high frequency applications in time or frequency domain.

The 3D reflectarray design can be modeled using this tool (CST Microwave studio (MWS)). We begin by drawing the feed antenna CAD and its excitation port. Next, the reflectarray panel, which contains the ground plane, the dielectric substrate and the array, is added to the design. The array is composed from identical cells arranged in a planar lattice. Next, we orientate the feed antenna to assure a good illumination on the panel. The radiating cells have via holes drilled through the ground plane to another substrate layer where tunable components, acting as reactive loads, are lying. The cells are connected to discrete ports to compute the EM quantities of the antenna. This configuration satisfies the requirements of our analysis and synthesis and provides the EM characteristics for our database.

At this step, the synthesis module can be used to find the reactive loads satisfying the radiation objective. All the performances are obtained analytically, without the need of full-wave simulations.

To validate the analytical formalism's calculus, we can launch validation simulations via CST by implementing the synthesized reactive loads inside the simulation (analytical solver) and exciting the feed antenna. This step is optional and we use it only to validate the theoretical formalism.

We can compare the following full-wave results with those given by the analytical solver:

1. The computed radiation pattern,
2. The <E,H> fields distribution on the panel,
3. The currents and voltages travelling through the cells ports.

Thanks to the full-wave simulations feedback we were able to validate the analytical solver and enhance its performances. Note that due the huge number of elements involved into the panel, we have developed a **VBA macro** that will automatically create N lumped elements and N discrete ports distributed in a 2D lattice and attached between the cells and the ground plane. One of the strong features offered by CST MWS is the possibility to write VBA Macro scripts and to act interactively with Matlab [6]. The powerful VBA (Visual Basic for Application) compatible macro language is equipped with a fully featured development environment including an editor and a debugger. An interface to OLE automation enables a seamless integration into the windows environment (e.g notepad, windows office (Excel, word…), Matlab etc...).

A *parametric study* is unavoidable to optimize an antenna's performances and reach a set of specifications, such as a desired gain, return losses, axial ratio, etc …. From a customer point of view, the performances of the reflectarray should be optimized due to its high cost, and to the complexity of manufacturing. The specifications can be maximizing the antenna directivity, decreasing the side-lobes levels or minimizing the cross-polar radiation, etc …

In our case, we shall optimize the phase shifts distribution /reactive loads inside the analytical formalism. Once the mathematical model of the reflectarray is validated, **we can perform any parametric study in a few seconds**. It is essential for an efficient and versatile reflectarray analysis and synthesis.

Our analytical solver is powered by Matlab. Thanks to its matrix based numerical analysis tool MATLAB also benefited greatly from the ability to extend its basic features through the use of the "Toolbox" concept. Toolbox such as the **Optimization Toolbox** and the **Global Optimization Toolbox** will make great use in the reflectarray pattern synthesis.

Matlab's Optimization Toolbox™ provides widely used algorithms for standard and large-scale optimization. These algorithms solve constrained and unconstrained continuous and discrete problems. The toolbox's optimization software includes functions for linear programming, nonlinear optimization, nonlinear least squares or multiobjective optimization as examples. We can use them to find optimal solutions, perform tradeoff analyses, balance multiple design alternatives, and incorporate optimization methods into algorithms and models [7].

During the thesis, several optimization solvers were tested successfully. I can name briefly the following: the ***fminimax*** minimization function, the ***lsqnonlin*** curve-fitting function and the ***genetic algorithm*.** These solvers are capable of interacting with the analytical formalism (synthesis module) in order to calculate nonstandard and specific phase shifts distributions for various applications (shaped beam synthesis, binary phase shifts synthesis etc …). I will present some results in the third chapter.

V - Conclusion

In this chapter I have presented an analysis and synthesis method which is developed to study reflectarray antennas and especially small-sized reflectarrays. A first step was to present the architecture used for the reflectarray panel and the equations to solve while defining a radiation objective. We have particularly demonstrate the dependence of the cells excitations weightings $\{a_i\}$ towards several parameters. In fact $\{a_i\}$ depend on:

- the scattering matrix [S],
- the incident coupled power waves from the feed antenna $b_{0\,I}$,
- the phase shift distribution to perform the radiation objective,
- a phase constant 'C'.

An important result to notice from the equation Eq.II.26 is also that the magnitude of $\{a_i\}$ is directly linked to the mutual couplings of the cells. This particular issue will be addressed in next chapters.

By combining an EM simulation software from the market (CST MWS 2012) with programs developed internally, we have now in our hands a tool capable of synthesizing a reflectarray antenna.

This tool is divided into two modules. The first module studies and characterizes the reflectarray antennas. It is essential to analyze the entire reflectarray design including the primary source with the real and physical dimensions of the cells. Full-simulations or measurements are required to fill a database for this particular reflectarray design. The second module is the analytical formalism for synthesizing the values of the reactive loads required to shape/steer the beam in a given direction.

By including the mutual couplings between the cells inside the analytical formalism we look forward to compute the required phase shifts and radiation pattern with a very good accuracy in a short time. A comparison between the full-wave simulations and the analytical formalism will give us a better idea in the following chapters.

The presented tool is easy to use since the different modules are computerized and automatized. Speaking of the full-wave simulations, a VBA Macro program is developed along CST MWS to automate the design of the radiating panel and the implementation of the discrete ports and lumped elements behind the cells. It will help the user overcome the large number of radiating elements in the structure. Speaking of the analytical formalism, Matlab

matches perfectly our objectives thanks to its high-level matrix/array based numerical language. It can also communicate easily and exchange the data with MWS CST through text files. These data can be scattering parameters, a radiation pattern or synthesized reactive loads.

The full-wave simulations are coupled to a powerful analytical formalism which calculates the required phase shifts for the reflectarray antenna. One needs to construct the database of the reflectarray antenna configuration. It contains the incident coupled waves, the diffracted fields on the reflectarray panel including the spillover pattern and edge diffractions, the element active pattern of the cells and the scattering matrix [S]. These parameters will help us synthesize the reactive loads versus a given radiation pattern **in a few seconds**.

I add one final note on the beam synthesis. In this chapter I have presented a solution for a focused beam using continuous phase shift distribution. But it is also possible to solve complex problems such as shaping the radiation pattern or adding constraints such as quantized phase shifts distribution.

In the next chapter, we will use the analytical formalism and tools presented in this chapter to make a design test.

VI - References

[1] M. Thevenot, A. El Sayed Ahmad C. Menudier, G. Zakka El Nashef, F. Fezai, Y. Abdallah, E. Arnaud, F. Torres, and T. Monediere, "Synthesis of Antenna Arrays And Parasitic Antenna Arrays With Mutual Couplings," *Special Issue of International Journal of Antennas and Propagation,Hindawi Publishers*, 2011.

[2] C. A. Balanis, "Antenna theory Analysis and Design," *WileyInterscience Editions*, 2005.

[3] CST MWS Studio, *http://www.cst.com/Content/Products/MWS/Overview.aspx*.

[4] T. Weiland, "A discretization method for the solution of Maxwell's equations for six component fields: Electronics and Communication," *AEÜ*, vol. 31, pp. 116-120, 1977.

[5] B. Krietenstein, R. Schuhmann, P. Thoma, and T. Weiland, "The Perfect Boundary Approximation technique facing the challenge of high precision field computation," *Proc of the XIX International Linear Accelerator Conference LINAC*, pp. 860-862, 1998.

[6] M. Gilbert and K. Getz, "VBA Developer's Handbook, 2nd Edition," 2001.

[7] Mathworks, *http://www.mathworks.co.uk/products/optimization/*.

Chapter III

DESIGN TEST: A SMALL SIZE REFLECTARRAY ANTENNA

I - Introduction

In this chapter, I will present a reflectarray design based on the architecture proposed in Chapter II. The objective is to numerically design a proof of concept according to the theoretical formalism detailed in the previous chapter.

For this purpose, we shall use a reflectarray with a small aperture $(10\lambda, 10\lambda)$. With such a dimension, the strength of the fields coming from the feed towards the cells can present an important variation between the cells. We have voluntarily chosen this dimension because it justifies a detailed and accurate analysis of the EM parameters to lead to an optimized result. Moreover, the overall volume of this design test is suitable with a full-wave extraction of the EM characteristics of the reflectarray.

The main goal of this numerical proof of concept is to demonstrate that the design of a reflectarray can be made efficiently by controlling the energy balance between the different elements, provided the theoretical formalism used allows to access to the suitable parameters. Some examples of beam steering will be used during this study.

The first part of the chapter is dedicated to the different steps of the design leading to a radiation objective. The setup of the database presented in the analysis module of chapter 2 will be detailed as well as the synthesis process. Notice that the conditions to extract the EM parameters at each step will be discussed. This is necessary to guarantee the energy balance in the overall volume.

The second part of this chapter focuses on the numerical validation of the proof of concept by comparing the results from the synthesis to the ones from a full-wave simulation (with CST MWS).

II - Design of a Reflectarray Antenna:

II.1 - Description of the RA and objectives

The favorable conditions to run this study are the following:

(1) The frequency bandwidth is defined in the X-band (10GHz)

(2) The reflectarray cells are identical and periodic

(3) The illumination spot should fit for a $10\lambda \times 10\lambda$ panel.

(4) The edge taper is around -13dB and the illumination efficiency is around 80%.

(5) The feed antenna is in offset configuration.

II.2 - Study of the primary feed antenna

We begin with the primary feed antenna. Usually, we aim to minimize the secondary lobes of the feed antenna to improve the aperture efficiency of the reflectarray panel (i.e reducing the spillover losses). Also we wish to obtain a symmetrical radiation pattern in the E and H-plane. Typically those specifications can be achieved with a Potter Horn or a corrugated horn. The phase center of the antenna is another critical parameter to consider and we usually seek to minimize the dispersion of the phase center versus the wavelength.

In our work, the objective is the accurate synthesis of the weightings of the RA cells. That is why we have not focused on the horn design. Therefore, a classical pyramidal horn in X-band has been chosen. It is a model that is especially used in the laboratory: Flann Microwave 16240-20. This feed antenna might present some secondary lobes and a non symmetric radiation pattern in the E and H-plane, but I have bypassed this 'brick' to move quickly to the numerical study of the reflectarray antenna. For a more detailed study on the horn feed for illumination purposes, the reader can refer to [1].

II.2.1 - Feed antenna Modeling

The horn antenna is well known in the literature. It can be described as the simplest and one of the most used of microwave antennas. Between the many possible horn shapes (pyramidal, conical), I have picked the standard gain pyramidal horn. It consists of an open waveguide connected to a flared aperture in both the E and H-planes, which results in narrow

beamwidths in both principal planes. The overall geometry of the antenna is shown in Fig .III.1. and the standard dimensions of the Flann Microwave 16240-20 can be found in [2]. They are depicted in Table.III.1 for this 20dB directivity horn in X-band.

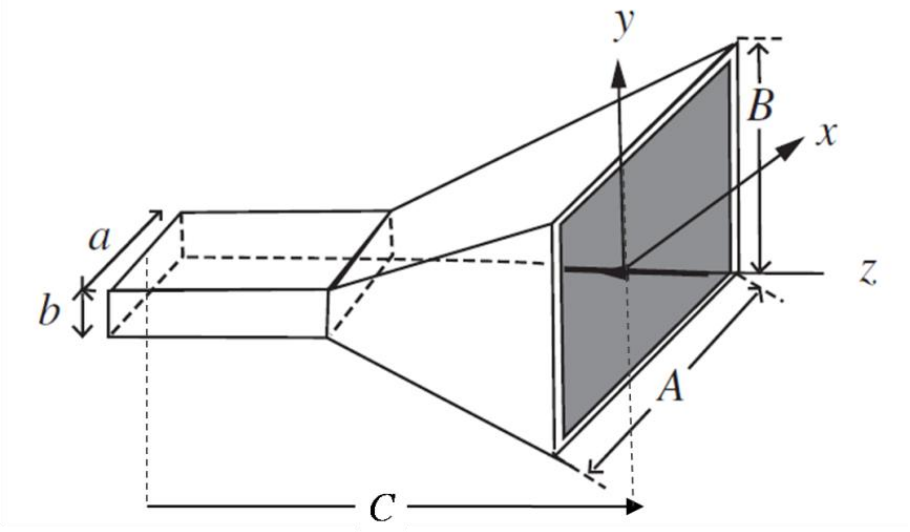

Figure.III.1. *Overall geometry of the pyramidal horn*

Frequency bandwidth	8.2-12.5 GHZ		
Desired directivity	20 dB		
Waveguide WR90	Width a	0.9”	22.86 mm
	Height b	0.4”	11.84 mm
Aperture width A	109 mm		
Aperture heigth B	79 mm		
Overall length C	245 mm		

Table.III.1: Standard dimensions of the horn Flann Microwave

When we are simulating the horn via CST MWS, we usually select the surface of the open end of the waveguide, then we add a waveguide excitation port. However, the EM simulator obligates us to keep the waveguide port parallel to one of the three planes of the simulation domain (XOY, YOZ or ZOX). As a consequence, the horn antenna can only be orientated in the direction of the axis of the coordinate system . In our case, we are looking to orientate the feed antenna with the direction unit vector $\overrightarrow{U_0}$. One solution to surpass this constraint is to replace the waveguide excitation with a discrete port excitation, close to the open end of the waveguide and add a cubic object inside the waveguide port as seen in Figure.III.2. The cubic shape allows the excitation to take place inside the waveguide;

therefore we can be sure that the simulation of the reflectarray is possible without any constraint in the direction of the excitation port.

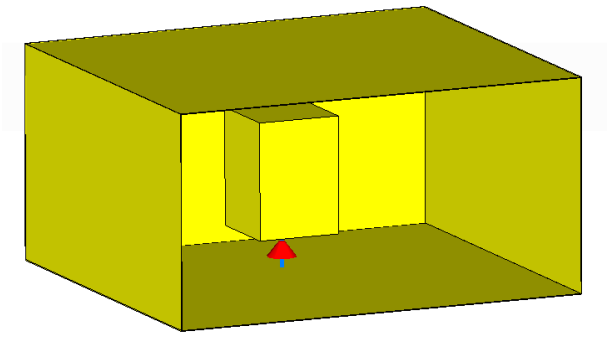

Figure.III.2. *Discrete port excitation of the horn antenna to allow a simulation in the case of a rotated horn (view of waveguide)*

The feed antenna is excited with the above technique. The z-axis is normal to the antenna aperture. The simulated return loss is shown in Figure.III.3. The antenna is well matched around the desired frequency 10 GHz.

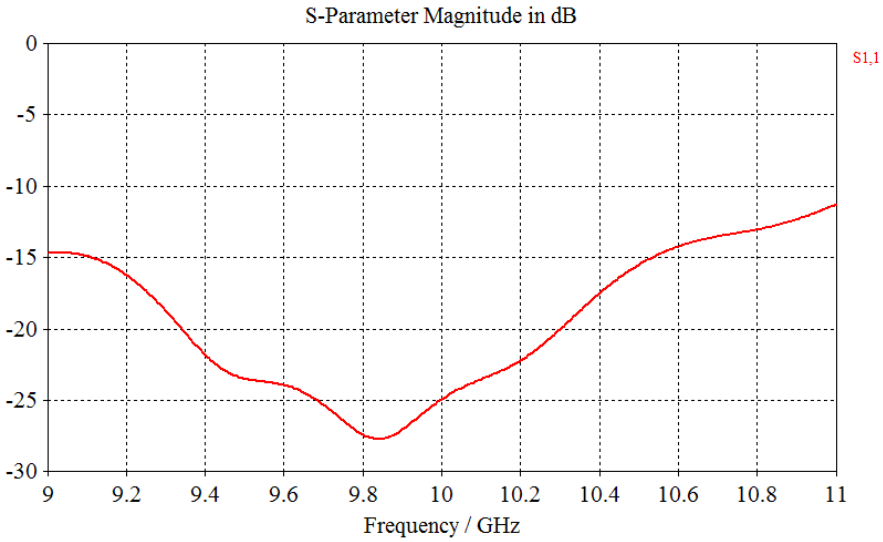

Figure.III.3. *Return loss of the feed antenna*

II.2.2 - Output format of the feed's radiation pattern

The radiation pattern of the antenna presents a 19.7dB of gain, as depicted in Fig .III.5. As can be seen, the wider aperture of the horn is oriented in the XOZ plane ($\varphi = 0°$). Therefore the major components of the electric fields are the $\overrightarrow{E_y}$ components. It is confirmed by the Co-polar and Cross-polar components of the radiation pattern. If we compare between

the radiations patterns of a horn excited with a normal waveguide port and with the above excitation technique we see a perfect agreement.

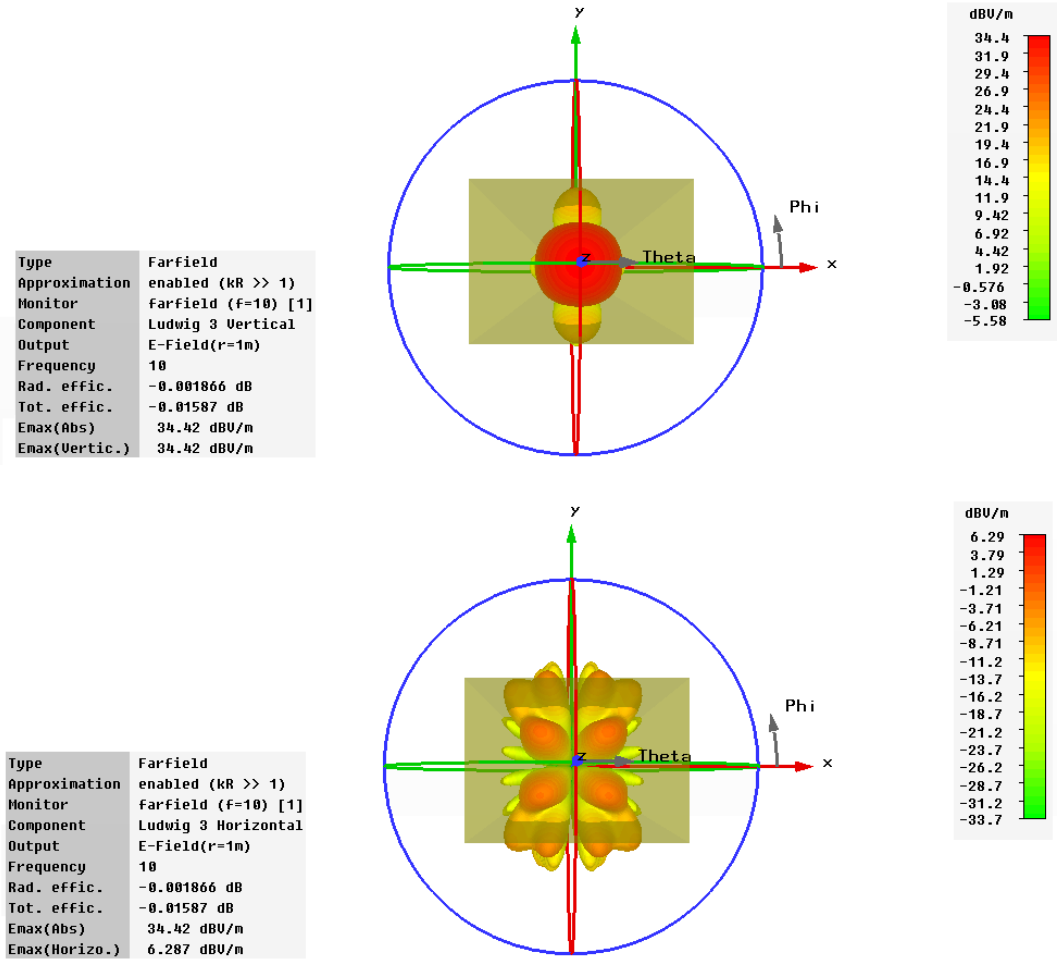

Figure.III.4. *3D Electric fields components as respect to the Ludwig 3 definition. (Top) Vertical Polarization (Co-polar). (Bottom) horizontal Polarization (Cross-Polar).*

Fig .III.5 shows the radiation pattern in terms of the realized gain in the E plane ($\varphi = 0°$) and in the H plane ($\varphi = 90°$). The maximum gain is about 19.7 dB in the plane ($\varphi = 90°$), whereas the cross polarization is below -40 dB in the plane ($\varphi = 0°$), as illustrated in Figure III.5

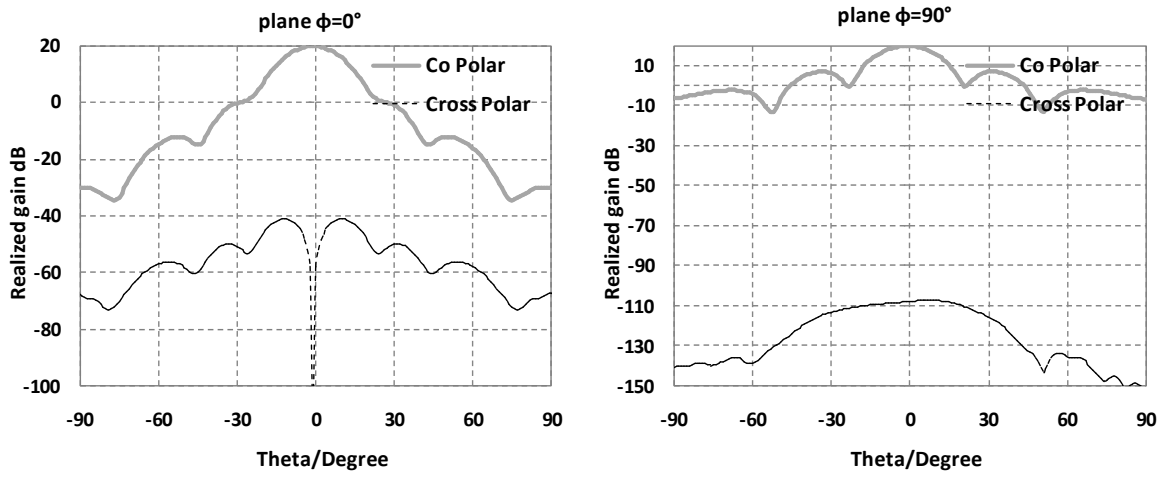

Figure.III.5. *Polarization Components of the radiation pattern of the feed antenna*

In order to be used as input for the synthesis, the radiation patterns are stored in the database with a normalized format. The standard defined by Ticra for their software GRASP was used [3]. This format has the advantage to be available in commercial softwares like CST MWS or FEKO and it is convenient to handle.

In CST MWS, we use the VBA Macro 'Farfield Export to GRASP' to export the radiation pattern through the third definition of Ludwig as illustrated in Fig .III.6. We should notice that the radiation pattern must be clearly defined in terms of origin for the radiated phase, designated as 'Farfield Origin'. We should also specify the direction of the principal polarization of the feed antenna. A multiple frequency patterns can be extracted in case we would like to study the reflectarray response over a bandwidth.

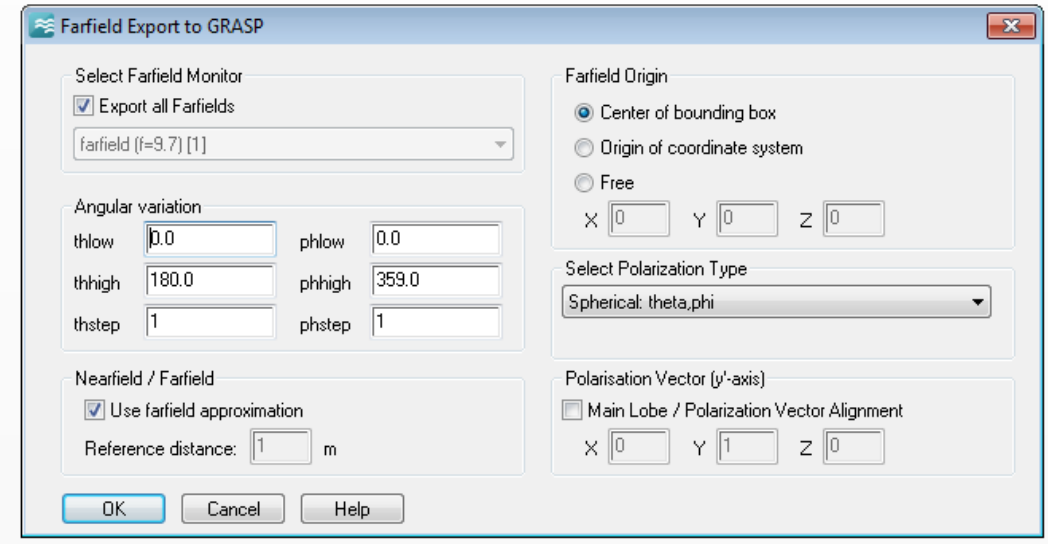

Figure.III.6. *Farfield Macro "Export to Grasp" inside CST MWS*

II.3 - **Illumination Study on the RA panel: Position and orientation of the feed**

Now, we have in our disposal the electrical fields in a text file. We can start optimizing the illumination on the reflectarray panel. The illumination setup of the feed (orientation, distance) can be defined through the aperture efficiency. If we consider only the taper efficiency and spillover losses the best tradeoff consists to place the horn in order to obtain a -13 dB taper.

The panel is made from 20x20 cells and it belongs to the XOY plane of the coordinate system. For a 10 GHz frequency, the dimensions of the panel are 30cmx30cm. We calculate the incident electromagnetic fields on the panel for any given position or orientation for the feed antenna. The geometrical parameters of the reflectarray are listed in Table III.2 below.

Panel configuration **(Data in the panel's coordinate system)**	
Center	$(0,0,1.56)\ mm$
Periodic cell dimension	$(7mm \times 7\text{mm})$
Reflectarray size	(20×19) cells
Dimensions of the aperture	$(30\ cm\ \times 30\ \text{cm})$
FEED-HORN (FLANN 16240-20) **(Data in the panel's coordinate system)**	
Phase center (M)	$(-190,0,330)\ mm$
Illumination point (P)	$(-10,0,1.56)\ mm$
Matrix of rotation Of the feed horn R_{horn}	$\begin{bmatrix} 0 & 0.8769 & 0.48 \\ 1 & 0 & 0 \\ 0 & 0.48 & -0.8769 \end{bmatrix}$
Illumination on the panel	
Spillover efficiency	83.5%
Taper efficiency	87.5 %
Aperture efficiency	73%

Table III.2: Main geometrical parameter of the reflectarray antenna

These parameters were optimized to produce the best aperture efficiency while as the feed-horn is in offset fed configuration (aperture efficiency = 73%). The distributions of the incident electric and magnetic fields on the panel for this particular geometrical configuration are shown in Fig .III.7. The fields are represented by their Cartesian components. The polarization angle of the feed antenna equals 90°.

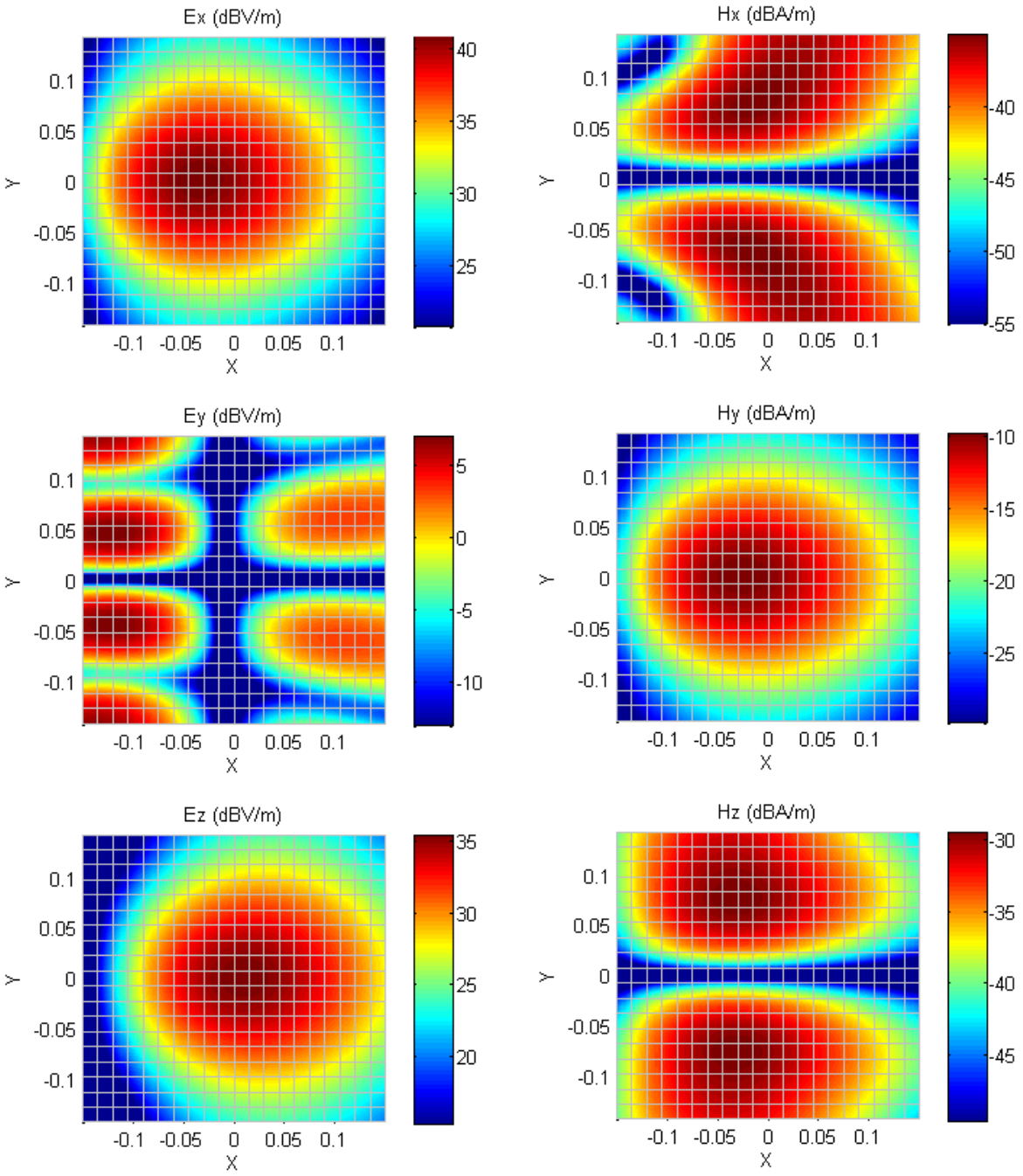

Figure.III.7. *Incident electromagnetic fields on the panel represented by their Cartesian components*

The illumination law which is defined by the magnitude of the total incident electrical fields on the panel, is illustrated in Fig .III.8. The incidence angle (θ_i) of these fields illuminating the surface of the cells is illustrated in Fig. III.9.

The maximum angle of incidence is located at the top right edge of the panel and it equals 48°.

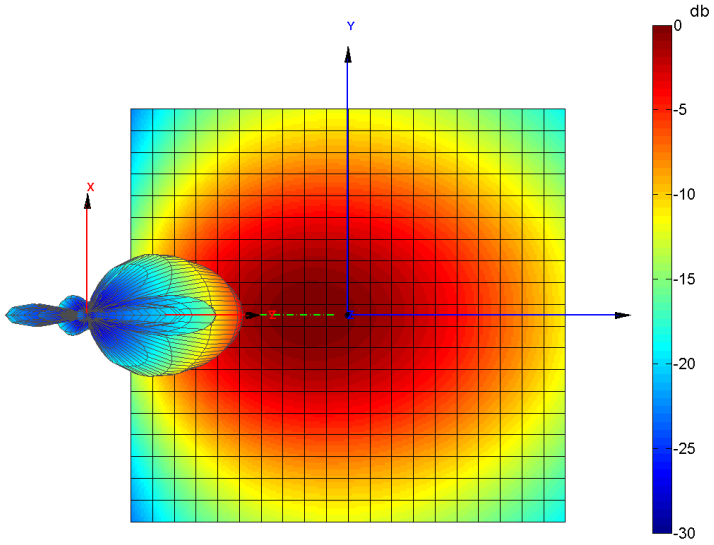

Figure.III.8. *Illumination on the panel: Offset fed with optimized aperture efficiency*

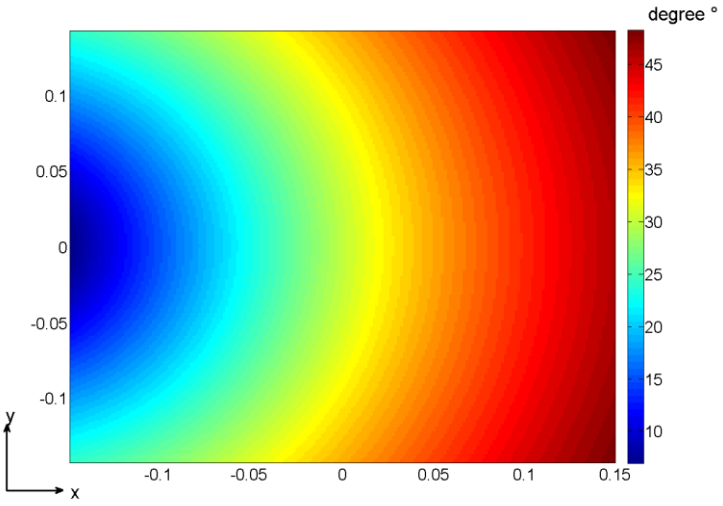

Figure.III.9. *Incidence (θ_i) of the EM waves* at each cell

II.4 - **Full-wave simulations: Building up the database**

II.4.1 - Designing the structure with CST MWS

An offset reflectarray antenna with a ten wavelength side (310mmx310mm) at the 10 GHz frequency will be simulated to focus the beam in different directions. The 20x19 cells are square patches with half-wavelength spacing as shown in Fig .III.12.The planar surface lies on a Rogers4003 substrate ($\varepsilon_r = 3.38,\ \tan(\delta) = 0$). The dielectric substrate is lossless in a preliminary study. Its height is 1.524 mm. The dimensions of a unit cell are ($7mm \times 7\text{mm}$). The edges of the cells on the panel are equispaced with ($dx = 8mm, \text{dy} = 8\text{mm}$). The feed antenna is a standard gain horn antenna with 19.7 dB gain with -15dB sidelobe level. The feed antenna is excited with a discrete port to enable the rotation and translation. Its position was optimized to produce a -13dB edge taper and 83.5% spillover efficiency as seen in the previous section.

The RA design in CST consists in placing the panel that contains the ground plane, the substrate and the array in the XOY plane. Then, the feed horn is added, as depicted in Table III.2.

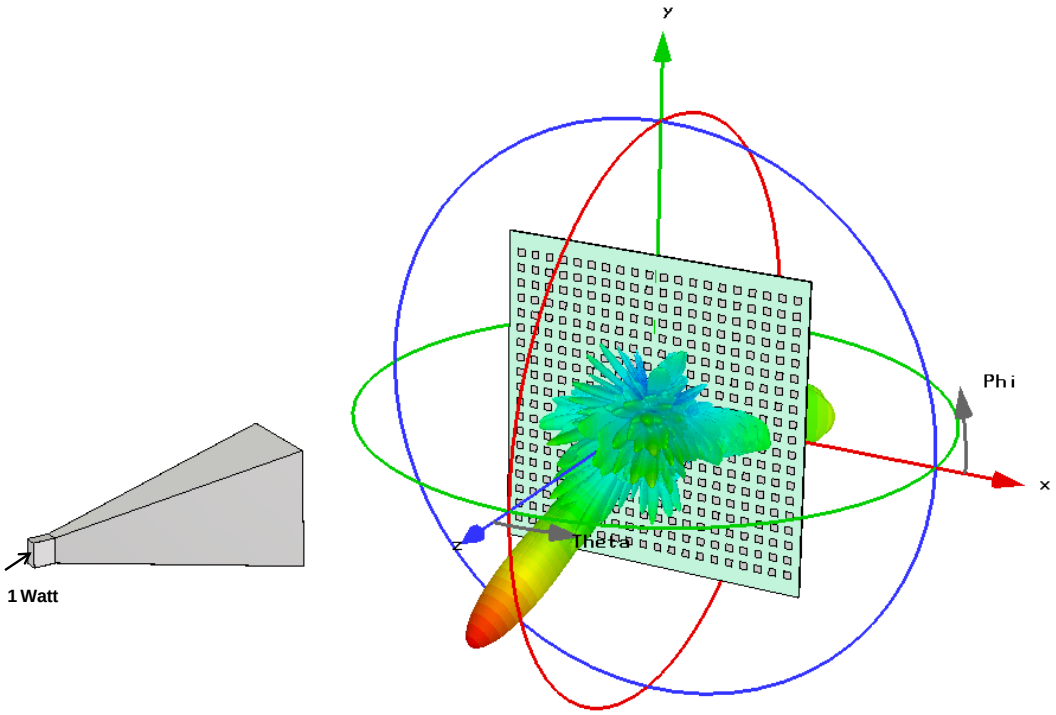

Figure.III.10. *Design of the reflectarray antenna via CST MWS*

The final reflectarray design is shown in Fig .III.12. As we see, the standard gain horn is polarized with the $\vec{x}$ direction and its position meets with the offset-fed requirements. The excitation power is set to 1Watt.

II.4.2 - Convergence study of the mesh settings

As the setup of the simulation is defined, we must address the particular point of accuracy. Notice that the presented analysis technique can be strongly affected by the meshing accuracy of the design [4]. To get accurate results for the phase of the incident coupled waves $b_{m,n}$, a study on the meshing tolerance should be considered. As finite integration technique (FIT) is a spatial discretization of the integral form of the Maxwell equations, the method requires the computational domain to be covered by a mesh. The mesh type used is hexahedral and it is generated by the adaptative mesh generator. The more the mesh used dense is, the more accurate results are obtained. At the same time the spatial computation domain gets bigger and the simulation time is extended. So there is a trade-off between accuracy and mesh volume. The study is performed by increasing the lines per wavelength in the global mesh properties and observing the variation of the phases on two receiving discrete ports of the reflectarray cells.

Fig .III.13 shows that the absolute phase difference between two receiving waves is not stable below certain mesh settings and an error on the phase of the incident coupled wave can reach 20°. The absolute phase starts to converge when we discretize the spatial volume of the structure at a rate of 17lines/wavelength or higher. It will be the minimum meshing setting used in the following simulations.

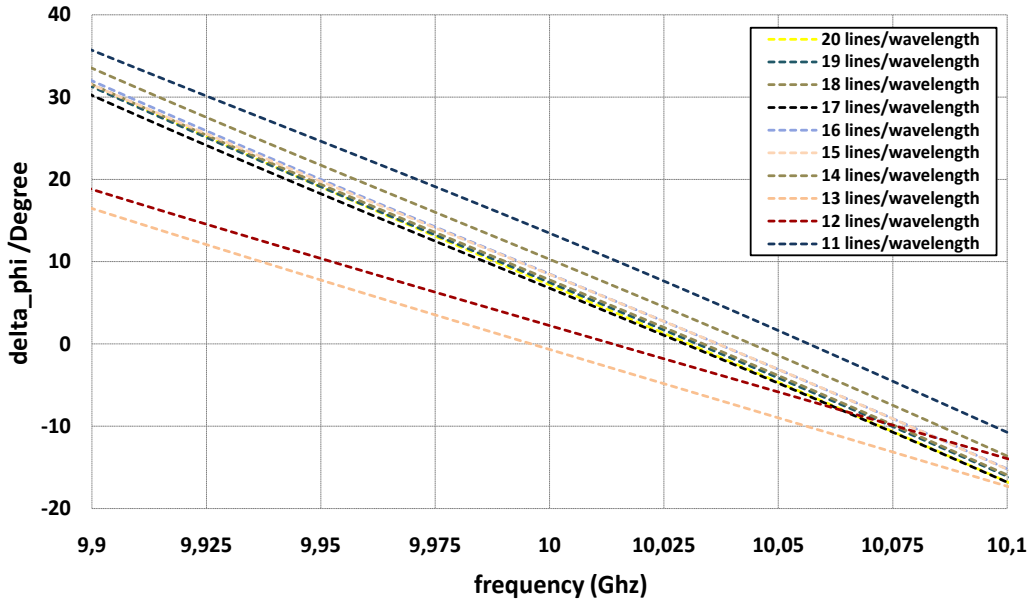

Figure.III.11. *The dispersion of the phase difference with the mesh setting*

II.4.3 - Stage one: Cells in reception mode

This step corresponds to the scheme model seen in chapter II (Fig. II.5). The feed horn antenna is excited and the cells are in reception mode. The return loss at the horn's port $S_{horn,horn}$ is around -18 dB, as seen in Fig .III.15. We compute the diffracted electromagnetic field as in Fig .III.12.

The diffracted field pattern contains the diffracted fields from the horn on the panel, which are visible in the region $\theta = 30°$, and the rear radiation pattern for the directions $\theta > 90°$. They also contain the edge diffractions and the spillover pattern. A small part of this diffracted pattern can also be caused by the interferences with the feed horn.

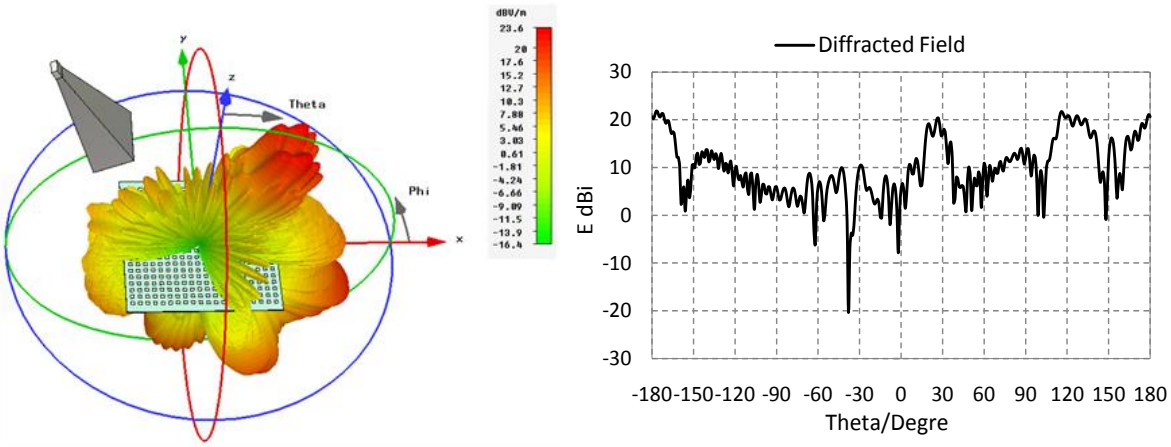

Figure.III.12. *The diffracted electromagnetic field on the panel. (Left) 3D view. (right) The diffracted electric field on the reflectarray panel in the XoZ plane* ($\varphi = 0°$)

The second computed parameter is the incident power waves $[b_0]$ inside the cells ports, both in magnitude and phase, as presented in Fig .III.23 (respectively left and right). We can notice clearly the illumination law on the panel through the magnitude of the incident power waves $[b_0]$, as well as the phase of the incident field at each cell in the argument of $[b_0]$. The -13 dB edge tapper can be seen clearly in the magnitude of $[b_0]$.

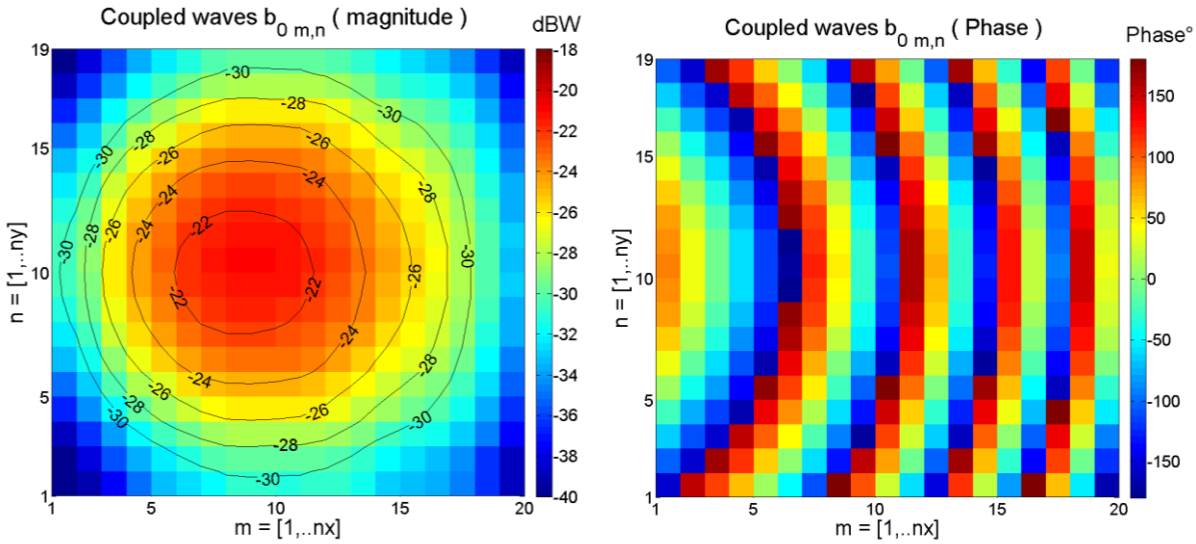

Figure.III.13. *Distribution of the complex incident coupled waves $b_{0,mxn}$ on the panel.(top) magnitude in dBW. (bottom) argument in degrees.*

II.4.4 - Stage two: Extraction of the Scattering Matrix

The reflectarray antenna is simulated with the above mesh setting. The full-wave simulations presented in the following sections are based on the full-wave analysis technique which was described in the chapter II. We remind that one cell is excited while the others are loaded on 50Ω.

In the first simulation, we aim at characterizing the scattering parameters of the cells and computing the active radiation patterns. These parameters serve as inputs for the analytical formalism. The return loss of the center surrounded cell is around -22 dB as can be seen in Fig .III.15. To evaluate the dispersion of the S-parameters on the array I have excited several cells separately. Results were taken for a center cell (k= 190), a cell located near the edge of the panel (k= 182) and a cell randomly located on the panel (k= 125).

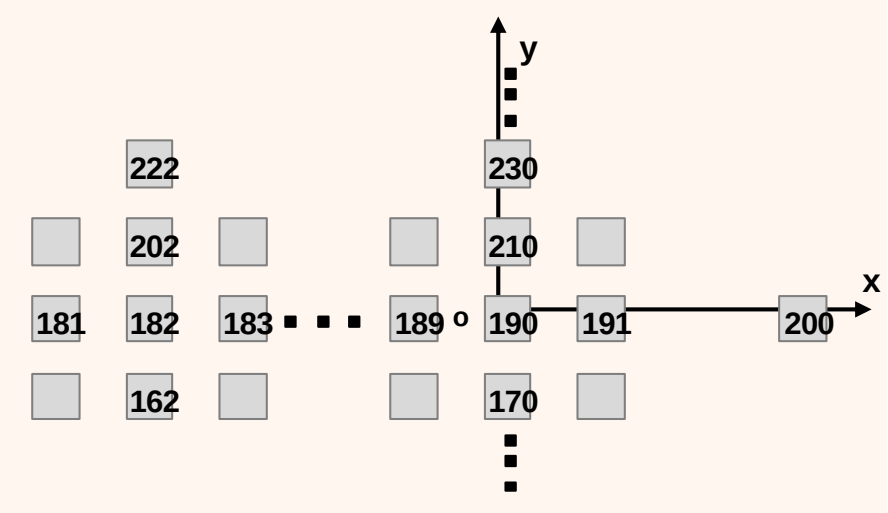

Figure.III.14. *Index of the cells on the panel*

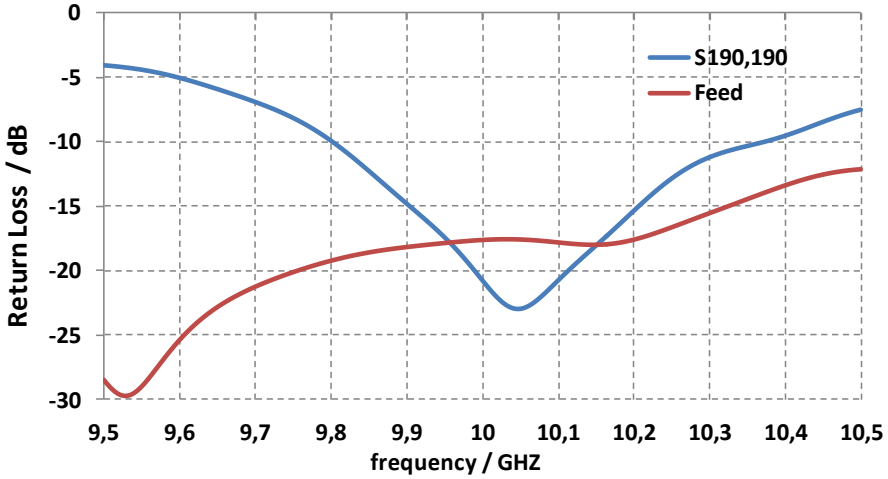

Figure.III.15. *Simulated Return loss of the excited cell and of the primary feed horn*

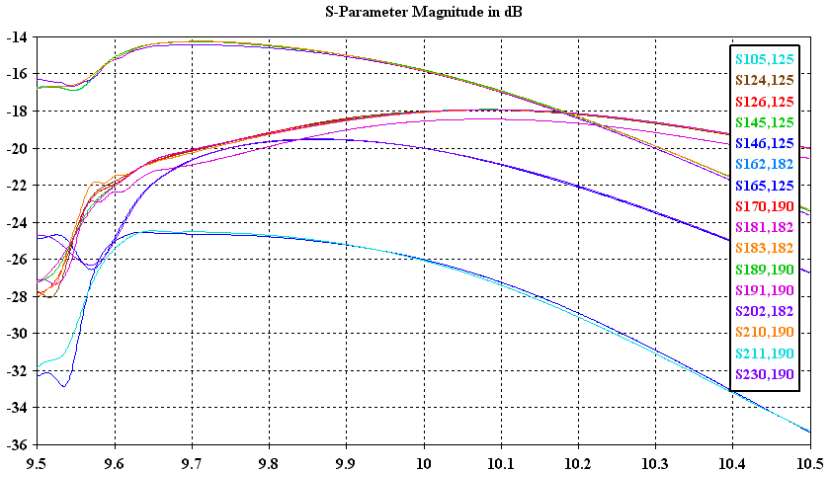

Figure.III.16. *Scattering parameters for different excited cells*

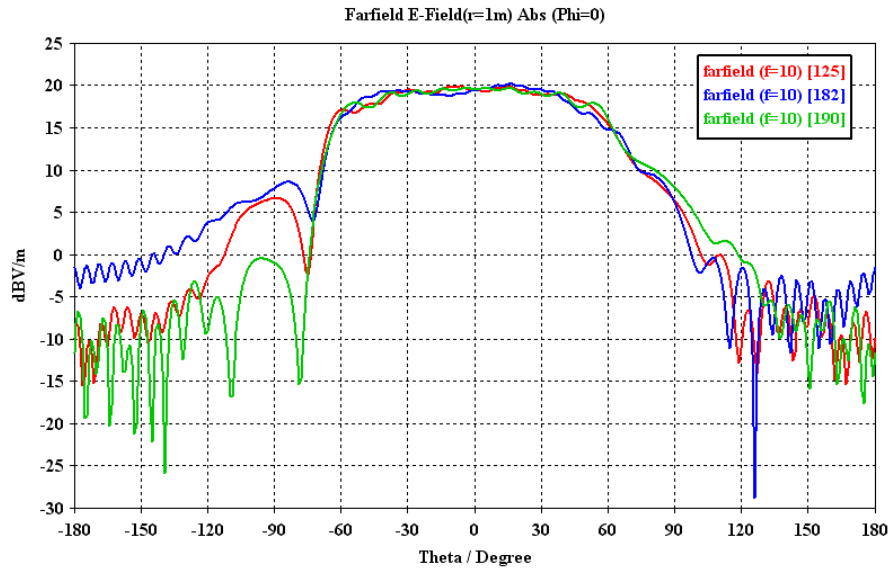

Figure.III.17. *Active radiation pattern $\vec{F}(\theta,\varphi)$ of a cell located in the middle of the panel (190), a cell located near the edge (182) and at a random location (125)*

By comparing their active patterns and the scattering parameters, we notice a reasonable accordance. This is mainly due to the geometry of the cells which are identical and periodical on the panel. The scattering parameters [$S_{i,cell}$] and the active radiation pattern $\vec{F}(\theta,\varphi)$ are shown in Fig .III.16 and Fig .III.17.

The center cell of the panel is positioned at the origin of the coordinate system. The position of the 50Ω discrete port that presents a good matching with the cell is at (p_x=1.3mm, p_y=0mm). Note that the excited cell is surrounded by an array of 379 cells. The ports on the surrounding cells are identically positioned. The indexes of the cells '*k*' on the panel are shown in Fig .III.17 where '190' refers to the center cell.

The scattering parameters and the active patterns can be considered identical. The results change slightly for the cells placed near the edges of the panel. The outcome of this study is that the entire scattering matrix [S] can be approximated and retrieved from the scattering parameters computed of the center cell. The second outcome of this study is that the cells are matched to their ports, allowing a reasonable between the cell and the port which is essential for a good efficiency of the design.

The mutual couplings between the cells is shown in Fig .III.18. The couplings between the adjacent cells are around -15 dB in the *y* direction and -17 dB in the *x* direction.

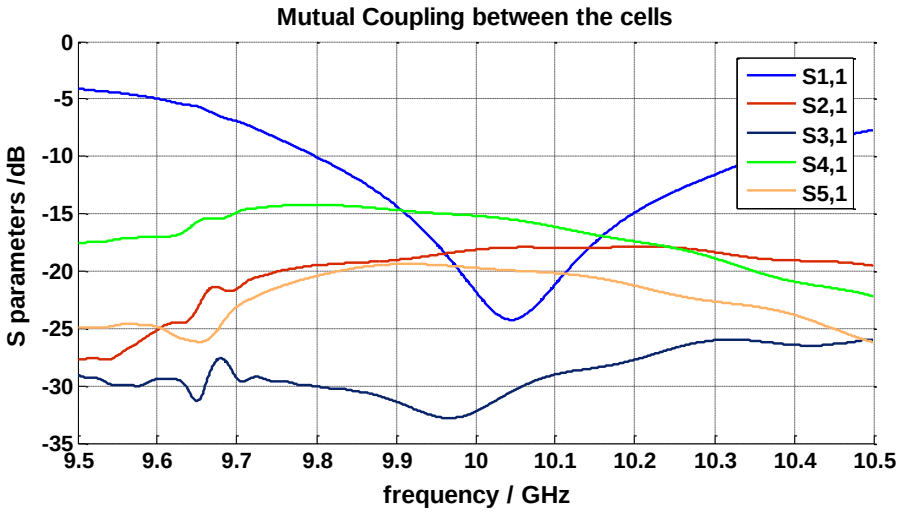

Figure.III.18. *Mutual coupling between the adjacent cells*

II.4.5 - Energy Balance of the previous simulations for the reflectarray design

By treating the Eq.II.10 and Eq.II.11 we can study the energy balance of the simulation performed during the phase one. We conclude that the ports of the cells absorb 78.6% of the energy radiated by the feed horn. Only 19.6% of the energy is lost in the diffracted electromagnetic fields, whereas 1.8% of the energy is lost due to the mismatching of the feed antenna.

On the other hand, by studying the scattering parameters and the active radiation pattern thanks to Eq.II.12 and Eq.II.13 a center cell radiates 77% of its energy and the remaining energy is coupled to its neighbors. A cell located at the edge radiates 91% of its energy. Consequently, the mutual coupling ranges from 9% to 24% depending on the cell's position on the panel. This study is based on the assumption that the structure is lossless. The energy absorbed by the cells is either radiated or transmitted to its neighbors.

We can perform the same study in case we add losses to the structure. It is recommended that we add each loss apart (such as metallic losses, dielectric losses etc …) and study the energy balance. Finally we will know how the energy is distributed inside a real practical design.

	Power normalized to 1W calculated for the lossless reflectarray antenna
Center cell excited	$Power_{coupling} = 0.240W$ $\iint \vec{F}(\theta,\varphi) = 0.760\ W$
Feed antenna	$Power_{mismatc\ hing} = \left\|b_{horn}\right\|^2 = 0.018$ W
Illumination on the panel	$Power_{absorbed} = \sum_{k=1}^{n} \|b_{0\,k}\|^2 = 0.786W$ $\iint_{\Omega} \left\|\overrightarrow{E_{diffracted}}(\theta,\varphi)\right\|^2 d\Omega = 0.196$W

Table III.3: Energy Balance of the reflectarray design

III - Focused Beam Synthesis using Reactive-loads

As all the parameters of the database are calculated ($b_{0\,m,n}$, [S], $\vec{F}(\theta,\varphi)$ and $\overrightarrow{E_{diffracted}}(\theta,\varphi)$) we define several objectives to radiate focused beams at different directions and we calculate analytically the required phase shifts and reactive loads. Once the synthesis procedure is achieved, the resulting radiation patterns are calculated analytically, allowing fast parametric studies if needed. Then, the full-wave simulation is performed to validate the results. In this section, different objectives have been considered. In all the examples shown, the feed horn is always located at the same position (offset-fed reflectarray). The different radiation objectives are obtained only through the reactive load synthesis.

III.1 - Computation of the excitation weightings

We have seen in chapter II the beam synthesis procedure that begins by fixing the argument of the excitation weightings $\angle(a_{m,n})$ as in Eq.II.18. By following the path of the equations Eq.II.22 ... Eq.II.26, we were able to find one equation (Eq.26) that links the modulus of the excitations weightings $|a_{m,n}|$ to their arguments $\angle(a_{m,n})$, the incident coupled waves $b_{0\,m,n}$, the phase constant C and the scattering matrix [S].

One way to check this procedure is to compare between $|a_{m,n}|$ and $\left\|\overrightarrow{b_0} + [S].diag\left(e^{+j(p+C)}\right).\|\vec{a}\|\right\|$ for two focused beam test cases $\{\theta_1 = 0°, \varphi_1 = 0°\}$ and $\{\theta_2 = 15°, \varphi_2 = 90°\}$. I define (*A*,*B*) as $A = |a_{m,n}|$ and $B = \left\|\overrightarrow{b_0} + [S].diag\left(e^{+j(p+C)}\right).\|\vec{a}\|\right\|$. Actually the convergence routine stops when the following condition is respected:

$$B_{i+1} - B_i < tolerance.$$

Where $tolerance$ is the minimum accepted convergence error (such as $tolerance = 10^{-5}$). At the iteration i=0, *B* is equal to the incident coupled waves $b_{0\,m,n}$. The convergence routine, in our case ***the fixed point method***, starts adding the mutual couplings and the desired phases to the magnitude of the excitations weightings.

While it is the first try we used this method to solve such a problem, we have performed a convergence to check the accuracy and the efficiency of the method in a reduced time. In Table III.4, I compare between *A* and *B* for the cells lying on the center line of the

panel (k=186:1:194) for several given iterations i. the cell indexed '190' is located at the origin of the coordinate system.

Index of the cells k	Focused beam test case $\{\theta_1 = 0°, \varphi_1 = 0°\}$					
	Start	Iterations *i*				Stop
	$B\ (i=0)$	$B\ (i=1)$	$B\ (i=2)$	$B\ (i=3)$	$B\ (i=4)$	$A = a_{m,n}$
K=186	8.013054e-002	6.696799e-002	6.656163e-002	6.667867e-002	6.666359e-002	6.666586e-002
K=187	8.577505e-002	9.402195e-002	9.403554e-002	9.400070e-002	9.405479e-002	9.403640e-002
K=188	8.844836e-002	1.157115e-001	1.165453e-001	1.167509e-001	1.167560e-001	1.167851e-001
K=189	8.847605e-002	9.945959e-002	1.003252e-001	1.004844e-001	1.005053e-001	1.005163e-001
K =190	8.653800e-002	7.135100e-002	7.089376e-002	7.107918e-002	7.107411e-002	7.108850e-002
K =191	8.295004e-002	7.550236e-002	7.451972e-002	7.463937e-002	7.461425e-002	7.461000e-002
K =192	7.650361e-002	9.673989e-002	9.719100e-002	9.726622e-002	9.729426e-002	9.728518e-002
K =193	6.808398e-002	7.639829e-002	7.736805e-002	7.744607e-002	7.745352e-002	7.745295e-002
K =194	6.012664e-002	4.824281e-002	4.805407e-002	4.798582e-002	4.796863e-002	4.793150e-002
Index k	Focused beam test case $\{\theta_2 = 15°, \varphi_2 = 90°\}$					
	$B\ (i=0)$	$B\ (i=1)$	$B\ (i=2)$	$B\ (i=3)$	$B\ (i=4)$	$A = a_{m,n}$
K=186	8.013054e-002	6.631853e-002	6.609548e-002	6.603315e-002	6.600665e-002	6.600759e-002
K=187	8.577505e-002	9.098893e-002	9.181697e-002	9.168700e-002	9.175271e-002	9.174818e-002
K=188	8.844836e-002	1.150863e-001	1.148545e-001	1.152553e-001	1.152350e-001	1.152465e-001
K=189	8.847605e-002	1.037518e-001	1.051687e-001	1.054672e-001	1.054844e-001	1.054912e-001
K =190	8.653800e-002	7.062362e-002	7.041393e-002	7.035402e-002	7.031393e-002	7.032133e-002
K =191	8.295004e-002	7.416508e-002	7.285111e-002	7.316540e-002	7.303466e-002	7.305254e-002
K =192	7.650361e-002	9.543795e-002	9.517666e-002	9.534474e-002	9.531193e-002	9.530568e-002
K =193	6.808398e-002	7.997840e-002	8.108605e-002	8.117979e-002	8.119706e-002	8.117135e-002
K =194	6.012664e-002	4.750961e-002	4.801646e-002	4.793332e-002	4.794797e-002	4.793630e-002

Table III.4: Convergence of the magnitude of the excitations weightings versus the objective radiation pattern. Test cases: $\{\theta_1 = 0°, \varphi_1 = 0°\}$ and $\{\theta_2 = 15°, \varphi_2 = 90°\}$

The ***fixed point method*** runs until the tolerance criterion is met, as we can see in the above table. For this first test case $\{\theta_1 = 0°, \varphi_1 = 0°\}$, the magnitude of the excitation weightings converged after 8 iterations. Starting the 9th iteration, the excitations weightings are no longer significantly affected; which means that *B* are the correct and actual excitations of the cells taking into account the mutual couplings between the cells.

Below in Fig .III.19 and Fig .III.20 I show the excitations weightings distribution $a_{m,n}$ for the two test cases $\{\theta_1 = 0°, \varphi_1 = 0°\}$ and $\{\theta_2 = 15°, \varphi_2 = 90°\}$ respectively.

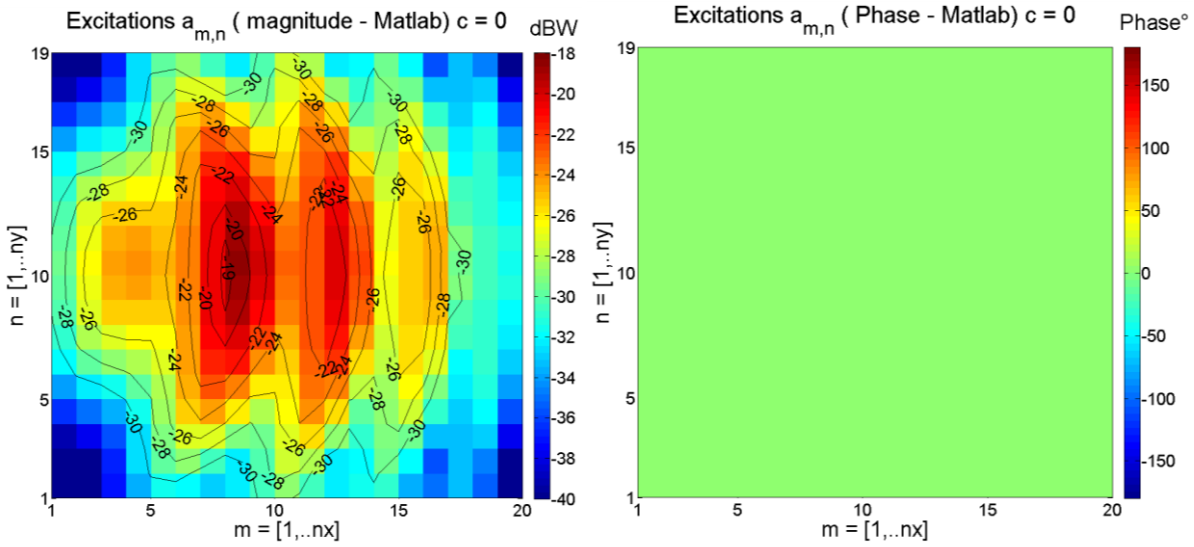

Figure.III.19. *Distribution of the excitations weightings of the cells on the panel for the test case* $\{\theta_1 = 0°, \varphi_1 = 0°\}$ *(left) magnitude (right) phase.*

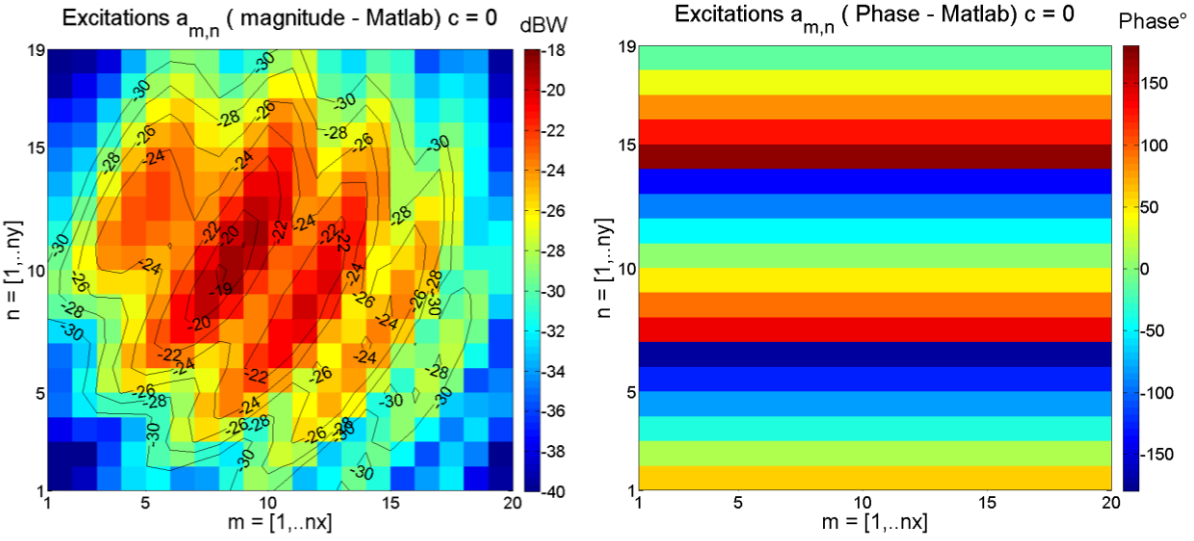

Figure.III.20. *Distribution of the excitations weightings of the cells on the panel for the test case* $\{\theta_2 = 15°, \varphi_2 = 90°\}$ *(left) in magnitude (right) in phase.*

III.2 - **Phase shifts and reactive loads distribution on the reflectarray panel**

Once we have computed the complex excitations weightings of the cells versus an objective radiation pattern using the convergence routine, we calculate the total incident waves $b_{tot\ m,n}$ using Eq.II.22:

$$b_{tot\ m,n} = b_{0\ m,n} + [S]a_{\ m,n}$$

The phase shift γ at each cell or the reflection coefficient $\Gamma_{m,n}$ is the ratio between the excitation weightings $a_{m,n}$ and the total incident wave $b_{tot\ m,n}$ at each cell as presented in Eq.II.9.

$$\Gamma_{m,n} = \frac{a_{m,n}}{b_{tot\ m,n}}$$

Using the equations Eq.II.27 we calculate the reactance of the reactive loads versus the phase shifts and the impedance of the cells. In this particular design we have matched the cells to 50Ω impedances.

$$\begin{cases} \gamma = argument(\Gamma) \\ X_{m,n} = img\left(\dfrac{50 + \Gamma_{m,n}}{50 - \Gamma_{m,n}}\right) \end{cases}$$

Finally the capacitances or inductances to be integrated behind the cells, to satisfy the radiation pattern objective, are deduced from the complex reactance, as shown in Eq.II.28:

$$\begin{cases} C_{m,n} = -\dfrac{1}{X_{m,n} \times \omega} \quad (F) & if\ X_{m,n} < 0 \\ L_{m,n} = +\dfrac{X_{m,n}}{\omega} \quad (H) & if\ X_{m,n} > 0 \end{cases}$$

In Fig .III.21 I show the phase shifts for two focused beam test cases $\{\theta_1 = 0°, \varphi_1 = 0°\}$ and $\{\theta_2 = 15°, \varphi_2 = 90°\}$. We notice that the phase shift distribution that focuses in the beam in the direction $\{\theta_1 = 0°, \varphi_1 = 0°\}$ is globally in phase opposition with the phase of the incident coupled waves $b_{0\ m,n}$ (Fig .III.13), a small distortion of phase appears because of the mutual couplings between the cells.

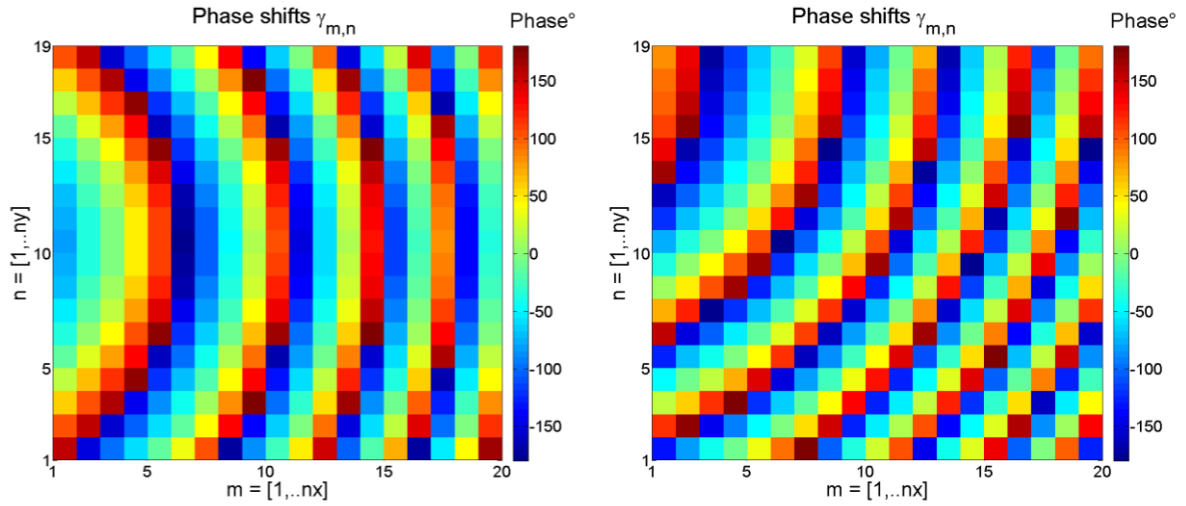

Figure.III.21. *Phase shift distribution $\gamma_{m,n}$ on the panel. (left)* $\{\theta_1 = 0°, \varphi_1 = 0°\}$. *(right)* $\{\theta_2 = 15°, \varphi_2 = 90°\}$

III.3 - **Radiation Pattern Computation**

The radiation patterns are calculated thanks to the analytical formalism, with the parameters extracted from CST MWS ($\vec{E}_{diffracted}\ (\theta, \varphi)$,$\vec{F}_{cell}\ (\theta, \varphi)$) and the excitations weightings computed in Matlab. The analytical formalism employs Eq.II.16 and Eq.II.17. The 3D radiation patterns for the test cases $\{\theta_1 = 0°, \varphi_1 = 0°\}$ and $\{\theta_2 = 15°, \varphi_2 = 90°\}$ are shown in Fig .III.22. The maximal directivity equals 28.76 dB for the first case and 28.68 dB for the second case. Fig .III.23 shows the directivity in the plane

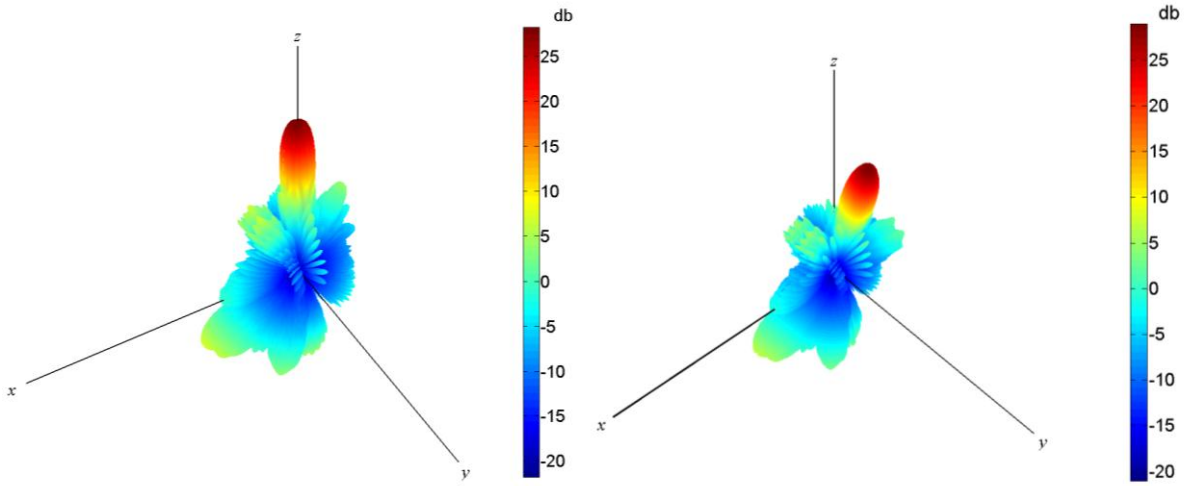

Figure.III.22. *3D view of the Calculated radiation pattern. (left)* $\{\theta_1 = 0°, \varphi_1 = 0°\}$. *(right)* $\{\theta_2 = 15°, \varphi_2 = 90°\}$

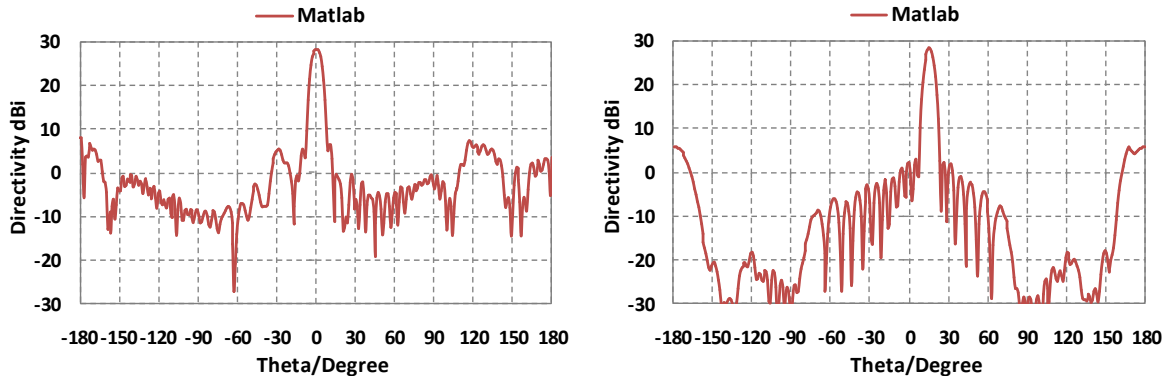

Figure.III.23. *Computed radiation pattern in the plane* $\varphi = 90°$. *(left)* $\{\theta_1 = 0°, \varphi_1 = 0°\}$. *(right)* $\{\theta_2 = 15°, \varphi_2 = 90°\}$.

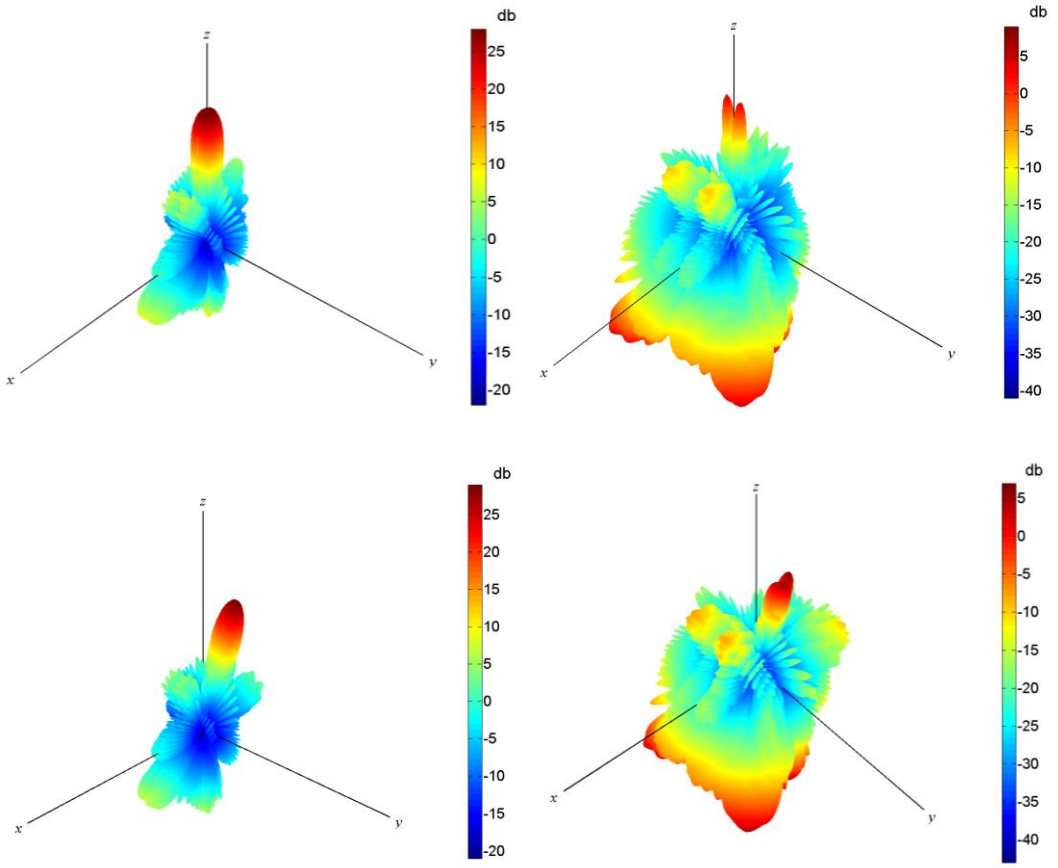

Figure.III.24. *3D representation of the Co-polarized field (left) and Cross-polarized field (right) for the two test cases: (top)* $\{\theta_1 = 0°, \varphi_1 = 0°\}$*; (bottom)* $\{\theta_2 = 15°, \varphi_2 = 90°\}$.

We can also compute the polarization components of the radiation pattern (i.e. Co- and cross- respectively) from their spherical components (θ,φ). The results are illustrated in Fig .III.24. The principal polarization is the horizontal one (H) according to the polarization of the feed antenna. The cross polarization level is at 7dB, 21dB below the principal polarization.

III.4 - **Summary of the physical characteristics obtained with the analytical formalism**

The different physical quantities that appears in the equations of the analytical formalism have been illustrated for the two focused beams test cases $\{\theta_1 = 0°, \varphi_1 = 0°\}$ and $\{\theta_2 = 15°, \varphi_2 = 90°\}$ in Fig .III.25 and Fig .III.26 respectively. The feed antenna is always located at the left edge of the panel.

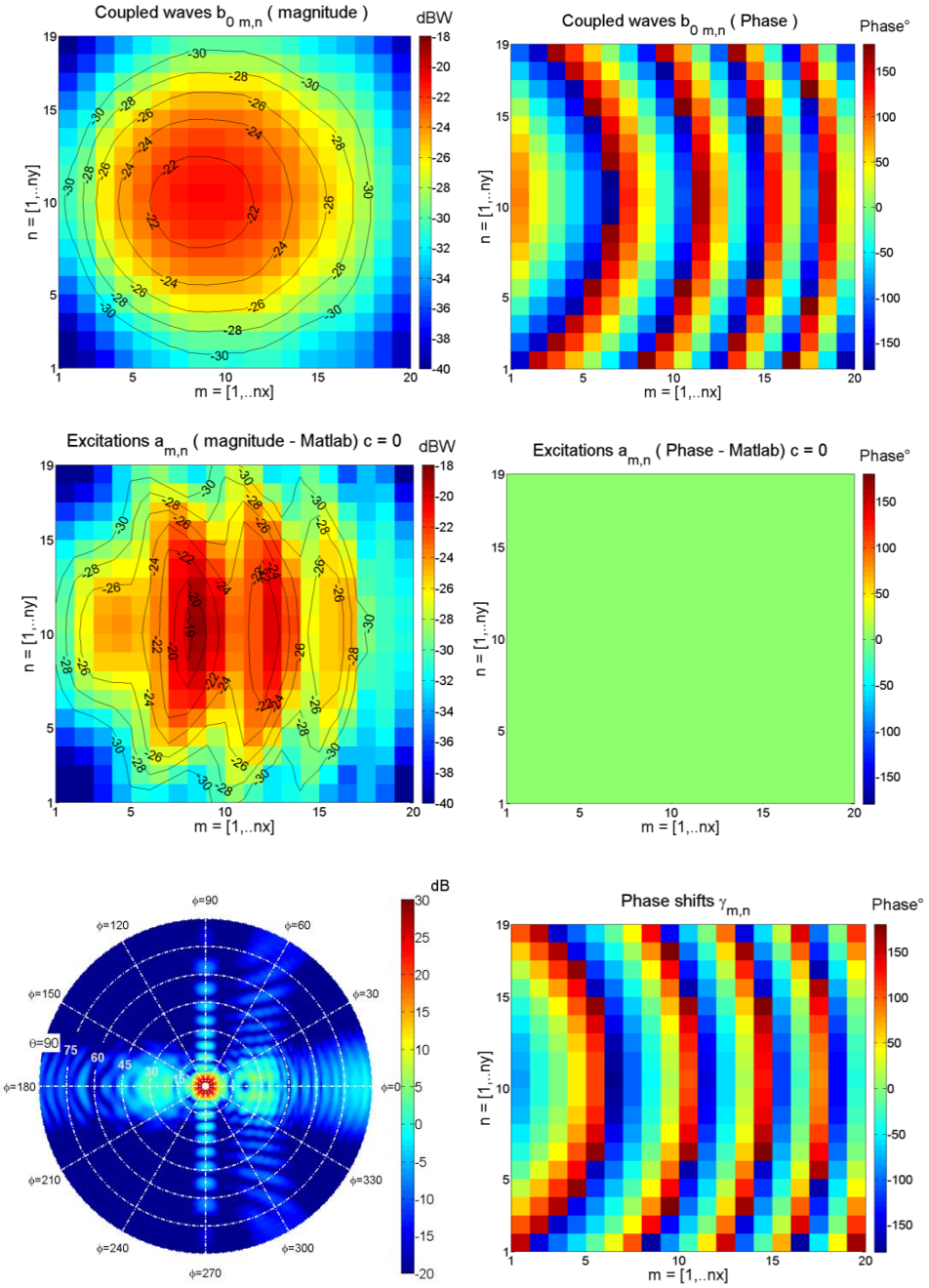

Figure.III.25. *Test case: focused beam* $\{\theta_1 = 0°, \varphi_1 = 0°\}$ $D1_{max} = 28.76\ dB$

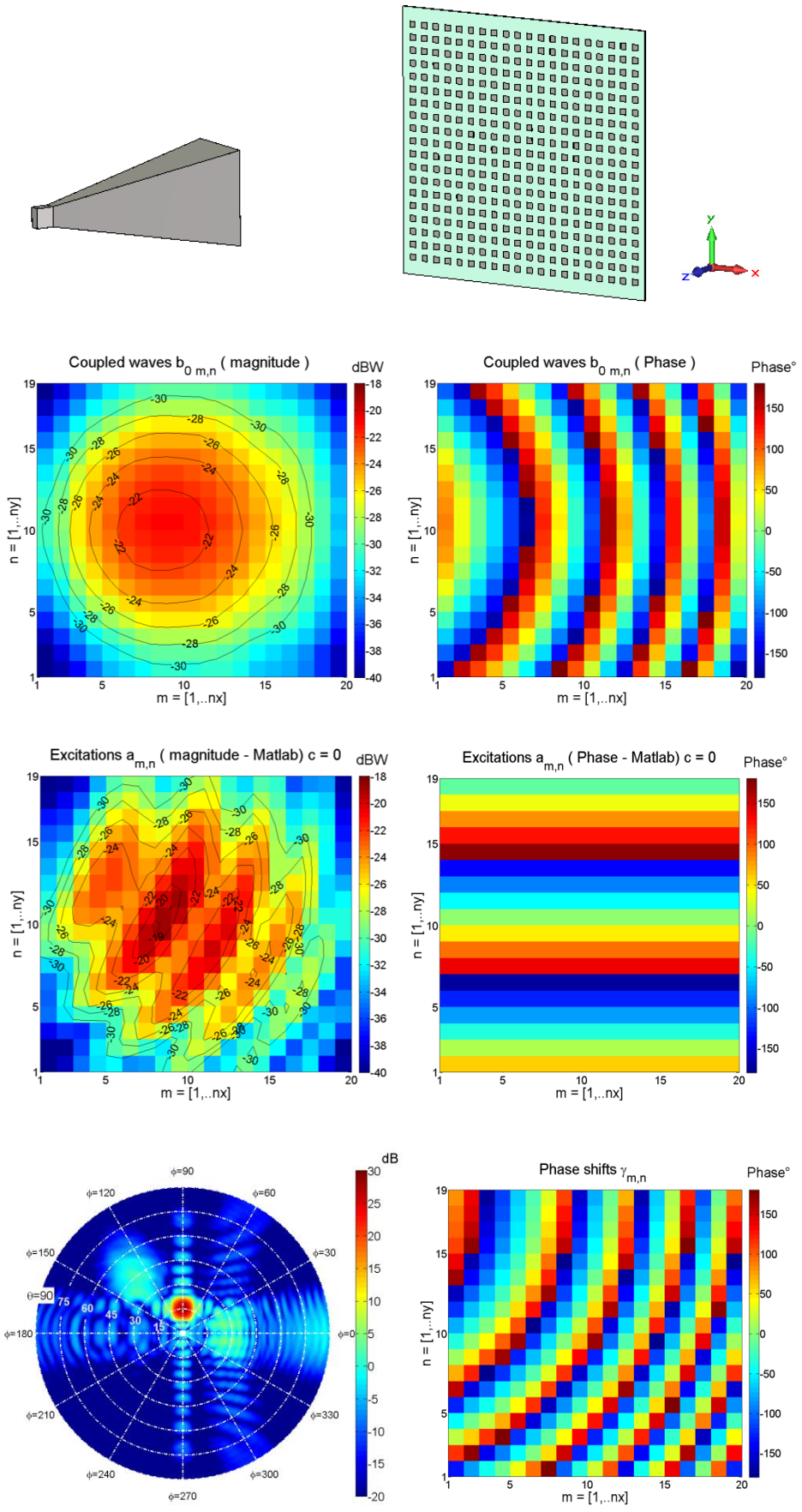

Figure.III.26. Test case: focused beam $\{\theta_2 = 15°, \varphi_2 = 90°\}$ $D2_{max} = 28.68\ dB$

IV - Full-wave Simulation of the Optimized Reflectarray antenna

The former results have been obtained through the design modules for analysis and synthesis of the RA. However, all the antenna elements have never been merged in a single full-wave study. In this part, all the resulting elements leading to the optimized antenna will be included in a same transient full-wave simulation with CST MWS.

This stage allows concluding on the design modular process developed in this thesis. Reactive loads are connected to the cells ports as described in phase three, and we excite the feed antenna. The resulting radiation patterns are shown in Fig .III.27. These figures are 2D polar representation of the front radiation patterns calculated via CST MWS. They include the edge diffracted fields and specular reflected field components, which can be clearly seen in the region (φ <60° and φ >300°). The rear radiation pattern (including spillover effects) has been truncated on this representation but all its effects are accounted for. Notice that the two radiation objectives have been voluntarily chosen in two different directions to show the different contributions. The computed phase shifts to radiate focused beams in the directions $\{\theta_1 = 0°, \varphi_1 = 0°\}$ and $\{\theta_2 = 15°, \varphi_2 = 90°\}$ are accurate by judging the computed radiation patterns in CST MWS in Fig .III.27 (to be compared with Fig .III.25 and Fig.III.26).

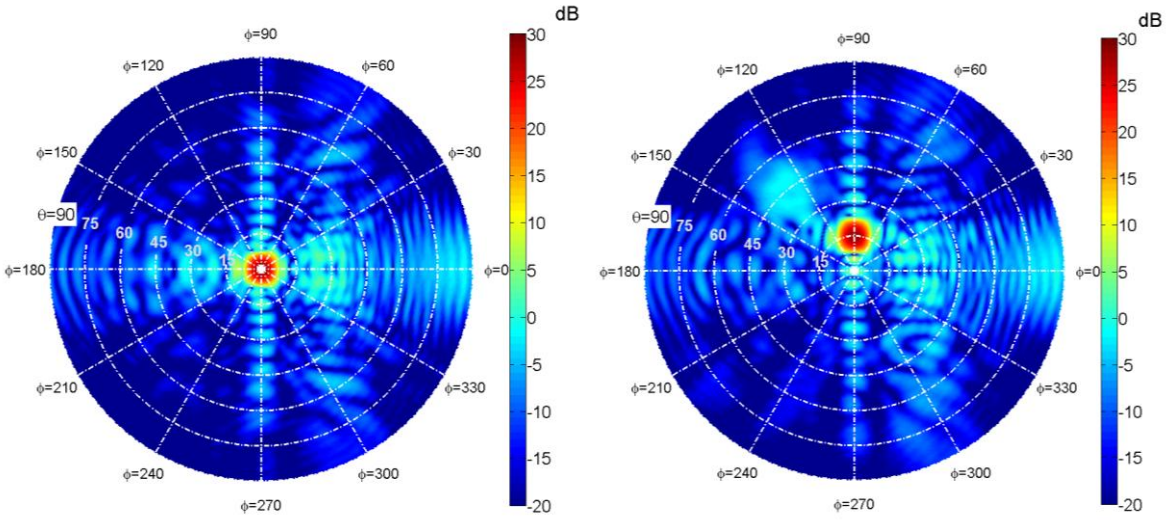

Figure.III.27. *Directivity of the radiation pattern computed in the full-wave simulation. Front radiation, test case: focused beams. (left) $\{\theta_1 = 0°, \varphi_1 = 0°\}$ $D1_{max} = 28.95$ dB. (right) $\{\theta_2 = 15°, \varphi_2 = 90°\}$ $D2_{max} = 28.75$ dB.*

The maximal computed directivity for the beams $\{\theta_1 = 0°, \varphi_1 = 0°\}$ and $\{\theta_2 = 15°, \varphi_2 = 90°\}$ are $D1_{max}$ = 28.95 dB and $D2_{max}$ = 28.75 dB. Notice that these values are in very close agreement from $D1_{max}$ = 28.76 dB and $D2_{max}$ = 28.68 dB with the analytical formalism. The dynamic range for the axis of the colobar is set to 50db to make the secondary lobes and diffracted fields visible.

IV.1 - Radiation pattern comparison between the analytical formalism and the full-wave simulations

Comparing between Matlab's and CST MWS's results shows a good agreement in the radiation patterns. As a matter of fact, the analytical analysis driven in Matlab takes into accounts the full-wave environment of CST MWS (such as the diffracted field on the reflectarray panel, the active radiation pattern and the scattering matrix).

Below in Fig .III.28, I compare between the radiation patterns computed in both Matlab and CST MWS.

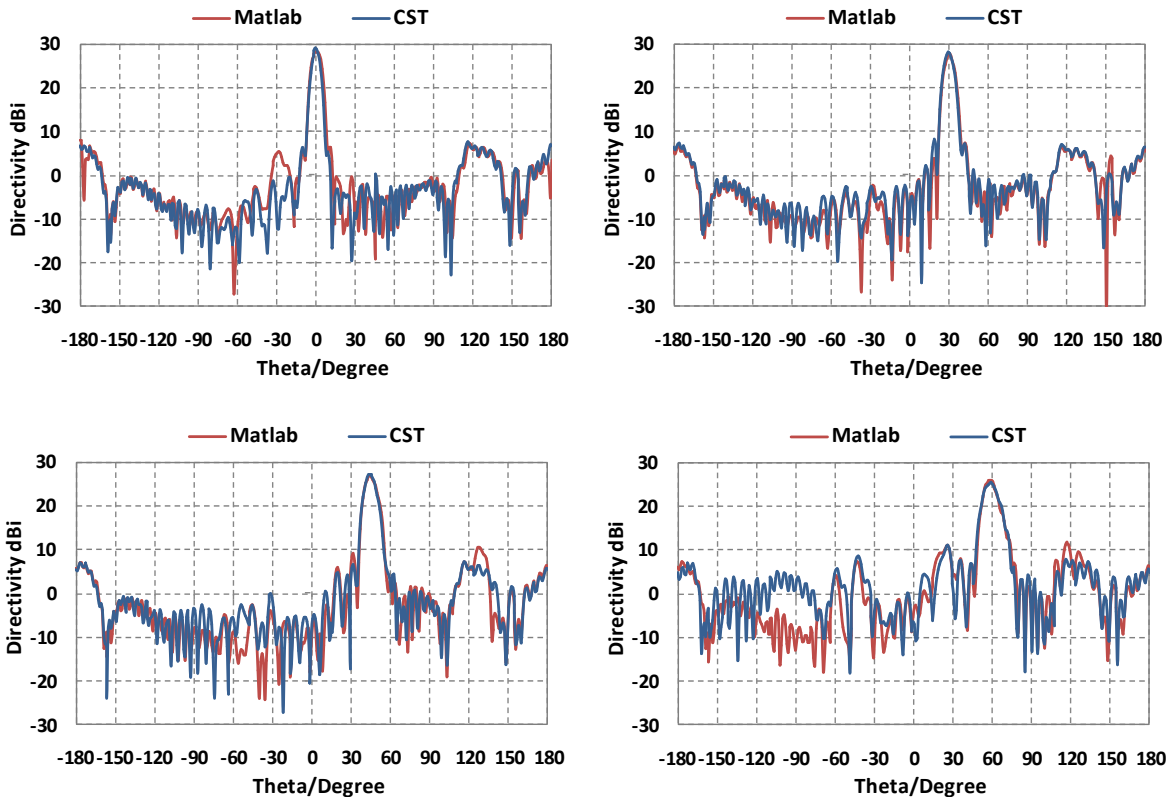

Figure.III.28. *Comparison between Matlab and CST for 4 different focused beams cases in the specular direction. View in the plane* $\varphi = 0°$.

The figures show focused beams radiating in different directions of the specular direction (in the plane $\varphi = 0°$). The directions of the focused beams are the following $\{\theta_1 = 0°, \varphi_1 = 90°\}$, $\{\theta_2 = 30°, \varphi_2 = 0°\}$, $\{\theta_3 = 45°, \varphi_3 = 0°\}$ and $\{\theta_4 = 60°, \varphi_4 = 0°\}$. The results show a good agreement. We start to notice a small disagreement on the rear radiation pattern when the boresight direction is important versus the elevation plane ($\theta_0 > 50°$).

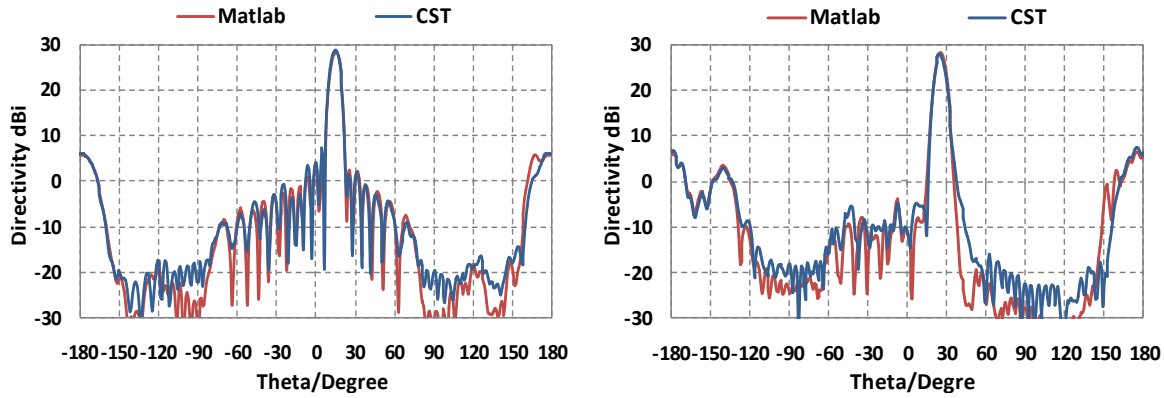

Figure.III.29. *Comparison between Matlab and CSTMWS for the test cases $\{\theta_1 = 15°, \varphi_1 = 90°\}$ and $\{\theta_2 = 25°, \varphi_2 = 135°\}$*

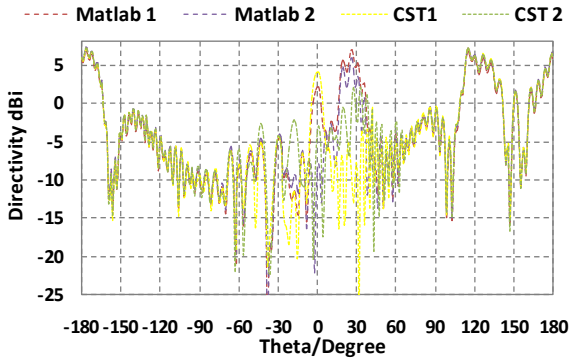

Figure.III.30. *Comparison on the diffracted fields patterns for the above focused beam cases.*

Above in Fig .III.34 I compare between the radiation patterns of focused beams radiating outside the specular direction ($\{\theta_1 = 15°, \varphi_1 = 90°\}$ and $\{\theta_2 = 25°, \varphi_2 = 135°\}$. The results show a good agreement in the overall. In Fig .III.35, I compare between the corresponding diffracted fields in the specular direction. The conclusion is the same.

Therefore, the use of CST MWS to calculate the radiated fields with the reactive loads is an optional step. In fact, in this validation, we have seen a good agreement between the predicted radiation patterns with Matlab and the ones obtained with the CST MWS full-wave simulation. This is an important result because it validates our synthesis process and thus,

optimizations or parametric studies on the reactive loads are possible in few seconds with a good accuracy on the radiation patterns.

IV.2 - **Antenna efficiency in the case of losses included in the structure**

In this section, I compare two structures. The first structure is ideal and lossless, the metal is set to PEC (perfect electric conductor), and the reactive load impedance is purely imaginary ($R_{load} = 0\ \Omega$). The dielectric losses are also null. The second structure is lossy making it closer to the reality. Conductive and dielectric losses are introduced. PEC is replaced with IASC (International Annealed Standard Copper). The reactive loads present ohmic losses ($R_{load} = 5\ \Omega$). Full details are illustrated in Table III.5.

The previous patterns (Fig .III.27 to III.32) were already computed for the lossless antenna. An overview on the efficiency for the lossy antenna is available in Table III.6. The computed directivity refers to the focused beam radiating at the direction (θ_0 =15°, φ_0 =90°), as already seen in Fig .III.27 and Fig .III.29 (right).

	Loss free reflectarray	Lossy reflectarray
Microstrip patch cell	Lx = 7mm, Ly = 7mm dx = 8mm, dy = 8mm	
panel	nx = 20, ny = 19 cells F/D = 1.254	
Feed antenna	Directivity = 19.7 dB RL = -18 dB	
Spillover efficiency	$\eta_s = 83\%$	
Tapper efficiency	$\eta_t = 87\%$	
Dielectric material	Rogers 4003 H= 1.425 mm $\varepsilon = 3.38$ $\tan\delta = 0$ Thermal Cond = 0 w/k/m	Rogers 4003 H= 1.425 mm $\varepsilon = 3.38$ $\tan\delta = 0.0027$ Thermal Cond = 0.64 w/k/m
Metallic properties	PEC $\sigma = \infty$ Thermal Cond = 0 w/k/m	IASC $\sigma = 5.8^7\ S/m$ Thermal Cond = 401 w/k/m
Reactive loads	R = 0 Ω	R = 5 Ω

Table III.5: Lossless reflectarray and a lossy reflectarray

As the table shows, the components that downgrade mostly the performances of a reflectarray antenna are the reactive loads. Besides causing thermal losses in the structure, introducing errors at the active loads damages the overall directivity. This study considers no phase errors. So we should expect a bigger damage in that case. Of course this study remains theoretical and not practical. Not all the type of errors can be studied in a simulation particularly the active components. Since they could present a non linear behavior and cause more thermal losses (pin diodes could add 3dB loss) or a distortion on the phase shift. So a measurement is a must in this case.

	Lossless design	Lossy design
Directivity	28.75 dB	28.45 dB
Total radiated power	0.98 W	0.84 W
Load losses	--	-0.48 dB
Metallic losses	--	-0.03 dB
Dielectric losses	--	-0.17 dB
Gain IEEE	28.75 dB	27.774 dB
Feed mismatching	-0.07 dB	-0.08 dB
Realized gain	28.68 dB	27.69 dB
Efficiency	74.8 %	59.5 %

Table III.6: Comparison on the efficiency between the lossless and the lossy reflectarray

I defined the final efficiency of the reflectarray as the ratio between the power contained in the pattern's main lobe and the power radiated by the feed antenna. In other words, the percentage of the useful electromagnetic fields radiated in the desired direction.

$$efficiency = \frac{\int_{\vartheta}\int_{\varphi} \left|\overrightarrow{E_{reradiated}}(\theta,\varphi)\right|^2 \sin\theta d\theta d\varphi \ /120\pi}{Power\ 3_{total}} \quad \text{(III.1)}$$

Where(ϑ,φ) are the solid angles defined in the area around the main lobe in which the directivity is -10dB below the maximum directivity.

It should be noted that when CST MWS computes the realized gain, it considers only the thermal losses in the structure plus the mismatching at the feed antenna. The illumination efficiency is not taken into account inside CST MWS.

V - Conclusion

In this chapter, I have shown a design test for our reflectarray analysis and synthesis approach. The antenna has a small size (380 elements) compared to other reflectarrays which can contain thousands of elements. The objective is to optimize the performance of the antenna by controlling the energy balance of the system.

Firstly I have studied the illumination law on the panel using a commercial standard horn gain as feed antenna. The illumination should fit to the small panel. The optimum position for the feed is chosen versus the taper and the illumination efficiencies.

Using the above parameters (feed horn, feed position and orientation, panel and cells size, etc ..) I have built the entire reflectarray design inside CST MWS and performed a convergence study on the mesh settings have to be sure that the computed parameters are accurate. Next, the full-waves simulations to prepare the reflectarray design database have been launched. This database contains the input parameters required for the analytical formalism (Scattering parameters, active pattern, incident coupled power waves and diffracted fields).

Then, several radiation objectives have been defined. To do that, we must compute the excitation weightings of the cells. The phases of the excitation weightings are given by the array factor and their modulus are computed thanks to a convergence routine that takes into account the mutual couplings of the cells. Once the excitations weightings of the cells are defined, we synthesize the reactive loads and calculate the final radiation pattern of the antenna. We have voluntary chosen different targets to illustrate the potentialities of such an antenna designed with this approach. In all the examples shown, the feed horn is always located at the same position (offset-fed reflectarray). The different radiation objectives are obtained only through the reactive load synthesis, and the mutual couplings are always considered.

To validate the analytical formalism the reactive loads are added to the full-wave simulation and then we computed the radiation pattern of the antenna via CST MWS. A comparison with Matlab demonstrated a good agreement, especially on the directivity level, side lobes and for the diffracted fields pattern which are usually the hardest to compute using a periodical approach. Notice that the distribution of the power among the elements is also clearly available.

The results were accurate because of the good knowledge and understanding of the energetic balance of the structure. This is possible thanks to the discrete ports that are added behind the reflectarray cells.

In the next chapter, as the analytical approach is validated, we will focus on the analysis of some important EM behaviors in RA and we will give some performances analysis of RA including technological constraints like the quantification effects.

VI - References

[1] A.D Olver, P.J.B. Clarricaats, A.A. Kishk, and I. Shafai, "Microwave horns and feeds," *IEEE Elect. waves series*, 1994.

[2] Flann microwave, "Standard gain horns," *http://www.flann.com/*.

[3] Ticra, *www.ticra.com*.

[4] Y. Abdallah, C. Menudier, M. Thevenot, and Monediere T., "Reflectarray Antennas with Accurate Calculation of Phase Shifts," *Proceedings of EUCAP, Rome*, April 2011.

[5] CST MWS Studio, "CST STUDIO SUITE™ Introduction in VBA Macro usage and programming," *www.cst.com*.

[6] C. Menudier and T. Koleck, "Sub-Reflectarrays Performances for Reconfigurable," *IEEE Trans. and Ant. Prop*, vol. 60, no. 7, pp. 3476-3481, July 2012.

[7] Y. Abdallah, C. Menudier, M. Thevenot, and T. Monediere, "Switchable Steerable Square Parasitic Monopole Array design using a Genetic Algorithm," *Int. Symp. Antem*, June 2012.

Chapter IV

INVESTIGATION ON ELECTROMAGNETIC PROPERTIES OF REFLECTARRAYS

I - Introduction

The reflectarray modeling techniques are mainly affected by the assumptions made on mutual couplings between the cells [1]. This parameter is hard to investigate because of very different geometries of the cells have been developed in the literature and also because of the important number of cells lying on a panel (typically several thousands). Full-wave simulations are difficult to perform because of a prohibitive memory and CPU cost. Even if multi-level formalisms have been develop, as the Multi-Level Fast Multipole Method (MLFMM) [2], this approach is suitable for analysis only and does not allow parametric or optimization processes. To overcome these limitations, a significant effort has been led on the mutual couplings assumptions. One of the well-known approaches is based on the local periodicity [3]. It consists in the modeling of a unit cell distributed on an infinite lattice thanks to Floquet modes [4]. It takes into account the effect of incidence of the impinging waves and the couplings are assumed identical whatever the position of the cell on the panel (identical cells). However, this approximation is inefficient with a limited number of cells (impact of edge effects becomes not negligible) or with different cells. To overcome these restrictions, significant efforts are performed in order to obtain a robust and versatile method to design reflectarrays. Among the promising contributions, the authors of [5] propose a Surrounded Element Approach (SEA). It consists in the simulation of a cell with its neighbors (no periodicity allowed), leading to a more precise assumption of mutual couplings even if several runs are required. More recent works use the compression method combined to the SEA to relate the couplings with more accuracy [6]. Recently, the concept of Extended Local Periodicity (ELP) has been developed [7]. It consists in the modeling of a repeating scheme with an extended unit cell with its nearest neighbors. Notice that a promising method, initially developed for arrays, has been derived for reflectarrays, it is the Scale Changing Technique (SCT) [8]. It consists of a sub-domain decomposition with Scale Changing Networks allowing to represent fine details and couplings. All these formalisms aim at finding the best trade-off between mutual coupling accuracy and computation time because it is recognized that the mutual couplings are the cause of discrepancy in the reflectarray design, dramatically reducing their development.

Even if significant advances are made on reflectarray modeling to analyze their final electromagnetic performances, some interesting behaviors are not well detailed. In this chapter, we focus on the effects of the mutual couplings on the cell excitation weightings.

Therefore, we want to insist on the accurate coupling modeling impact. Such a study needs several parametric changes, which are tough to investigate with FW simulations. That is why we will use our synthesis module and the formalism described in the previous chapters. The full-wave simulations will be used only for validation purposes.

In this chapter, we will use our analytical formalism to demonstrate the effects of couplings on the RA EM characteristics. We will also study the effect of the phase reference that can be applied to the reflectarray weightings. These two particular points will be addressed to focus on the importance of a fine study of the EM properties of the RA, which is a physical point of view.

However, the analytical formalism developed can also be used for practical design. As an example case, we will also study the effects of quantized states of the phase shifts, which can be directly linked to a phase shifter or cell technology (PIN diodes, MEMS, etc…). This last part is an engineering point of view. As a result, we want to show that the formalism developed for a specific architecture of RA can be very helpful either to understand physical aspects of the RA or to design the RA.

II - Effects of the mutual couplings on the excitations weightings of the reflectarray cells

II.1 - Heritage of phased arrays to be applied on the reflectarray antennas

When antenna elements are placed in an array, they interact with each other. This interaction between elements due to their close proximity is called mutual coupling. The electromagnetic behavior of each *surrounded element* changes in comparison with an *isolated element* case.

It is well known that one of the main concerns of phased array antennas is the mutual coupling between the radiating elements [9]. The performances of phased array antennas are affected in many aspects [10]; Firstly, the input impedance of each radiating element changes from its initial value due to the mutual coupling. This variation is unstable when we change the direction of the radiated beam. This phenomenon causes a mismatching between the output impedance of the beam-forming network and the input impedance of the elements at different given beam directions if the BFN is not properly designed. Secondly the array can radiate no power in certain angles; this issue is called angle blindness [11].

Similarly to phased array, we will encounter those phenomena on the reflectarray panel in the excitations weightings of the cells. Once we have access to the electromagnetic quantities at the reflectarray cells thanks to the EM access/Ports, the panel is treated as a phased array composed from hundred of radiating elements. Instead of dealing with incident and reflected electromagnetic field components, we are dealing with incident and reflected power waves which were computed inside the discrete ports both in magnitude and phase. These power waves are the cells excitation weightings as if they were the output of a BFN. We will benefit from the heritage of phased array to have a better understanding of the reflectarray pattern synthesis by including the mutual couplings between the cells.

II.2 - **Calculus of the excitations weightings**

We have seen in the second chapter that the excitation weightings of the cells are related to the Scattering matrix, the incident coupled power waves and the reflection coefficients/phase shifts. The corresponding equation (Eq.II.24) is reminded in Eq.IV.1.

(IV.1) *(Eq.II.24)* $\vec{a} = \left[[\Gamma]^{-1} - [S]\right]^{-1}\overrightarrow{b_0}$

The above equation is related to Fig .IV.1, already presented in chapter 2. We remind that once the radiation objective has been set, the analytical formalism synthesis is used with the elements provided to the database ([S], $\vec{E}_{diffracted}\ (\theta,\varphi)$, $\vec{F}_{cell}\,(\theta,\varphi)$, $\overrightarrow{b_0}$).

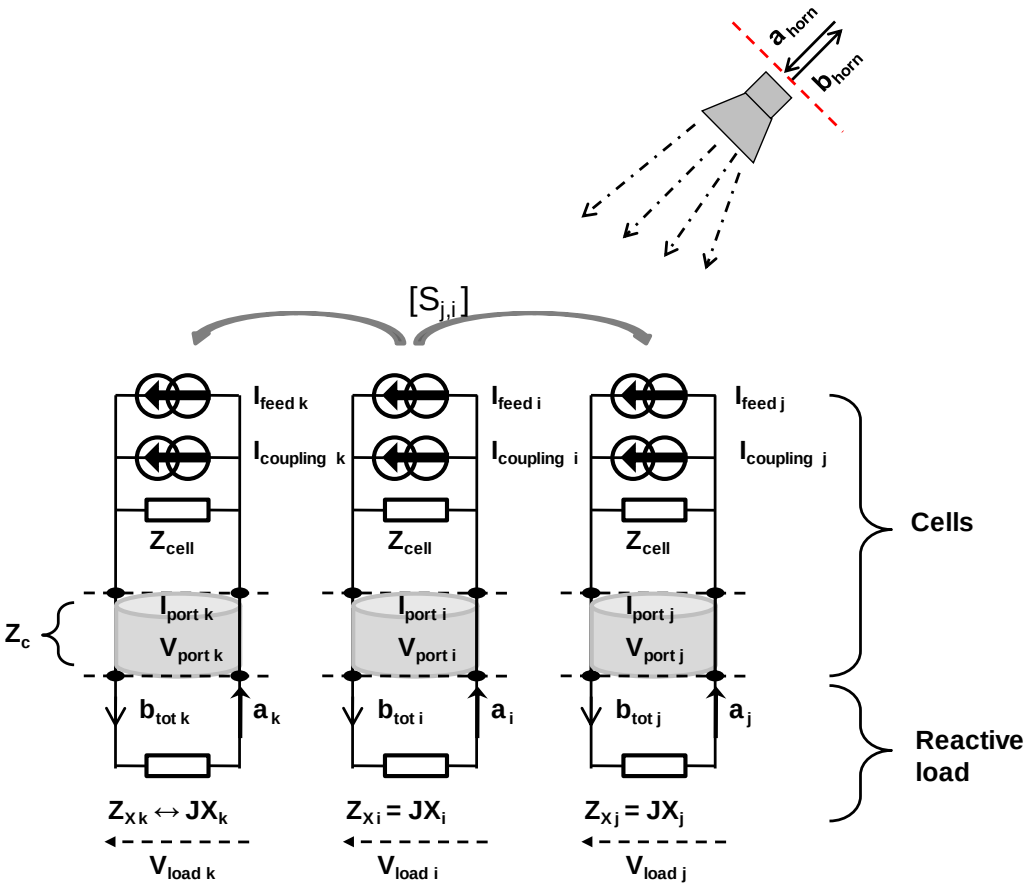

Figure. IV.1. *Circuit model of the reflectarray antenna*

When simulating the antenna via the commercial software CST MWS we remember to configure the discrete ports and the reactive loads as voltages and currents monitors behind the cells.

In this case, the excitation weighting of the cell is directly related to the currents I_{port} passing through the ports and the voltages V_{load} around the reactive load according to Eq.IV.2:

$$a_{m,n} = \frac{(V_{load\ ,\ m,n}) - 50 * I_{port\ ,\ m,n}}{2\sqrt{50}} \quad \text{(IV.2)}$$

The above equation can be used to study the effects of the mutual couplings [12]. Similarly to the previous logic, the electric currents and voltages are related to the excitations weightings and the total incident coupled waves, as illustrated in Eq.IV.3:

$$\begin{cases} I_{port\ m,n} = \frac{a_{m,n} - b_{tot\ m,n}}{\sqrt{50}} \\ V_{port\ m,n} = R_{port\ m,n} * I_{port\ m,n} = R_{port\ m,n} * \frac{a_{m,n} - b_{tot\ m,n}}{\sqrt{50}} \end{cases} \quad \text{(IV.3)}$$

II.3 - **Investigation on the mutual couplings**

In this section, we will use the methodology defined to study the RA in order to detail the effects of couplings. In order to compare different states of couplings, we have computed several beam directions {θ_0 =15°; φ =90°}, {θ_0 =45°; φ =245°} and {θ_0 =45°; φ =245°} as illustrated in Fig .IV.3, Fig .IV.5 and Fig .IV.7. The corresponding excitation weightings $a_{m,n}$ were computed *analytically* and they are illustrated in Fig .IV.4, Fig .IV.6 and Fig .IV.8 (Left). The excitations weightings distributions are computed also via the full-wave simulations from the electric currents and voltages as seen in Eq.IV.2. They are illustrated in Fig .IV.4, Fig .IV.6 and Fig .IV.8 (Right). By comparing the analytical formalism to the full-wave results we notice a great agreement. The modulus of the excitation weightings lead to an interesting observation which is visible thanks to our analysis technique. We can notice the difference between the modulus of the incident waves $b_{0,m,n}$ (Fig .IV.2) and the excitation weightings $a_{m,n}$ in both cases (Fig .IV.4 and Fig .IV.6).

The common assumption today is that reflectarray cells radiate an energy proportional to the one captured from the primary feed. This could be true if we neglect the mutual couplings between the cells ([S] = [0]). In such a case, we would simplify (Eq.IV.1) into the following expression:

$$\vec{a} = [\Gamma].\overrightarrow{b_0} \quad \text{(IV.4)}$$

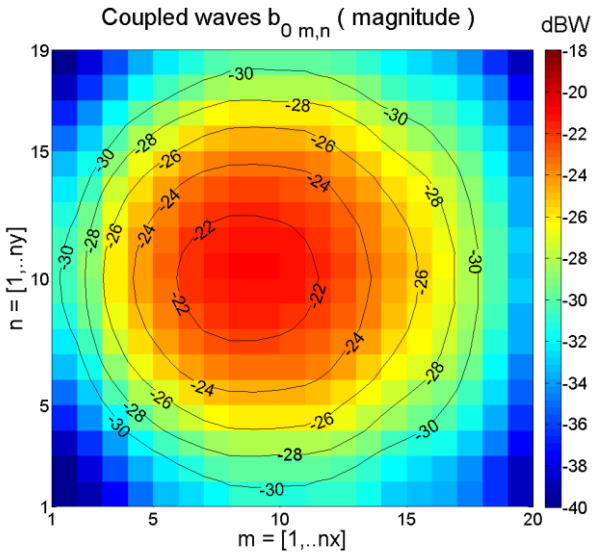

Figure. IV.2. *Distribution of the modulus of the complex incident coupled waves $b_{0,mxn}$ on the panel in dBW*

However it is very important to notice that when we take the scattering matrix into account, a difference appears between the magnitude of the incident waves $b_{0,m,n}$ and the excitation weightings $a_{m,n}$ in both cases (Fig .IV.2, Fig .IV.4 and Fig .IV.6). Also we can notice that the magnitude of $a_{m,n}$ is not the same when the radiation pattern objective changes.

A strong distortion on the excitations weightings is observed because of couplings. This could be explained by Eq.IV.1. In fact, the beam direction related to the argument of $\vec{a}$ is also related to the parameters $a_{m,n}$, [S] and $b_{0,m,n}$. The contribution of the cells in the radiation pattern changes on the panel. The mutual coupling is added to the incident waves in a constructive way at some cells leading to a higher level of energy or in a destructive way in some other cells causing a particular behavior, in the way that each cell accepts the energy from the primary feed.

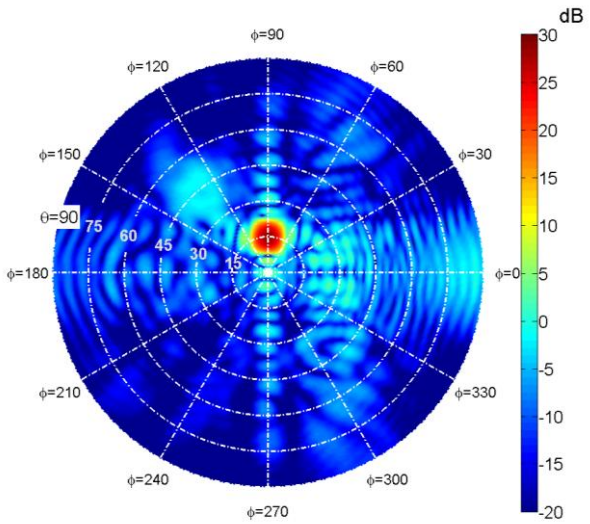

Figure. IV.3. *Directivity of the radiation pattern computed in the full-wave simulation. Front radiation, test case: focused beam {θ_0 =15°; φ_0 =90°} D_{max} =28.75dB*

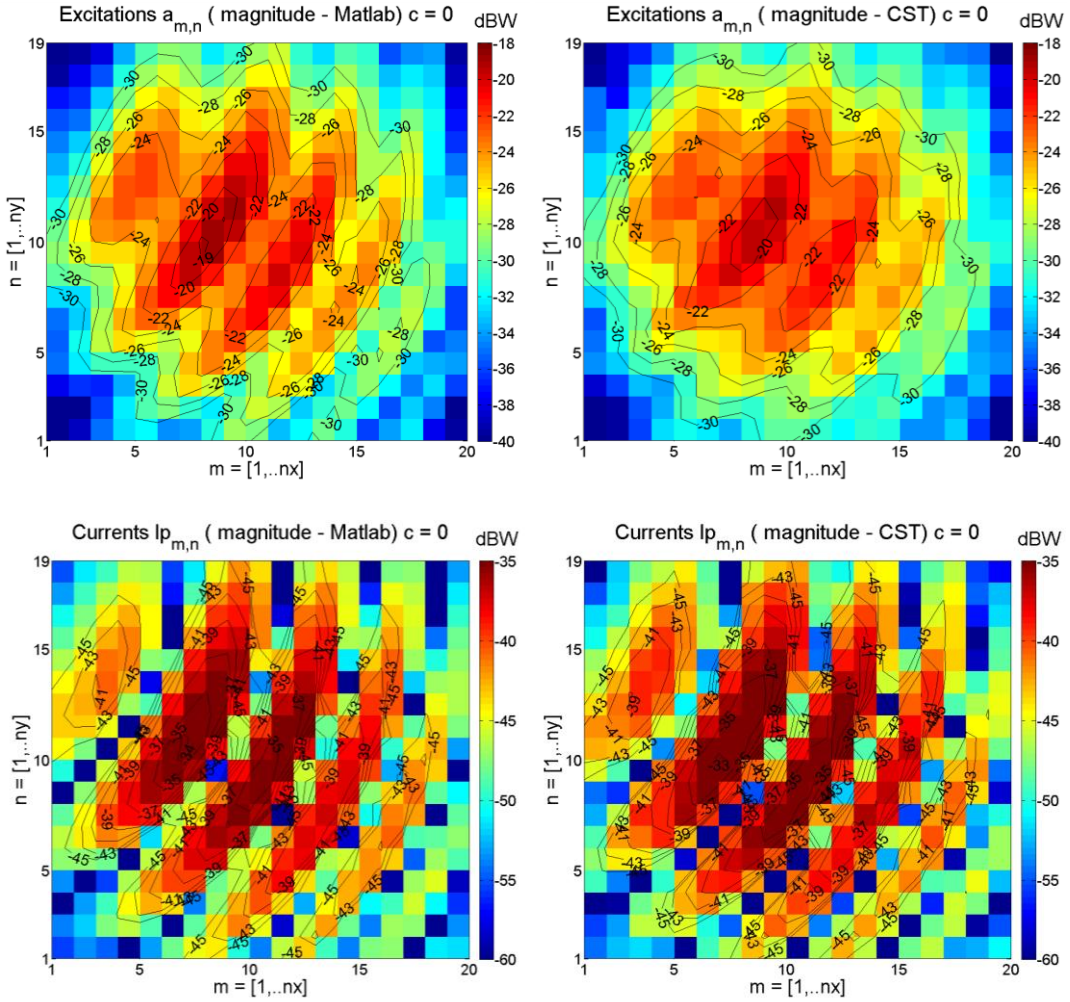

Figure. IV.4. *Distribution of the magnitude of the excitation weightings a_{mxn} on the panel, in the first test case {θ_0 =15°; φ_0 =90°}, phase constant C = 0°. (Left) for the analytical formalism, (Right) for the full-wave simulation*

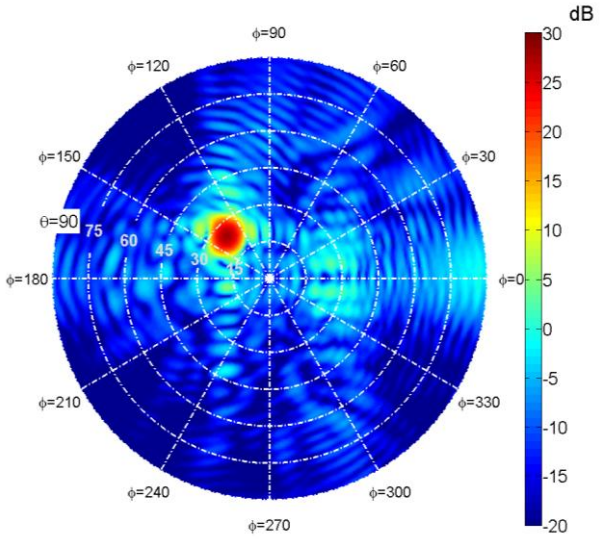

Figure. IV.5. *Directivity of the radiation pattern computed in the full-wave simulation. Front radiation, test case: focused beam {θ_0 =25°; φ_0 =135°} D_{max} =27.8 dB*

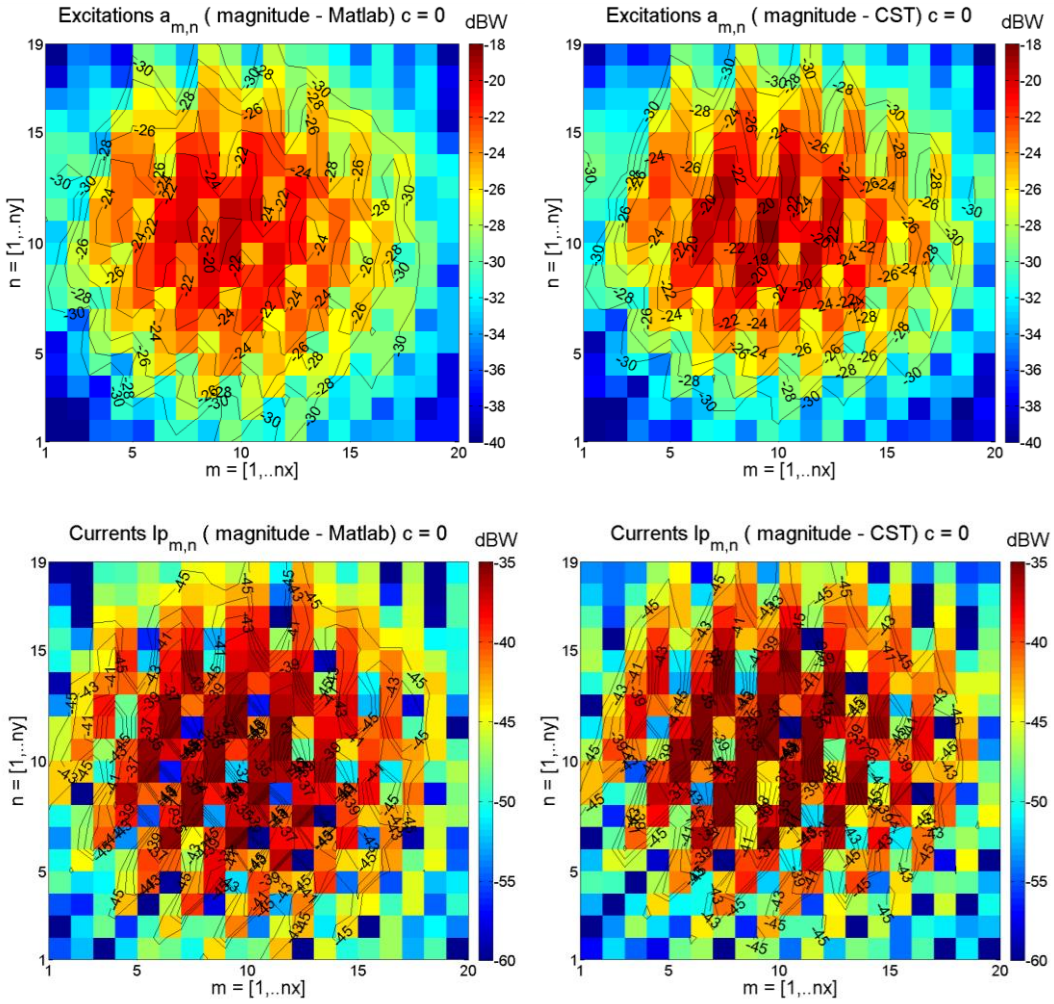

Figure. IV.6. *Distribution of the magnitude of the excitation weightings a_{mxn} (top) and of the current Ip_{mxn} (bottom) on the panel in the test case {θ_0 =25°; φ_0 =135°}, phase constant C = 0°. (Left) for the analytical formalism, (Right) for the full-wave simulation*

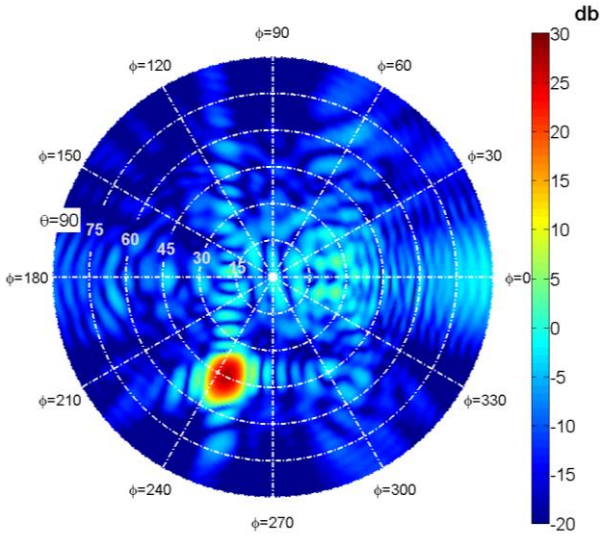

Figure. IV.7. *Directivity of the radiation pattern computed in the full-wave simulation. Front radiation, test case: focused beam {θ_0 =45°; φ_0 =245°} D_{max} =27.28 dB*

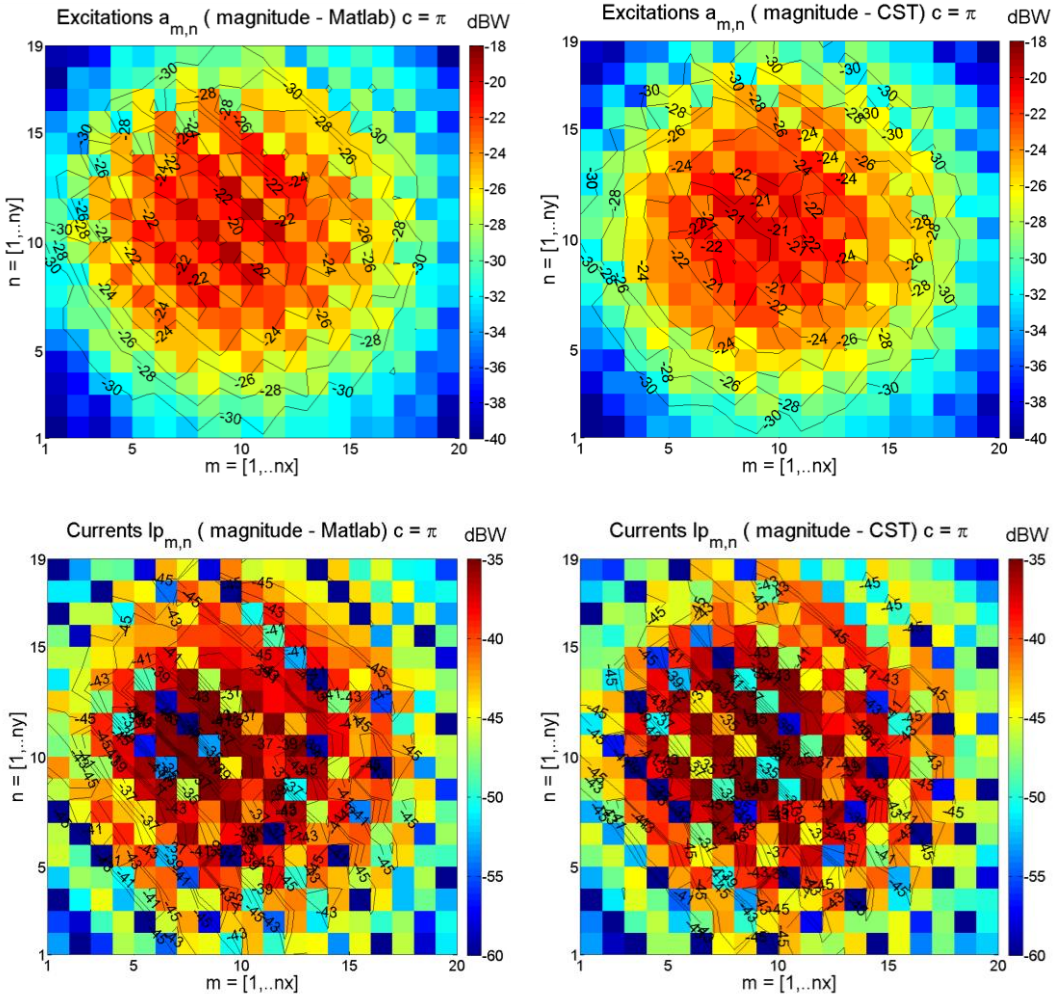

Figure. IV.8. *Distribution of the magnitude of the excitation weightings a_{mxn} (top) and of the current Ip_{mxn} (bottom) on the panel in the test case {θ_0 =45°; φ_0 =245°}, phase constant C = 180°. (Left) for the analytical formalism, (Right) for the full-wave simulation.*

II.4 - **Correlation between the modulated excitation weightings and the phase shift distributions**

A good agreement between the analytical formalism and the full-wave results is spotted, as seen in the previous figures. The first remark is that the shape of the excitation weightings distribution is subject to complex forms and sharp variations. The second remark is that these variations or modulations on the panel are correlated to the phase shifts γ, as illustrated in Fig .IV.9.

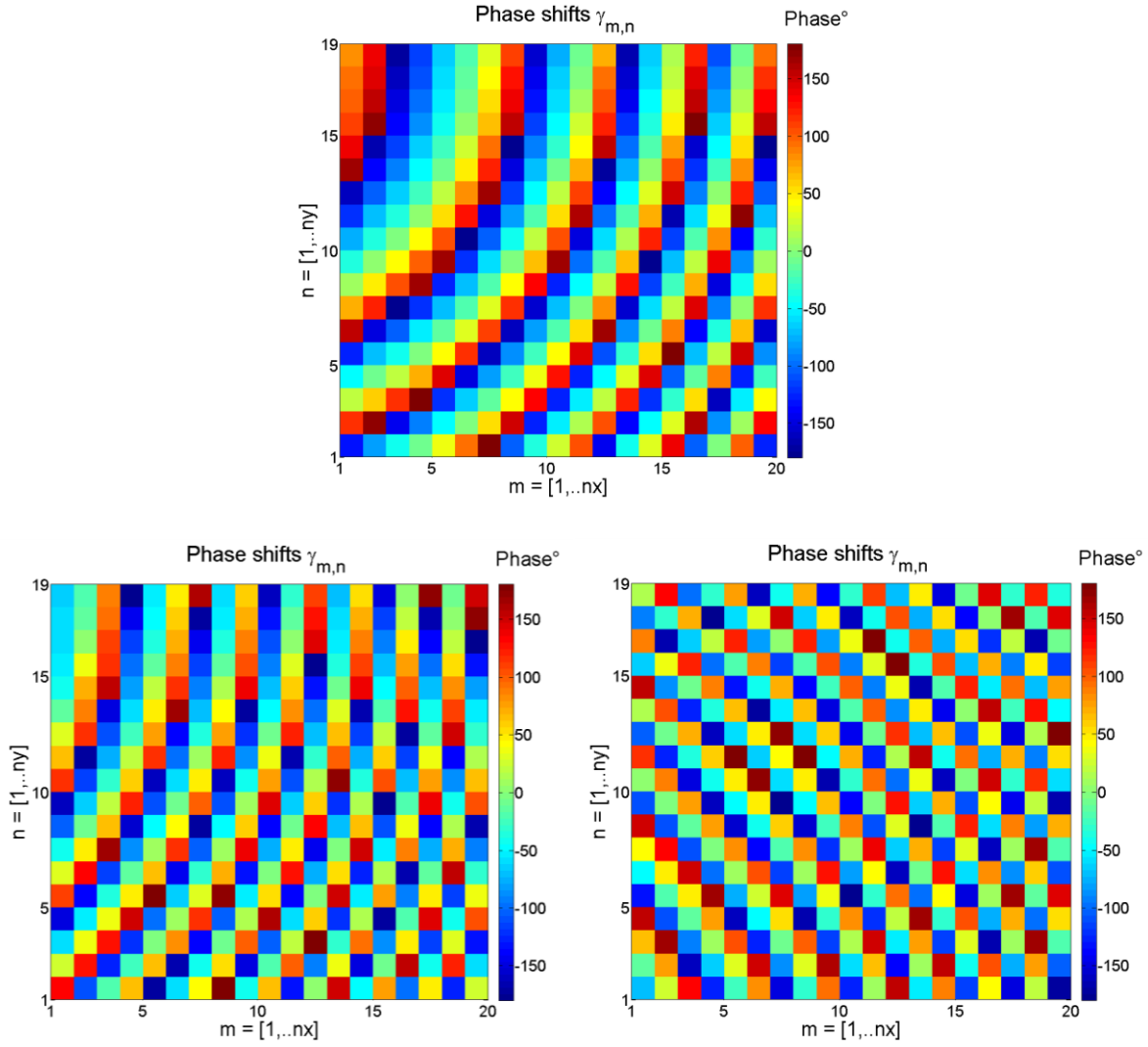

Figure. IV.9. *Distribution of the phase shifts γ_{mxn} on the panel. (Top) test case: {θ_0 =15°; φ_0 =90°}, c=0°. (Bottom-left) test case: {θ_0 =25°; φ_0 =135°}, c=0°. (Bottom-right) test case: {θ_0 =45°; φ_0 =245°}, c=180°*

III - Effects of the phase constant 'C' on the EM behavior of the cells

III.1 - Case of a Continuous phase shift synthesis

Another interesting parameter impacting the results is the phase constant *C* introduced in Eq.II.18. In this section, two beam directions have been studied, $\{\theta_0 = 30°; \varphi = 0°\}$ and $\{\theta_0 = 60°; \varphi = 0°\}$. Fig .IV.13 shows spots with different widths; they are computed with different phase constants *C=0:60°:300°*. This option allows optimizing the excitation magnitudes on the panel, which is recommended for shaped beam applications, where the magnitude of the weightings can be as much important as the phase in order to shape the radiation pattern efficiently. In other words, it means that neglecting the couplings and the phase constant in a shaped beam synthesis can drastically affect the performances. Fig .IV.15 shows progressive 'waves' shifting the excitations weightings on the panel in the horizontal plane as the phase constant changes.

Beside controlling the magnitude of $a_{m,n}$, the phase constant *C* will affect the summation between the radiated field by the cells and the diffracted field. This parameter is neutral in the case $\{\theta_0 = 30°; \varphi = 0°\}$ as we can see in Fig .IV.10, nevertheless it affects the results in the case $\{\theta_0 = 60°; \varphi = 0°\}$. Therefore, it can be used to optimize the radiation pattern as shown in Fig .IV.11 and Fig .IV.12, and an improvement of 0.6 dB in the directivity is observed.

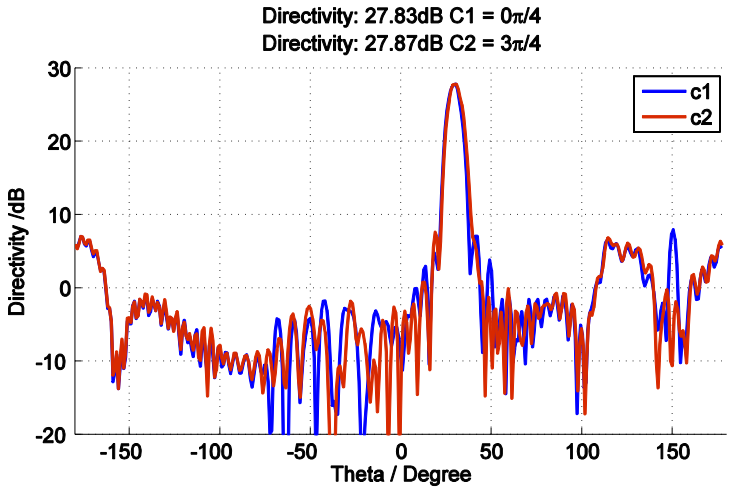

Figure. IV.10. *Calculated radiation pattern in the case $\{\theta_0 = 30°; \varphi_0 = 0°\}$ for 2 phase constants (c1=0 and c2=3π/4). $D1_{max}$ =27.87dB & $D2_{max}$ =27.83 dB*

The computed radiation patterns for these test cases shown in Fig .IV.10, Fig .IV.11 and Fig .IV.12 include spillover losses and the diffracted field on the panel. Notice that even if we do not see the impact of the phase constant *C* on the radiation pattern in the first case, the impact is real on the phase shifts and consequently the values of the reactive loads, as shown in Fig .IV.14 and Fig .IV.16. It gives a degree of freedom to choose realistic values of reactive loads. Below in Fig .IV.11 and Fig .IV.12 I present the radiation patterns computed via the FW simulations for the same objective $\{\theta_0 = 60°; \varphi_0 = 0°\}$. The only difference is in the phase constant C1 =0 and C2=$3\pi/4$, requiring to implement two different sets of reactive loads behind the cells before starting the full-wave simulations.

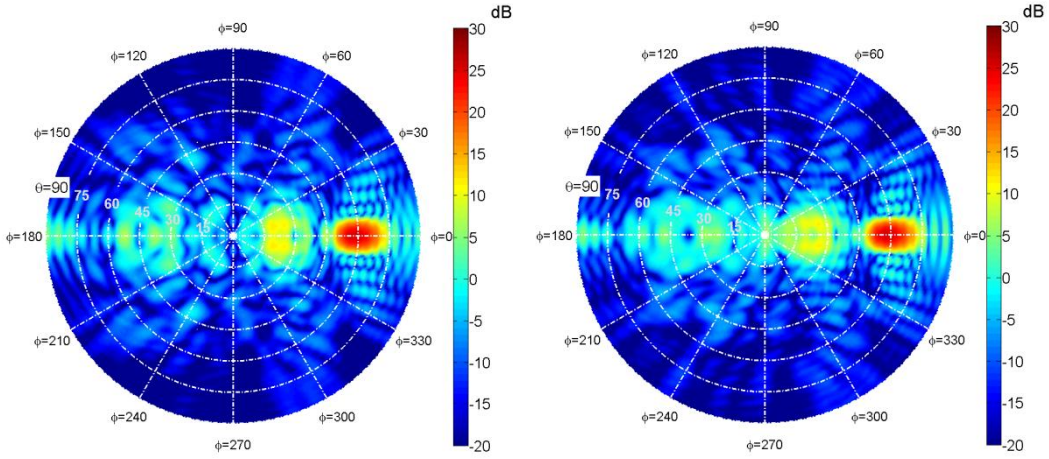

Figure. IV.11. *Calculated radiation pattern in the case $\{\theta_0 = 60°; \varphi_0 = 0°\}$ for 2 phase constants (c1=0 and c2=$3\pi/4$) $D1_{max}$ =25.66 dB & $D2_{max}$ =25.24 dB*

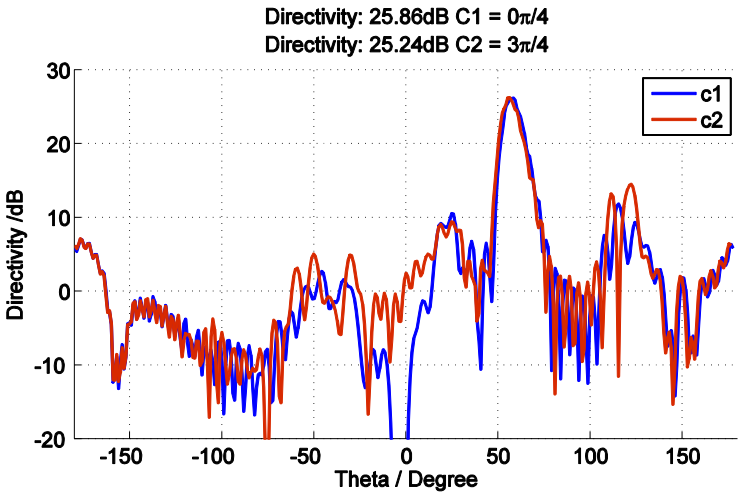

Figure. IV.12. *Calculated radiation pattern in the case $\{\theta_0 = 60°; \varphi_0 = 0°\}$ for 2 phase constants (c1=0 and c2=$3\pi/4$). $D1_{max}$ =25.66 dB & $D2_{max}$ =25.24 dB*

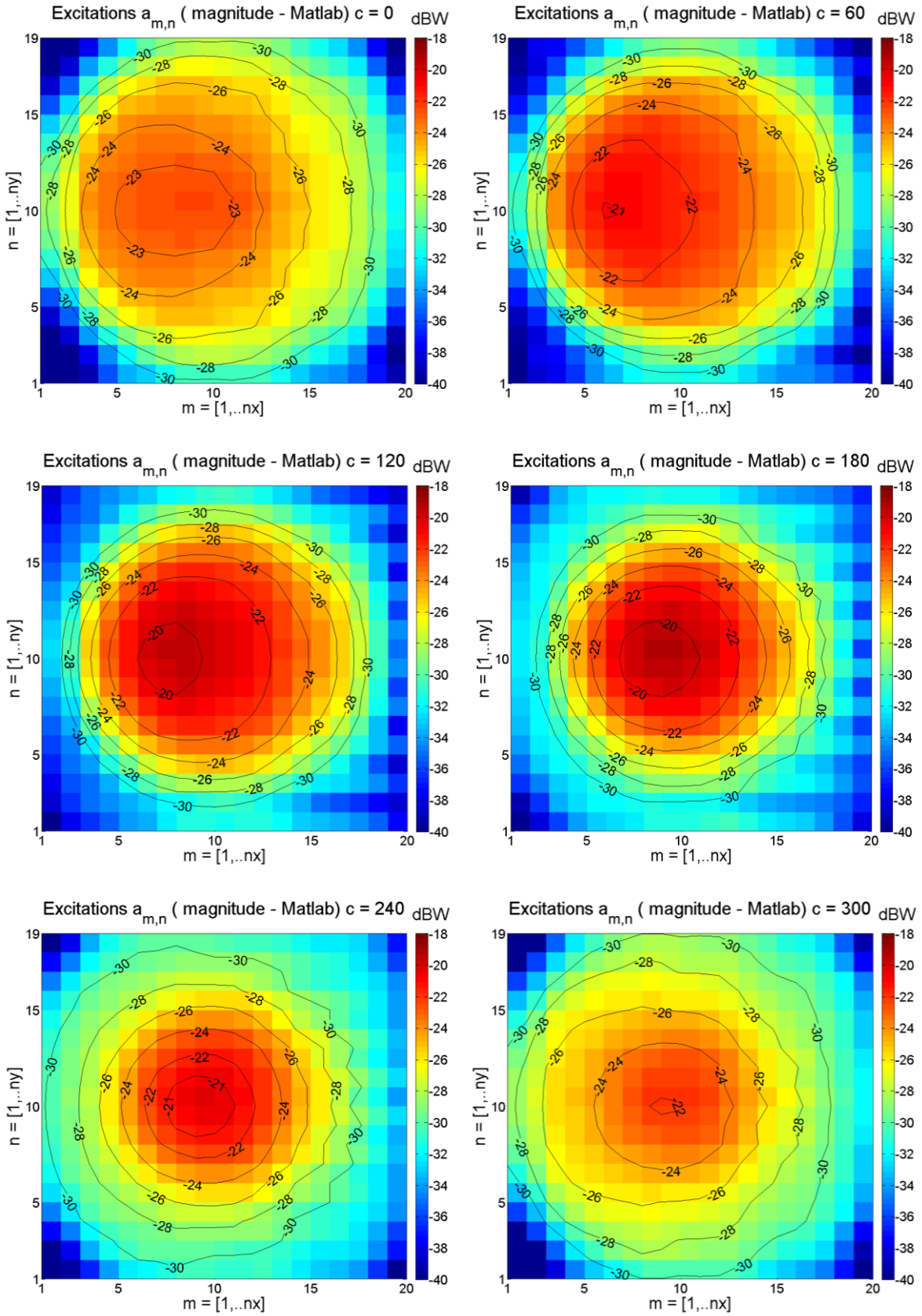

Figure. IV.13. *Distribution of the magnitude of the excitations a_{mxn} on the panel in the case {θ_0 =30°; φ_0 =0°} for several phase constants (C=0°:60°:300°).*

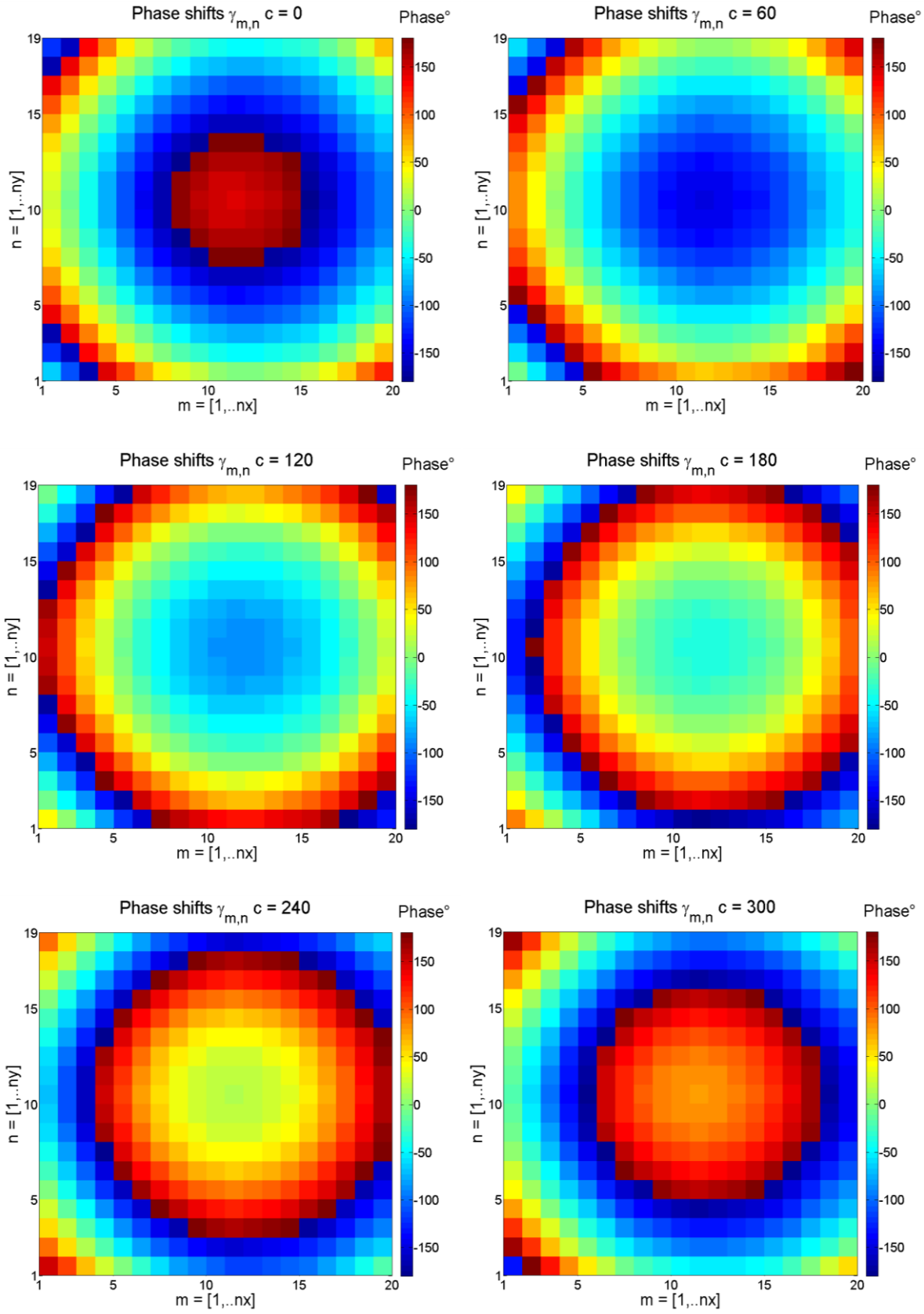

Figure. IV.14. *Distribution of the phase shifts $\gamma_{m,n}$ on the panel in the test case $\{\theta_0 = 30°; \varphi_0 = 0°\}$ for several phase constants (C=0°:60°:300°).*

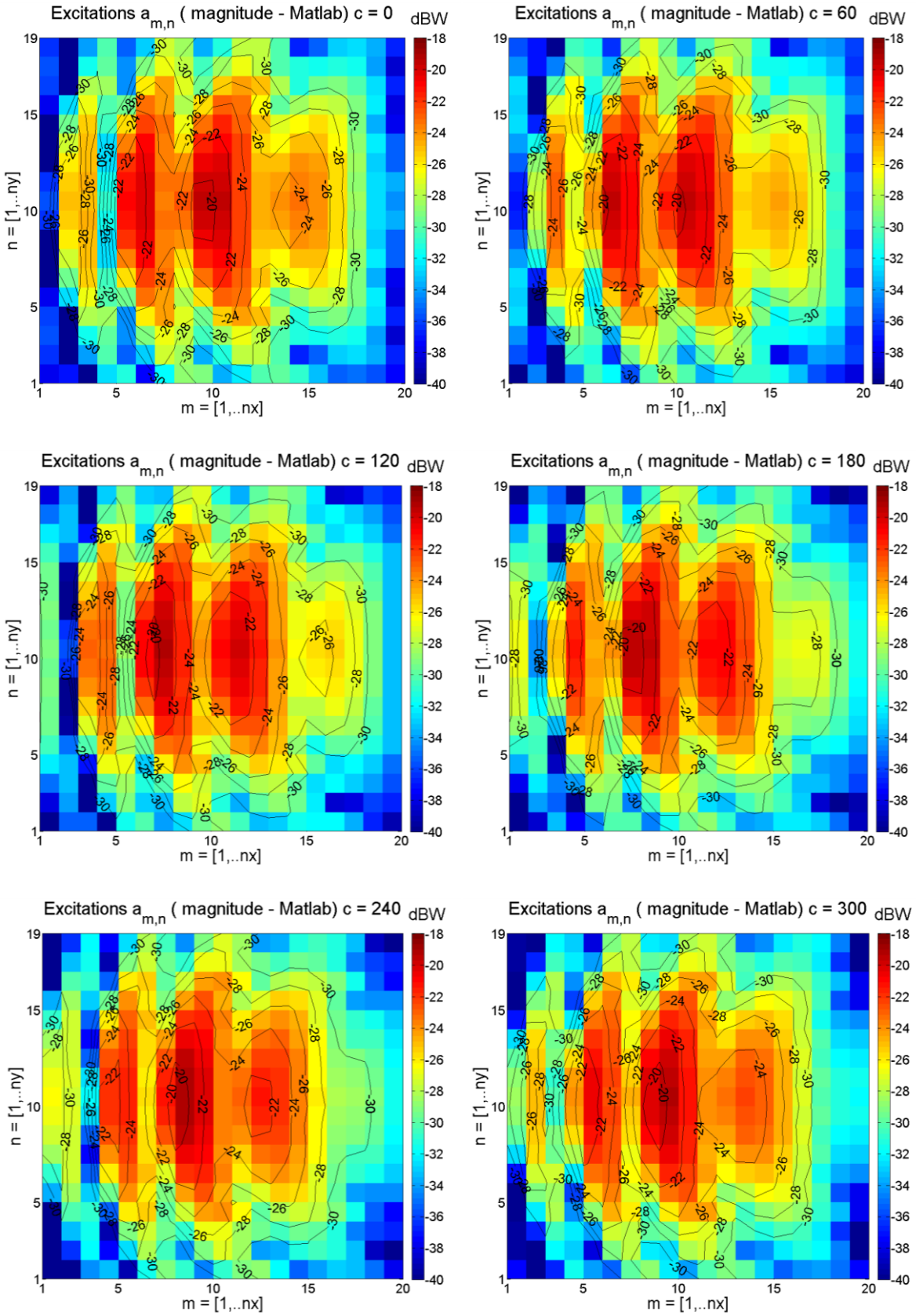

Figure. IV.15. *Distribution of the magnitude of the excitations a_{mxn} on the panel in the case {θ_0 =60°; φ_0 =0°} for several phase constants (C=0°:60°:300°).*

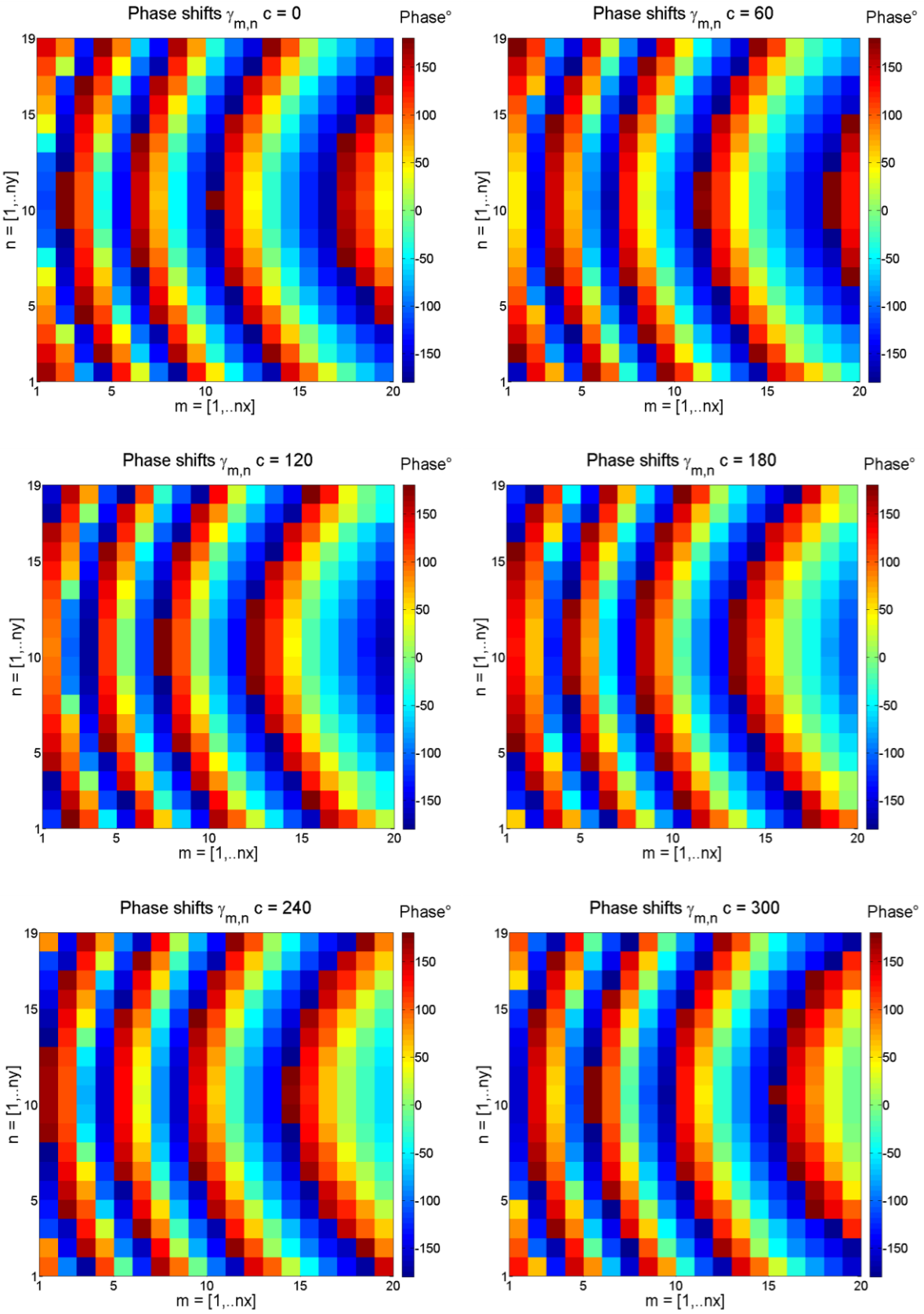

Figure. IV.16. *Distribution of the phase shifts $\gamma_{m,n}$ on the panel in the test case $\{\theta_0 = 60°; \varphi_0 = 0°\}$ for several phase constants (C=0°:60°:300°).*

III.2 - **Case of a prescribed discrete phase shift synthesis**

Similarly to the continuous phase shift synthesis, the phase constant 'C' impacts the results in the case of a discrete prescribed phase shift distribution. Below in Fig .IV.17 and Fig .IV.18 the phase shifts are computed to steer the beam in the direction $\{\theta_0 = 0°; \varphi_0 = 0°\}$, for two different levels of quantization, $(nb = 1)$ and $(nb = 2)$ respectively.

In Fig .IV.17, two different states for the reflectarray cells allows us to satisfy the objective radiation pattern. The maximum directivity is equal to 24.8 dB for the optimized phase constant $C_1 = 90°$ and to 23.9 dB for the un-optimized phase constant $C_2 = 290°$.

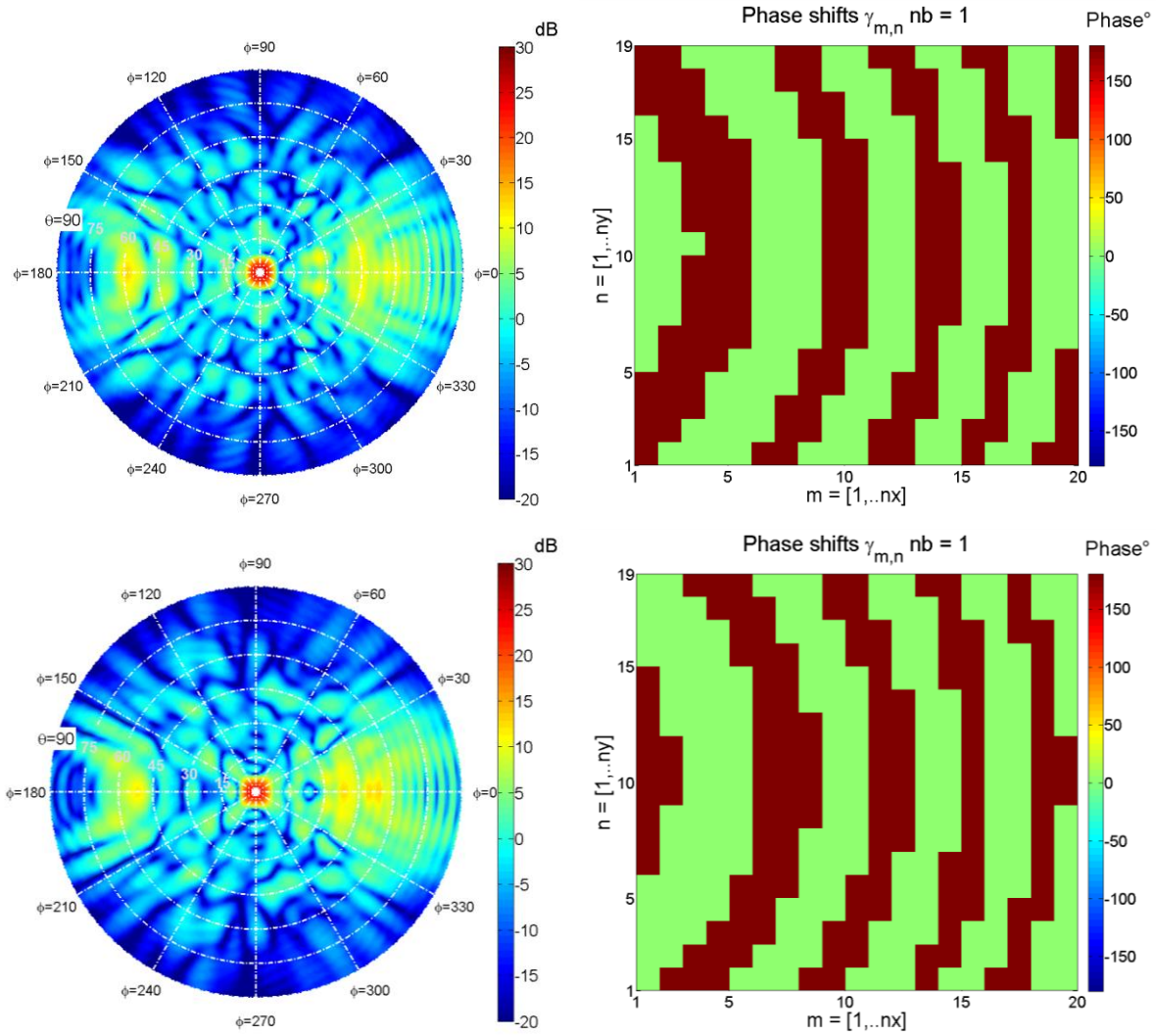

Figure. IV.17. *Computed phase shifts and radiation pattern for two values of the phase constant. (Top) Optimized C1 =90°; (Bottom) Un-Optimized C2 = 290°. Test case: focused beam $\{\theta_0 = 0°; \varphi_0 = 0°\}$, level of quantization* ***nb=1***

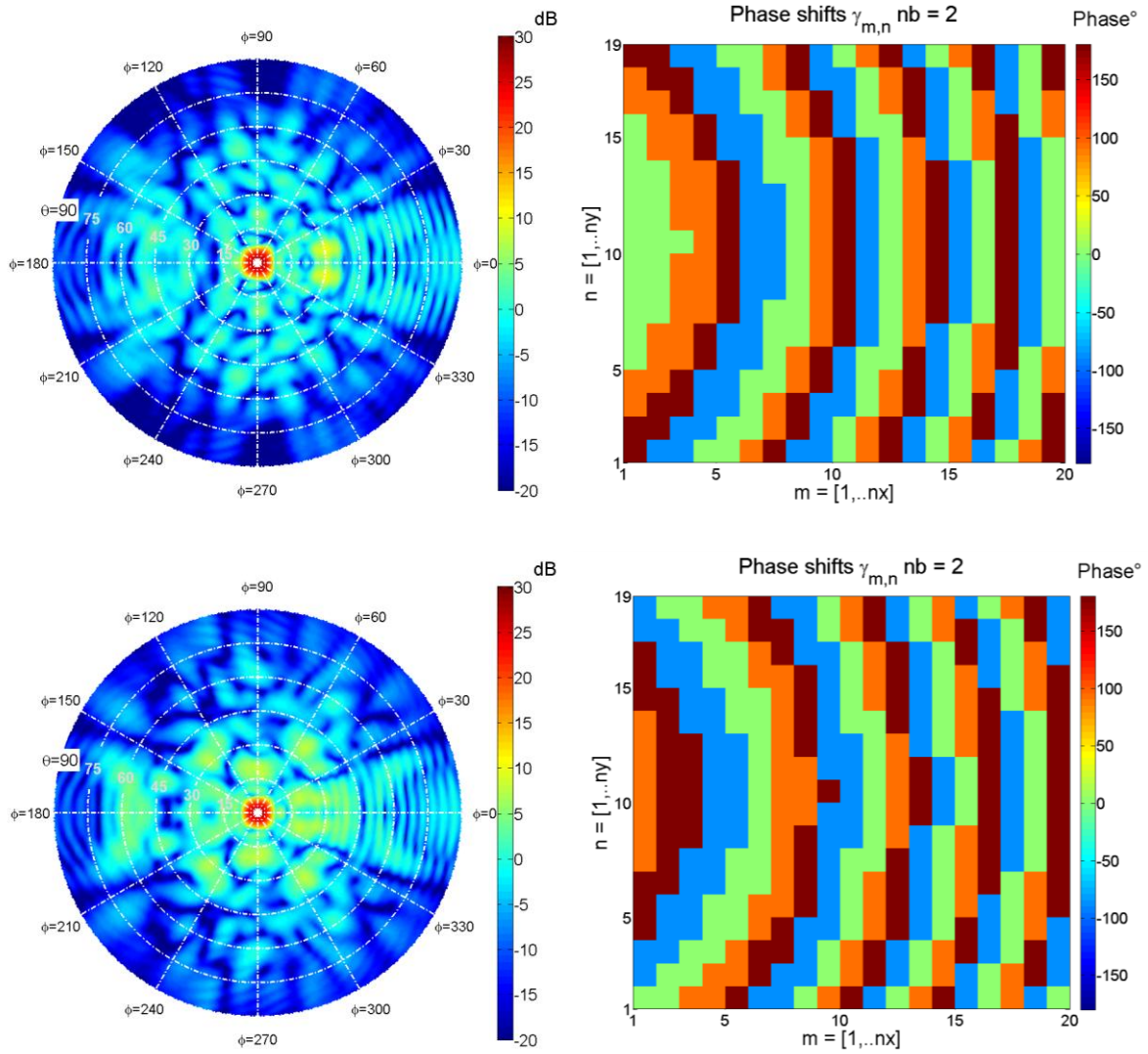

Figure. IV.18. *Computed phase shifts and radiation pattern for two values of the phase constant 'C'. (Top) Optimized C_1 =50°; (Bottom) Un-Optimized C_2 = 180°. Test case: focused beam {θ_0=0°;φ_0=0°}, level of quantization* ***nb=2***

In Fig .IV.18 two different phase shifts distribution for the reflectarray cells are computed for a higher level of quantization ($nb = 2$). The maximum directivity equals 27.42 dB for the optimized phase constant C_1=50° and equals 26.85 dB for the un-optimized phase constant C_2=180°. The side lobe level difference is also visible in the area ($15° < \theta < 45°$).

In a practical reflectarray design where the phase shift distribution is prescribed, the phase constant 'C' shall allow us to optimize the directivity of the beam by simply assigning the optimized phase shifts for the reflectarray cells. Note that the impact of the phase constant on the computed radiation patterns is bigger when the level of quantization is lower. (0.9dB for *nb=1*, and 0.57 dB for *nb=2* in this example).

IV - Quantization of the Optimum Continuous Phase Shifts Distribution

In a practical case, the active reflectarray cells have limited number of states for the phase shifts [13]. The continuous phase is theoretical and cannot be achieved physically. Moreover, phase shifts with high level of quantization imply high costs. The easiest and direct solution to take into account the quantization effect is to quantize the computed continuous phase shifts. It means that each reflectarray cell continuous phase shift is replaced with the closest discrete value as presented in Eq.IV.5-6 and illustrated in Fig .IV.19 and Fig .IV.20.

Let us define *nb* as the number of bits of quantization. *Nb* depends on the number of PIN-diodes or MEMS included in the design of the tunable cell. The number of allowed discrete phase shifts n_γ is equal to 2^{nb}.

In this section I consider the case of an equally spaced discrete phase shifts distributed along the following interval $[-180: 180]$.

$phase_{stepper}$ defines the partitions in which the prescribed discrete phases $discrete_{phase}$ are assigned to the continuous ones. Below in Fig .IV.19 and Fig .IV.20 I present the phase quantization for two levels $(nb = 1)$ and $(nb = 2)$.

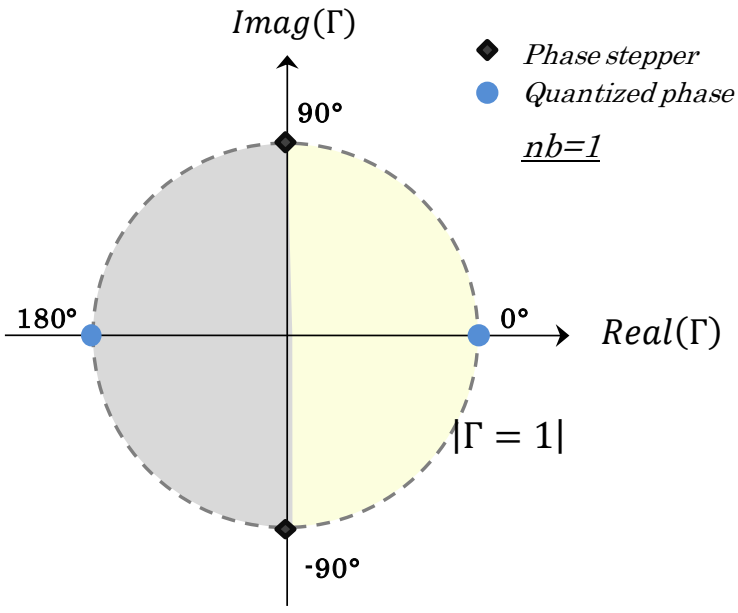

Figure. IV.19. *Quantization of the continuous phases shifts assuming* $|\Gamma| = 1$ *and nb=1*

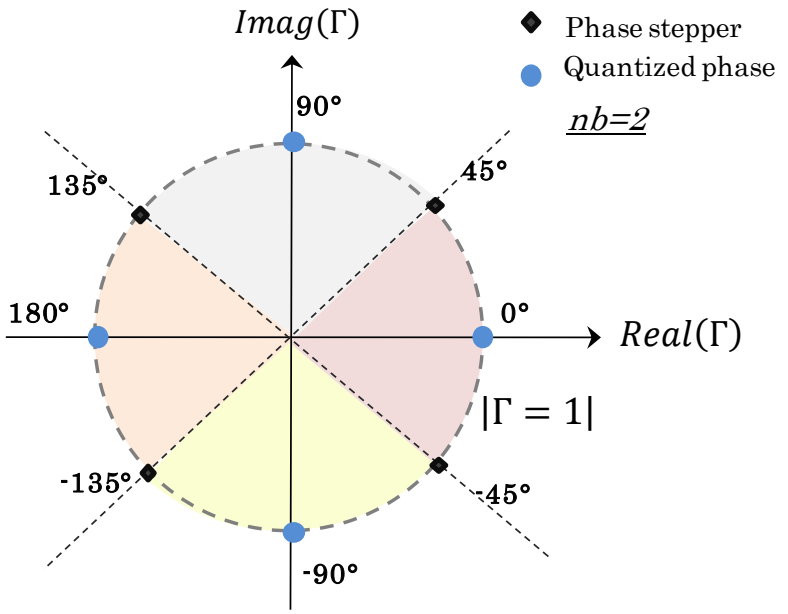

Figure. IV.20. *Quantization of the continuous phases shifts assuming* $|\Gamma| = 1$ *and nb=2*

In Matlab the quantization is applied as follows.

$$\text{(IV.5)}\quad \begin{cases} phase_{step} = \frac{360°}{nb} \\ discrete_{phase} = [0°{:}\,phase_{step}\,{:}\,360°] - 180°; \\ \%\; n_\gamma = numel(discrete_{phase}); \\ phase_{stepper} = \left[\frac{phase_{step}}{2}{:}\,phase_{step}\,{:}\,360°\right] - 180°; \\ \%\; numel(phase_{steper}) = (n_\gamma - 1); \\ \gamma_{quantized} = quantiz(\gamma, phase_{steper}, discrete_{phase}) \end{cases}$$

$$\text{(IV.6)}\quad \begin{cases} a_{quantized\ m,n} = \left[\left[\Gamma_{quantized}\right]^{-1} - [S]\right]^{-1} \overrightarrow{b_0} \\ \Gamma_{quantized} = diag(e^{j(\gamma_{quantized})}) \end{cases}$$

Once we calculate the optimum continuous phase shifts versus an objective radiation pattern using Eq.II.18 –II.24, we compute the quantized phase shifts using Eq.IV.5. The new phases lead us to a new distribution of reflection coefficients $\Gamma_{quantized}$ and excitation weightings for the cells $a_{quantized\ m,n}$ as seen in Eq.IV.6.

IV.1 - **Focused beam test cases using quantized phase shift distribution**

As an example, let me consider the case of a 1bit reflectarray. It means that the cells can only have 2 phase shifts. The different parameters which were defined in Eq.IV.2 have the following values: $(nb = 1)$, $(n_\gamma = 2)$, $phase_{step} = 180°$; $discrete_{phase} = [-180°\ 0°\ 180°]$; $phase_{stepper} = [-90°\ 90°]$;

Below in Fig .IV.21 and Fig .IV.22 I present the results for two focused beams test cases $\{\theta_1 = 0°, \varphi_1 = 0°\}$ and $\{\theta_2 = 45°, \varphi_2 = 245°\}$. The quantized phase shifts and the corresponding radiation patterns are computed for 5 different levels of quantization:

$(nb = [1\ 2\ 3\ 4\ 5]) \Leftrightarrow (n_\gamma = [2\ 4\ 8\ 16\ 32])$;

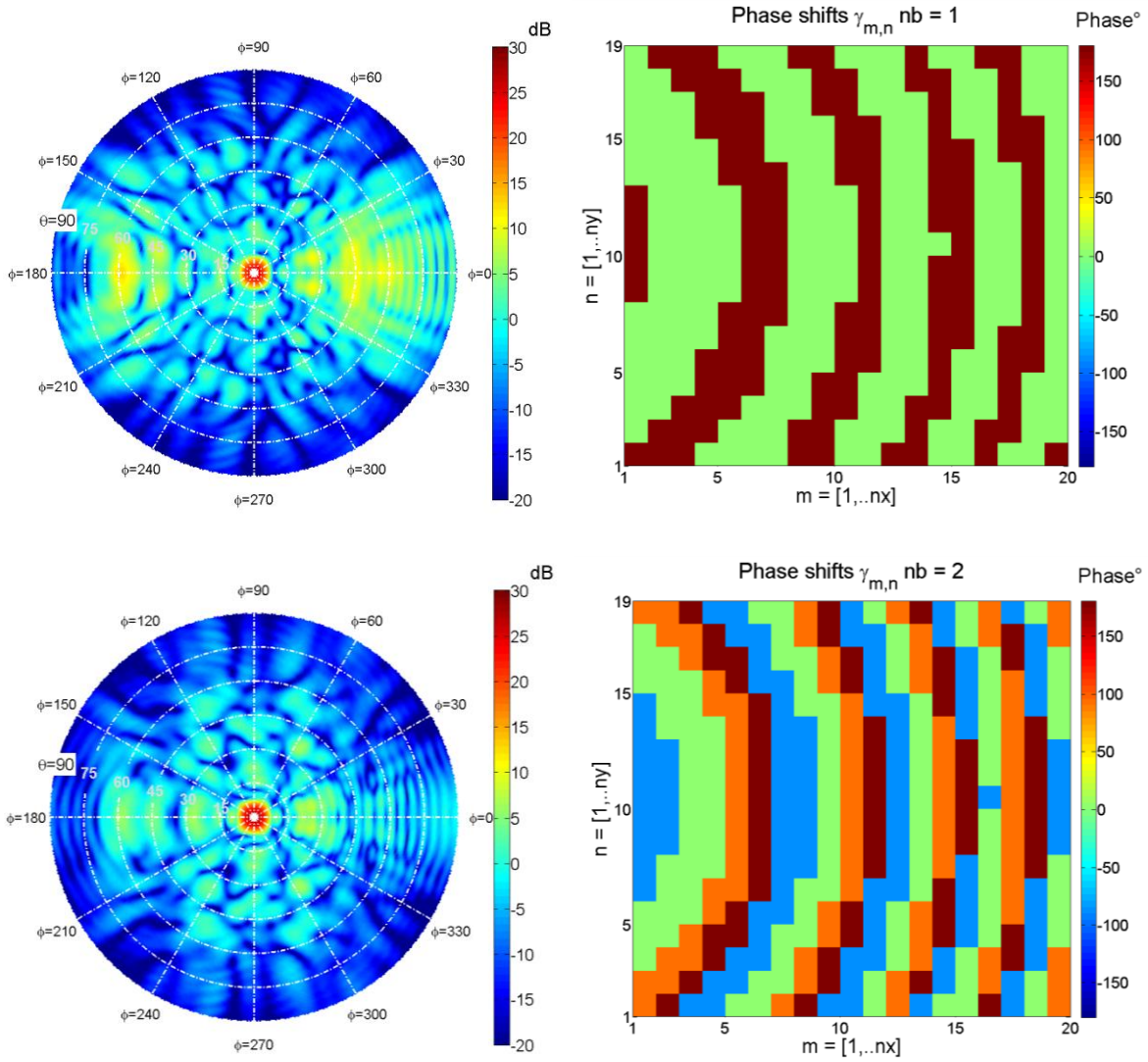

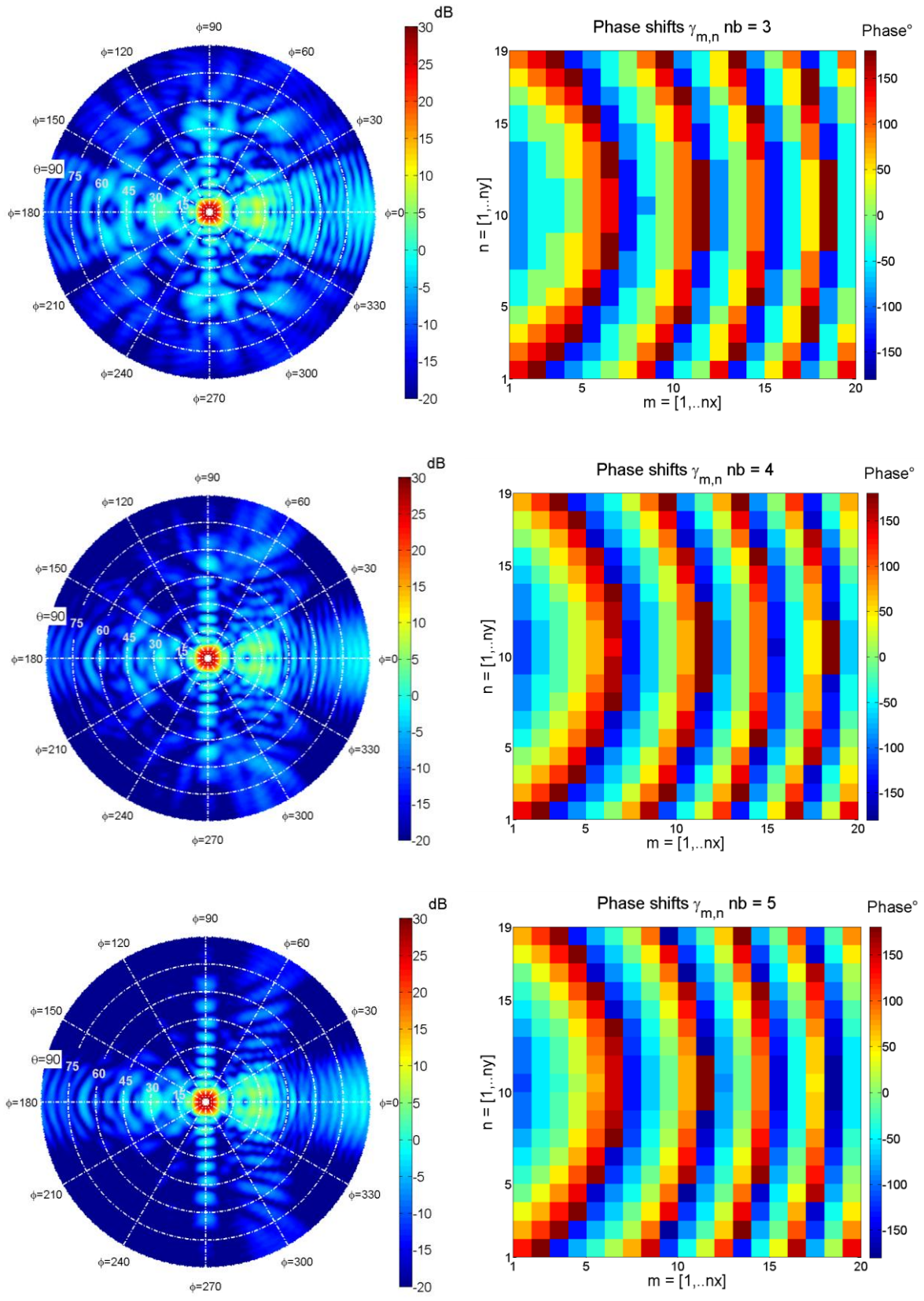

Figure. IV.21. *Computed radiation patterns of the reflectarray versus the number of bits of the phase shift quantization. Test case: focused beam {θ_1 =0°, φ_1 =0°}.*

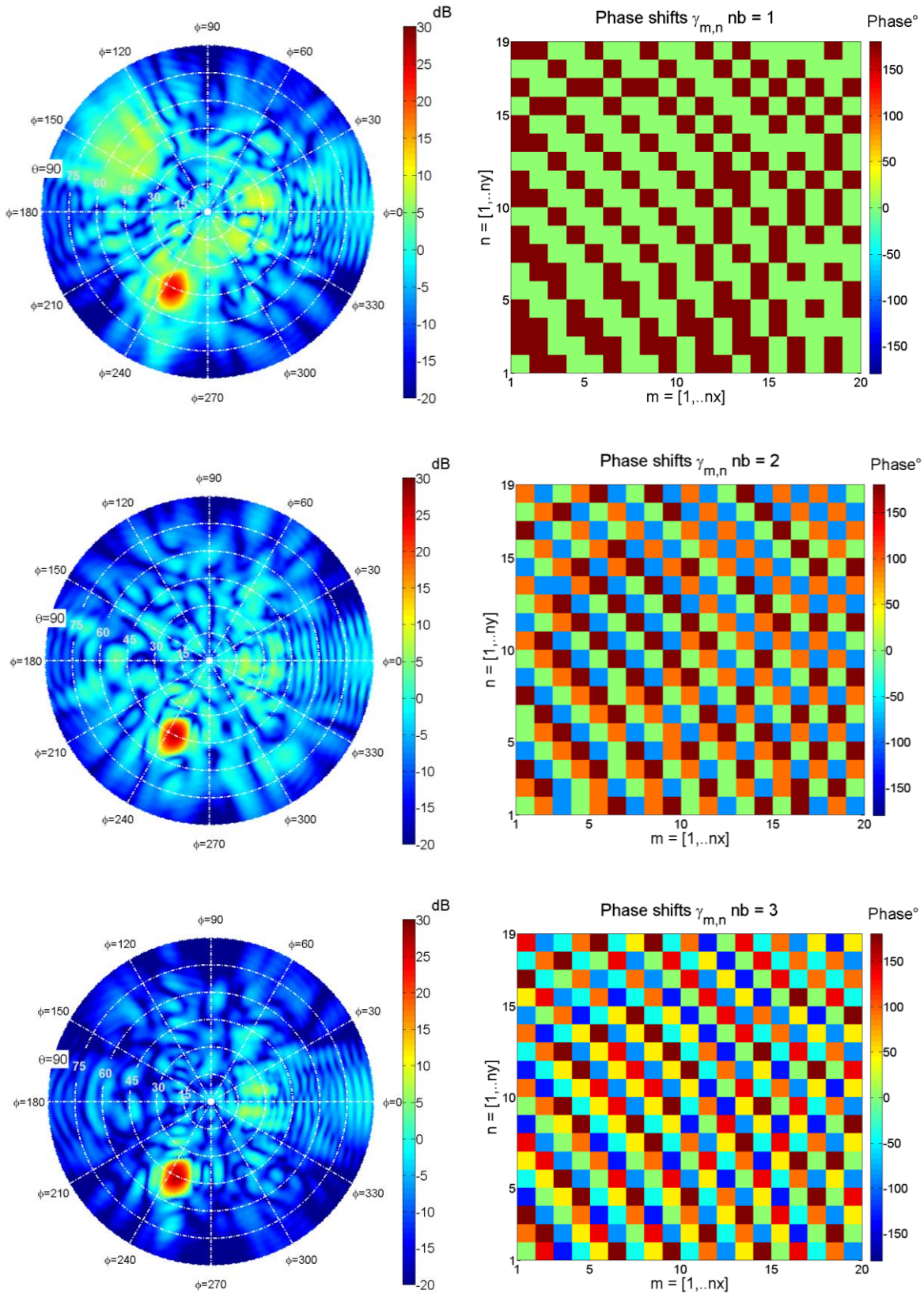
dB
Phase shifts $\gamma_{m,n}$ nb = 1
Phase°
n = [1,..ny]
m = [1,..nx]
dB
Phase shifts $\gamma_{m,n}$ nb = 2
Phase°
n = [1,..ny]
m = [1,..nx]
dB
Phase shifts $\gamma_{m,n}$ nb = 3
Phase°
n = [1,..ny]
m = [1,..nx]

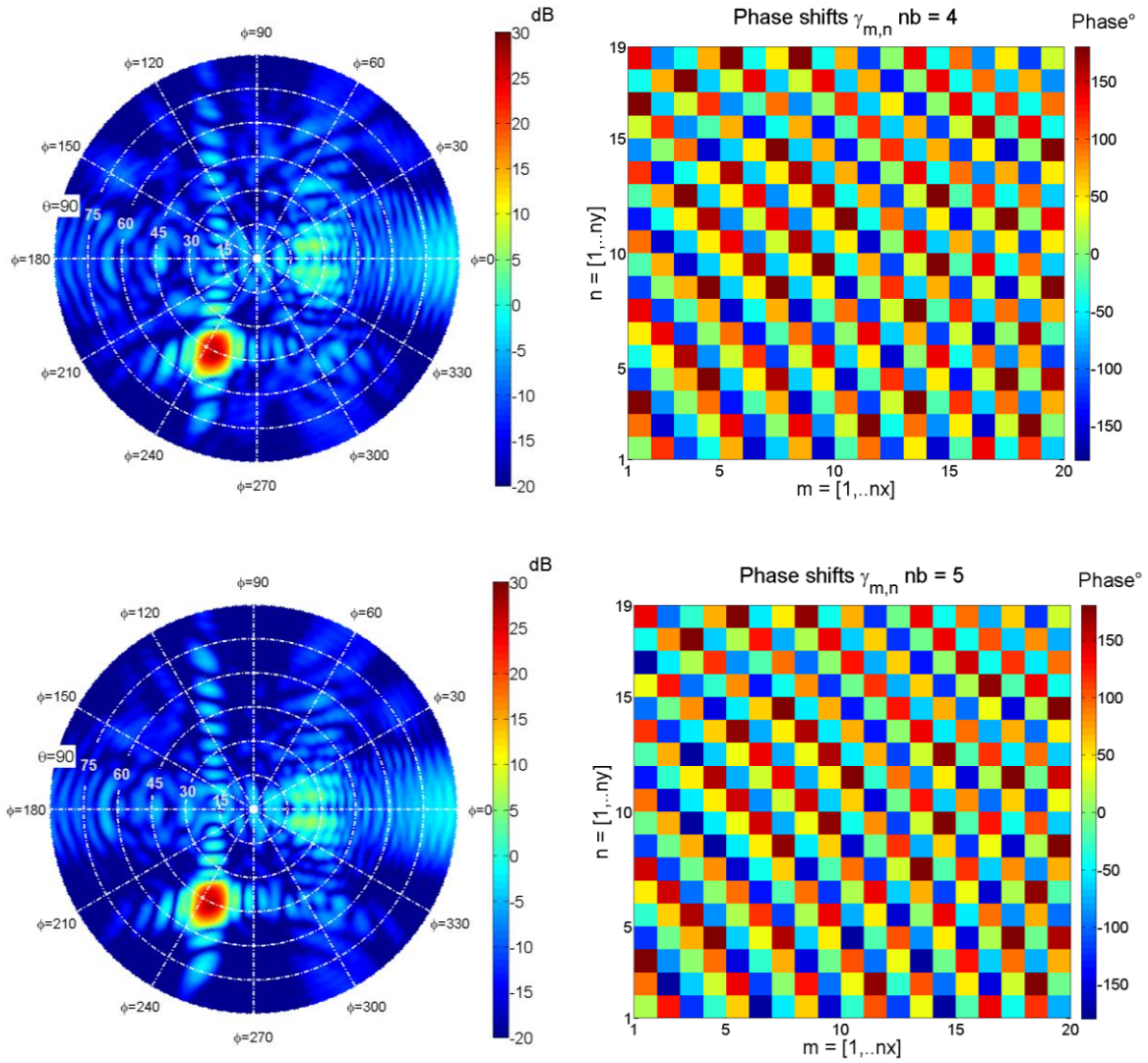

Figure. IV.22. *Computed radiation patterns versus the number of bits of the phase shift quantization. Test case: focused beam {θ_2 =45°, φ_2 =245°}.*

We can steer the beam thanks to quantized phase shifts instead of continuous phase shifts. The reflectarray cells have now prescribed discrete phase shifts that depend on the level of the quantization. The radiation pattern becomes more directive and the side lobes becomes cleaner when the level of the quantization increases. After a given value $(nb \geq 4)$ we can claim that the radiation pattern converges to the ideal one with a reduced comprehensible dispersion. The quantization losses are estimated to 3-4 dB when $nb = 1$ and to 0.7-0.8 dB when $nb = 2$. The losses become negligible $(< 0.2\, dB)$ when $nb \geq 3$. The computed directivities and the estimated quantization losses, for different focused beams test cases and different quantization levels are illustrated in Fig .IV.23 and Fig .IV.24. The reason why the directivity starts to converge with a higher level of quantization is because the maximum

phase error between the real continuous phase and the quantized one decreases and becomes negligible, as we can see in Fig .III.41.

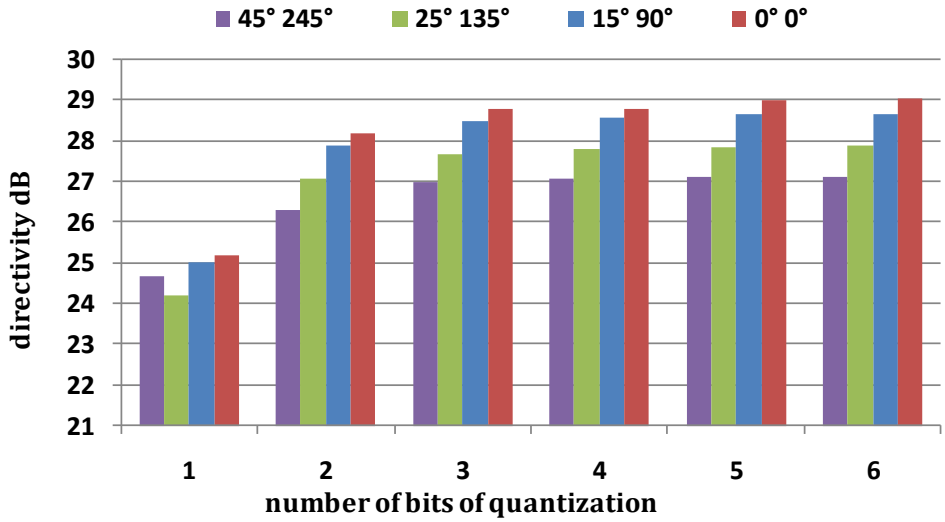

Figure. IV.23. *Evolution of the directivity of the reflectarray versus the number of bits of quantization for different objective radiation patterns*

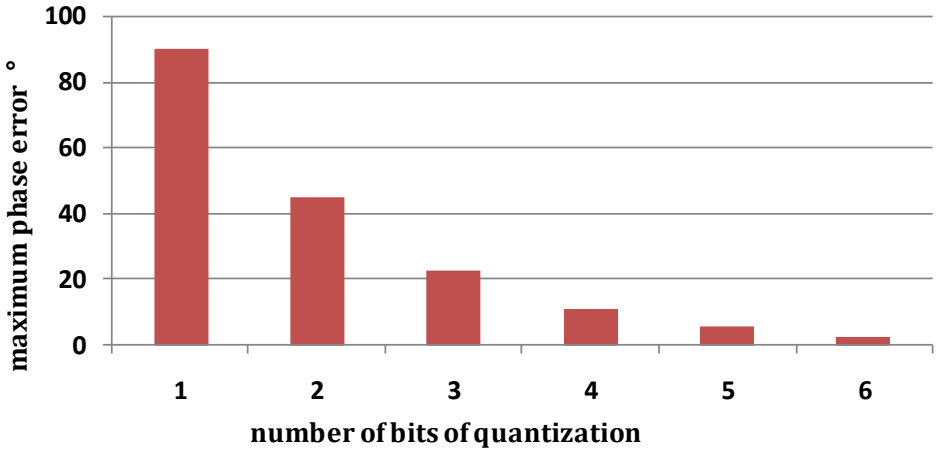

Figure. IV.24. *Maximum phase error between the continuous optimum phase shift and the quantized phase shift versus the level of quantization*

We can design a cheap and tunable reflectarray with 2bits cells and steer the beam at any direction. I have tried to focus the beam at random directions such as $\{\theta_0 = 63°, \varphi_0 = 123°\}$ and the results were interesting while the pointing degree error were around 1°. The 0.8dB losses due the quantization can be considered reasonable when compared with the lower cost of the antenna and the easiest deployment and control of PCB circuit behind the panel. It can be interesting for applications where a moderate cost if preferred to accuracy (especially for tertiary or terrestrial applications).

IV.2 - **Reflectarray Optimization of quantized phase shifts**

Another alternative to the direct synthesis lies with the optimization algorithms. Besides optimizing the radiation pattern (by lowering the side lobes level and maximizing the directivity of the main lobe), these algorithms such as the genetic algorithm or particle swarm, provide more options and control than a simple direct synthesis. They offer us the possibility to add complex constraints, define null-matching in certain directions or create complex masks of directivity to shape the radiation pattern.

In this section I present a simple case where we want to focus the beam using quantized phase shifts. However, the quantized phase shifts are no longer the direct output of the quantization of the continuous phase shift distribution. Instead, we will be asking to the genetic algorithm to look for the optimum quantized phase shifts distribution during the radiation pattern synthesis.

The genetic algorithm is related to a mathematical model based on the nature selection and reproduction principles (Crossover and mutation). We classify the GA as a ***Stochastic Optimizer*.** It is a candidate since it is capable of solving *mixed integer optimization* problems. In this type of problem, solving the variables can be defined as a set of fixed values. Their values can be integer or real numbers, such as $\text{discrete}_{\text{phase}} = [-60.5° \; 0° \; 35.5° \; 95.8° \; 180°]$. As an application, this algorithm was successfully applied on a switchable parasitic elements square monopole array [14].

In Fig.IV.25, I show an example of focused beams using 1-bit quantized phase shifts radiating at the directions $\{\theta_1 = 0°, \varphi_1 = 0°\}$, $\{\theta_2 = 25°, \varphi_2 = 135°\}$ and $\{\theta_3 = 45°, \varphi_3 = 245°\}$. As we can notice the solution given by the genetic algorithm resembles slightly to the solution given by a direct quantization solution. If we compare the computed radiation patterns with (Fig .IV.21 and Fig .IV.22), we notice that the optimized phase shifts distributions present higher directivities and lower side lobe levels. In Fig .IV.23, the maximum directivities of the focused beams (without the GA) are: $D1_{max}$ = 25.4 dB, $D2_{max}$ = 24.23 dB and $D3_{max}$ = 24.7 dB, with the GA these directivities are equal to: $D1_{max}$ = 25.4 dB, $D2_{max}$ = 25.3 dB and $D3_{max}$ = 24.76 dB, as seen in Fig .IV.25.

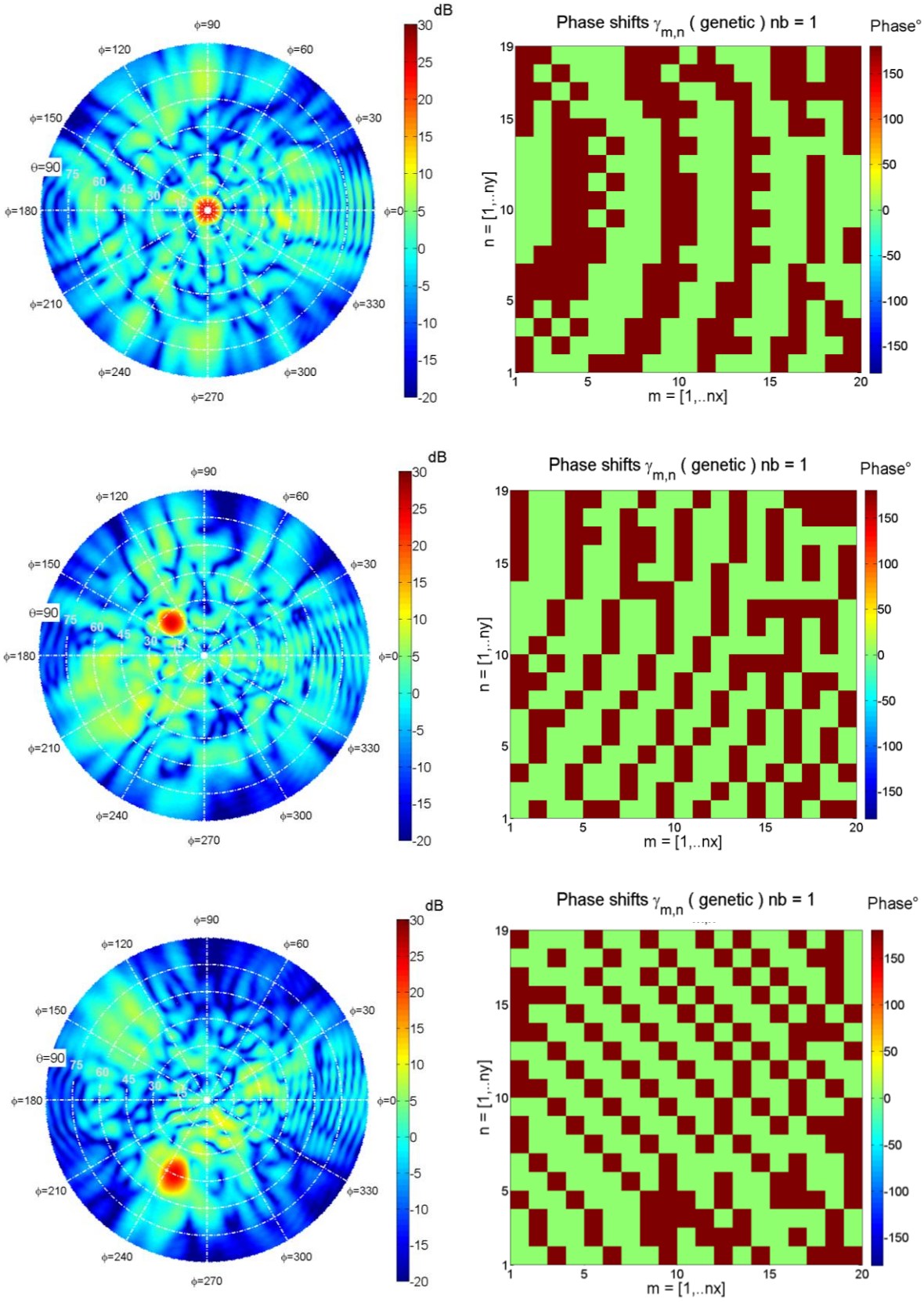

Figure. IV.25. *Discrete quantized optimization using the genetic algorithm. Test case: focused beams {θ_1 =0°, φ_1 =0°} , {θ_2 =25°, φ_2 =135°} and {θ_3 =45°, φ_3 =245°} [nb=1]. $D1_{max}$ = 25.4 dB, $D2_{max}$ = 25.3 dB and $D3_{max}$ = 24.76 dB*

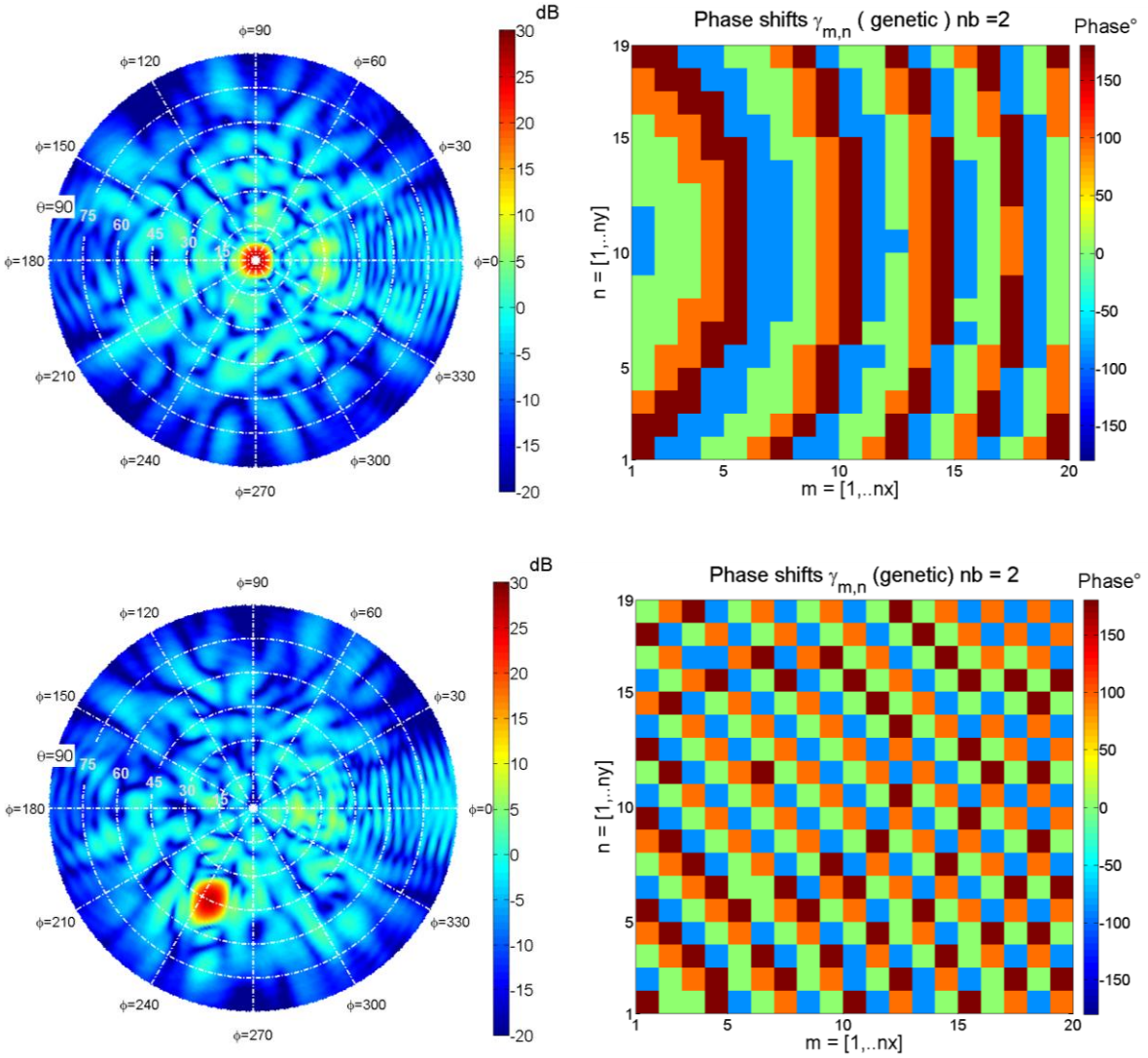

Figure. IV.26. *Discrete quantized optimization using the genetic algorithm. Test case: focused beams {θ_1 =0°, φ_1 =0°} and {θ_2 =45°, φ_2 =245°}. [nb=2]. $D1_{max}$ = 28 dB and $D2_{max}$ = 26.7 dB*

In Fig .III.44 I present the optimization of a 2-bit reflectarray using quantized phase shifts. The discrete variables are bounded to the following values: $\text{discrete}_{\text{phase}} = [-90°\ 0°\ 90°\ 180°]$. The initial population is set to the phase shifts given by the fixed point method. The computed directivities were higher than the original population but not classified as significant improvements over the already existing solutions (fixed-point).

At a higher level of quantization the improvements given by the GA were not significant. This might have two possibilities. One, the GA used (Matlab Toolbox) cannot find the global minimum (best solution) due to the huge size of the search domain. For example, if nb=2, the search domain is equal to $4^{380} = 6 \times 10^{228}$. Two, the given solution is the best physical allowed since we are limited to fixed number of quantized phase shifts.

Notice that in our case, we have used the GA because it is easily available in a Matlab toolbox. However, a specifical study can be made on the most suited algorithm for RA (PSO, gradient based Least-square, MinMax, ..). We do not give more details on these algorithms because it is not the scope of this thesis.

Nevertheless, in this part, we have seen that including the quantization directly in the load synthesis could lead to better results than a simple quantization of final continuous phase shifts.

V - Comparison between our approach and the Classical Assumption

V.1 - Phase shift calculus in the case of a classical Assumption

In a classical procedure, the magnitude of the reradiated fields is directly related to the magnitude of the incident electromagnetic fields. This approximation will be compared with the proposed approach in this section, on both the excitations of the cells and the radiation pattern. To make this comparison feasible, two phase shift distributions were synthesized for the same antenna configuration to radiate a focused beam at $\{\theta_0 = 15°; \varphi = 90°\}$ and another one at $\{\theta_0 = 25°; \varphi = 135°\}$. The first phase shift distribution was already treated in a previous section and corresponds to our synthesis approach, where we compute them versus incident waves and reflected excitations weightings, as given by Eq.IV.8. The second phase shift distributions were computed versus the phase of incident EM fields and the array factor as it was given by [3], and illustrated in Eq.IV.7. This equation is a result of the approximations made in Eq.IV.4.

Classical assumption to compute the phase shifts distributions:

(IV.7) $$\Gamma_{m,n}(\theta_0, \varphi_0) = e^{j\left(p_{m,n}(\theta_0,\varphi_0) - \angle b_0(m,n)\right)}$$

Our approach to compute the phase shift distributions:

(IV.8) $$\Gamma_{m,n} = \frac{a_{m,n}}{b_{tot\ m,n}}$$

We define several reactive loads sets behind the cells (for our approach and for the assumption of Eq.1V.4) and we compare the corresponding full-wave simulations. Notice that, in these simulations, the interactions between the cells are accounted. The presented phase shift distribution sets were synthesized assuming that the magnitude of the reflected fields is the same as the incident fields, i. e., the scattering matrix does not interfere in the calculus of the phase shifts. As a whole, the impact should be clearly visible on the resulting radiation pattern. The results of our approach are already illustrated in Fig .IV.3 and Fig .IV.5. The results of the second approach are illustrated in Fig .IV.27 and Fig .IV.28.

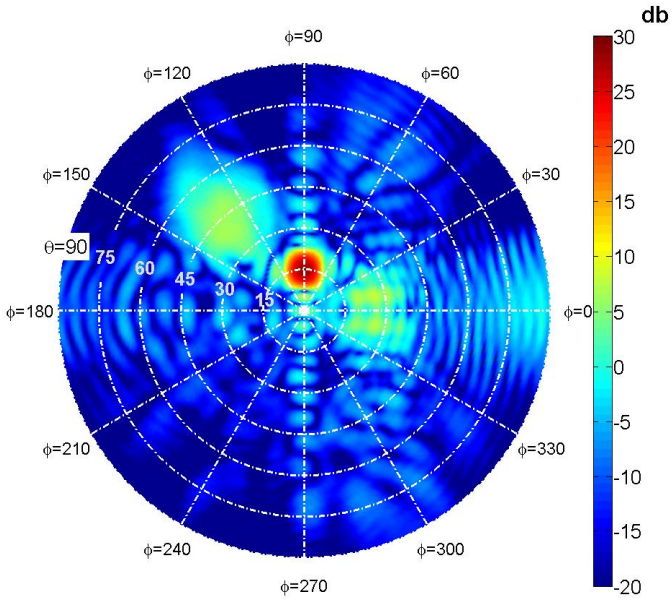

Figure. IV.27. *Directivity of the radiation pattern computed in the full-wave simulation using phase shifts computed with Eq.IV.4-5. Front radiation, test case: focused beam at {θ_0 =15°; φ_0 =90°} D_{max} =28.46 dB. To be compared with Fig .IV.3.*

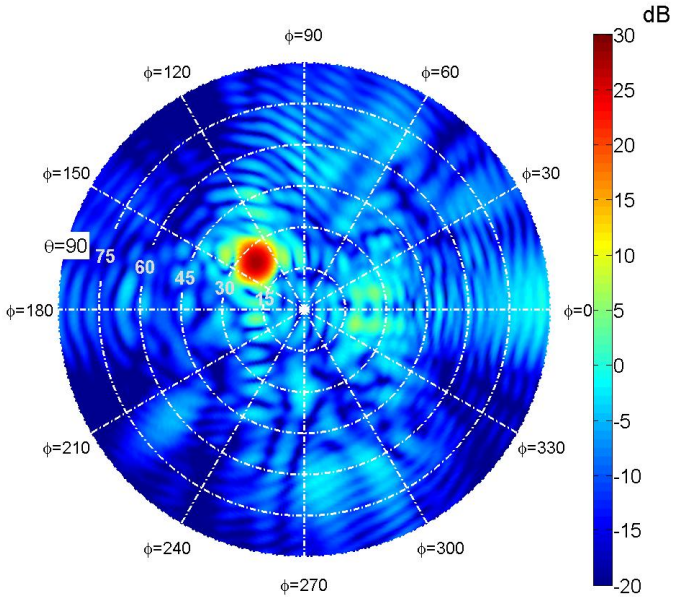

Figure. IV.28. *Directivity of the radiation pattern computed in the full-wave simulation using phase shifts computed with Eq.IV.4-5. Front radiation, test case: focused beam at {θ_0 =25°; φ_0 =135°} D_{max} =27.7 dB. To be compared with Fig .IV.5.*

As we can see in Fig .IV.27 and Fig .IV.28, the phase shifts/reactive loads computed with Eq.IV.5 meet with our objective to radiate focused beams at {θ_0 =15° and φ_0 =90°} and {θ_0 =25° and φ_0 =135°}. The directivity of the first beam (28.46 dB) is not far from the beam (28.79 dB) presented in Fig .IV.3. However, we can see that the level of the side-lobes (one is

located in the specular direction (φ =0°) and the second lobe is located in the plane φ =130°) are clearly higher.

A closer look to the results given by the full-wave simulations is presented in Fig .IV.29. In the tilted beam plane (φ =90°), the difference is minimal, only 0.33 dB is observed. When looking in the direction of the side lobe (φ =135°), the difference can reach 8 dB. This spurious radiation does not appear if the synthesis is performed including couplings, with Eq.IV.1 & Eq.IV.8. For the second test case, the comparison is illustrated in Fig .IV.30.

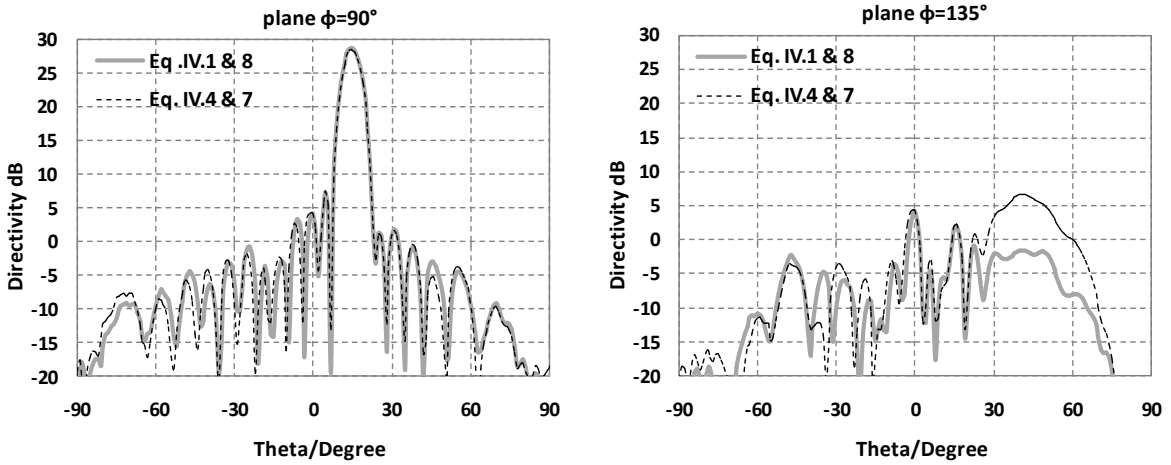

Figure. IV.29. *Comparison between radiation patterns computed with 2 different sets of phase shifts. One refers to Eq.IV.1. The second refers to Eq.IV.7. (Left) Full-wave simulation results in the plane φ =90°. (Right) in the plane φ =135°, test case: focused beam at {θ_0 =15°; φ_0 =90°}.*

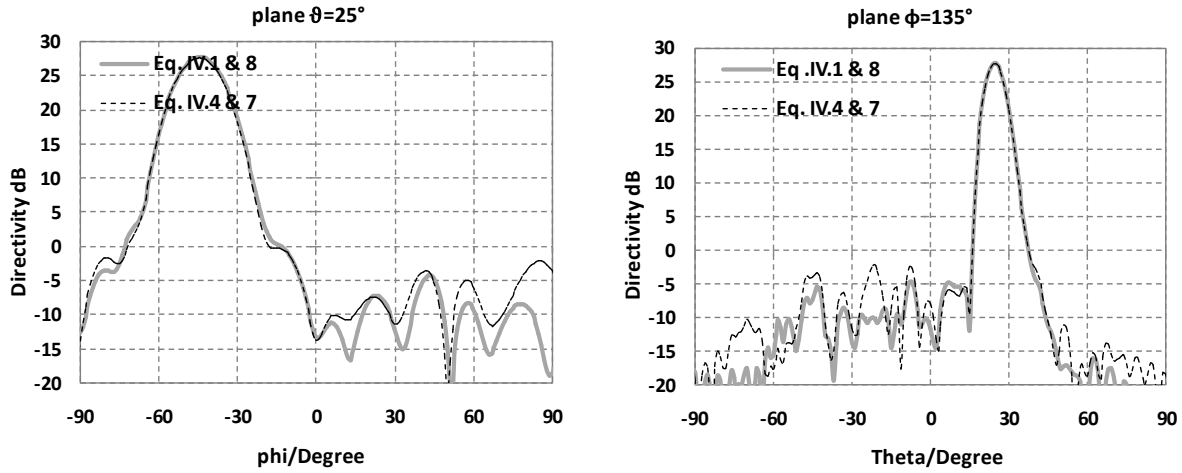

Figure. IV.30. *Comparison between radiation patterns computed with 2 different sets of phase shifts. One refers to Eq.IV.1. The second refers to Eq.IV.7. (Left) Full-wave simulation results in the plane θ =25°. (Right) in the plane φ =135°, test case: focused beam at {θ_0 =25°; φ_0 =135°}.*

V.2 - **Noise on the excitation weightings phases**

This noise which appears in the radiation pattern can be explained by the phase of the excitations weightings $a_{m,n}$. When the phase shift distribution is calculated directly from Eq.IV.5, the phases of the reradiated fields are affected by the mutual couplings, as illustrated in Fig .IV.31 (right) and Fig .IV.32 (right). Ideally they should be equal to the array factor as illustrated in Fig .IV.31 (left) and Fig .IV.32 (left).

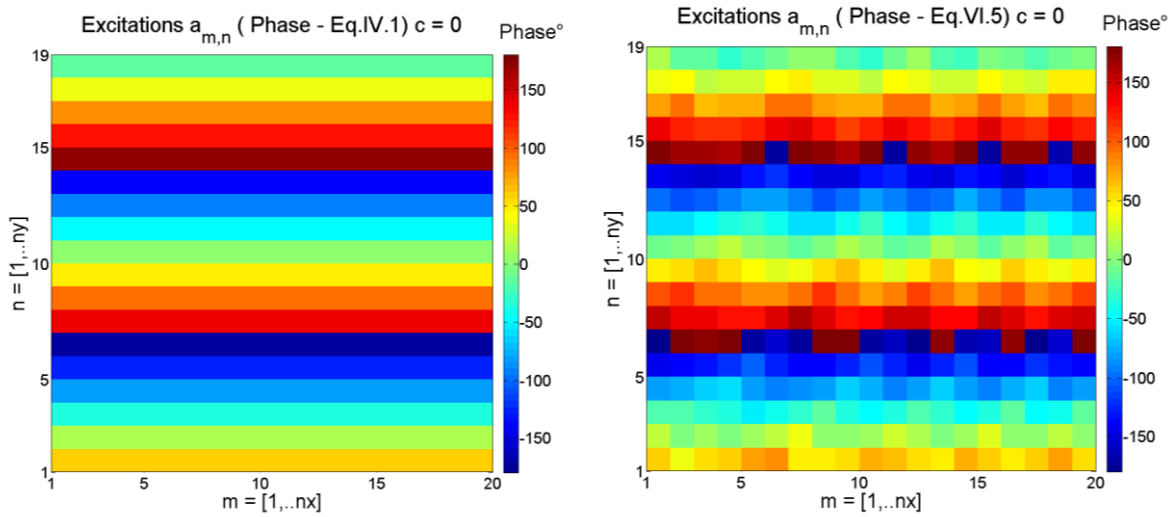

Figure. IV.31. *Phase of the excitations weightings a_{mxn} when the phase shifts are calculated to radiate a focused beam at {θ_0 =15°; φ_0 =90°}, with the proposed approach in Eq.IV.1 (left) and with approximation of Eq.IV.7 (right)*

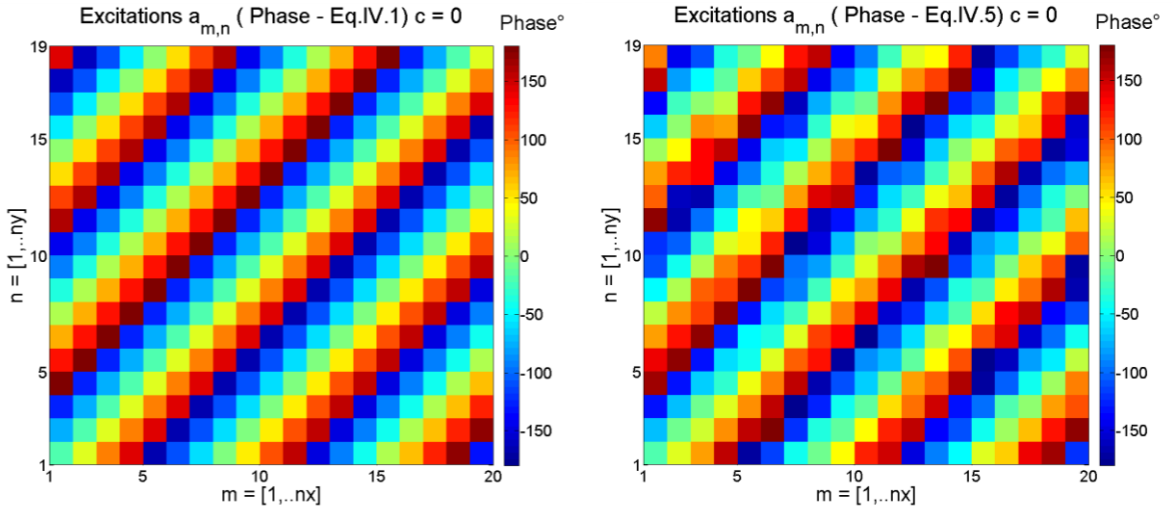

Figure. IV.32. *Phase of the excitations weightings a_{mxn} when the phase shifts are calculated to radiate a focused beam at {θ_0 =25°; φ_0 =135°}, with the proposed approach in Eq.IV.1 (left) and with approximation of Eq.IV.7 (right)*

We can see the impact of the mutual couplings [S] on the performances of the reflectarray. Calculating the phase shifts with the assumption of equations Eq.IV.4 and Eq.IV.7 induces an error on the phases of the reradiated fields. It is visible in the radiation pattern calculated with the full-wave simulation. The results computed by considering the scattering matrix present lower spurious radiation and side lobe level, which is of interest to increase the performances of the antenna and to avoid interferences in a non desired direction. These results demonstrate the interest of taking into account the couplings in the synthesis process.

VI - Conclusion

In this chapter I have discussed the effects of the mutual couplings between the cells on the reflectarray performances.

Our synthesis procedure demonstrates that the couplings impact both the phases and the amplitude of the excitation weightings, whereas the classical assumption is to consider that their amplitudes are only proportional to the primary feed illumination. This contribution is actually correlated to the scattering matrix, incident coupled waves and the reactive loads. The effect of an arbitrary phase constant on each cell is also investigated. The results have been validated with a full-wave simulation.

On a second note, the phase constant C is a parameter that we can control and optimize in order to maximize the directivity of the focused beam. Besides controlling the magnitude of the excitation weightings, the phase constant C affects the summation between the radiated field by the cells and the diffracted field.

Then, I have a presented a comparison between our synthesis procedure with the classical assumption. In a classic procedure, the magnitude of the reradiated fields is directly related to the magnitude of the incident electromagnetic fields. The phase shifts/reactive loads were computed with and without taking note of the scattering matrix. A comparison on the computed radiation pattern in full-wave simulations for both cases is performed. The presented results show the interest of using our synthesis procedure if we are looking to improve the performances of the reflectarray given an objective radiation pattern. By opting this new strategy for the calculus of the reactive loads we could lower the side-lobes and spurious radiation levels.

Notice that a specifical study has been performed on the quantization effects. This work has been made to evaluate of the number of phase shifts states on the RA performances.

VII - References

[1] D. M. Pozar, "Microstrip Reflectarrays Myths and Realities," *Proceedings of JINA*, 2004.

[2] K. D'Ambrosio, R. Pirich, A. Kaufman, D. Mesecher, and P. Anumolu, "Parallel Computation Methods for Enhanced MOM and MLFMM Performance," *IEEE Systems Applications and Technology Conference*, vol. 1, pp. 1-4, May 2009.

[3] J. Huang and J. A. Encinar, "Reflectarray antennas," *John Wiley & sons publication*, 2008.

[4] A. K. Bhattacharyya, "Phased Array Antennas: Floquet Analysis, Synthesis, BFNs and Active Array Systems," *John Wiley and Sons Editor*, 2005.

[5] M. A. Milon, D. Cadoret, R. Gillard, and H. Legay, "Surrounded-element Approach for the Simulation of Reflectarray Radiating Cells," *IET Microwave Antennas and Propagation*, vol. 1, pp. pp. 289-293, April 2007.

[6] C. Yann, R. Loison, R. Gillard, M. Labeyrie, and J-P Martinaud, "Global Technique Analysis for Reconfigurable Reflectarray Antennas," *Proceedings of EUCAP, Rome*, 2011 April.

[7] M. Zhou, S. B. Sørensen, O. S. Kim, S. Pivnenko, and G. Toso, "Investigations On Accurate Analysis Of Microstrip Reflectarrays," *Proceedings of the 33rd ESA antenna workshop on Challenges for Space Antenna Systems, Estec*, Oct 2011.

[8] H. Aubert, "The Concept of Scale-changing Network in Global Electromagnetic Simulation of Complex Structures," *Progress In Electromagnetics Research B*, vol. 16, pp. 125-154, 2009.

[9] S. Rabinowitz and J. Blass, "Mutual coupling in two-dimensional arrays," *IEEE Conf WESCON*, pp. 134-150, 1957.

[10] S. Edelberg and A. Oliner, "Mutual coupling effects in large antenna arrays II: Compensation effects," *IRE Transactions on Antennas and Propagation*, pp. 360–367, 1960.

[11] H. C. Hansen, "phased array antennas," *New York: John Wiley and Sons*, p. 254, 1998.

[12] Y. Abdallah, C. Menudier, M. Thevenot, and T. Monediere, "Examining the Energetic Contribution of Reflectarray Cells Using Circuit Model and Full-wave Simulations," *Proccedings of EUCAP*, 2012.

[13] C. Menudier and T. Koleck, "Sub-Reflectarrays Performances for Reconfigurable," *IEEE Trans. and Ant. Prop*, vol. 60, no. 7, pp. 3476-3481, July 2012.

[14] Y. Abdallah, C. Menudier, M. Thevenot, and T. Monediere, "Switchable Steerable Square Parasitic Monopole Array design using a Genetic Algorithm," *Int. Symp. Antem*, June 2012.

CONCLUSIONS

AND

PROSPECTS

The topic of this thesis concerned the design of reflectarray antennas with a particular attention on the elements that could affect their performances. In order to accurately characterize reflectarray antennas, a detailed theoretical formalism was defined in chapter 2. In order to establish the different relations, a particular architecture has been described. It consists of a reflectarray panel made of identical and periodical microstrip patches with via holes. The most important point is that each radiating element includes an electromagnetic port, allowing an accurate calculation of all electromagnetic contributions in each cell. Thanks to this formalism that can be easily implemented in a design, we have demonstrated theoretically that the reflectarray cell's weightings depends on the incident coupled waves b_0, the scattering matrix of the reflectarray [S], the prescribed phase shift distribution to obtain a specific beam, and a constant phase reference *C*. Even if this result is relatively obvious from a physical point of view, it must be noticed that couplings clearly affect both magnitudes and phases of the cells weigthings a_i, and not only the phases.

Then, this formalism has been implemented in an analytical solver for reflectarray antennas. The synthesis of the phase shift distribution rests on an accurate and rigorous EM approach where the reflectarray cells are identical and periodical and connected to EM ports/ access previously defined. These ports are a key element to characterize the EM behavior of the reflectarray, especially in terms of couplings and power balance. The analytical solver is divided into two separated modules.

The first one is in charge of analysis and characterization of the EM behavior of the reflectarray antenna. The aim is to obtain a precise 'identity card' of the reflectarray, in order to fast synthesize an objective pattern through the second module of the analytical solver. At the end of this analysis stage, four parameters are computed and they form the database of the reflectarray design. These parameters are:

- the scattering matrix [S],
- the active elements pattern,
- the incident coupled waves $\{b_{0i}\}$,
- diffracted fields pattern.

It must be clearly noticed that these parameters are all obtained through a full-wave simulation thanks CST Microwave Studio. This is the most consuming step of our design approach. However, the object of this work was to obtain the most accurate elements for the database rather than to focus on computation time. However, it is also obvious that this stage can be improved without changing anything to the synthesis process (because the full-wave

simulation is only used to feed a database in our case). Other formalism, like the Scale Changing Technique mentioned in Chapter one, as example, would be another way to fill the database in a reduced time.

The second module concerns the synthesis of the ractive loads to produce the required phase shift distribution for the radiation pattern. We use the database as input and we define different objective radiation patterns. This solver allow us to synthesize the phase distributions / reactive, compute the radiation pattern of the antenna, perform a parametrical study on the phase shift distribution of the cells as well the breakdown effects. This analytical solver is coupled to the Matlab Optimization toolbox to operate with some included algorithms (MinMax, Genetic Algorithm) in addition to the fixed point method, which is the basic algorithm used for simple task. This link affords some flexibility. These algorithms allow us to define masks of directivity and null-matching at some given directions or add constraints on the phase shifts.

Concerning the time consumption, a direct synthesis of the phase shifts costs only a few seconds to some minutes for complex cases. Thanks to the time saved, a detailed study of electromagnetic properties is then possible. The optimization of an arbitrary phase constant or the design of a complete reflectarray with another type of cell (provided it is contained in the database) is possible in a few minutes.

To validate this analytical solver, we have designed a numerical proof of concept. It consists of a moderate size reflectarray (380 elements) with patch radiating elements linked to the synthesized reactive loads through metallic via holes. A comparison between the analytical solver and the full-wave simulation demonstrated a good agreement; especially on the diffracted field pattern which. The results were accurate because of the good knowledge and understanding of the energetic balance of the structure and because we take into account the scattering matrix in the reactive loads synthesis.

The commercial EM simulator software CST MWS is used for the characterization (analysis) of the design and for the validation of the synthesized reactive loads. To be sure that the results given by the full-simulation are accurate, I have performed a study on the global mesh settings of the antenna. A full-simulation of the antenna is quite costly in terms of memory and time consumption. In a machine that has 32GB of ram and Multi-core 2.4 GHz processors, we should wait 4 hours for the full-simulation to finish. Even if it is a long time, it was necessary to validate the analytical solver. Notice that, once the database is filled, this one needs only a few second to give a result similar to the full-wave solver.

Once this step was validated, the analytical solver was used to study some interesting electromagnetic properties of reflectarray antennas. I have performed a study on the effects of the mutual couplings that occur between the cells on the behavior of the antenna. Indeed, we treat the reflectarray panel as a classical array antenna where each cell is excited with a complex excitation weighting and the final radiation pattern is calculated as the linear combination of the elementary patterns added to the diffracted field patterns. The results have shown us that the EM behavior of the panel is quite similar to the array antenna, apart on the aspect of "Active SWR". On this particular point, the reflectarray is less sensitive than phased arrays, as seen in the field distribution of Chapter 4. This is a very important point to notice in favor of reflectarray antennas.

The mutual couplings impact the magnitude of the excitations weightings $a_{m,n}$ as well as their phases, whereas the classical assumption for reflectarrays considers that their magnitude is related to the illumination law on the panel. The energetic contribution of the reflectarray cells changes versus the objective radiation pattern. By looking at the different EM quantities, we have concluded that the energetic contribution is essentially modeled by the phase shifts distribution.

We have particularly demonstrated the dependency of the cells excitation weightings $a_{m,n}$ towards several parameters. In fact $a_{m,n}$ depend on:

- the scattering matrix [S]
- the incident coupled power waves from the feed $b_{0\,i}$
- the phase shift distribution required for the objective radiation pattern,
- a phase constant 'C'.

These different studies confirm the formalism and dependencies described in Chapter 2. It can also be noticed that the phase constant 'C' is a parameter of optimization. By simply shifting the relative phase of the cells we can optimize the directivity while respecting the objective radiation pattern. Besides controlling the magnitude of the excitation weightings, the phase constant '*C'* affects the summation between the radiated field by the cells and the diffracted field.

In another part of the thesis, I have performed a study on the quantization of the phase shift distribution of the cells. This particular point does not concern directly the physical aspect but it can be very helpful from a technological point of view. In fact, tunable reflectarrays involve discrete phase shifters whose quantization effects must be evaluated. In

this work, we have studied some steered beam configurations with quantized phase shifts as well to continuous phase shifts. This was also to incorporate some practical tool in our analytical solver. The most evident result is that the radiation pattern becomes more directive and the side lobes becomes cleaner when the level of the quantization was increased. After the fourth's level of quantization (4 bits/16 phase shifts) we can claim that the radiation pattern converges to the ideal one (using continuous phase shifts) with a comprehensible dispersion. The quantization losses on directivity are estimated to 3-4 dB when the phase shifts are limited to 2 values (0° 180°) and to 0.7-0.8 dB when the phase shifts are bounded to four values. The losses become negligible with a higher level of quantization. The reason why the directivity starts to converge with a higher level of quantization is because the phase error dispersion decreases and becomes negligible.

Actually two strategies are offered to compute quantized phase shifts. One is the direct quantization of the optimum continuous phase shifts distribution and the other is done by using optimization engines such as the genetic algorithm, during the synthesis process.

I have used global and local optimization solvers such as the genetic algorithm, the least-square algorithm and the minimax minimization to synthesize continuous and quantized phase shifts distribution in the following conditions: 1-maximize the directivity at one direction, 2- add null-matching at some directions while focusing the beam in some other direction, 3- define masks of directivity to shape the radiation pattern. The obtained results on a parasitic elements array as well as on a reflectarray antenna were encouraging even though all the results are not presented in this manuscript. They confirmed that the analytical solver can be extended to fit with such optimization routines and that we are not limited to the case of focused beam synthesis. Concerning the quantization effects, if we are looking only to focus the beam at one direction, we can say a direct quantization of the continuous phase shifts provided the optimum phase constant 'C' is satisfying.

All these conclusions and studies must be related to the accuracy and validation step. In fact, the analytical solver gives accurate results if we provide it the accurate data. It is driven by a database, so the accuracy of the results is directly linked to the exactness of the input parameters, which are the EM characteristics of the reflectarray panel (dispersion of the components, scattering parameters, active element pattern, etc …). Our main care while using this analytical solver can be summarized in one sentence: in any future measurement, the analytical solver should remain out of the 'suspicious zone'. The focus should be rather on an

accurate analysis and characterization of the reflectarray antenna. This particular point will be addressed in the prospects.

The immediate ***prospects*** are oriented towards the experimental research to support this analytical solver. The XLIM-OSA laboratory has planned to build a tunable reflectarray prototype. For this reason, we have to our disposal a driving and acquisition bench dedicated for the following tasks:

1. Providing the EM characteristics of the reflectarray cells which are required to drive the analytical solver, i.e. the database.
2. Driving the reactive loads leading to the required phase shifts on the reflectarray cells, according to the synthesis process of our analytical solver.
3. Measuring the radiation pattern of the reflectarray and evaluating its performance

These different steps will be fulfilled thanks to a test bench dedicated to multi-element antennas. It is composed of several apparatus (DC supplies and DC bias matrix for reactive loads, RF multiplexers to acquire scattering matrix, Vectorial Network Analyzer for measurement) able to complete the previous tasks. It is also connected to the analytical solver and the Compact Antenna Test Range. The entire process will be automated for a faster reflectarray analysis and synthesis.

The different elements and features of this analysis and design chain can be summarized in the very last schematic. We can notice that the different elements have been chosen to be as most versatile as possible:

- The scattering matrix will be performed through an arrangement of RF multiplexers. They can be extended to any number of elements on the elementary panel used.
- The DC supplies are suitable to voltage between +/-60V, allowing to drive different cells topology of the reflectarray (Pin-diodes, MEMS, Varactors...).
- The phase shifters are enslaved to the radiation pattern synthesis. The DC bias voltages are able to address 16 states of quantized phase shifts at.
- A diagnostic process will be possible thanks to the feedback of the measurement base (CATR) and the analytical solver

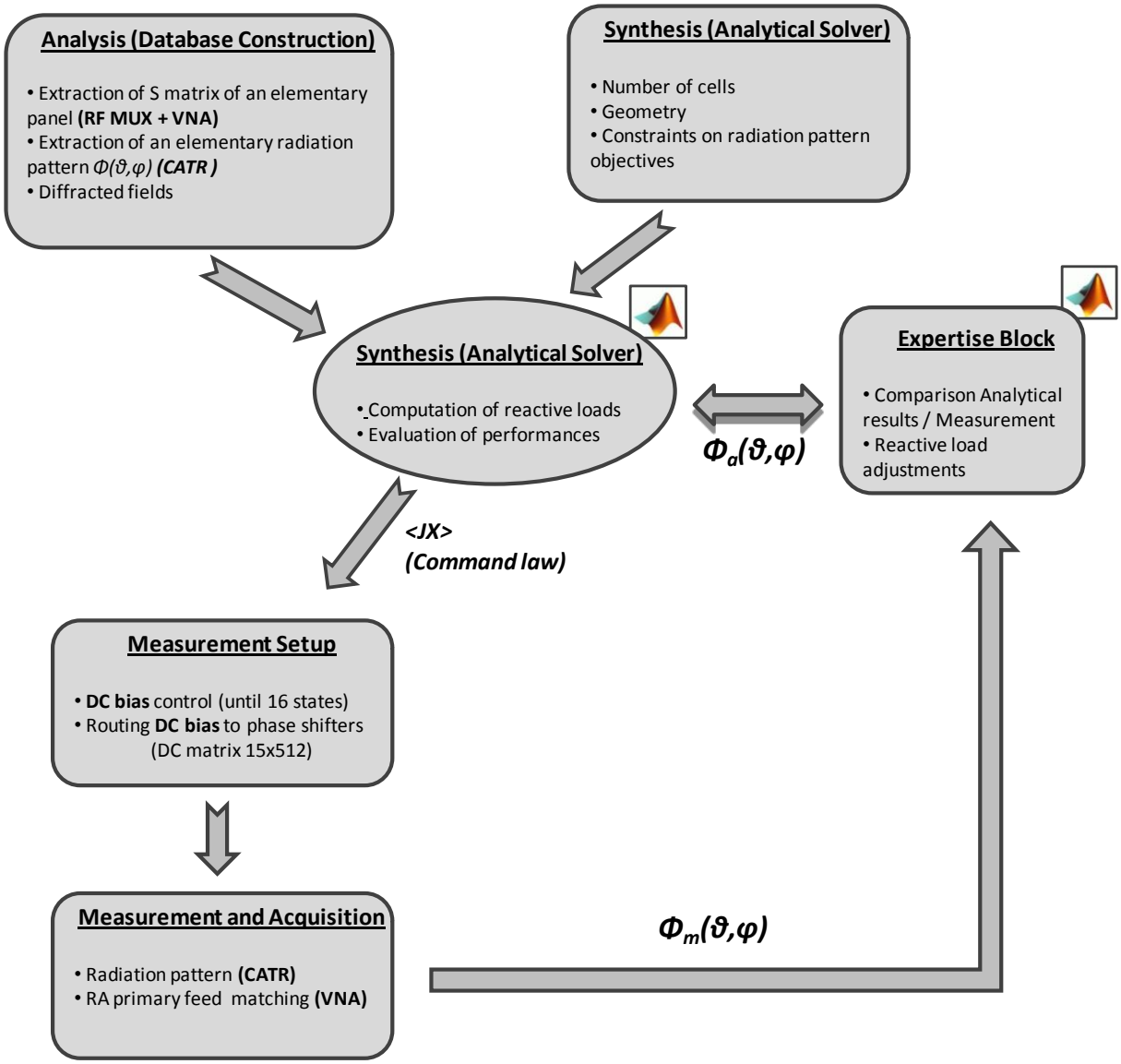

This chain will capitalize on the work accomplished during this thesis in order to design with as most accuracy as possible tunable reflectarrays, to detail their physical properties and to include technological constraints (phase shifter models obtained from measurement, quantization states, …)

LIST OF PUBLICATIONS

International Journal Publications

- Abdallah Y., Menudier C., Thevenot M. and Monediere T., “Mutual Coupling Effect Investigation in Reflectarray antennas”, *IEEE Antennas and Propagation Magazine*, Accepted for publication in 2013.
- Zhang H., Abdallah Y., Chantalat R., Thevenot M, Monediere T. and Jecko B., “Low Profile and High Gain Yagi Wire-Patch Antenna for WIMAX Applications”, *IEEE Antennas and Wireless P. Letters*, 2012.
- Thevenot M., El Sayed Ahmad, Menudier C., El Nashef G., Fezai F., Abdallah Y., Arnaud E., Torres F., and Monediere T., "Synthesis of Antenna Arrays And Parasitic Antenna Arrays With Mutual Couplings," *Special Issue of International Journal of Antennas and Propagation, Hindawi Publishers*, 2012.

International Conference Publications

- Abdallah Y., Fezai F., Menudier C., Thevenot M., and Monediere Thierry, "Switchable Steerable Square Parasitic Monopole Array Design Using a Genetic Algorithm," *Int. Symp. Antem* , Toulouse, June 2012.
- Abdallah Y., Menudier C., Thevenot M., and Monediere T., "Examining the Energetic Contribution of Reflectarray Cells Using Circuit Model and Full-wave Simulations," *Proccedings of EUCAP*, Prague, March 2012.
- Abdallah Y., Menudier C., Thevenot M., and Monediere Thierry, “A Method to Analyze Reflectarray Antennas Using Local Ports”, *Worshop ESA/ESTEC*, Noordwijk, Oct 2011.
- Abdallah Y., Menudier C., Thevenot M., and Monediere Thierry, "Reflectarray Antennas with Accurate Calculation of Phase Shifts," *Proceedings of EUCAP, Rome*, April 2011.
- Koubeissi M, Abdallah Y., Thevenot M, Monediere T, Koleck T and Peragin E., “WideBand WideAngle Circular Polarization of a Multilayer Patch Antenna”, *Proceed. of EUCAP*, Barcelona, April 2010.

National Conference Publications

- Abdallah Y., Menudier C., Thevenot M., and Monediere T., "Methode d'Analyse et de Synthèse des Charges pour Reflectarray," *17ème Journées Nationales Microondes JNM*, Brest, Mai 2011.

Résumé :

L'objectif de la thèse est étudier de façon précise et rigoureuse les propriétés électromagnétiques des antennes reflectarray (RA). Pour atteindre cet objectif, ce travail de thèse propose une architecture de reflectarray spécifique associée à une méthodologie de synthèse. Après avoir présenté un état de l'art sur les reflectarray et leurs applications, une méthodologie complète de conception sera détaillée. Celle-ci sera ensuite mise en œuvre, notamment pour montrer l'impact des couplages et la nécessité de les considérer dans la conception d'un Reflectarray. L'intérêt de ce travail consiste aussi à améliorer la compréhension des propriétés EM du RA afin d'optimiser leurs performances. La démarche adoptée permet également d'analyser des contraintes particulières comme celles lies à la technologie des cellules utilisées dans un RA agile. A cette fin, l'effet de la quantification des états de phase des cellules sera étudié.

INFLUENCE DES COUPLAGES SUR LES PROPRIETES DES ANTENNES A RESEAU REFELCTEUR. DEFINITION D'UNE METHODOLOGIE DE CONCEPTION

Abstract :

This thesis aims to present an accurate and a rigorous study of the electromagnetic properties of reflectarray antennas. To reach this objective, this work proposes a specific architecture of reflectarrays associated with a synthesis approach. After presenting a state of the art of reflectarrays and their application domain, a conception method will be detailed. Then, we will present a design test, particularly to demonstrate the effects of mutual couplings between the cells, and the need of taking them into account in the synthesis of the reflectarray. This work will also improve the comprehension of the electromagnetic behaviour of the reflectarray in order to enhance its performance. The proposed approach allows also to perform a study on some particular constraints such as those related to the technology of the cells. For this purpose, the effects of the quantization of the phase shifts will be studied.

Discipline : "Electronique des Hautes Fréquences, Optoélectronique"

Mots clés :

Reflectarray antenna	Antennes à réseau réflecteur
Directive antenna	Antennes directives
Mutual couplings	Couplages Mutuels
weightings	Pondérations
Pattern synthesis	Synthèse des diagrammes
Quantization	Quantification
Phase shifts	Déphasages
Optimization	Optimisation

Adresse du laboratoire : XLIM, UMR CNRS n°7252, Département OSA, Faculté des Sciences – Université de Limoges, 123 avenue Albert Thomas – 87060 Limoges Cedex